Stony Brook University

OFFICIAL COPY

The official electronic file of this thesis or dissertation is maintained by the University Libraries on behalf of The Graduate School at Stony Brook University.

© All Rights Reserved by Author.

The Brown Dwarf Kinematics Project

A Dissertation Presented

by

Jacqueline K. Faherty

to

The Graduate School

in Partial Fulfillment of the Requirements

for the Degree of

Doctor of Philosophy

in

Physics

Stony Brook University

December 2010

Copyright by

Jacqueline K. Faherty

2010

Stony Brook University

The Graduate School

Jacqueline K. Faherty

We, the dissertation committee for the above candidate for the Doctor of Philosophy degree, hereby recommend acceptance of this dissertation.

Frederick M. Walter – Dissertation Co-Advisor
Professor, Department of Physics and Astronomy, Stony Brook

Michael M. Shara – Dissertation Co-Advisor
Curator, Department of Astrophysics, American Museum of Natural History

Adam J. Burgasser – Dissertation Co-Advisor
Assistant Professor, Department of Physics, UC San Diego

Michael Zingale – Chairperson of Defense
Assistant Professor, Department of Physics and Astronomy, Stony Brook

Anand Sivaramakrishnan
Adjunct Professor, Department of Physics and Astronomy, Stony Brook

Dan M. Davis
Professor, Geosciences, Stony Brook

This dissertation is accepted by the Graduate School.

Lawrence Martin
Dean of the Graduate School

Abstract of the Dissertation

The Brown Dwarf Kinematics Project

by

Jacqueline K. Faherty

Doctor of Philosophy

in

Physics

Stony Brook University

2010

Brown dwarfs are a recent addition to the plethora of objects studied in Astronomy. With theoretical masses between 13 and 75 $M_{Jupiter}$, they lack sustained stable Hydrogen burning so they never join the stellar main sequence. They have physical properties similar to both planets and low–mass stars so studies of their population inform on both.

The distances and kinematics of brown dwarfs provide key statistical constraints on their ages, moving group membership, absolute brightnesses, evolutionary trends, and multiplicity. Yet, until my thesis, fundamental measurements of parallax and proper motion were made for only a relatively small fraction of the known population. To address this deficiency, I initiated the Brown Dwarf Kinematics (BDKP). Over the past four years I have re-imaged the majority of spectroscopically confirmed field brown dwarfs (or ultracool dwarfs–UCDs) and created the largest proper motion catalog for ultracool dwarfs to date. Using new astrometric information I examined population characteristics such as ages calculated

from velocity dispersions and correlations between kinematics and colors. Using proper motions, I identified several new wide comoving companions and investigated binding energy (and hence formation) limitations as well as the frequency of hierarchical companions.

Concurrently over the past four years I have been conducting a parallax survey of 84 UCDs including those showing spectral signatures of youth, metal-poor brown dwarfs, and those within 20 pc of the Sun. Using absolute magnitude relations in J,H, and K, I identified overluminous binary candidates and investigated known flux-reversal binaries. Using current evolutionary models, I compared the M_K vs J-K color magnitude diagram to model predictions and found that the low-surface gravity dwarfs are significantly redward and underluminous of predictions and a handful of late-type T dwarfs may require thicker clouds to account for their scatter.

In loving memory of Rachel Faherty

Contents

List of Figures

List of Tables

Acknowledgements

I like the saying "It takes a village to raise a child" and how it applies to my thesis. This work was made possible by the love and support of a number of people (and places). First I must acknowledge my academic parents. Like many other aspects of life I took a non-standard path during my PhD and had three supervisors. Each one of them helped me tremendously in producing this work.

Adam Burgasser shaped my writing style and approach to science. He took me on as his first student in the first few moments of his career as a tenure track astronomer. The majority of our mentor-mentee relationship was conducted long-distance via emails, phone calls or video chats, but somehow I managed to learn an enormous amount of Brown Dwarf science from him. While the deadly red-penning that Adam loves to do to paper manuscripts wasn't always the most pleasant thing to receive, it is one of the main reasons I am so proud of my work over the past few years. I might never get the Burgasser voice out of my head correcting my grammar, re-writing sentences, telling me to add more references, but without it I wouldn't be half the scientist I am today.

Mike Shara allowed me to return to my home away from home, the American Museum of Natural History. As I stumbled to find where I could fit into the academic world 4 years ago Mike made me feel that I was already an expert. Even though his science interests are (quite literally) completely opposite to what I proposed to study in my thesis, Mike took me under his wing and supported my research. He was a picture perfect academic father, gently prodding to make sure I was making progress on a regular basis but always encouraging me when I was down on myself. Even if I was faltering, Mike seemed to have the utmost faith that I was blazing on to be a fantastic scientist. For that undying support and encouragement I am a better and more confident scientist and person.

Fred Walter was my Stony Brook advisor and while it was a rocky four years together, I learned a great deal about academics and myself from our relationship. I worked with Fred on a first year research project in 2005, measuring a parallax to the neutron star Geminga. That project and the

Yale Astrometry conference that I attended as a result, are the main reasons I pursued astrometry in my thesis. There seemed to be few things that Fred and I agreed on over the years (anything from science to Baseball seemed to cause a fight); but, the constant challenging of my knowledge and work did push me to become a better researcher.

I also acknowledge the support of the remainder of my thesis committee including the chair Mike Zingale, the late add-in Dan Davis, and one of my best supporters, Anand Sivaramakrishnan.

There is a core group of people who have greatly influenced my career path over the past four years. Kelle Cruz has been the springboard that I bounced ideas off of, a safety net when I was in the academic doldrums, and my personal cheerleader through tricky situations. Dagny Looper was my long-distance academic sister. John Bochanski and Andrew West became my older academic brothers. Whether I liked it or not they treated me like their kid sister, teasing my research choices, pushing me around for not knowing things, but coaching me through the difficult situations and choices faced in academia. Ben Oppenheimer was a huge support during the first few years of graduate school. He introduced me to Adam 5 years ago which kick-started my entire thesis. I am extremely grateful for the advice and encouragement he supplied early on.

While I spent very little time at Stony Brook during the research portion of my thesis, I spent all of my time there in the first two years. I survived the course work period of graduate school because of Jason Reeves, Steve Stewart, Saul Lapidus, and the Starbucks on the corner of 347 and Stony Brook road. I can't remember how many nights we spent there over two years but it was probably a high percentage of 730.

A large portion of my thesis was spent observing at Cerro Tololo in Chile. I have to thank the outstanding staff at Tololo for making that part of research so exciting. I would especially acknowledge the great friendships developed with Jose Velazquez (who got me addicted to Sahne Nuss chocolate) and Nicole van der Bliek (who helped to advance the addiction).

Over the years I have had numerous stimulating conversations with members of the Astrophysics department at AMNH including David Zurek, Colin McNally, Sebastien Lepine, Mordecai-Mark Mac Low, Emily Rice, and Ryan Wyatt that helped shape the work here-in. I especially thank Brian Abbott, the Digital Universe manager at AMNH who originally brought me into the Astro department as a volunteer in 2001. He has been a source of inspiration for the past 9 years.

Outside of academia several people including Aisling McKenna, Dina Holinka, and Richard Shackell, helped me stay sane while working on this project.

Emily Fellman, Mandë Holford and Tina Romero provided constant and priceless amounts of advice on all aspects of life. I am in debt to them for their unwavering loyalty.

Lastly I acknowledge the love and support of my father Richard Faherty, sisters and brother Colleen, Erin, and Scott Faherty and brother-in law Paul Rooney. If this project had completely failed (which at times seemed possible) I knew that these five people would not have thought any different of me. We would have just laughed about it and probably blamed one of the dogs (the prime culprit would have been Ruby. Miracle, Kelly, or Charley would have just been co-conspirators).

This thesis was made possible in part due to the financial support of Hillary Lipschitz, a patron of AMNH and lover of Astronomy.

Chapter 1

Introduction

1.1 Brief History of Astrometry

In ancient times stars were thought to be fixed points in the sky, drilled into a celestial sphere that circled the Earth as it stayed in its central position of the Universe. Our acceptance of stars having their own intrinsic proper motion and a detectable parallax is grounded in the assertion that the stars are not fixed points in the sky and the Earth is moving and not the center of the Universe. Thus early astrometrists were the true scientific rebels of the astronomical community seeking to overthrow the traditional model of the cosmos in which the Earth was central and immobile.

1.1.1 Astrometric Measurements

The term 'Astrometry' was not coined until the 19^{th} century but the history of astrometric measurements traces as far back as Ancient Egypt and Mesopotamia when star charts first appeared. By the age of antiquity, Greek and Roman astronomers such as Hipparcos and Claudius Ptolemy were creating stellar catalogs that eventually served as references for thousands of years. Prominent Greek astronomers identified that the ecliptic provided a fundamental astronomical coordinate system. They noted that the geometrical points in the sky where the ecliptic and equatorial planes intersected formed a natural origin for coordinate systems. Ptolemy as well as his contemporaries designated the ascending node of the ecliptic as the delineator for the stellar day and the reference position for navigational stars. This "First Point of Aries" was recognized to change, an observation which marked the establishment of Earth's precession, a fundamental achievement of early astrometric work.

By the late 16^{th} century , the Copernican revolution had occurred and it

was surmised that if the Earth was indeed moving around the Sun the geometry of the constellations should shift seasonally. Tycho Brahe was among the early astronomers who unsuccessfully attempted to measure the first stellar parallax. His failed attempts led him to identify three major factors that were necessary for advances in high precision astrometric measurements: instrument innovation, refined techniques, and an alertness to potential sources of error. The development of instruments in the 17^{th} and 18^{th} centuries such as astronomical quadrants, telescopic sights, micrometers and verniers, was strongly driven by astronomical desire to detect the elusive stellar parallax. The search also led to advances in other areas of astronomical research. For instance, in 1650 Christian Huygen's recognized that graduated scales were insufficiently refined to detect a parallax. Up until that time it was thought that the brightest stars had to be the closest. Many failed parallax attempts were targeting stars such as Sirius which were bright but had stellar parallaxes well outside the bounds of possibility for the precision possible in the 17^{th} and 18^{th} centuries.

The quest for stellar parallax also led Robert Hooke, John Flamsteed, and James Bradley to the invention of the zenith sector (a long-focus telescope hung to point exactly at the zenith). Independent attempts at stellar parallaxes by each, but most noteably by Bradley, led to the discovery of a "New Found Motion". This stellar aberration was quickly understood to be the apparent displacement of a star from its mean position on the celestial sphere due to the velocity of the Earth in its orbit around the Sun. While this was not the long sought parallactic motion; the discovery was considered a triumph of refined astrometric techniques and proof of the Earth's motion in space.

One important advancement in early astrometric studies was in our understanding about the motion of stars. Through the 17^{th} century it was generally assumed that stars were fixed in their positions. But in 1718 Edmund Halley published a paper which showed that Aldebaran, Sirius, and Arcturus displayed independent motion against the stellar background. This measurement was a product of a catalog comparison between the positions recorded by Hipparcos, and Ptolemy against positions current in Halley's time. The paper is the first recorded publication of proper motion and was a key to advancing all other astrometric measurements. The discovery and increasingly accurate quantification of stellar proper motion over the decades that followed identified a means for differentiating the relative closeness of stars and hence their suitability for parallax measurements.

By the middle of the 19^{th} century all the great observatories of Europe were primarily dedicated to astrometric work. In the years between 1838 and 1840 bonafide parallaxes were reported by Friederich Bessel, Thomas Henderson,

and Friederich Wilhem Struve all using different instruments and astronomical techniques. These parallax measurements were made possible because of the discovery of proper motion as a target criterion, the innovation of instrumentation, and the advancement in our understanding of positional uncertainties (most prominent stellar aberration and atmospheric distortion).

1.1.2 Modern Day Astrometry

Astrometric work blossomed in the 20^{th} century. The invention of photography in 1839 and the introduction of photographic plates led to major advances . In addition to allowing significantly more precise measurements, it liberated the astronomer from the eyepiece of a telescope. In the 1960's the advent of large-aperture, high precision reflector telescopes as well as more recent technological advances in silicon based CCD instruments provided the largest modern day advances in ground-based astrometric programs.

Numerous large-scale ground-based astrometric surveys have been conducted over the past century. The Guide Star Catalog (GSC) was prepared to support the operation and requirements of the Hubble Space Telescope (HST) by providing accurate positions of nearly 20 million stars (Lasker et al. 2008). The United States Naval Observatory (USNO) has published stellar positions and proper motions for almost half a billion stars (Monet 1998; Monet et al. 2003). Many large scale proper motion surveys have been published including notable ones by Wolf (1919), Ross (1926), Luyten (1979), Lépine et al. (2002). Optical ground-based parallax surveys have been conducted in the North and South and prominent catalogs include the General Catalogue of Trigonometric Stellar Parallaxes (Jenkins 1952; van Altena et al. 1995), and the CTIOPI catalog (Henry et al. 2006, Weichun et al. 2005, Costa et al. 2006).

Atmospheric distortion remains the largest deterrent to precise ground-based astrometry. Therefore space based observatories were the last and most significant advancement in astrometry. The High Precision Parallax Collecting Satellite, Hipparcos, is responsible for the largest parallax sample to date and the most precise proper motion catalog (Perryman et al. 1997).

1.1.3 ASIDE: How to Measure Proper Motion and Parallax

Proper motion, the angular change in stellar position over time, can be measured with just two images separated by a significant time baseline (typically several years). Parallactic motion is a subtle effect. As the Earth orbits the Sun, several observations over a six month period of a nearby star against

the background of distant, stationary stellar objects reveal an annual shift in its position. Parallax, π, is related to the distance to a star, r, by $\pi=\frac{1}{r}$ where π is expressed in arcseconds and r is in parsecs. To be precise, the instantaneous motion of a star must be measured relative to the Solar System barycentre in a plane perpendicular to the line of sight. Figure 1.1 demonstrates the annual parallactic displacement, p_t, which can be written as

$$\begin{aligned} \theta_1 - \theta &= \pi\ R\ sin\ \theta \\ &\quad or \\ p_t &= \pi\ R\ sin\ \theta \end{aligned} \tag{1.1}$$

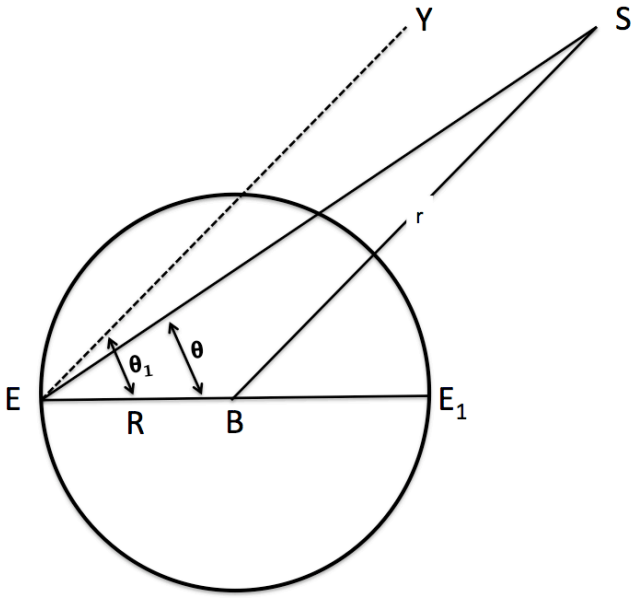

Figure 1.1: Plotted is a circular representation of the Earths orbit at position E and E_1 (six months later). B indicates the Solar System barycenter, R is the Earth's orbital radius, S is the position of a star at distance r, and θ is an angle (varying with time) between the direction to the Sun and to the star.

The annual parallax factor is separated as

$$P_t = R\ sin\theta \tag{1.2}$$

A textbook description of parallax and proper motion using classic astrometric modeling dealing with angles and geodescic triangles can be found in van de Kamp (1967). As described there-in, the parallax displacement of a star toward the Solar System barycenter can be calculated with parallactic displacement in longitude and latitude as:

$$\begin{aligned} x_\lambda &= \pi\ R\ sin\ \theta\ sin\ \phi \\ y_\beta &= -\pi\ R\ sin\ \theta\ cos\ \phi \end{aligned} \tag{1.3}$$

where π is the parallax, ϕ is shown on Figure 1.2, λ and β are the longitude and latitude of the parallax star, and x and y are the displacements in the two directions.

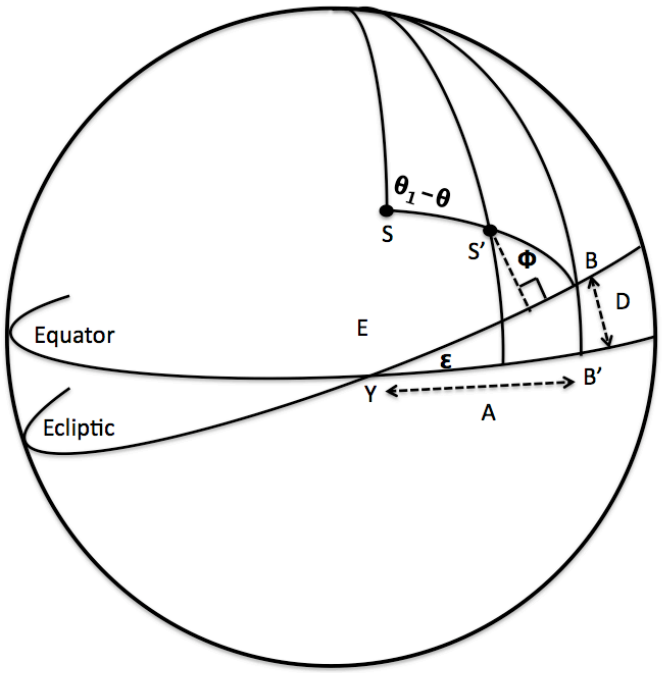

Figure 1.2: S is the star and S' is the stellar position seen from Earth (E). B is the Solar System barycenter at coordinate (A,D), Y is the position of the vernal equinox, and ϵ is the obliquity of the ecliptic.

Applying spherical trigonometry the parallactic ellipse is described as:

$$\frac{x_\lambda^2}{\pi^2 R^2} + \frac{y_\beta}{\pi^2 R^2 sin^2\beta} = 1 \tag{1.4}$$

The small inclination of the ecliptic relative the Earth's equator leads to the majority of parallactic displacement occurring in the right ascension direction. Therefore, the parallax factors can be further re-written as:

$$\begin{aligned} P_\alpha &= R\,(cos\,\epsilon\,cos\,\alpha\,sin\,B - sin\,\alpha\,cos\,B) \\ P_\delta &= R\,[(sin\,\epsilon\,cos\,\delta - cos\,\epsilon\,sin\,\alpha\,sin\,\delta)\,sin\,B - cos\,\alpha\,sin\,\delta\,cos\,B] \end{aligned} \tag{1.5}$$

where ϵ is the obliquity of the ecliptic, (α,δ) are the right ascension, declination positions of the star, and B is the Solar System barycenter (see Figure 1.2).

The final equations for decoupling the proper motion from the parallax are:

$$x = x_0 + \mu_\alpha(t - t_0) + P_\alpha\pi \tag{1.6}$$

$$y = y_0 + \mu_\delta(t - t_0) + P_\delta\pi \tag{1.7}$$

where x_0, y_0 are initial positions; μ_α, μ_δ are the proper motion in right ascension, declination (respectively); P_α, P_δ are the parallactic factors, (t-t_0) is the baseline between measurements, and π is the parallax.

1.2 Modern Day Astrometric Accomplishments

Over the past 150 years, astrometric measurements have significantly changed our understanding of the local solar neighborhood, the Galaxy and beyond. In the following section I detail a number of the major advances astrometry has contributed to over the years. These highlights primarily target contributions that are discussed within this thesis (in the context of Brown Dwarfs) so this is by no means a complete discussion of the vast contributions of astrometric measurements.

1.2.1 3D Space Motions

Understanding the motion of a star or population of objects can be informative about parameters such as age or origin and can provide crucial information regarding both the structure and evolution of the Milky Way. Combining proper motion, parallax and radial velocity (the element of stellar motion toward or away from the Sun) the full space motion or velocity of an

object can be calculated. There are three components of space velocity in the Milky Way's Galactic coordinate system (using a right-handed coordinate system): U which is positive in the direction of the Galactic center, V which is positive in the direction of Galactic rotation, and W which is positive in the direction of the North Galactic Pole. The Sun has its own peculiar motion with respect to the Local Standard of Rest (LSR)[1] which is (U,V,W) = (10.00±0.36, 5.25±0.62, 7.17 ±0.38) km s^{-1} (Dehnen & Binney 1998) .

As early as 1908, Karl Schwarzschild interpreted a sample of stellar random velocities as forming a triaxial 'velocity ellipsoid' which Oort B. Lindbland and Stromberg related to the large-scale structure of the Galactic disc. Subsequent studies by Parenago (1950) and Roman (1952, 1950) noted that stellar kinematics systematically vary with stellar type identifying that younger stars have (on average) smaller velocity dispersions and larger mean Galactic rotation velocities than older stellar constitutents. Multiple authors explained this correlation between age and velocity in terms of the diffusion of stars through phase space as the Galactic disk ages (Wielen 1977, Spitzer & Schwarzschild 1953, Barbanis & Woltjer 1967).

The Geneva-Copenhagen survey of the solar neighborhood has produced one of the most up to date kinematic samples by combining Hipparcos parallaxes and proper motions with measured high precision radial velocities. They used this sample to investigate ages and metallicities for a sample of over 14,000 F and G dwarfs and to assign Galactic disk membership to investigate large scale structure (Nordstrom et al. 2008; Nordström et al. 2004). The space motions and Galactic orbits of stars as a function of age provide key information regarding the parallel dynamical evolution of the Galaxy and the degree of mixing of stellar populations from different regions of the disk (see Freeman & Bland-Hawthorn 2002 and references there in).

Substructures of the Galactic disk have also been identified using space motion. Aside from the overall Galactic structure of a young thin disk, older thick disk, and a halo population (Eggen 1989; Gilmore et al. 1989; Gilmore & Reid 1983; Chiba & Beers 2000; Soubiran et al. 2003) co-moving associations of stars including young moving groups, open clusters, and Galactic streams have been identified (Chereul et al. 1999; Montes et al. 2001; Bensby et al. 2007; Dehnen & Binney 1998). Such kinematic associations are key clues to understanding stellar dynamics and the Galactic history.

[1]A point defined as instantaneously centered on the Sun and moving in a perfectly circular orbit along the solar circle about the Galactic center

1.2.2 Identifying Companions

Multiple stellar systems (with two or more bound objects) are ubiquitous in the Milky Way. They have been found in a wide range of configurations, from tight spectroscopic binaries with separations < 10 AU to loosely bound wide binaries with separations $> 20{,}000$ AU (e.g. Halbwachs et al. 2003, Chanamé & Gould 2004). Multiplicity characteristics such as periods, mass ratios, and eccentricities provide key constraints on theoretical models of star formation (e.g. Bate 2000, Delgado-Donate et al. 2004, Goodwin et al. 2007). Specifically the separation distribution of low mass star and brown dwarf companions has been used as a constraint on the low mass end of star formation (Reid et al. 2001; Burgasser et al. (2003c)). The observed distribution of wide binaries is of particular interest, because the low binding energy of these systems makes them susceptible to disruption. Models suggest that over timescales comparable with the age of the Milky Way, these weakly bound systems should be disrupted due to repeated and separate encounters with other field stars, giant molecular clouds, and/or hypothetical dark matter bodies (Retterer & King 1982; Weinberg et al. 1987; Yoo et al. 2004).

The main problem in searching for wide systems is distinguishing between chance alignments and true physical pairs. Astrometric measurements have been instrumental in both identifying and confirming wide multiple system candidates. Using catalogs of high proper motion stars (typically > 100 mas yr^{-1}) searches for common proper motion candidates greatly reduces the probability of chance alignment. Early studies by Luyten (1988) catalogued over 6000 wide systems. Luyten noted at the 1969 Double Star Conference in Nice that these common proper motion pairs constituted the most common, and the most representative physical binaries in space (at least based on what was known through the middle of the 20^{th} century). More wide binaries were detected through common proper motion searches of the Hipparcos catalog where precise parallaxes were also available for critical mapping of the HR diagram of co-eval stars as well as investigations of the projected physical separation between components which can be directly compared with theoretical models. Hundreds of wide Hipparcos pairs were investigated in Chanamé & Gould (2004) and Lépine & Bongiorno (2007).

1.2.3 Color Magnitude and HR Diagrams

The Hertzsprung-Russell diagram, developed independently by Hertzsprung in 1911 and Henry Norris Russell in 1913, empirically illustrates the relationship between stellar spectral types and luminosities. It stems from the basic relation for an object emitting thermal radiation as a black body:

$$L = 4\pi\sigma R^2 T_{eff}^4 \tag{1.8}$$

where L is the luminosity, σ is the Stefan-Boltzmann constant, R is the radius and T_{eff} is defined as the effective temperature of a hypothetical black body of the same radius R radiating the same luminosity L. The structure of a star changes with time due to nuclear fusion. As a result, L and T_{eff} change as a star evolves. On an HR-diagram, any given star will follow a path that is a function of its mass and chemical composition so it is a powerful diagnostic of a star's structure and evolution during its whole life. In order to construct an observational HR diagram, stellar luminosities and therefore precise distances are required. Until the publication of the Hipparcos catalog (Perryman et al. 1997), the several thousand ground-based stellar parallax measurements with precisions on the order of 10-20% were the foundation for our understanding of stellar luminosity. This collection of stars was used to develop various methods for indirect distance estimates including spectroscopic and photometric parallaxes, secular and statistical parallaxes, the moving-cluster method, and main-sequence fitting to specific features in the observational HR diagram of open and globular clusters Mihalas & Binney 1981).

Different populations of stars have different loci in the HR-diagrams. Globular clusters (GC) have sequences in which almost all evolutionary phases, including a stellar main sequence, the horizontal and asymptotic giant branches, are detectable. Close examination of GC HR and color-magnitude diagrams revealed that metallicity was the most influential factor governing their horizontal branch morphologies but a second parameter effect, most likely age, must be included to completely describe the horizontal branch sequence (e.g. Arp et al. 1952, Sandage 1953, Sandage & Wallerstein 1960, Searle & Zinn 1978, Dotter et al. 2010). HR diagrams of nearby well observed star clusters such as the Pleiades and the Hyades, have led to an improved understanding of stellar physics. They serve as excellent tests for how well interior models, which make use of model atmospheres, can reproduce observations (e.g. Mitchell & Johnson 1957, Johnson & Mitchell 1958, Vandenberg & Bridges 1984; Perryman et al. 1998). For instance, a detailed look at the HR diagram of the Hyades cluster shows a well-defined main sequence with two "gaps" or "turn-offs" showing observational support for the theoretical prediction of the onset of surface convection (de Bruijne et al. 2001).

As a whole, HR diagrams provide sharp constraints on stellar evolutionary theories and a rigorous framework for exploring the evolutionary history of the Milky Way.

1.3 Brown Dwarfs

The last quarter of the 20th century was marked, within a small portion of the astronomical community, by a race to detect the first substellar mass object. The quest began on the heels of the pioneering theoretical works of Kumar (1962) and Hayashi & Nakano (1963). Both groups independently predicted that below stellar masses between roughly 0.07-0.08 $M_{\odot}$ central temperature and density would be too low to sustain nuclear fusion reactions. These so-called brown dwarfs (Tarter 1975) were thought to have significantly different characteristics than stars thereby necessitating an entirely new class of objects.

1.3.1 Formation

The standard model for stellar formation is through the gravitational collapse and subsequent fragmentation of dense gas within giant molecular cloud cores (e.g., Shu et al. 1987). Initially, radiant energy is generated through the transformation of gravitational potential energy into heat. In the process, the core becomes dense enough to trap radiation and the central temperature (T_c) and density rise rapidly enough to slow the contraction (with temperature scaling roughly as $T_c \propto R^{-1}$; Stahler 1988). The conditions eventually reach a level where thermonuclear fusion is possible within the core of the protostar (for solar type stars T_C ~3 x 10^6K). Gas and radiation pressure generated by initial nuclear burning support the protostar against any further gravitational contraction bringing it into hydrostatic equilibrium on the stellar main sequence.

For lower mass objects, higher densities are required for the collapse before achieving the critical temperature required for fusion. In the perfect gas regime, the thermal energy and gravitational potential energy are in balance: $GM^2/R \sim (M/m_p)kT_c$ or $M/R \sim$ constant for a given T_c. Consequently, the density $<\rho>$ scales as M^{-2}. At a high enough density, the stellar core becomes partially degenerate measured by the parameter α (Reid & Hawley 2005):

$$\alpha_E = \frac{N_e h^3}{2(2\pi M - EkT)^{3/2}} \sim \frac{electron\ chemical\ energy}{kT} \tag{1.9}$$

where $\alpha_E <$ -4 implies that the material can be treated as a perfect gas governed by Maxwell Boltzmann statistics and $\alpha_E > 20$ implies that the material is fully electron degenerate governed by Fermi-Dirac statistics.

As the degeneracy parameter rises, the potential energy is increasingly absorbed into reducing the separation between degenerate electrons rather

than transformed into thermal energy. The core pressure (Burrows & Liebert 1993):

$$P_C \sim 10^{13}(\frac{\rho}{\mu_e})^{5/3}(1+\frac{5\mu_e}{2\mu\eta})\, dyne\, cm^{-2} \tag{1.10}$$

increases under the influence of electron degeneracy pressure and eventually halts further contraction. If this occurs before the protostar has reached the critical temperature for sustained stable Hydrogen fusion (below a mass of $\sim 0.072 M_\odot$; Chabrier & Baraffe 1997); the object simply continually cools off and is categorized as a brown dwarf. Figure 3.11 demonstrates the core temperature versus age based on the evolutionary models of Burrows et al. (1997).

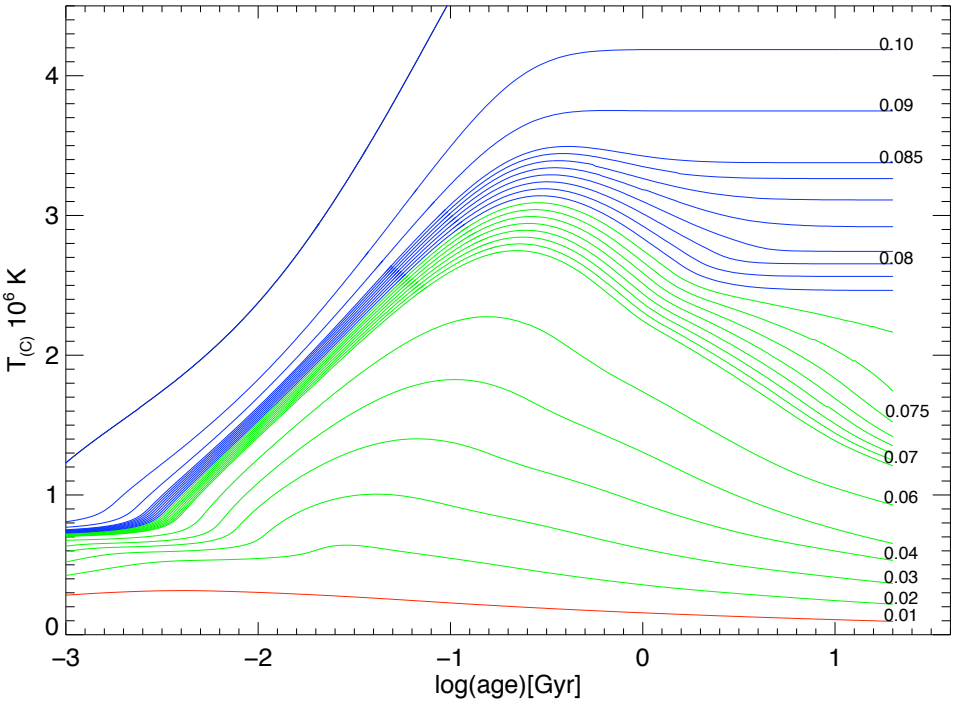

Figure 1.3: The core temperature (T_c versus age of low mass stars and brown dwarfs based on the Burrows et al. (1997) evolutionary models. Lines of constant mass are labeled in $M_\odot$. As in Burrows et al. 2001 the red lines are for models with masses equal to or below 13 $M_{Jupiter}$, the green lines are for objects above 13 $M_{Jupiter}$ and below the edge of the main sequence (here marked at 78 $M_{Jupiter}$), and the blue are for Hydrogen burning stars.

Some initial nuclear burning is possible in brown dwarfs before electron

degeneracy reduces the temperature below what is required for fusion. The nuclear energy generation can be reduced to one branch of the $p-p$ chain (Burrows & Liebert 1993):

$$p + p \rightarrow d + e^{+} + \nu_e \tag{1.11}$$

$$p + d \rightarrow^{3} He + \gamma \tag{1.12}$$

Depending on the mass, nuclear burning is achieved for $0.1< \tau <10$ Myr during which 95% of the total emitted luminosity is generated via the above branch of the $p-p$ chain (Grossman et al. 1974). For objects less massive than 0.013 $M_{\odot}$, temperatures do not reach a level where this initial deuterium fusion is possible (Burrows et al. 1997; Chabrier et al. 2000). Oppenheimer et al. (2000) proposed this mass cut-off as the boundary between low-mass brown dwarfs and planets, and subsequent works (such as Basri & Brown (2006)) have adopted this designation.

1.3.2 Detection and Observable Properties

The lack of stable hydrogen burning in brown dwarfs makes them intrinsically very dim. They peak in brightness in the near-IR (due to their low effective temperatures) and because of their intrinsic faintness (see Figure 1.4), they are primarily detected in the nearby solar neighborhood. The first bonafide brown dwarf discoveries came after many false positives and null results were reported in the literature from deep cluster surveys, radial velocity monitoring, and companion searches (e.g. Leggett & Hawkins 1988; Forrest et al. 1989; Murdoch et al. 1993). In the mid 90's Gliese 229B, a faint < 1200 K companion to a nearby M dwarf, was reported by Nakajima et al. (1995). This is often considered the first bonafide brown dwarf verified in the literature although GD 165B (Becklin & Zuckerman 1988); Teide 1 (Rebolo et al. 1995); and PPl 15 (Basri et al. 1996) also stake that claim.

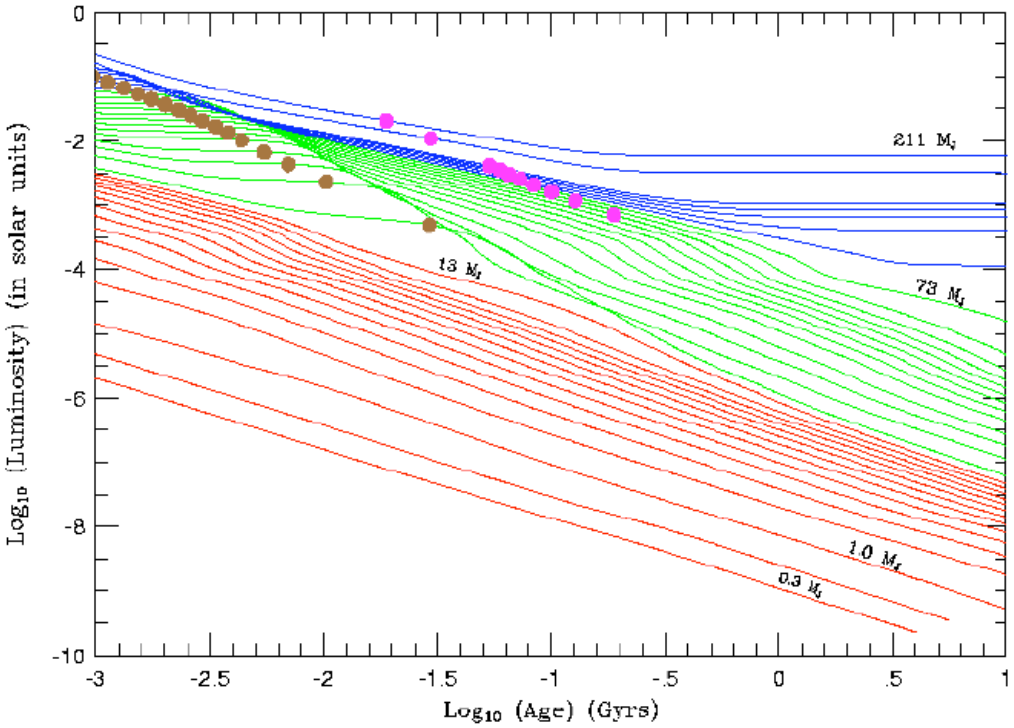

Figure 1.4: Luminosity versus age of low mass stars and brown dwarfs as published in Burrows et al. (2001). Lines of constant mass are labeled in $M_{Jupiter}$ ($\sim 10^{-3}$ $M_{\odot}$.)

By the end of the 20^{th} century a number of surveys made possible what is now called substellar observational astronomy. Astronomers working with the Two Micron All-Sky Survey (2MASS; Skrutskie et al. 2006), the Deep Near-Infrared Survey of the Southern Sky (DENIS; Epchtein et al. 1997), and the Sloan Digital Sky Survey (SDSS; York et al. 2000) identified hundreds of brown dwarf candidates that were confirmed with spectroscopic follow-up (e.g. Cruz & Reid 2002; Cruz et al. 2003; Burgasser et al. 1999, 2003d; West et al. 2004; Kirkpatrick et al. 2000; Chiu et al. 2006, 2008; Knapp et al. 2004). The spectral classification scheme was expanded to encompass the variety of new objects. The standard $OBAFGKM$ classifications were extended to include "L" dwarfs (objects with temperatures typically between 2400<T<1300K) and "T" dwarfs (objects with temperatures typically below ∼1300K; see Kirkpatrick 2005 and references there in).

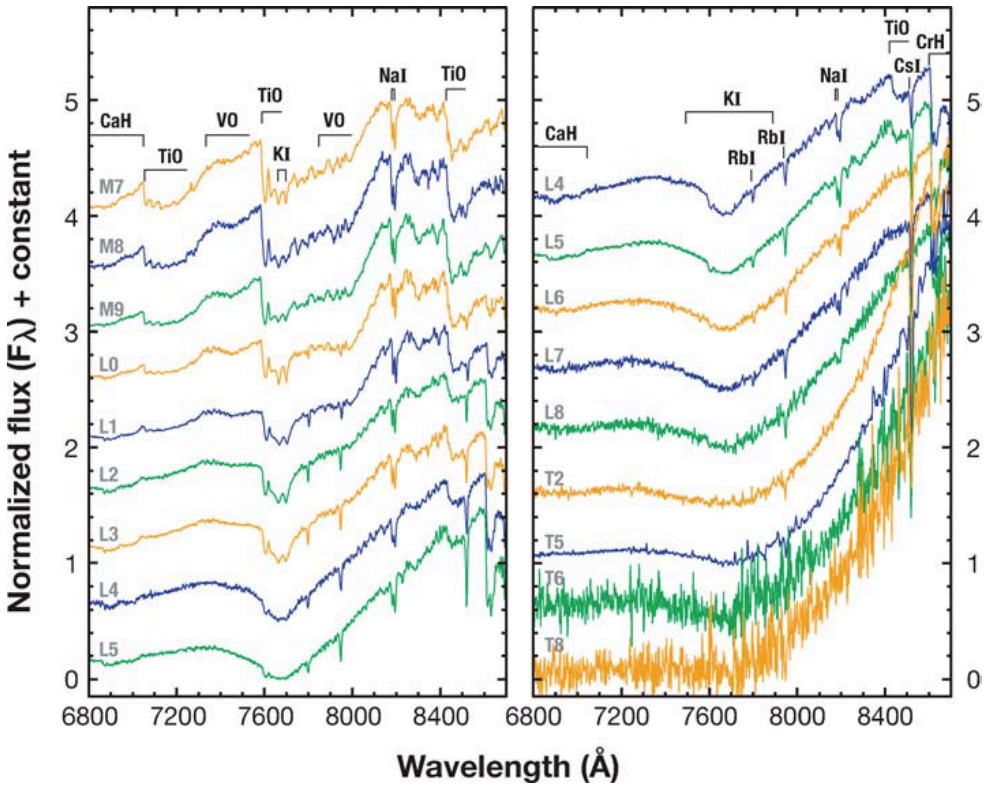

Figure 1.5: The optical spectral sequence from M7 to T8 dwarfs as published in Kirkpatrick (2005).

As objects cool from M dwarfs into L dwarfs, their optical spectra become dominated by strong metal hydride bands (FeH, CrH, MgH, CaH) and prominent alkali metal lines (Na I, K I, Cs I, Rb I). Titanium oxide (TiO) and vanadium oxide (VO), which are dominant in M dwarfs, are depleted with decreasing temperature as dust formation is believed to remove these molecules from the atmosphere. As objects cool even further into the T dwarfs, astronomers turn to near-IR spectra as a classification scheme where CH_4, the distinguishing T dwarf spectral feature, and H_2O dominate. Figure 1.5 shows the optical spectral sequence of M7 through T8 dwarfs taken from Kirkpatrick (2005), and Figure 1.6 shows the near-IR spectral sequence of L dwarfs taken from Kirkpatrick et al (2010) and T dwarfs taken from Burgasser et al (2006). The standard spectral classification for L dwarfs is in the optical using the Kirkpatrick et al (1999) scheme and for T dwarfs is in the near-IR using the Burgasser et al (2006) scheme (see also Geballe et al. 2002; Kirkpatrick et al. 2010; Cushing et al. 2005).

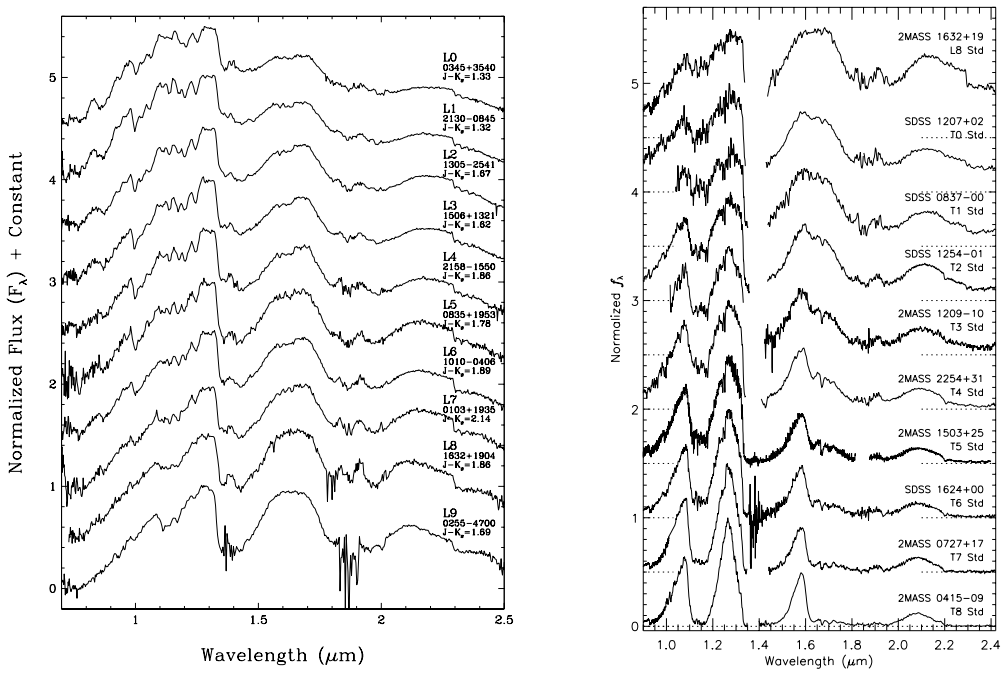

Figure 1.6: At left, the near-IR spectral sequence from L0 to L9 taken from Kirkaptrick et al (2010). At right, the near-IR spectral sequence from L8 to T8 taken from Burgasser et al (2006). The standard classification scheme for L dwarfs is from Kirkpatrick et al 1999 using optical data. The standard for T dwarfs is from Burgasser et al (2006) using near-IR data.

Using a combination of optical and near-IR filters, apparent magnitude differences in near-IR bandpasses have been used to photometrically select brown dwarf candidates as well as study overall population characteristics. The latest type T dwarfs emit a significant percentage of their light in mid-IR wavelengths therefore Spitzer Infrared Array Channel (*IRAC*) bands have also been used to study photometric characteristics of the coldest brown dwarfs (Leggett et al. 2010; Patten et al. 2006). The most widely used color for studying L and T dwarfs in the field has been *J*-*K*. L dwarfs have increasingly red *J*-*K* colors due to decreasing T_{eff} and condensate dust in their photospheres. T dwarfs have increasingly blue *J*-*K* colors as CH_4 absorption removes significant longer wavelength flux and their photospheres are generally considered cloudless or clear of dust. Figure 1.7[2] shows the *J*-*K* color difference versus spectral type for the L and T dwarfs listed on dwarfarchives.org as well as the recent SDSS

[2]The dwarfarchives website is a compendium of spectroscopically confirmed field L and T dwarfs maintained by Chris Gelino, Davy Kirkpatrick, and Adam Burgasser

sample from Schmidt et al. (2010).

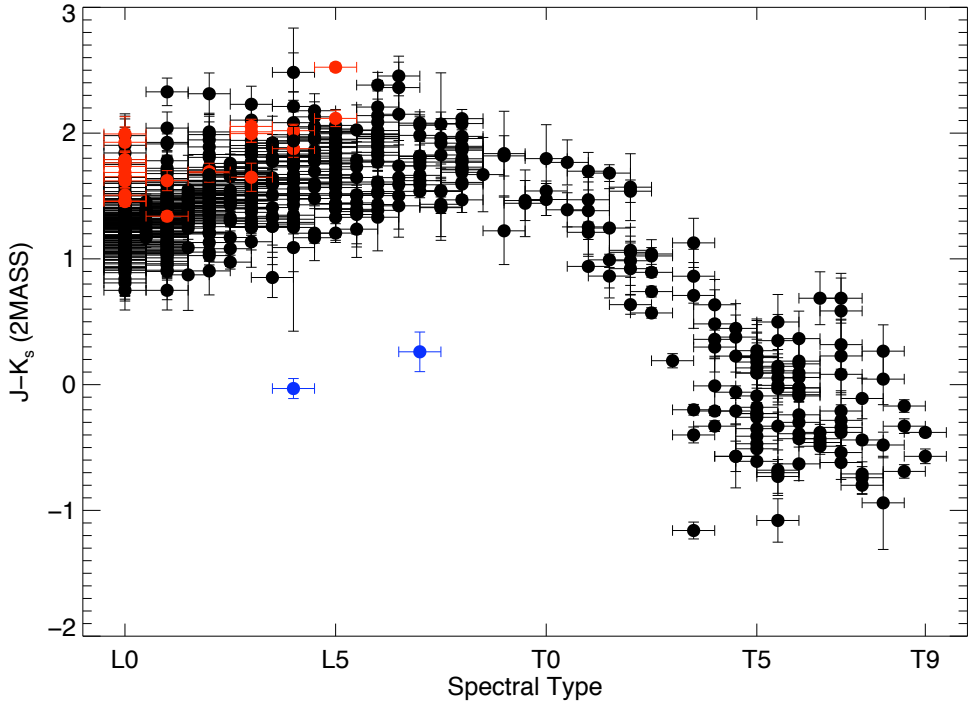

Figure 1.7: 2MASS near-IR J-K$_s$ color of L and T dwarfs listed on the dwarfarchives.org website (as of September 2010) as well as those listed in a recent SDSS study by Schmidt et al. (2010). Low surface gravity dwarfs are marked by red filled circles, subdwarfs are marked with blue filled circles, and normal field dwarfs are marked as black filled circles.

1.3.3 Influence of Clouds, Gravity, and Metallicity

The early models of brown dwarfs predicted a sensitivity of observables to different surface gravities, metallicity, and dust precipitation (Burrows et al. 2002; Marley et al. 2002). The range of photospheric pressures (0.1-10 bar) and temperatures (∼500-3000 K) covered by brown dwarfs leads to complex atmospheric chemistry. The atmospheres of substellar mass objects contain clouds of oxides, iron, silicates and various other refractory condensates which cause a reddening of the spectral energy distribution and a shallowing of absorption bands (Tsuji et al. 1996). The elemental depletion and wavelength distribution of the opacity of these dust clouds influence the photometry as well as the emergent spectral energy distribution.

A range in age among the known field population leads to gravity and/or metallicity differences. The surface gravity modulates the photospheric gas pressure. This affects both pressure-sensitive features as well as gas/condensate chemistry which in turn influences colors and spectral features. Low-surface gravity objects have weakened alkali lines, enhanced metal oxide absorption and reduced H_2 absorption all leading to a redder near-IR color. High surface gravity objects have inverse features all leading to a bluer near-IR color.

Differences in metallicity influence brown dwarf colors and spectral features (e.g. Burrows et al 2006). For metal-poor brown dwarfs there is an enhancement in collision-induced H_2 absorption that preferentially supresses flux at K band (Linsky 1969; Saumon et al. 1994). Combined with a reduction in metal opacity at shorter wavelengths; low-metallicity results in bluer near-IR colors (see Burgasser et al. 2008c, Bowler et al. 2009, Cushing et al. 2010). Conversely, metal-rich dwarfs have greater dust production due to the availability of metals for grain condensation.

Relative to the mean J-K_s colors of known L and T dwarfs, both red and blue photometric outliers have been observationally identified. They have spectral peculiarities attributable to suppressed or enhanced metallicity, gravity or atmospheric properties as described above. The red photometric outliers have their observable features attributed to low-surface gravity; dusty photospheres; or a high metallicty (e.g. Kirkpatrick et al. 2006; Cruz et al. 2009; Allers et al. 2007; Looper et al. 2008b). Low-surface gravity outliers tend to have weak Na and K lines as well as reduced VO bands in their optical spectra. The near-IR spectra of the blue photometric outliers show strong H_2O, FeH and K I features (e.g. Cruz et al. 2003, Cruz et al. 2007; Knapp et al. 2004, Chiu et al. 2006, Burgasser et al. 2008c, Bowler et al. 2009, Cushing et al. 2010). Their observable features have been attributed to low-metallicty, old age, or patchy-cloud atmospheres. Extreme examples of these are the handful of halo brown dwarfs identified in the field (Burgasser et al. 2003a; Burgasser et al. 2004; Burgasser 2004a; Sivarani et al. 2009; Cushing et al. 2009).

Several models are available for testing the effects of clouds, gravity, and metallicity on brown dwarf observables. Prominent evolutionary models include Chabrier et al. (2000), Burrows et al. (1997), and Saumon & Marley 2008. Prominent atmospheric models include: PHOENIX models (Hauschildt et al. 1999, 1997; Allard et al. 2001, 2003; Helling et al. 2008), Burrows models (Burrows et al. 2006; Burrows & Liebert 1993); Marley & Saumon models (Ackerman & Marley 2001; Saumon & Marley 2008); and Tsuji models (Tsuji 2005, 2002). Each approaches the problem of dust condensation and opacity with a different methodology. Helling et al. (2008) shows that even with vastly different approaches, atmospheric models agree on the global cloud structure

but differ in opacity relevant details such as grain size, dust quantity, etc., leading to slightly different theoretical predictions. Testing the predictions of both model atmospheres and brown dwarf isochrones requires knowledge of critical brown dwarf parameters such as well defined distances and ages.

1.4 Determining Brown Dwarf Ages

Determining the age of an individual brown dwarf is challenging. Their thermal evolution leads to a degeneracy between mass, age, and physical properties derived from observables such as luminosity and effective temperature (T_{eff}). One method for breaking this degeneracy is to sample the age of the population using kinematics. Combining distance with proper motion yields the tangential velocity (v_{tan}) of an individual source. The dispersion of v_{tan} for a population reveals high or low velocity outliers as well as age information about the population (Wielen 1977). Vrba et al. (2004) compared the distribution of v_{tan} among L and T dwarfs and conclude that the kinematics indicate that, in general, the T dwarfs are an older population than the L dwarfs. Combining proper motion, distance, and radial velocity, Zapatero Osorio et al. (2007) examined the space motion of a sample of 18 ultracool dwarfs. They concluded that L and T dwarfs are kinematically younger than solar-type to early M stars with likely ages in the interval 0.5-4 Gyr.

Individual brown dwarf ages have been determined by tying them to objects with well defined ages. Brown dwarfs have been found in very young star-forming regions such as Orion and Taurus (ages <1-2 Myr); intermediate-age moving groups such as β Pictoris and AB Doradus (< 10 Myr); and older associations such as the Hyades ($\sim$ 600 Myr) and Pleiades ($\sim$ 100 Myr) open clusters (e.g. Bouvier et al. 2008; Bihain et al. 2006; Jameson et al. 2008b; Ribas 2003). They have also been found as companions to well characterized main-sequence stars (e.g. Kirkpatrick et al. 2001a, Wilson et al. 2001, Burgasser et al. 2000a, Nakajima et al. 1995). Assuming co-evality between the pair; the age of the main-sequence star can be applied to the brown dwarf. For these objects, ages can range from as low as a few hundred Myr to several Gyr.

Spectral analysis techniques have also proven effective for determining individual brown dwarf ages. For T dwarfs, comparing the H_2O and H_2–sensitive spectral ratios between empirical data and theoretical atmospheric models calibrated to brown dwarfs with well-characterized ages yields effective temperatures and surface gravities (Burgasser et al. 2006a). These in turn can be combined with evolutionary models to yield individual age estimates. Several groups have successfully applied such age dating methods within the litera-

ture (Saumon et al. 2007; Warren et al. 2007; Cushing et al. 2008), although this method relies on having well calibrated brown dwarf benchmarks (such as those described above) to anchor the analysis.

1.5 Astrometry of Brown Dwarfs

The first multi-object brown dwarf astrometric program was by Dahn et al. (2002). In that work astrometry was reported for 17 L dwarfs and three T dwarfs. One year later Tinney et al. (2003) reported astrometry for 10 T dwarfs and the following year Vrba et al. (2004) reported measurements for 22 L dwarfs and 18 T dwarfs. Some overlap exists between the various programs; but with these three samples in combination with companions to nearby parallax stars (e.g. Nakajima et al. 1995; Kirkpatrick et al. 2001a; Wilson et al. 2001) and a handful of individual measurements (Thorstensen & Kirkpatrick 2003; Burgasser et al. 2008c; Smart et al. 2010), the sample of brown dwarfs with well defined distance and proper motion measurements was defined.

A number of intrinsic characteristics of the brown dwarf population emerged from early astrometric studies. By combining parallax measurements with bolometric corrections (Golimowski et al. 2004b) and an assumed radius (see Vrba et al. 2004), the mean luminosity and temperature ranges were defined for spectral types. Spectrophotometric relations were defined in the near-IR and optical enabling distance calculations for objects without trigonometric parallax measurements. Close examination of absolute magnitude as a function of spectral type revealed a brightening in near-IR color (primarily in the J band) for T0-T5 dwarfs (Dahn et al. 2002; Vrba et al. 2004). Further studies revealed this to be an intrinsic feature of brown dwarfs with the most probable explanation being complex atmospheric physics (Burgasser et al. 2002b; Looper et al. 2008a; Liu et al. 2006).

A number of parallax sources were followed up with adaptive optics imaging and resolved into close binary companions (Bouy et al. 2008;Martín et al. 2006; Burgasser et al. 2003c). A number of groups have been monitoring these sources to measure orbital parameters and consequently the dynamical masses (Dupuy et al. 2008; Dupuy et al. 2009; Konopacky et al. 2010a). The handful of objects with precise mass measurements have been used to test the accuracy of evolutionary models. The most recent studies have found significant discrepancies between empirical measurements tracing brown dwarf isochrones to those predicted by the most reliable models (Burrows et al. 1997; Chabrier et al. 2000; Zapatero Osorio et al. 2004).

The scatter of brown dwarfs in color-magnitude diagrams has been at-

tributed to a second parameter influence which could be gravity, metallicity, unresolved binarity, and/or atmospheric differences within the brown dwarf population (Saumon & Marley 2008). The J band brightening is now firmly attributed to atmospheric effects largely caused by either cloud disruption or a sharp variation in the efficiency of condensation across the temperature regime of the early type T dwarfs (Burgasser et al. 2002b; Knapp et al. 2004). The scatter of luminosity among the latest-type T dwarfs has been attributed to gravity or metallicity effects (Leggett et al. 2009; Patten et al. 2006). Novel techniques have successfully identified an increasingly large population of unresolved close binaries (Burgasser et al. 2010a). Such systems would appear as over-luminous sources on color-magnitude diagrams. Increasing the number of brown dwarfs with well-characterized distances, ages, metallicities, and/or surface gravities will enable robust investigations of the second parameter effect.

1.6 The Brown Dwarf Kinematics Project

In order to address pressing issues with our understanding of brown dwarf evolutionary trends, multiplicity, and atmospheric properties, I and collaborators at the American Museum of Natural History, MIT, United States Naval Observatory (USNO), Cerro Tololo Inter-American Observatory (CTIO), and the University of Washington initiated the Brown Dwarf Kinematics Project (BDKP). We set out to measure proper motions for all known L and T dwarfs and determine parallax as well as radial velocity measurements for all brown dwarfs within 20pc of the Sun and select sources of scientific interest. The scientific goals of this project are to (1) construct a "clean" (free of binary and spectrally-peculiar objects) sample for luminosity function measurements, (2) search for spatial and kinematic structure associated with moving groups, (3) construct robust absolute magnitude, luminosity and T_{eff} relations particularly across the poorly-sampled L dwarf/T dwarf transition region, (4) examine correlations between kinematics and physical properties, and (5) identify unresolved multiples and wide companions to nearby stars.

The following chapters describe the results of the first few years of the BDKP and the projects for which I was the lead investigator. Chapter 2 describes a campaign to re-image known L and T dwarfs. With this work I created an astrometric catalog of the majority of known brown dwarfs and examined kinematic trends within the population. Chapter 3 describes a cross-correlation between the BDKP astrometric catalog and the Hipparcos and Lepine Shara Proper Motion North (LSPM-N) catalog in search of companions to nearby stars. Extensive follow-up of 9 systems is described in that chapter

where I test age-diagnostic tools for brown dwarfs and stars and examine the stability of the low-binding energy systems discovered. Chapter 4 describes an extensive parallax campaign in the South to determine distances to all late-type L and T dwarfs within 20pc of the Sun as well as select sources of scientific interest (namely low-surface gravity dwarfs and subdwarfs). In that chapter I create robust absolute magnitude diagrams and explore various color magnitude diagrams which test various levels of gravity, metallicity, and atmospheric properties. Finally, in Chapter 5 I discuss the impact of this work and the future of brown dwarf astrometry.

Chapter 2

Proper Motions and Tangential Velocities

At the start of my thesis it was clear that there was a large gap in our understanding of the basic astrometric properties of the brown dwarf population because the majority of L and T dwarfs were missing proper motion measurements. As a result myself, and collaborators initiated the Brown Dwarf Kinematics Project (BDKP) with one of the primary goals being to re-image all known L and T dwarfs lacking proper motion measurements. In this chapter I describe the results of a 1.5 year observing campaign using optical and near-IR imaging facilities in the North and the South to obtain accurate kinematic data for ultracool dwarfs. This chapter is a reprinting of a paper, of which I am the primary author, published in the Astronomical Journal with co-authors Adam J Burgasser, Michael M. Shara, Frederick M. Walter, Kelle L. Cruz, and Chris Gelino.

2.1 Introduction

Kinematic analyses of stars have played a fundamental role in shaping our picture of the Galaxy and its evolution. From early investigations (e.g. Lindblad 1925, Oort 1927) where the large scale structure of the Galactic disk was first explored, through more recent investigations (e.g. Gilmore & Reid 1983, Gilmore et al. 1989, Dehnen & Binney 1998, Famaey et al. 2005) where the structure of the Galaxy was refined to include a thick disk and prominent features such as streams, moving groups, and superclusters, kinematics have played a vital role in understanding the Galactic origin, evolution, and structure. Combining kinematics with spectral features, several groups have mapped out ages and metallicities for nearby F,G,K, and M stars (e.g.

Nordström et al. 2004). The ages of these stars have become an important constraint on the Galactic star formation history and their kinematics have become a vital probe for investigating membership in the young thin disk, intermediate aged thick disk or older halo portion of the Galaxy.

One population that has yet to have its kinematics exploited is the recently discovered population of very low-mass ultracool dwarfs (UCDs). These objects, which include those that do not support stable hydrogen fusion (Kumar 1962; Hayashi & Nakano 1963), occupy the late-type M through T dwarf spectral classifications (e.g., Kirkpatrick, 2005, and references therein). UCDs emit the majority of their light in the infrared and thus were only discovered in large numbers with the advent of wide-field near-infrared imaging surveys such as the Two Micron All Sky Survey (hereafter 2MASS; Skrutskie et al. 2006), the Deep Infrared Survey of the Southern Sky (hereafter DENIS; Epchtein et al. 1997) and the Sloan Digital Sky Survey (hereafter SDSS; York et al. 2000). Their very recent discovery has largely precluded astrometric measurements which require several-year baselines to produce useful measurements. Therefore, while UCDs appear to be comparable in number to stars (e.g., Reid et al. 1999), their role in the structure of the Galaxy has yet to be explored.

In addition, the thermal evolution of brown dwarfs (the lowest temperature ultracool dwarfs) implies that there is no direct correlation between spectral type and mass, leading to a mass/age degeneracy which makes it difficult to study the mass function and formation history of these objects. While some benchmark sources (e.g. cluster members, physical companions to bright stars) have independent age determinations, and spectroscopic analyses are beginning to enable individual mass and age constraints (e.g. Burgasser et al. 2006a; Saumon et al. 2007, Mohanty et al. 2004), the majority of brown dwarfs are not sufficiently characterized to break this degeneracy. Kinematics can be used as an alternate estimator for the age of the brown dwarf population.

Moreover, kinematics can also be used to characterize subsets of UCDs. With hundreds of UCDs now known[1], groupings of peculiar objects - sources whose photometric or spectroscopic properties differ consistently from the majority of the population - are becoming distinguishable. Currently defined subgroups of late-type M, L and T dwarfs include 1) low surface-gravity, very low-mass objects (e.g. McGovern et al. 2004, Kirkpatrick et al. 2006, Allers et al. 2007, Cruz et al. 2007), 2) old, metal-poor ultracool subdwarfs (e.g. Burgasser et al. 2003a, Lépine et al. 2003, Gizis & Harvin 2006, Burgasser et al. 2007a), 3) unusually blue L dwarfs (hereafter UBLs; e.g. Cruz et al. 2003, Cruz et al. 2007; Knapp et al. 2004, Chiu et al. 2006), and 4) unusually red

[1]An up-to-date list of known L and T dwarfs is maintained by C. Gelino, D. Kirkpatrick and A. Burgasser at http://www.dwarfarchives.org

and possibly dusty L dwarfs (e.g. (Looper et al. 2008b; McLean et al. 2003). While observational peculiarities can overlap between these groups (e.g. both young and dusty L dwarfs can be unusually red), they appear to encompass objects with distinct physical traits (e.g., mass, age, composition, and cloud properties) so they are important for drawing a connection between observational characteristics and intrinsic physical properties. Kinematics can be used to investigate the underlying physical causes for the peculiarities of these groups.

In the past decade a number of groups have conducted astrometric surveys of UCDs, including subsets of low mass objects (e.g. Vrba et al. 2004, Dahn et al. 2002, Gizis et al. 2000b, Tinney et al. 2003, Schmidt et al. 2007, Jameson et al. 2008a, Zapatero Osorio et al. 2007, and West et al. 2008, 2006). We have initiated the Brown Dwarf Kinematics Project (BDKP) which aims to measure the positions and 3D velocities of all known L and T dwarfs within 20 pc of the Sun and selected sources of scientific interest at larger distances (e.g. low surface-gravity dwarfs, subdwarfs). In this article we add 332 new proper motion measurements and combine all published proper motion measurements and distance estimates into a uniform sample to examine the ultracool dwarf population as a whole. Section 2 of this paper outlines the observed sample and describes how proper motion measurements were made. Section 3 discusses the expanded sample and how distances and V_{tan} measurements were calculated. Section 4 examines the full astrometric sample and subsets. Section 5 reviews the high tangential velocity objects in detail. Finally, section 6 applies an age-velocity relation and examines resultant ages of the full sample and red/blue outliers.

2.2 Observations and Proper Motion Measurements

2.2.1 Sample Selection

Our goal is to re-image all known late-type M, L, and T dwarfs to obtain accurate uniformly measured proper motions for the entire ultracool dwarf population. In our sample we focused on the lowest temperature L and T dwarfs that were lacking proper motion measurements or whose proper motion uncertainty was larger than 40 mas/yr. We gave high priority to any dwarf that was identified as a low surface-gravity object in the literature. Our sample was created from 634 L and T dwarfs listed on the Dwarf Archives website as well as 456 M7-M9.5 dwarfs gathered from the literature (primarily from Cruz et al. 2003, 2007). The sample stayed current with the Dwarf Archives

website through April 2008. Figure 2.1 shows the histogram of spectral type distributions for the entire sample. The late-type M and early-type L dwarfs clearly dominate the ultracool dwarf population. Plotted in that figure is the current distribution of objects with proper motion values and the distribution of objects for which we report new proper motions. To date we have re-imaged 427 objects. As of June 2008 and including all of the measurements reported in this article, 570 of the 634 known L and T dwarfs and 277 of the 456 late-type M dwarfs in our sample have measured proper motions.

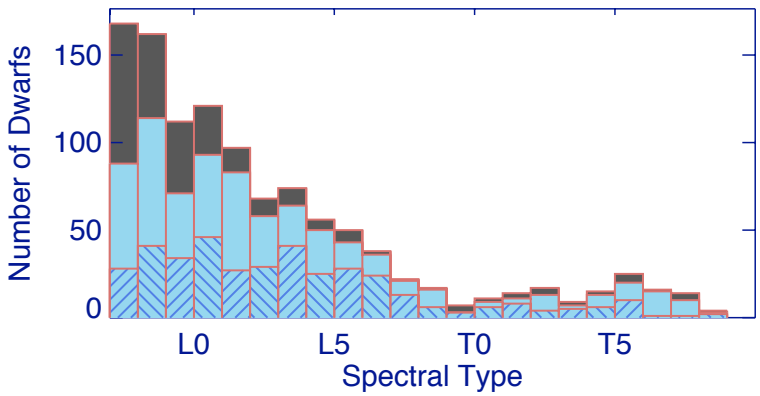

Figure 2.1: Spectral type distribution of all late-type M, L, and T dwarfs. The overall histogram is the distribution of all ultracool dwarfs in our sample. The blue shaded histogram shows ultracool dwarfs with proper motion measurements. The diagonally shaded histogram shows the distribution of ultracool dwarfs with new proper motions reported in this paper.

2.2.2 Data Acquisition and Reduction

Images for our program were obtained using three different instruments and telescopes in the northern and southern hemispheres. Table 2.1 lists the instrument properties. For the northern targets the 1.3m telescope at MDM with the TIFKAM IR imager in J band was used. For the southern targets the 0.9m and 1.5m telescopes at CTIO with the CFIM optical imager in I band and the CPAPIR wide field-IR imager in J band (respectively) were used. The CTIO data were acquired through queue observing on 11 nights in March, September and December 2007, and standard user observing on 9 nights in January 2008. The MDM targets were imaged on five nights in November 2007 and 7 nights in April 2008. Objects were observed as close to

the meridian as possible up to an airmass of 1.80, and with seeing no greater than 2.5″ FWHM. Exposure times varied depending on the target and the instrument. For CPAPIR the exposure times ranged over 15−40s with 4 co-adds per image and a five-point dither pattern. At MDM the exposure times ranged over 30−120s with up to 6 co-adds per image and a three to five-point dither pattern. For the 0.9m observations the exposure times ranged over 180−1800s per image with no co-adds and a three-point dither pattern. The dither offset between positions with each instrument was 10″.

All data were processed in a similar manner using standard IRAF and IDL routines. Domeflats were constructed in the J or I band. CPAPIR and CFIM domeflats were created from 10 images illuminated by dome lamps, and TIFKAM domeflats were created by subtracting the median of 10 images taken with all dome lights off from the median of 10 images taken with the dome lights on. A dark image constructed from 25 images taken with the shutter closed was used to map the bad pixels on the detector. Domeflats were then dark subtracted and normalized. Sky frames were created for each instrument by median-combining all of the science data taken on a given night. Science frames were first flat-fielded, then sky-subtracted. Individual frames were shifted and stacked to form the final combined images.

2.2.3 Calculating Proper Motions

The reduced science frames were astrometrically calibrated using the 2MASS Point Source catalogue. 2MASS astrometry is tied to the TYCHO 2 positions and the reported astrometric accuracy varies from source to source. In general the positions of 2MASS sources in the magnitude range $9 < K_s < 14$ are repeatable to 40-50 mas in both RA and DEC.

Initial astrometry was fit by inputting a 2x2 transformation matrix containing astrometry parameters which were first calculated from one image in which two stars with known 2MASS RA and DEC values and second epoch X,Y pixel positions were known. The reference RA, DEC and pixel values were first set to the pointing RA and DEC values and the center of the chip respectively.

RA and DEC values for all stars in the field were then imported from the 2MASS point source catalogue and converted to X,Y pixel positions using the initial astrometric parameters. We worked in X,Y positions of the second epoch image so we could overplot point source positions on an image and visually check that we converged upon a best fit solution. We detected point sources on the second epoch image with a centroiding routine which used a detection threshold of 5 sigma above the background. We matched the 2MASS X,Y positions to the second epoch positions by cross-correlating the two lists. We

Table 2.1. Properties of Instruments Used for Astrometric Measurements

Telescope	Instrument	Band	FOV (arcminutes)	Plate Scale (arcsecond/pixel)	Dates	Seeing (arcseconds)	Sources Observed
CTIO 0.9m	CFIM	I	4.5	0.40	2007 Sep 23 - 26	0.8 - 2.0	42
MDM 1.3m	TIFKAM	J	5.6	0.55	2007 Nov 20 - 24	1.0 - 2.5	66
					2008 Apr 22 - 28	0.8 - 2.5	80
CTIO 1.5m	CPAPIR	J	35.0	1.02	2005 Oct 19	1.0 - 1.5	4
					2006 Aug 21	1.0 - 2.0	7
					2007 Mar 04	0.9 - 1.8	28
					2007 Mar 23	0.9 - 1.3	39
					2007 Dec 03 - 06	1.0 - 2.0	35
					2008 Jan 15 - 23	0.7 - 2.5	248

refined the astrometric solution by a basic six parameter, least-squares, linear transformation where we took the positions from the 2MASS image (X_1,Y_1) and the positions from the second epoch image (X_0,Y_0) and solved for the new X,Y pixel positions of the second epoch image in the 2MASS frame. Due to the large field of view, we checked for higher order terms in the CPAPIR images and found no significant terms. The following equations were used:

$$X = x_{2o} + A(X_1 - X_0) + B(Y_1 - Y_0) \tag{2.1}$$

$$Y = y_{2o} + C(X_1 - X_0) + D(Y_1 - Y_0) \tag{2.2}$$

where x_{2o} and y_{2o} were set to the center of the field, A, B, C, D solve for the rotation and plate scale in the two coordinates.

The sample of stars used to compute the astrometric solution for each image were selected according to the following criteria:

1. Only stars in the 2MASS J magnitude range $12 < J < 15$ were used, as objects in this intermediate magnitude range transformed with the smallest residuals from epoch to epoch.

2. The solution reference stars were required to transform with total absolute residuals against 2MASS of < 0.2 pixels. From testing with images taken consecutively using each instrument, the best astrometric solution always generated between 0.1 and 0.2 pixel average residuals. Therefore the stars used to calculate the solution were required to fall in or below that range.

As the solution was iterated, the residuals were examined at each step, and stars that did not fit the above criteria were removed. For CPAPIR, the process converged on a solution that had between 100 and 200 reference stars with average residuals < 0.15 pixels. TIFKAM and CFIM have smaller fields of view ($\sim$6 arcmin and $\sim$ 5 arcmin respectively as opposed to 35 arcmin for CPAPIR) so there were far fewer stars to work with. For these imagers the process converged on a solution that had between 15 and 60 reference stars. The astrometric solution was required to converge with no less than 15 reference stars and when this criterion could not be met, the other two criteria above were relaxed. As a result TIFKAM and CFIM had slightly larger residuals on the astrometric solution (average residuals < 0.25 pixels).

Once an astrometric solution was calculated, final second epoch positions were computed using a Gaussian fit for each 2MASS X,Y position on an image. For the science target, a visual check was employed to ensure that it had been detected and X,Y positions were manually input for the Gaussian fit. Final X,Y positions were then converted back into RA and DEC values using the best

astrometric solution and the proper motion was calculated using the positional offset and time difference between the second epoch image and 2MASS.

The residuals of the astrometric solution were converted into proper motion uncertainties by multiplying by the plate scale of the instrument and then dividing by the epoch difference. The baselines ranged from 6-10 years and our astrometric uncertainties range from 5 to 50 mas/yr. Positional uncertainties for each source were also calculated by comparing the residuals of transforming the X,Y position for our target over consecutive dithered images. These uncertainties are dominated by counting statistics with the high S/N sources having negligible positional uncertainties compared to the uncertainties in the astrometric solution. We added the positional and astrometric solution uncertainties in quadrature to determine the total proper motion uncertainty. Figure 2.2 shows the distribution of proper motion uncertainties and baselines for all new proper motion measurements reported in this paper. The median uncertainty was 18 mas/yr.

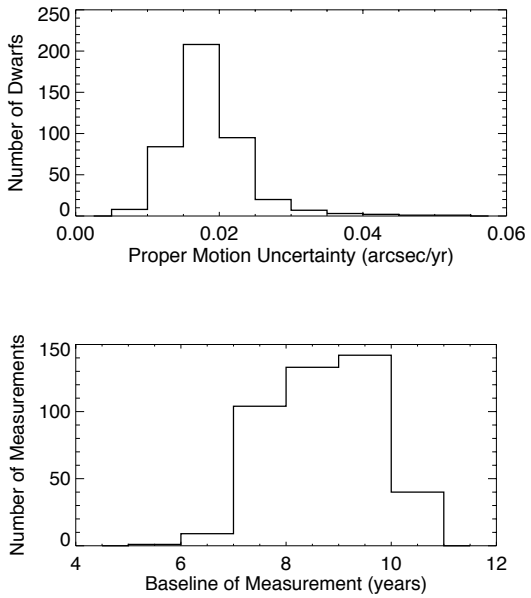

Figure 2.2: (Top): Distribution of proper motion uncertainties for the sample of 427 measurements reported in this paper. The median value is 18 mas yr^{-1}. (Bottom): Distribution of proper motion baselines (time between first and second epoch measurements) used in this survey.

Of the 427 proper motion measurements we report in this paper, 332 are presented here for the first time. Twelve objects were purposely remeasured with multiple instruments as a double check on the accuracy of the astrometric solution, and 42 objects were remeasured to refine the proper motion uncertainties. Thirty-two measurements were published in Jameson et al. 2008a-hereafter J07-, and 11 in Caballero (2007) while our observations were underway. The proper motion measurements presented in this paper agree to better than 2σ in 84 of the 97 cases of objects with prior measurements. Table 2.2 lists those cases where the proper motions are discrepant by more than 2σ with a published value. For nine of the objects, there is a third (fourth or fifth) measurement by an independent group with which we are in good agreement. We are discrepant with six objects reported in Deacon et al. (2005) but we note that there are no position angle uncertainties reported for these objects in that catalogue therefore we cannot fully assess the accuracy of the proper motion components. The difference in proper motion for 2MASSW J1555157-095605 is quite large ($>$ 1"/yr difference) but there are two other measurements for this object with which we are in close agreement. We have examined all of the discrepant proper motion images carefully and see no artifacts that could have skewed our measurements. Figure 2.3 compares the proper motion component measurements from this paper with those from the literature for objects with μ < 0.5 $''$/yr and $\mu_{err} < 0.1$ $''$/yr. With$\sim$90% agreement with published results, this indicates that the 332 new measurements are robust. Table 2.11 contains all new measurements reported in this article, and Table 2.12. contains the astrometric measurements for the full sample.

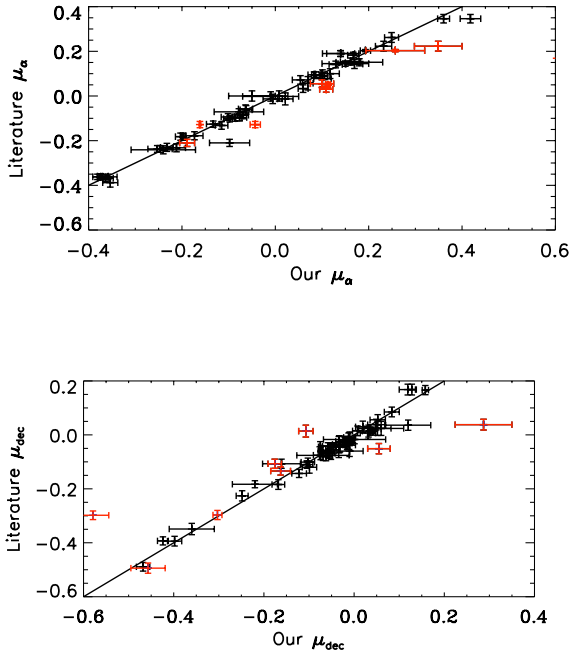

Figure 2.3: Comparison of Right Ascension (top) and Declination (bottom) proper motion measured in this paper and those measured in the literature. The straight line represents a perfect agreement between measurements. The red highlighted objects are the discrepant proper motion measurements (see Table 2.2.)

2.3 Distances, Tangential Velocities, and Reduced Proper Motion

2.3.1 Expanded Sample

We extended our observational sample to include published late-type M, L, and T dwarfs with proper motion measurements yielding a full combined sample containing 841 objects. Thirty-three percent of ultracool dwarfs in the full sample have multiple proper motion measurements. In these cases we chose the measurement with the smallest uncertainty for our kinematic analysis, typically objects from high precision astrometric surveys such as Vrba et al 2004 or Dahn et al 2002. If there was a value discrepant by more than 2σ amongst multiple measurements (> 2) for an object then regardless of

Table 2.2. Discrepant Proper Motion Values

Name	$\mu_\alpha cos(\delta)$ ($''$/yr) This Paper	μ_{dec} ($''$/yr) This Paper	$\mu_\alpha cos(\delta)$ ($''$/yr) Literature	μ_{dec} ($''$/yr) Literature	Reference
SIPS J0050-1538	-0.229 ± 0.018	-0.494 ± 0.019	-0.495 ± 0.039	-0.457 ± 0.038	16
2MASSJ0227-1624	0.426 ± 0.016	-0.297 ± 0.017	0.509 ± 0.016	-0.303 ± 0.010	16
2MASSJ0939-2448	0.592 ± 0.019	-1.064 ± 0.021	0.486 ± 0.031	-1.042 ± 0.055	41
2MASSJ1155-3727	0.050 ± 0.012	-0.767 ± 0.015	0.113 ± 0.005	-0.861 ± 0.039	16
			0.013 ± 0.015	-0.778 ± 0.013	9
			0.06 ± 0.04	-0.82 ± 0.07	36
2MASSJ1341-3052	0.030 ± 0.013	-0.134 ± 0.015	0.109 ± 0.014	-0.163 ± 0.022	17
2MASSJ1347-7610	0.203 ± 0.005	0.038 ± 0.020	0.257 ± 0.063	0.287 ± 0.063	22
			0.193 ± 0.011	0.049 ± 0.019	35
2MASSJ1448+1031	0.262 ± 0.022	-0.120 ± 0.022	0.70 ± 0.15	-0.10 ± 0.16	36
			0.249 ± 0.015	-0.099 ± 0.016	10
2MASSJ1507-1627	-0.128 ± 0.014	-0.906 ± 0.015	-0.043 ± 0.011	-1.037 ± 0.255	16
			-0.1615 ± 0.0016	-0.8885 ± 0.0006	15
			-0.147 ± 0.003	-0.890 ± 0.002	12
			-0.09 ± 0.11	-0.88 ± 0.06	36
2MASSJ1548-1636	-0.210 ± 0.016	-0.107 ± 0.017	-0.189 ± 0.016	-0.176 ± 0.015	17
			-0.098 ± 0.043	-0.161 ± 0.042	22
2MASSJ1555-0956	0.950 ± 0.015	-0.767 ± 0.015	0.929 ± 0.014	-2.376 ± 0.017	10
			0.961 ± 0.017	-0.835 ± 0.014	16
			-0.400 ± 1.200	-1.900 ± 1.100	9
2MASSJ1936-5502	0.169 ± 0.009	-0.298 ± 0.016	0.603 ± 0.037	-0.579 ± 0.035	16
			0.22 ± 0.29	-0.19 ± 0.28	36
2MASSJ2255-5713	-0.216 ± 0.011	-0.260 ± 0.020	0.394 ± 0.321	-1.525 ± 0.319	22
			-0.16 ± 0.11	-0.32 ± 0.13	36
2MASSJ2330-0347	0.223 ± 0.022	0.014 ± 0.022	0.349 ± 0.051	-0.107 ± 0.016	16
			0.232 ± 0.017	0.032 ± 0.013	10

Note. — Details on the discrepant proper motion objects. We note only objects whose proper motion values were discrepant by more than 2σ. Proper motion references are listed in Table 2.12.

uncertainty we defaulted to the numbers that were in agreement and chose the one with the smaller uncertainty. Otherwise, if there was a discrepancy and only two measurements, we quoted the one that had the smaller uncertainty and made note of it during the analysis.

2.3.2 Distances and Tangential Velocities

True space velocities are a more fundamental measure of an object's kinematics than apparent angular motions, so proper motions for the complete sample were converted to tangential velocities using astrometric or spectrophotometric distances. As of January 2008, only 79 of the 634 L and T dwarfs and 64 of the 456 late-type M dwarfs in our sample had published parallax measurements. Therefore to include the other 83% of L and T dwarfs and 87% of late-type M dwarfs in a population analysis, published absolute magnitude/spectral type relations were used for calibrating distances. Dahn et al. (2002) and Vrba et al. (2004) both showed that M_J is well correlated with spectral type for late-type M, L, and T dwarfs (see alsoWest et al. 2005, and Covey et al. 2007). Since the initial relations were published several investigators have revised the absolute magnitude/spectral type relation after including new measurements and removing resolved binaries. In this paper, the distances for the M7-L4.5 dwarfs were calculated using the absolute 2MASS J magnitude/spectral type relation in Cruz et al. (2003) and the distances for the L5 –T8 dwarfs were calculated using the absolute MKO K magnitude/spectral type relation in Burgasser (2007)[2]. Both optical and near-IR spectral types are reported for ultracool dwarfs. For late-type M through the L dwarfs, we use the optical spectral type in the distance relation when available but use near-IR spectral types when no optical spectral types are reported. We use the near-IR spectral type in the distance relation for all T dwarfs. The Cruz et al. (2003) relation was derived for the 2MASS magnitude system, while the Burgasser (2007) relation was derived using the MKO system. In reporting distances we maintain the magnitude system for which the relation was calculated, converting a 2MASS magnitude to an MKO magnitude or vice versa using the relation in Stephens & Leggett (2004) when necessary. The most recent precision photometry for many L and T dwarfs (e.g. Knapp et al 2004; Chiu et al. 2006, 2008) are reported on the MKO system; yet the majority of objects explored in this paper have measured 2MASS magnitudes. We con-

[2]The coefficients of this polynomial relation reported in Burgasser (2007) did not list sufficient significant digits, yielding a slightly different numerical relation than that used in the paper's analysis. The coefficients as defined should be $\{c_i\}$ = [10.4458, 0.232154, 0.0512942, -0.0402365, 0.0141398, -0.00227108, 0.000180674, -6.98501e-06, 1.05119e-07], where $M_K = \sum_{i=0}^{6} c_i \mathrm{SpT}^i$ and SpT(T0) = 10, SpT(T5) = 15, etc.

vert MKO filter measurements to the 2MASS system when available using the conversion relations of Stephens & Leggett (2004) so all of the ultracool dwarf photometry in Table 2.12 is reported on the 2MASS system.

The uncertainty in the derived distance is dominated by the uncertainty in the spectral type (the photometric uncertainties are typically between 0.02-0.1 mag whereas the spectral type uncertainties are typically 0.5-1.0). This leads to a systematic over- or underestimation of distance of up to 30%. Therefore the kinematic results presented in this paper are largely sensitive to the reliability of the spectrophotometric distances used to calculate V_{tan}. Furthermore, unresolved multiplicity leads to an underestimation of distance. Recent work has shown that roughly 20% of ultracool dwarfs are likely to be binary (Allen 2007, Reid et al. 2008a), and this fraction may be even higher across the L dwarf/T dwarf transition (Burgasser et al. 2006b). Seven percent (56) of the dwarfs analyzed in this paper are known to be close binaries and of these, most appear to be near equal-mass/equal brightness (e.g. Bouy et al. 2003; Burgasser et al. 2006b). For these objects we use the distances quoted in the binary discovery papers where the contribution of flux from the secondary was included in the distance estimate. Any remaining tight binaries probably constitute no more than 10-20% of the sample and the contamination of their inclusion in the kinematic analysis is relatively small.

2.3.3 Reduced Proper Motion Diagram

A reduced proper motion diagram is a useful tool for distinguishing between kinematically-distinct stellar and substellar populations. This parameter was used extensively in early high proper motion catalogues to explore Galactic structure (Luyten 1973). Proper motion is used as a proxy for distance measurements following the expectation that objects with large proper motions will be nearest to the Sun. The definition is analogous to that of absolute magnitude:

$$H = m + 5.0 + 5.0log_{10}(\mu) \tag{2.3}$$

or

$$H = M + 5.0log_{10}(V_{tan}) - 3.38 \tag{2.4}$$

where m and M are the apparent and absolute magnitudes (respectively), V_{tan} is measured in km/s and μ is measured in $''$/yr.

We can use reduced proper motion to search for the lowest temperature objects. In Figure 2.4, we show the reduced proper motion at K_s for our astrometric sample. We find that below an H_{K_s} of 18 there are only L and T dwarfs regardless of near-IR color. Since the discovery of the first brown

dwarfs, near-IR color selection has been the primary technique for identifying strong candidates. But because M dwarfs dominate photometric surveys (they are bright, nearby and found in large numbers), near-IR color cut-offs were administered to maximize the L and T dwarfs found in searches. These cut-offs have caused a gap in the near-IR color distribution of the brown dwarf population, particularly around $J - K_s$ of 1 where early-type T dwarfs and metal weak L dwarfs are eliminated along with M dwarfs. A reduced proper motion diagram with the cut-off limit cited above allows a search which eliminates the abundant M dwarfs and probes the entire range of $J - K_s$ colors for the ultracool dwarf population.

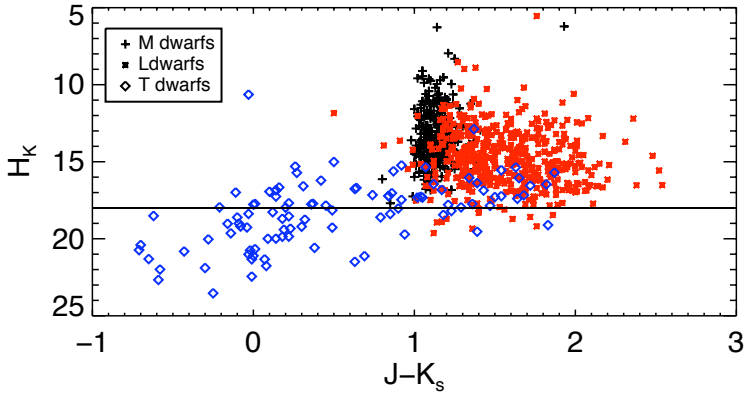

Figure 2.4: Reduced proper motion diagram using the 2MASS J and K_s magnitudes. Late-type M dwarfs are marked with a black plus sign, L dwarfs are marked as a red 5 point star and T dwarfs are marked as blue diamonds. The line at H_K of 18 marks where M dwarfs are segregated from the L and T dwarfs regardless of near-IR color. This cut-off will also include subdwarfs and cool white dwarfs but these objects will be rare.

Note that, while our cut-off limits are good guidelines for segregating the coolest temperature dwarfs within the ultracool dwarf population, there is likely to be contamination in selected regions of the sky from relatively rare ultracool subdwarfs and cool white dwarfs, which are nonetheless of scientific interest.

2.4 Analysis

2.4.1 Kinematic Characteristics of the UCD Population

The ultracool dwarfs analyzed in this paper have a range of proper motion values from $0.01-4.7''$/yr and a range of proper motion uncertainties from $0.0002 - 0.3\ ''$/yr. While one of our goals is to refine proper motion measurements of ultracool dwarfs to have uncertainties < 40 mas/yr, there are still 86 or 10% that have larger errors. Since the uncertainty in V_{tan} is generally dominated by the uncertainty in distance (see subsection 3.2 above) we make no restrictions on the accuracy of the proper motion measurements used in the kinematic analysis. The median 1σ detection limit for proper motion measurements in this paper was 18 mas/yr (see Figure 2.2). We use this number as a proxy for the L and T dwarfs (where we are looking at all known field objects as opposed to the late-type M dwarfs where we are looking at only a subset) to determine the percentage of objects with appreciable motion. We find that 32 move slower than our 2σ detection limit and ten of those are at or below our 1σ limit. This indicates that according to our astrometric standard, less than 6% of L and T dwarfs have no appreciable motion. Conversely, 32 objects (or 6% of the population) move faster than $1.0''$/yr making them some of the fastest proper motion objects known. As late-type dwarfs are intrinsically quite faint and have only been detected at nearby distances (generally ≤ 60 pc), the high proper motion values measured are not surprising. Using the median proper motion values listed in Table 2.3 as a proxy , we can also conclude that at least half or more of the brown dwarf population would be easily detectable on a near-IR equivalent of Luyten's 2-tenth catalog (Luyten 1979) where the limiting proper motion was $\sim 0.15\ ''$/yr.

Table 2.3 lists the average proper motion values and photometric data for the entire population binned by spectral type. There is a trend within these data for larger proper motion values with increasing spectral type. This is clearest within the L0-L9 population where the sample is largest. We further bin this group into thirds to compare a statistically significant sample. We examine the L0-L2, L3-L5, and L6-L9 populations and find the median proper motion values increase as (0.174, 0.223, 0.289) $''$/yr. This trend most likely reflects the fact that earlier type sources are detected to further distances. Indeed when we examine the median distance values for these same groupings we find values of (31, 27, 20) pc respectively.

Table 2.3. Median Photometric and Kinematic Properties of UCDs

SpT	N_μ	μ_{med} ($''$/yr)	σ_μ ($''$/yr)	Med Dist (pc)	σ_{dist} (pc)	N_{J-K_s}	$(J-K_s)_{avg}$	$2^*\sigma_{J-K_s}$	N_{Red}	N_{Blue}
(1)	(2)	(3)	(4)	(5)	(6)	(7)	(8)	(9)	(10)	(11)
M7	88	0.261	0.553	25	10	160	1.08	0.19	0	1
M8	114	0.210	0.403	23	8	147	1.14	0.18	1	1
M9	71	0.204	0.357	22	10	107	1.20	0.22	1	0
L0	93	0.111	0.211	32	19	92	1.31	0.37	4	1
L1	83	0.208	0.301	31	21	82	1.39	0.37	4	1
L2	58	0.185	0.209	32	17	63	1.52	0.40	5	1
L3	64	0.189	0.398	33	17	67	1.65	0.39	1	1
L4	50	0.183	0.284	27	12	44	1.73	0.40	2	2
L5	43	0.323	0.281	24	12	43	1.74	0.40	0	1
L6	36	0.215	0.339	26	12	31	1.75	0.40	4	2
L7	21	0.247	0.186	23	9	15	1.81	0.40	0	2
L8	16	0.280	0.368	19	8	16	1.77	0.33	2	0
L9	3	0.424	0.200	20	6	7	1.69	0.19	0	0
T0	9	0.333	0.165	18	4	8	1.63	0.40	0	0
T1	11	0.289	1.336	23	9	10	1.31	0.40	1	1
T2	13	0.350	0.285	15	7	15	1.02	0.40	1	0
T3	7	0.183	0.135	26	6	5	0.63	0.40	1	0
T4	13	0.323	0.219	23	9	6	0.26	0.40	0	0
T5	20	0.340	0.351	15	3	12	0.07	0.39	0	0
T6	15	0.594	1.217	11	18	5	-0.30	0.40	2	1
T7-T8	13	1.218	0.764	9	3	6	-0.08	0.40	0	1
M7-M9	273	0.222	0.445	23	9	414	1.12	0.22	2	2
L0-L9	467	0.189	0.292	29	17	460	1.53	0.40	22	11
T0-T9	101	0.373	0.801	15	10	67	0.74	0.40	5	3

Note. — To calculate the $(J-K_s)_{avg}$ for each spectral type, we chose only objects that were not identified as binaries,young cluster members, subdwarfs and/or had σ_J and $\sigma_{K_s} < 0.20$.

2.4.2 Kinematics of Full and 20pc Samples

We have conducted our kinematic analysis on two samples: the full astrometric sample and the 20 pc sample. Figure 2.5 shows the distance distribution for all ultracool dwarfs regardless of proper motion measurements to demonstrate the pertinence of the 20 pc sample. In this figure, both the late-type M and L dwarfs diverge from an N $\propto$ d^3 density distribution around 20 pc. The T dwarfs diverge closer to 15 pc. Within the literature (e.g Cruz et al. 2003) complete samples to 20 pc have been reported through mid-type L dwarfs so we use this distance in order to establish a volume-limited kinematic sample. We also examine the two samples with and without objects with V_{tan} $>$ 100 km s^{-1} in order to remove extreme outliers that may comprise a different population.

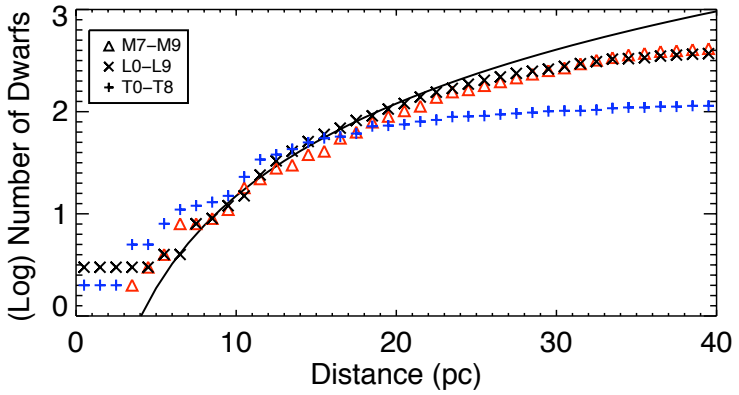

Figure 2.5: Cumulative distance distribution of all late-type M, L, and T dwarfs in our database. Triangles refer to the M7-M9 dwarfs, the 'X' symbols refer to all L0-L9 dwarfs and the plus symbols refer to all T0-T8 dwarfs. The solid line corresponds to a constant density distribution (N $\propto$ d^3). The L and M dwarfs deviate from this distribution around 20 pc but the T dwarfs fall off closer to 15 pc.

Tables 2.4 – 2.5 contain the mean kinematic properties for the 20 pc sample and the full astrometric sample respectively. Figure 2.6 shows V_{tan} vs. spectral type for both samples. As demonstrated in Figure 2.6, we find no difference between the two samples, with median V_{tan} values of 26 km s^{-1} and 29 km s^{-1} and σ_{tan} values of 23 km s^{-1} and 25 km s^{-1} for M7-T9 within the full sample and the 20 pc sample respectively. Within spectral class bins, namely the M7-M9, L0-L9, or T0-T9 groupings, we find no significant kinematic differences.

This indicates that we are sampling a single kinematic population regardless of distance and spectral type.

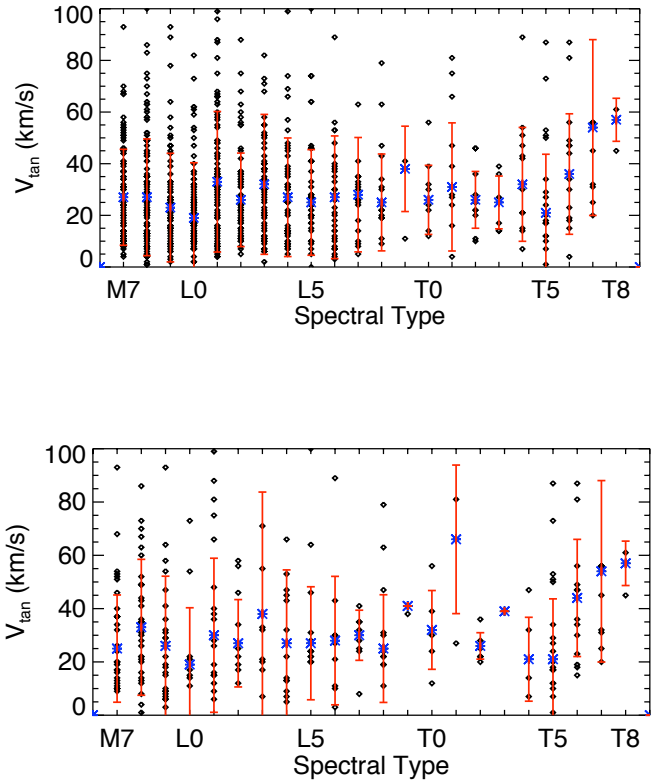

Figure 2.6: Distribution of V_{tan} values binned by spectral type. The top panel is the full astrometric sample and the bottom panel is the 20 pc sample. The asterisks refer to the median V_{tan} values and the vertical bars refer to the standard deviation or dispersion of velocities.

Figure 2.7 shows the distribution of tangential velocities. There are 14 objects with $V_{tan} > 100$ km s^{-1} that fall at the far end of the distribution. Exclusion of these high velocity dwarfs naturally reduces the median V_{tan} and σ_{tan} values. The most significant difference in their exclusion occurs within the L0-L9 group as 10 of the 14 objects belong to that spectral class. We explore the importance of this subset of the ultracool dwarf population in section 5.

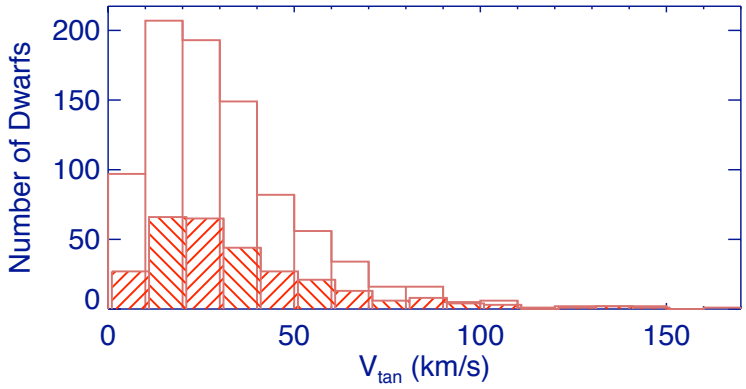

Figure 2.7: The overall histogram is the tangential velocity distribution for the entire sample and the diagonally shaded histogram is the 20 pc sample. Both V_{tan} distributions peak in the 10-30 km s^{-1} bins.

In order to put our kinematic measurements in the context of the Galaxy we compare with Galactic U,V,W dispersions. Proper motion, distance, and radial velocity are all required to compute these space velocities. Therefore, a direct Galactic U,V,W comparison with the ultracool dwarf population is not possible because radial velocity measurements for ultracool dwarfs are sparse, with only 48 of the L and T dwarfs to date having been reported in the literature (e.g. Mohanty & Basri 2003, Zapatero Osorio et al. 2007, Bailer-Jones 2004). This is a similar problem to that for precise brown dwarf parallax measurements, but there is no relationship for estimating radial velocities as there is for estimating distances. However, we can divide our sample into three groups along Galactiocentric coordinate axes (toward poles, in direction of Galactic rotation and radially to/from Galactic center) in order to minimize the importance of radial velocity in 2 out of the 3 space velocity components. We create cones of 0 (all inclusive), 30, and 60 degrees around the galactic X,Y, and Z axes. Inside of each cone we set either the U,V, or W velocity to zero if the cone surrounds the galactic X,Y or Z axis respectively. In this way we can set the radial velocity of each source to zero with minimum impact on the component velocities of the entire sample and gather U,V,W information for the known ultracool dwarf population. We emphasize that this analysis is crude as the distribution of ultracool dwarfs is not isotropic (the Galactic plane has largely not been explored), and while the cones help to minimize the importance of radial velocity unless an object is directly on the X,Y, or

Table 2.4. 20 pc Sample

SpT	N	N High V_{tan}	med V_{tan} (km s^{-1})	med V_{tan} w/ high V_{tan} (km s^{-1})	σ_{tan} (km s^{-1})	σ_{tan} w/ high V_{tan} (km s^{-1})	Age (Gyr)	Age w/ high V_{tan} (Gyr)
(1)	(2)	(3)	(4)	(5)	(6)	(7)	(8)	(9)
M7	29	0	25	25	20	20	—	—
M8	37	1	33	33	20	25	—	—
M9	27	1	26	26	22	26	—	—
L0	9	0	19	19	21	21	—	—
L1	19	0	30	30	29	29	—	—
L2	10	0	27	27	16	16	—	—
L3	12	3	32	38	20	46	—	—
L4	15	1	27	27	20	28	—	—
L5	16	0	27	27	21	21	—	—
L6	10	0	28	28	24	24	—	—
L7	9	0	30	30	9	9	—	—
L8	12	0	25	25	20	20	—	—
L9	2	0	41	41	0	0	—	—
T0	6	0	32	32	15	15	—	—
T1	3	0	66	66	28	28	—	—
T2	8	0	26	26	5	5	—	—
T3	1	0	39	39	0	0	—	—
T4	5	0	21	21	16	16	—	—
T5	20	0	21	21	23	23	—	—
T6	14	0	44	44	22	22	—	—
T7	10	1	45	54	15	34	—	—
T8	3	0	57	57	8	8	—	—
M7-M9	93	2	29	29	21	24	$3.0^{+1.0}_{-0.8}$	$5.0^{+1.7}_{-1.4}$
L0-L9	114	5	27	27	21	26	$3.2^{+1.1}_{-0.9}$	$6.6^{+2.2}_{-1.8}$
T0-T9	70	1	30	31	20	24	$2.8^{+1.0}_{-0.8}$	$4.6^{+1.6}_{-1.3}$

Note. — The age range is calculated from the Wielen (1977) age-velocity relation for the disk which uses a value of α of (1/3).

Z axis, the radial velocity component will contribute to the overall velocities. Therefore, the spread of U,V,W velocities will be biased toward a tighter dispersion than the true values. In order to calculate total velocities (V_{tot}) for objects, which requires U,V, and W velocities we choose a cone of 30 degrees which provides a statistically significant sample. We create the cone around the X,Y, or Z axis and assume that within that cone either the V,W or U,Z or U,V components respectively are correct. To obtain the third component we assume it to be the average of the two calculated ones. In this way we can gather V_{tot} information which will be used for age calculation purposes in Section 6.

Table 2.5. Full Astrometric Sample

SpT	N	N High V_{tan}	med V_{tan} (km s^{-1})	med V_{tan} w/ high V_{tan} (km s^{-1})	σ_{tan} (km s^{-1})	σ_{tan} w/ high V_{tan} (km s^{-1})	Age (Gyr)	Age w/ high V_{tan} (Gyr)
(1)	(2)	(3)	(4)	(5)	(6)	(7)	(8)	(9)
M7	88	0	27	27	19	19	—	—
M8	114	1	27	27	21	23	—	—
M9	71	1	23	23	19	21	—	—
L0	93	1	19	19	16	21	—	—
L1	83	2	32	33	23	27	—	—
L2	58	0	26	26	18	18	—	—
L3	64	3	30	32	18	27	—	—
L4	50	1	25	27	20	23	—	—
L5	43	0	25	25	20	20	—	—
L6	36	1	26	27	18	24	—	—
L7	21	1	28	28	13	22	—	—
L8	16	0	25	25	19	19	—	—
L9	3	0	38	38	17	17	—	—
T0	9	0	26	26	13	13	—	—
T1	11	0	31	31	25	25	—	—
T2	13	0	26	26	11	11	—	—
T3	7	0	25	25	10	10	—	—
T4	13	0	32	32	22	22	—	—
T5	20	0	21	21	23	23	—	—
T6	15	0	36	36	23	23	—	—
T7	10	1	45	54	15	34	—	—
T8	3	0	57	57	8	8	—	—
M7-M9	273	3	26	26	19	21	$2.5^{+0.9}_{-0.7}$	$3.2^{+1.1}_{-0.9}$
L0-L9	467	10	26	26	19	23	$2.5^{+0.9}_{-0.7}$	$4.5^{+1.6}_{-1.3}$
T0-T9	101	1	29	29	20	23	$2.7^{+1.0}_{-0.8}$	$4.0^{+1.4}_{-1.1}$

Note. — The age range is calculated from the Wielen (1977) age-velocity relation for the disk which uses a value of α of (1/3).

Figure 2.8 shows our resultant U,V,W distributions where we measure $(\sigma_U, \sigma_V, \sigma_W)$=(28, 22, 17) km s^{-1}. We compare these dispersions with the kinematic signatures of the three Galactic populations, namely the thin disk, the thick disk, and the halo. The overwhelming majority of stars in the solar neighborhood are members of the Galactic disk and these are primarily young thin disk objects as opposed to older thick disk objects. The halo population of the Galaxy encompasses the oldest population of stars in the Galaxy but these objects are relatively sparse in the vicinity of the Sun. Membership in any Galactic population has implications for the age and metallicity of the object and kinematics play a large part in defining the various populations. Soubiran et al. (2003) find $(\sigma_U, \sigma_V, \sigma_W)$=(39 $\pm$ 2, 20 $\pm$ 2, 20 $\pm$ 1) km s^{-1} for the thin disk and $(\sigma_U, \sigma_V, \sigma_W)$=(63 $\pm$ 6, 39 $\pm$ 4, 39 $\pm$ 4) km s^{-1} for the

thick disk, and Chiba & Beers (2000) find $(\sigma_U, \sigma_V, \sigma_W)$=(141 $\pm$ 11, 106 $\pm$ 9, 94 $\pm$ 8) km s^{-1} for the halo portion of the Galaxy. Our U,V,W dispersions are consistent (albeit narrower in U) with the Galactic thin disk.

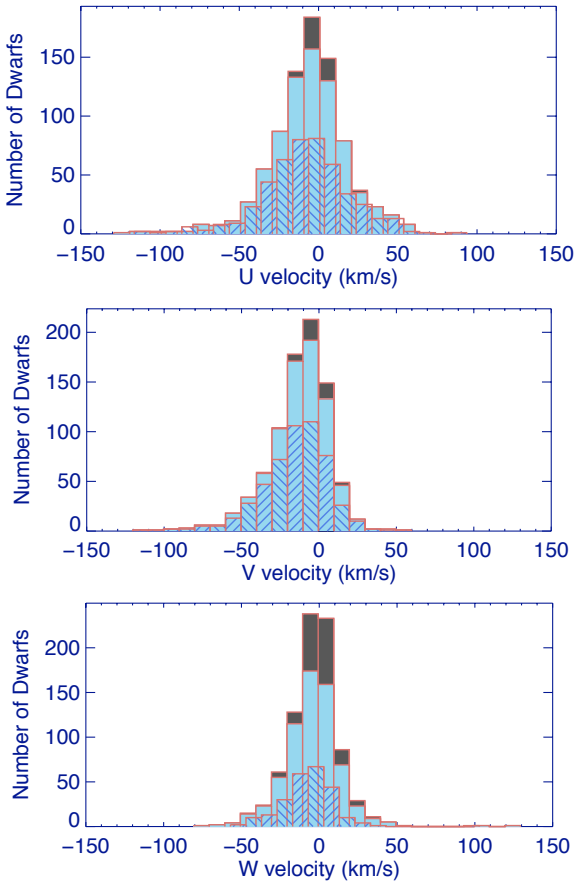

Figure 2.8: Histogram of U,V,W velocities. Plotted for each velocity is 1) each object in the astrometric sample (large histogram) 2) a 30 degree restriction on objects and 3) a 60 degree restriction (smallest histogram). The 30 and 60 degree restrictions are placed on the X,Y or Z axis and correspond to removing the U,V, or W velocity respectively for objects in cones of noted radius around the respective axis.

Zapatero Osorio et al. (2007) – hereafter Os07– examined 21 L and T dwarfs and found $(\sigma_U, \sigma_V, \sigma_W)$=(30.2, 16.5, 15.8) km s^{-1}. Their velocity dispersions are tighter than what is expected from the Galactic thin disk population. Our calculated dispersions are tighter at U than the Os07 result (which is expected due to the stated bias) but broader in V and W. In section 6 we discuss the

implications on age of the differences calculated from our astrometric sample.

2.4.3 Red and Blue Photometric Outliers

As discussed in Kirkpatrick et al. (2005) the large number of late-type M, L, and T dwarfs discovered to date has revealed a broad diversity of colors and spectral characteristics, including specific subgroups of peculiar sources that are likely related by their common physical properties. As a very basic metric, near-IR colors provide one means of distinguishing between "normal" and "unusual" objects. To investigate our sample for kinematically distinct photometric outliers, we first defined the average color ($(J-K_s)_{avg}$) as well as standard deviation (σ_{J-K_s}) as a function of spectral type using all known ultracool dwarfs (i.e., both with and without proper motion measurements). Defining the $(J-K_s)_{avg}$ for spectral bins has been done in previous ultracool dwarf studies such as Kirkpatrick et al. (2000), Vrba et al. (2004), and West et al. (2008) but we have included all ultracool dwarfs in the dwarfarchives complilation and the updated photometry reported in Chiu et al. (2006, 2008) and Knapp et al. (2004) which we have converted from the MKO system to the 2MASS system. Objects were eliminated from the photometric sample if they fit any of the following criteria:

1. Uncertainty in J or $K_s > 0.2$ magnitude;

2. Known subdwarf;

3. Known binaries unresolved by wide-field imaging surveys (i.e. separations $\lesssim 1\ ''$ e.g. Martin et al. 1999; Bouy et al. 2003; Burgasser et al. 2006b; Close et al. 2003; Liu et al. 2006; Reid et al. 2006); and

4. Member of a star forming region (such as Orion) or open cluster (such as the Pleiades) indicating an age $\lesssim$ 100 Myr (e.g. Allers et al. 2007; Zapatero Osorio et al. 2002)

We then designated objects as photometric outliers if they satisfied the following criterion :

$$\Delta_{J-K_s} = \mid (J-K_s) - (J-K_s)_{avg} \mid \geq \max(2\sigma_{J-K_s}, 0.4) \tag{2.5}$$

In other words, if an object's $J-K_s$ color was more than twice the standard deviation of the color range for that spectral bin than we flagged it as a red or blue photometric outlier. If twice the standard deviation was larger than 0.4 magnitudes then it was automatically reset to 0.4. We chose 0.4 as the

maximum upper limit for $2\sigma_{J-K_s}$ as this is the Δ_{J-K_s} for the entire ultracool dwarf population.

There are relatively few objects in each spectral bin beyond L9. For spectral type (SpT) $<$ L9 there is a mean of 45 objects used per bin whereas for SpT$>$ L9 there is a mean of only 7 objects. So photometric outliers are difficult to define for the lower temperature classes and may contaminate the analysis. We grouped T7-T8 dwarfs to improve the statistics used to calculate average values. The kinematic results for this subset of the ultracool dwarf population are reported with and without the T dwarfs in Table 2.6. Figure 2.9 shows the resulting $J - K_s$ color distribution and highlights the photometric outliers. Tables 2.7 - 2.8 list the details of the red and blue photometric outliers respectively. Table 2.3 lists the resultant mean photometric values for each spectral type.

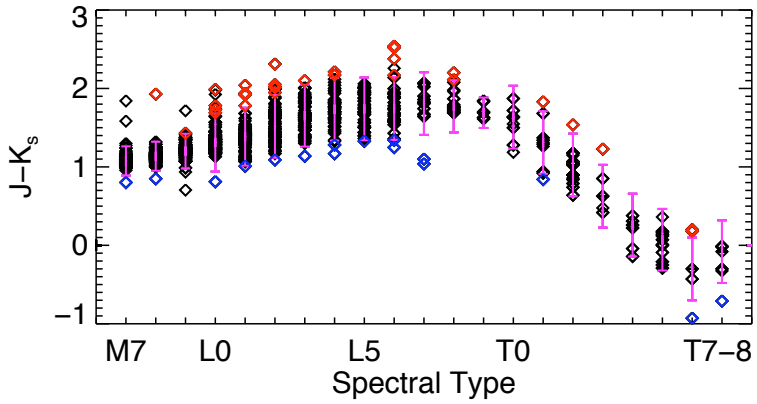

Figure 2.9: $J - K_s$ colors of late-type dwarfs. We compute the average values for each spectral type (binned by 1 subtype) from the 2MASS photometry of a select sample of dwarfs and then flag objects as photometric outliers when they are either twice the standard deviation of $J - K_s$ or 0.4 magnitude redder or bluer than the average value. Red symbols above the plotted range of $J - K_s$ colors are the red outliers and blue symbols below the plotted range of $J - K_s$ colors are the blue outliers.

Table 2.6. Average Kinematics and Ages for the Subgroups

SpT	N	Median V_{tan} km s^{-1}	σ_{tan} km s^{-1}	Age Range Gyr
(1)	(2)	(3)	(4)	(5)
M7-T9/BLUE	16	53	47	$37.9^{+12.6}_{-10.3}$
M7-T9/RED	29	26	16	$1.2^{+0.5}_{-0.4}$
M7-L9/BLUE	13	56	50	$46.0^{+15.2}_{-12.4}$
M7-L9/RED	24	26	15	$1.0^{+0.4}_{-0.3}$
UBLs	10	99	47	$37.9^{+12.6}_{-10.3}$
Low Gravity	26	18	15	$1.0^{+0.4}_{-0.3}$

Note. — The age range is calculated from the Wielen (1977) age-velocity relation for the disk which uses a value of α of (1/3).

Table 2.7: Details on Red Photometric Outliers[1]

Source Name	2MASS J (mag)	2MASS K_s (mag)	$\mu_\alpha cos(\delta)$ ($''$/yr)	μ_δ ($''$/yr)	μ Ref.	SpT (opt)	SpT (IR)	V_{tan} (km s^{-1})	Note[2]
(1)	(2)	(3)	(4)	(5)	(6)	(7)	(8)	(9)	(10)
2MASS J00374306-5846229	15.37 ± 0.05	13.59 ± 0.05	0.049 ± 0.010	-0.051 ± 0.020	19	L0	—	18 ± 5	LG
SDSSp J010752.33+004156.1	15.82 ± 0.06	13.71 ± 0.04	0.628 ± 0.007	0.091 ± 0.004	44	L8	L5.5	46.9 ± 3.3	—
2MASS J01244599-5745379	16.31 ± 0.11	14.32 ± 0.09	-0.003 ± 0.010	0.018 ± 0.019	19	L0	—	7 ± 7	LG
2MASS J01415823-4633574	14.83 ± 0.04	13.10 ± 0.03	0.104 ± 0.017	-0.026 ± 0.024	19	L0	L0	21 ± 4	LG
2MASS J01490895+2956131	13.45 ± 0.02	11.98 ± 0.02	0.1757 ± 0.0008	-0.4021 ± 0.0007	15	M9.5	—	46.8 ± 0.7	—
2MASSI J0243137-245329	15.42 ± 0.06[c]	15.22 ± 0.06[c]	-0.288 ± 0.004	-0.208 ± 0.003	44	—	T6	18.0 ± 0.7	—
2MASS J03231002-4631237	15.39 ± 0.07	13.70 ± 0.05	0.060 ± 0.013	-0.010 ± 0.019	19	L0	—	16 ± 4	LG
2MASS J03264225-2102057	16.13 ± 0.09	13.92 ± 0.07	0.108 ± 0.014	-0.146 ± 0.015	19	L4	—	35 ± 5	—
2MASS J03421621-6817321	16.85 ± 0.14	14.54 ± 0.09	0.064 ± 0.007	0.021 ± 0.018	19	L2	—	26 ± 5	—
2MASS J03552337+1133437	14.05 ± 0.02	11.53 ± 0.02	0.192 ± 0.017	-0.613 ± 0.017	19	L5	—	25 ± 5	LG
2MASS J04351455-1414468	11.88 ± 0.03	9.95 ± 0.02	0.009 ± 0.014	0.016 ± 0.014	19	M8	—	1 ± 1	LG
2MASS J05012406-0010452	14.98 ± 0.04	12.96 ± 0.04	0.158 ± 0.014	-0.139 ± 0.014	19	L4	—	24 ± 5	LG
2MASSI J0512063-294954	15.46 ± 0.06	13.29 ± 0.04	-0.028 ± 0.016	0.099 ± 0.018	19	L4.5	—	13 ± 3	—
2MASS J05361998-1920396	15.77 ± 0.08	13.85 ± 0.06	0.017 ± 0.017	-0.024 ± 0.018	19	L1	—	8 ± 5	—
AB Pic b	16.18 ± 0.10	14.14 ± 0.08	0.0141 ± 0.0008	0.0452 ± 0.0010	34	—	L1	10.2 ± 0.4	VLMC
SDSS J080959.01+443422.2	16.51 ± 0.06[c]	14.34 ± 0.06[c]	-0.198 ± 0.014	-0.214 ± 0.019	19	—	L6	35 ± 7	—
SDSS J085834.42+325627.7	16.52 ± 0.06[a]	14.69 ± 0.06[a]	-0.760 ± 0.023	0.075 ± 0.023	19	—	T1	66 ± 3	—
G 196-3B	14.83 ± 0.05	12.78 ± 0.03	-0.133 ± 0.040	-0.185 ± 0.015	10	L2	—	35 ± 5	VLMC
2MASS J12123389+0206280	16.13 ± 0.13	14.19 ± 0.09	0.065 ± 0.021	-0.141 ± 0.021	19	—	L1	49 ± 9	—
2MASS J13243559+6358284	15.60 ± 0.07	14.06 ± 0.06	-0.343 ± 0.064	-0.260 ± 0.048	32	—	T2	26 ± 6	—
SDSSp J132629.82-003831.5	16.37 ± 0.06[c]	14.17 ± 0.06[c]	-0.226 ± 0.008	-0.107 ± 0.006	44	L8	L5.5	23.8 ± 3.2	—
SDSS J141530.05+572428.7	16.72 ± 0.06[a]	15.49 ± 0.06[a]	0.043 ± 0.013	-0.345 ± 0.025	19	—	T3	36 ± 12	—
2MASS J15311344+1641282	15.58 ± 0.06	13.80 ± 0.05	-0.076 ± 0.025	0.040 ± 0.026	19	—	L1	21 ± 8	—
2MASSI J1726000+153819	15.67 ± 0.07	13.66 ± 0.05	-0.031 ± 0.013	-0.048 ± 0.014	10	L2	—	13 ± 3	—
SDSS J175805.46+463311.9	16.17 ± 0.06[c]	15.99 ± 0.06[c]	0.026 ± 0.015	0.594 ± 0.016	10	—	T6.5	34 ± 4	—
2MASS J21481633+4003594	14.15 ± 0.03	11.77 ± 0.02	0.770 ± 0.018	0.456 ± 0.024	19	L6.5	—	30 ± 5	—
2MASS J21512543-2441000	15.75 ± 0.08	13.65 ± 0.05	0.278 ± 0.014	-0.021 ± 0.015	19	L3	—	55 ± 6	—
2MASSW J2206450-421721	15.56 ± 0.07	13.61 ± 0.06	0.111 ± 0.013	-0.182 ± 0.018	19	L2	—	45 ± 5	—
2MASSW J2244316+204343	16.47 ± 0.06[c]	13.93 ± 0.06[c]	0.252 ± 0.014	-0.214 ± 0.011	10	L6.5	L7.5	30 ± 3	—

[1] See Table 2.12 for references and notes referred to in this table.

[2] VLMC is a wide companion, UBL is an Unusually Blue L dwarf, LG is a low-gravity dwarf, YC is in a young cluster, CB is a binary unresolved in 2MASS

Amongst the full sample, we find 16 blue photometric outliers and 29 red photometric outliers. Many of the objects have already been noted in the literature as having unusual colors, and several of these have anomalous spectra and have been analyzed in detail (e.g. Burgasser et al. 2008a, Knapp et al. 2004, Folkes et al. 2007, Chiu et al. 2006). Table 2.6 lists the mean kinematic properties for the blue and red subgroups of the ultracool dwarf population and Figure 2.10 isolates the outliers and plots their tangential velocity vs. spectral type. The blue outliers have a median V_{tan} value of 53 km s^{-1} and a σ_{tan} of 47 km s^{-1} while the red outliers have a median V_{tan} value of 26 km s^{-1} and a σ_{tan} of 16 km s^{-1} .

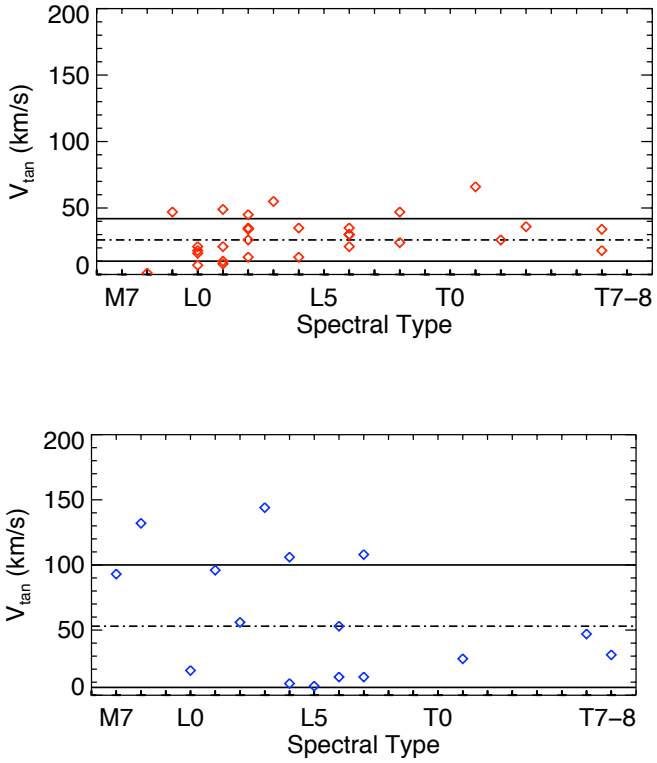

Figure 2.10: The spread of tangential velocities for objects marked as red outliers (top panel) and blue outliers (bottom panel). The red population has a fairly tight dispersion and the blue population has a fairly wide dispersion compared to the full sample suggesting a link between near-IR color and age. The dashed line in each plot represents the median V_{tan} value for the outlier group and the solid black lines represent the dispersion.

Table 2.8. Details on Blue Photometric Outliers

Source Name	2MASS J	2MASS K_s	$\mu_\alpha cos(\delta)$	μ_δ	μ Ref.	SpT	SpT	V_{tan}	Note[r]
	(mag)	(mag)	($''$/yr)	($''$/yr)		(opt)	(IR)	(km s^{-1})	
(1)	(2)	(3)	(4)	(5)	(6)	(7)	(8)	(9)	(11)
HD 3651B	16.16 ± 0.03	16.87 ± 0.05	-0.4611 ± 0.0007	-0.3709 ± 0.0007	34	—	T7.5	31.2 ± 0.3	VLMC
SSSPM J0134-6315	14.51 ± 0.04	13.70 ± 0.04	0.077 ± 0.008	-0.081 ± 0.009	30	—	L0	19 ± 2	—
2MASS J02530084+1652532	8.39 ± 0.03	7.59 ± 0.05	3.404 ± 0.005	-3.807 ± 0.005	23	M7	—	92.9 ± 1.0	—
SDSS J090900.73+652527.2	16.00 ± 0.06[a]	15.16 ± 0.06[a]	-0.217 ± 0.003	-0.138 ± 0.008	19	—	T1	28 ± 1	—
2MASS J09211410-2104446	12.78 ± 0.02	11.69 ± 0.02	0.244 ± 0.016	-0.908 ± 0.017	19	L2	—	56 ± 4	UBL
SDSS J093109.56+032732.5	16.75 ± 0.10[c]	15.65 ± 0.10[c]	-0.612 ± 0.018	-0.131 ± 0.018	19	—	L7.5	108 ± 23	UBL
2MASSI J0937347+293142	14.58 ± 0.06[c]	15.51 ± 0.12[c]	0.973 ± 0.005	-1.298 ± 0.006	44	d/sdT6	T6	47.2 ± 1.1	—
SDSS J103321.92+400549.5	16.88 ± 0.06[a]	15.63 ± 0.10[a]	0.154 ± 0.013	-0.188 ± 0.018	19	—	L6	53 ± 10	UBL
SDSS J112118.57+433246.5	17.19 ± 0.10[a]	16.15 ± 0.08[a]	-0.057 ± 0.024	0.026 ± 0.033	19	—	L7.5	14 ± 6	UBL
2MASS J11263991-5003550	14.00 ± 0.03	12.83 ± 0.03	-1.570 ± 0.004	0.438 ± 0.011	20	L4.5	L9	106 ± 11	UBL
SDSS J114805.02+020350.9	15.52 ± 0.07	14.51 ± 0.12	0.237 ± 0.026	-0.322 ± 0.013	10	L1	—	96 ± 8	—
2MASS J12162161+4456340	16.35 ± 0.10	15.02 ± 0.12	-0.035 ± 0.014	-0.004 ± 0.019	19	L5	—	7 ± 3	—
SDSS J142227.25+221557.1	17.01 ± 0.06[a]	15.67 ± 0.06[a]	0.047 ± 0.019	-0.054 ± 0.020	19	—	L6.5	14 ± 6	UBL
DENIS-P J170548.38-051645.7	13.31 ± 0.03	12.03 ± 0.02	0.129 ± 0.014	-0.103 ± 0.015	10	—	L4	9 ± 1	—
2MASSI J1721039+334415	13.63 ± 0.02	12.49 ± 0.02	-1.854 ± 0.017	0.602 ± 0.017	10	L3	—	144 ± 13	UBL
2MASS J18261131+3014201	11.66 ± 0.02	10.81 ± 0.02	-2.280 ± 0.010	-0.684 ± 0.010	28	M8.5	—	132 ± 9	—

Note. — See Table 2.12 for references and notes referred to in this table.

Figure 2.11 shows the tangential velocity vs. J-K_s deviation for all objects in the sample with the dispersions of the red and blue outliers highlighted. There is a clear trend for V_{tan} values to decrease from objects that are blue for their spectral type to those that are red. This is particularly significant at the extreme edges of this diagram. The dashed line in Figure 2.11 marks the spread of V_{tan} values for the full sample and demonstrates the significant deviations for the color outliers. We explore the age differences from these measurements in section 6.

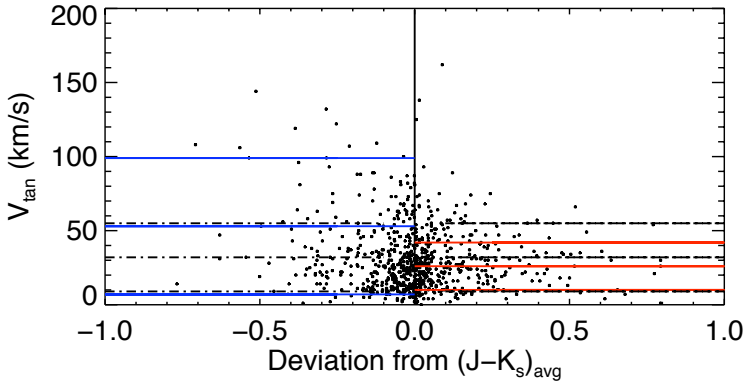

Figure 2.11: A scatter plot showing V_{tan} as a function of the deviation in $J - K_s$ color from the average at a given spectral type. The blue outliers appear to move faster on average than the red outliers. To demonstrate this we have over-plotted the average V_{tan} with dispersion for the blue and red photometric outliers as well as for the full astrometric sample (dashed lines).

2.4.4 Low Gravity Objects

A number of ultracool dwarfs that exhibit low surface-gravity features have been reported in the literature within the past few years (e.g. Cruz et al. 2007, Luhman & Rieke 1999; McGovern et al. 2004, Kirkpatrick et al. 2006; Allers et al. 2007). Low surface-gravity dwarfs are distinguished as such by the presence of weak alkali spectral features, enhanced metal oxide absorption, and reduced H_2 absorption. They are most likely young , with lower masses than older objects of the same spectral type. For ages $\lesssim$ 100 Myr these objects may also have larger radii than older brown dwarfs and low mass stars with similar spectral types, as they are still contracting to their final radii (e.g., Burrows et al. 1997).

We examine the kinematics of 37 low surface-gravity dwarfs in this paper. Seven of these objects are flagged as red photometric outliers and were examined in the previous subsection. The overlap between these two subgroups is not surprising as the reduced H_2 absorption in low surface-gravity dwarfs leads to a redder near-IR color. The median V_{tan} value for this subgroup is 18 km s^{-1} and the σ_{tan} value is 15 km s^{-1} which is smaller than that of the red photometric outliers as a whole and therefore points to the same conclusion. The smaller median V_{tan} and tighter dispersion of the low surface-gravity dwarfs as compared to either the full or 20 pc sample indicates that they are kinematically distinct.

2.4.5 Unusually Blue L Dwarfs

A subgroup of unusually blue L dwarfs (UBLs) has been distinguished based on strong near-IR H_2O, FeH and K I spectral features but otherwise normal optical spectra. Burgasser et al. (2008a) –hereafter B08– identify ten objects that comprise this subgroup (see Table 6 in B08). With the kinematics reported in this article we are able to analyze all ten. There are several physical mechanisms that can contribute to the spectral properties of UBLs. High surface-gravity, low metallicity, thin clouds or unaccounted multiplicity are amongst the physical mechanisms most often cited. B08 has demonstrated that while sub-solar metallicity and high surface-gravity could be contributing factors in explaining the spectral deviations, thin, patchy or large-grained condensate clouds at the photosphere appears to be the primary cause for the anomalous near-IR spectra (e.g. Ackerman & Marley 2001, Burrows et al. 2006).

The median V_{tan} value for this subgroup is 99 km s^{-1} with σ_{tan} of 47 km s^{-1} and this subgroup consists of dwarfs with the largest V_{tan} values measured in this kinematic study. These kinematic results strengthen the case that the UBLs represent an older population and that the blue near-IR colors and spectroscopic properties of these objects are influenced by large surface-gravity and/or slightly subsolar metallicities. Both of these effects may be underlying explanations for the thin clouds seen in blue L dwarf photospheres. Subsolar metallicity reduces the elemental reservoir for condensate grains while high surface-gravity may enhance gravitational settling of clouds. In effect, the clouds of L dwarfs may be tracers of their age and/or metallicity.

Eight of the ten UBLs examined in this subsection are also flagged as blue photometric outliers and examined in detail above. The overlap between these two subgroups is not surprising as many of the UBLs were initially identified by their blue near-IR color (e.g. Cruz et al. 2007, Knapp et al. 2004). There are 8 other blue photometric outliers, one of which has a V_{tan} value exceeding 100

km s^{-1}. We plan on obtaining near-IR spectra for these outliers to investigate the possibility that they exhibit similar near-IR spectral features to the UBLs.

While the UBLs are the most kinematically distinct subgroup analyzed in this paper, their kinematics do not match those of the ultracool subdwarfs. The subdwarfs were excluded from the kinematic analysis in this paper because they are confirmed members of a separate population. The median V_{tan} value for this subgroup is 196 km s^{-1} with σ_{tan} of 91 km s^{-1}. The UBLs move at half this speed indicating there is a further distinction between UBLs and the metal-poor halo population of ultracool dwarfs.

2.5 High Velocity Dwarfs

Table 2.9 summarizes the properties of the 14 high velocity dwarfs whose V_{tan} measurements exceed 100 km s^{-1}. A number of these have been discussed in the literature, having been singled out in their corresponding discovery papers as potential members of the thick disk or halo population. One high velocity dwarf is presented here for the first time. SDSS J093109.56+032732.5 is an L7.5 dwarf and is classified as both a UBL and a blue photometric outlier. We calculate V_{tan} for this object to be 108 $\pm$ 23 km s^{-1}.

Among the high velocity dwarfs, 11 have colors that are blue and 3 have colors that are normal for their spectral type. Three objects belong to the UBL subgroup. Three of the objects are late-type M dwarfs (2MASS J18261131+3014201, 2MASS J03341218-4953322, and 2MASS J132352+301433), one is a late T7.5 dwarf (2MASSJ 11145133-2618235) and the rest are early to mid-type L dwarfs. Four of the objects are flagged as blue photometric outliers. We explore the possibility that these objects are thick disk or halo objects in detail in a forthcoming paper.

2.6 On the Age of the Ultracool Dwarf Population

2.6.1 Kinematics and Ages

A comparison of the velocity dispersion for nearby stellar populations can be an indicator of age. While individual V_{tan} measurements cannot provide individual age determinations due to scatter and projection effects, the random motions of a population of disk stars are known to increase with age. This effect is known as the disk age-velocity relation (AVR) and is simulated by

Table 2.9. High V_{tan} Objects

Discovery Name	J-K_s	2MASS J (mag)	2MASS K_s (mag)	$\mu_\alpha cos(\delta)$ ($''$/yr)	μ_δ ($''$/yr)	SpT (opt)	SpT (IR)	Distance (pc)	V_{tan} (km s^{-1})	Note[r]
(1)	(2)	(3)	(4)	(5)	(6)	(7)	(8)	(9)	(10)	(11)
DENIS-P J1253108-570924	1.40	13.45 ± 0.02	12.05 ± 0.02	-1.575 ± 0.005	-0.434 ± 0.014	L0.5	—	21 ± 3	162 ± 20	—
2MASSIJ1721039+334415	1.14	13.63 ± 0.02	12.49 ± 0.02	-1.854 ± 0.017	0.602 ± 0.017	L3	—	16 ± 1	144 ± 13	UBL
2MASSJ11145133-2618235	-0.25	15.86 ± 0.08	< 16.11	-3.03 ± 0.04	-0.36 ± 0.04	—	T7.5	10 ± 2	140 ± 22	—
2MASSWJ1411175+393636	1.40	14.64 ± 0.03	13.24 ± 0.04	-0.911 ± 0.015	0.137 ± 0.016	L1.5	—	32 ± 2	138 ± 10	—
2MASS J182611.31+301420.1	0.85	11.66 ± 0.02	10.81 ± 0.02	-2.280 ± 0.010	-0.684 ± 0.010	M8.5	—	12 ± 1	132 ± 9	—
2MASSJ21501592-7520367	1.38	14.06 ± 0.03	12.67 ± 0.03	0.980 ± 0.048	-0.281 ± 0.014	L1	—	26 ± 3	125 ± 18	—
2MASSIJ0251148-035245	1.40	13.06 ± 0.03	11.66 ± 0.02	1.128 ± 0.013	-1.826 ± 0.020	L3	L1	12 ± 1	122 ± 11	—
SDSS J133148.92-011651.4	1.35	15.48 ± 0.06[c]	14.12 ± 0.06[c]	-0.407 ± 0.019	-1.030 ± 0.014	L6	L8	23 ± 2	119 ± 11	UBL
SDSSp J120358.19+001550.3	1.53	14.01 ± 0.03	12.48 ± 0.02	-1.209 ± 0.018	-0.261 ± 0.015	L3	—	19 ± 2	109 ± 10	—
SDSS J093109.56+032732.5	1.10	16.75 ± 0.10[c]	15.65 ± 0.10[c]	-0.612 ± 0.018	-0.131 ± 0.018	—	L7.5	36 ± 8	108 ± 23	UBL
2MASS J033412.18-495332.2	0.98	11.38 ± 0.02	10.39 ± 0.02	2.308 ± 0.012	0.480 ± 0.019	M9	—	10 ± 1	107 ± 7	—
2MASSJ11263991-5003550	1.17	14.00 ± 0.03	12.83 ± 0.03	-1.570 ± 0.004	0.438 ± 0.011	L4.5	L9	14 ± 1	106 ± 11	UBL
GJ 1001B, LHS 102B	1.71	13.11 ± 0.02	11.40 ± 0.03	0.6436 ± 0.0032	-1.4943 ± 0.0021	L5	L4.5	13.0 ± 0.7[j]	100.4 ± 5.2	CB
2MASS J132352.1+301433	1.10	13.68 ± 0.02	12.58 ± 0.02	-0.695 ± 0.023	0.156 ± 0.027	M8.5	—	30 ± 4	100 ± 15	—

Note. — See Table 2.12 for references and notes referred to in this table.

fitting well-constrained data against the following analytic form:

$$\sigma(t) = \sigma_0(1 + \frac{t}{\tau})^{\alpha} \tag{2.6}$$

where $\sigma(t)$ is the total velocity dispersion as a function of time, σ_0 is the initial velocity dispersion at t=0, τ is a constant with unit of time, and α is the heating index (Wielen 1977). $\sigma(t)$ is defined for U,V,W space velocities but we can estimate the total velocity dispersion using our measured tangential velocities assuming the dispersions are spread equally between all three velocity components, such that:

$$\sigma(t) = (3/2)^{(1/2)}\sigma_{tan} \tag{2.7}$$

Hänninen & Flynn (2002) calculate α from seven distinct data sets (both pre and post- Hipparcos) and find α ranges from 0.3 to 0.6. This is a large range of values and the authors are reluctant to assign a higher likelihood to any given value as each have nearly equal uncertainties. One possible explanation for the spread of values is that σ should be mass dependent [3]. If so, this would make a large difference in the age calculations for the low mass ultracool dwarf population. While the age-velocity relation in the nearby disk remains only roughly determined, there is strong observational evidence for a relation so we proceed with caution in examining the broad age possibilities implied by the AVR for the ultracool dwarf population.

Recent findings have suggested that late-type M stars in the solar neighborhood are younger on average than earlier type stars (Hawkins & Bessell 1988; Kirkpatrick et al. 1994; Reid et al. 1994). Several investigators have combined kinematics with the Wielen (1977) relationship (which uses a value of 1/3 for α) to estimate age ranges for the ultracool dwarf population and concluded that it is kinematically younger than nearby stellar populations (e.g. Dahn et al. 2002, Schmidt et al. 2007, Gizis et al. 2000b, Zapatero Osorio et al. 2007). We conducted a direct V_{tan} comparison with nearby stellar populations to draw conclusions about the kinematic distinguishability of our ultracool dwarf sample. We compared the kinematics of a 20 pc sample of F,G,K, and early M stars from Soubiran et al. (2003), Kharchenko et al. (2004) and Nordström et al. (2004) using a limiting proper motion of 25 mas/yr to our 20 pc sample and examined the resultant median V_{tan}, σ_{tan}, and V_{tot} , σ_{tot} values (where V_{tot} comes from the U,V,W velocities). Figure 2.12 shows our resultant velocity dispersions for nearby stellar populations along with the dispersions of our 20 pc sample. We show both the dispersions calculated using tangential

[3]Indeed Iwanowska 1980 proposes the introduction of a mass term to account for the importance of the exchange of energy between stars in the Galactic disk

velocities and those calculated using U,V,W velocities. As expected the dispersions are tighter for the UCDs when U,V,W values are used since we have attempted to minimize the importance of radial velocity. This effect is also reflected in the younger ages estimated from these dispersions. The tangential velocity dispersions are in good agreement between the UCDs and nearby stellar populations (see also West et al. 2008,Bochanski et al. 2007a, and Covey et al. 2008). Table 2.10 contains the calculated kinematic measurements and Wielen ages using both σ_{tan} and σ_{tot}. With Wielen ages of 3-8 Gyr calculated from σ_{tan}, we conclude that our 20 pc sample is kinematically indistinct from other nearby stellar populations and hence is not kinematically younger. The ages calculated by the AVR for the 20 pc sample are in good agreement with those predicted in population synthesis models where the mean ages for the ultracool dwarf population range from 3-6 Gyr (Burgasser 2004b; Allen et al. 2005).

We do find younger ages for the ultracool dwarf population when the high velocity dwarfs are excluded. As stated in section 4, the median V_{tan} and σ_{tan} values are naturally reduced when the high velocity dwarfs are excluded and consequently the ages are also reduced. Kinematic analyses of the past have regarded these objects as a separate older population and omitted them from an age calculation (e.g. Schmidt et al. 2007). Table 2.10 presents the ages with and without the high velocity dwarfs for the 20 pc sample. When the high velocity dwarfs are excluded the age ranges are reduced from 3-8 Gyr to 2-4 Gyr, which is still consistent with population synthesis models.

The Os07 study estimated mean ages of $\sim$ 1 Gyr for the L and T dwarf population . Even with the exclusion of the kinematic outliers, the ages calculated in our full and 20 pc samples do not match this very young age. Os07 combined proper motions, precise parallaxes, and radial velocities to study the 3D kinematics of a limited sample of 21 objects. When we apply an age velocity relation to the red photometric outliers and the low gravity dwarfs we do find ages that are on the order of $\sim$ 1 Gyr. We discuss the red outliers below but conclude that the low surface-gravity dwarfs are kinematically younger than the full or 20 pc sample. This result is consistent with what has already been reported through spectroscopic studies. There do not appear to be any low surface-gravity dwarfs flagged in the Os07 sample however further examination of their L and T dwarf spectra might be warranted by the discrepancy in ages between our samples. We suggest that kinematic studies of UCDs to date, including Os07, may have been plagued by small number statistics or a bias in the sample analyzed.

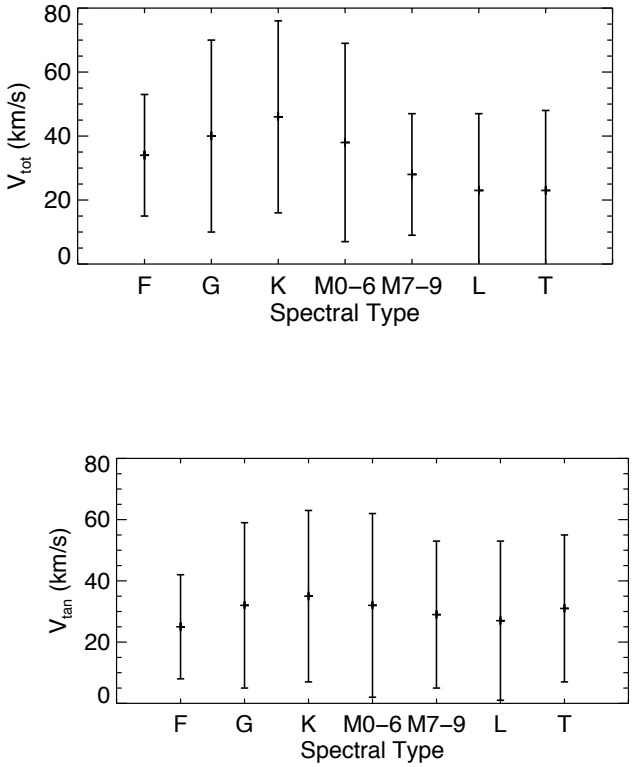

Figure 2.12: Top: A plot of median V_{tot} and σ_{tot} values calculated from the U,V,W velocities for the 20 pc sample of F through T objects. Bottom: A plot of median V_{tan} and σ_{tan} values calculated from the proper motions and distances for the 20 pc sample of F through T objects.

Table 2.10. Median Kinematics and Ages for the 20 pc sample

SpT	N[a]	U (km/s)	σ_U (km/s)	V (km/s)	σ_V (km/s)	W (km/s)	σ_W (km/s)	V_{tan} (km/s)	σ_{tan} (km/s)	Age from V_{tan} (Gyr)	N[b]	V_{tot} (km/s)	σ_{tot} (km/s)	Age from V_{tot} (Gyr)
(1)	(2)	(3)	(4)	(5)	(6)	(7)	(8)	(9)	(10)	(11)	(12)	(13)	(14)	(15)
F	139	-6	28	-8	18	-6	16	25	17	$1.7^{+0.6}_{-0.5}$	139	34	19	$1.2^{+0.5}_{-0.4}$
G	221	-16	38	-15	29	-5	21	32	27	$7.3^{+2.5}_{-2.0}$	221	40	30	$5.4^{+1.9}_{-1.5}$
K	308	-13	42	-20	30	-8	18	35	28	$7.8^{+2.6}_{-2.2}$	308	46	30	$5.2^{+1.8}_{-1.5}$
M0-M6	60	-8	45	-14	22	-7	21	32	30	$9.5^{+3.2}_{-2.6}$	60	38	31	$6.0^{+2.0}_{-1.7}$
M7-M9	93	-6	26	-14	20	-7	20	29	24	$5.0^{+1.7}_{-1.4}$	81	28	21	$1.7^{+0.6}_{-0.5}$
L0-L9	114	-8	28	-15	23	-5	15	27	26	$6.6^{+2.2}_{-1.8}$	168	25	24	$2.6^{+0.9}_{-0.7}$
T0-T8	70	-8	33	-12	21	-8	16	31	24	$4.6^{+1.6}_{-1.3}$	35	23	23	$2.2^{+0.8}_{-0.7}$

[a]The number of objects used to calculate median V_{tan} values.

[b]The number of objects used to calculate median V_{tot} values and thus used in the U,V,W analysis.

Note. — Kinematic data for F,G,K, and early M stars gathered from the Soubiran et al. (2003), Kharchenko et al. (2004) and Nordström et al. (2004) catalogues. We restricted to distances < 20 pc and proper motions > 20 mas/yr for comparison with our 20 pc ultracool dwarf sample.

2.6.2 Ages of the Red and Blue Outliers

We have defined two subgroups of the ultracool dwarf population in this article that are both photometrically and kinematically distinct from the full or 20 pc samples. Objects whose $J - K_s$ colors are sufficiently deviant are also kinematically different from the overall population. While we again advise caution in using the AVR, we can use it to compare the predicted ages of the photometric outliers to the predicted ages for the full or 20 pc samples. We find that the kinematics for the red outliers are consistent with a younger population of ultracool dwarfs whereas the kinematics for the blue outliers are consistent with an older population. The $\sim$ 1 Gyr mean age for the red outliers coincides with the prediction of Os07 for the entire L and T population. We have examined the photometry of their sample and concluded that the $J - K_s$ colors of their objects are normal so the age calculation of their sample is not influenced by a bias from inclusion of photometric outliers. The $\sim$ 38 Gyr mean age for the blue outliers is misleading. It indicates a large divergence from the full and 20 pc samples but also indicates that the AVR must be incorrect for these objects. The more informative number in this case is the median V_{tan} which, at 56 km/s, is nearly twice the expected value for the thin disk (see Reid & Hawley 2005). The blue photometric outliers most likely belong to an older population of the Galaxy such as the thick disk or the halo. The Wielen AVR is only valid for thin disk objects and we are unaware of an equivalent age relation for the halo or thick disk population.

From our kinematic analysis we conclude that there is an age-color relation that can be derived for the UCD field population. A change in broad-band collision-induced H_2 absorption that suppresses flux at K-band is partially responsible for the near-IR color and consequently the age of the photometric outliers (Linsky 1969; Saumon et al. 1994; Borysow et al. 1997). H_2 absorption is pressure and hence gravity sensitive. Changes in H_2 absorption effect gravity sensitive features which are used as an indicator of age. The overlap of red photometric outliers with low surface-gravity dwarfs and the concensus within the literature that low-g dwarfs are young demonstrates the age sensitivity of H_2 absorption.

Cloud properties have also been linked to a change in near-IR color. The analyses of B08, and Cushing et al. 2008 have shown that the thickness of patchy or large-grained condensate clouds at the photospheres of dwarfs will lead to redder (thick clouds) or bluer (thin clouds) near-IR colors. The old age implied by the kinematics of the blue outliers and the overlap with the UBLs suggests that there is a correlation between cloud properties and age or metallicity; but further investigation is warranted in this area.

Jameson et al. (2008b) have proposed a relation for inferring the ages of

young L dwarfs using only near-infrared photometry and estimated distances. Their work supports the argument for an age-color relation for the ultracool dwarf population. The ages that they work with are no larger than $\sim$ 0.7 Gyr. At these young ages, the surface gravities of UCDs change more rapidly than for ages greater than a few Gyr, so the age-color relation may be much stronger in the Jameson et al. (2008b) sample than that seen for field dwarfs.

2.7 Conclusions

We present new proper motions for 427 late-type M, L, and T dwarfs and combine all previous proper motion measurements with either parallax measurements or spectrophotometric distances to compute tangential velocities for 841 M7–T9 dwarfs. We derive average kinematic and photometric values for individual spectral types as well as for the late-type M,L, and T populations as a whole. We conduct a crude U,V,W analysis and find that the full and 20 pc samples examined in this article have space velocities consistent with the Galactic thin disk population. However, there are 14 objects in the ultracool dwarf population that lie at the tail end of the velocity distribution and are likely to be part of an older Galactic population. Ages for the 20 pc sample of this kinematic study are consistent with the 3-6 Gyr values derived in population synthesis models; we propose that one reason for prior kinematic reports of $\sim$1 Gyr mean ages for the L and T dwarf population is due to small number statistics or a bias in the sample analyzed.

We find a large difference in the kinematics between red and blue photometric outliers and conclude that their velocity dispersions are kinematically distinct from the full or 20 pc samples. Analysis of the low surface-gravity and UBL subgroups also shows a distinction from the full and 20 pc samples. Applying an age-velocity relation we conclude that the red outliers and low surface-gravity subgroups are younger than the full and 20 pc samples and the blue outliers and UBLs are older.

2.8 Post-Publication

Several pertinent papers have been published since this work. Schmidt et al (2010) presented a study reviewing the kinematic and photometric details of 210 L dwarfs discovered in SDSS. Combining their sample with 274 previously identified SDSS L dwarfs, they concluded that the spectroscopically-identified sample was $\sim$0.1 mag bluer in J-K_s color at a given spectral type (L0-L4) than the photometrically selected sample. The color selections chosen by previous

groups biased the known selection toward redder colors. Schmidt et al (2010) used radial velocity measurements for the L dwarf sample (totaling 484 objects) and searched for correlations between kinematic and photometric properties. Comparing to a Galactic model, they found evidence for both cold and hot dynamical populations consistent with both young and old disk components. Similar to our result, they found that J-K_s color is correlated with velocity dispersion with bluer objects sharing kinematics with the older population and redder objects the younger.

Reiners & Basri (2009) reported on the kinematics of a sample of 63 ultracool dwarfs (spectral type M7 – M9.5). Those authors examined U,V,W velocities using proper motion, spectrophotometric distance and radial velocity and concluded that the stars were predominantly members of the young disk with a kinematic age consistent with 3.1 Gyr. Seifahrt et al. (2010) conducted a similar kinematic analysis for 43 L0-L8 dwarfs. They found nine candidate members of young moving groups (50- 600 Myr) but report an average kinematic age of $\sim$5 Gyr for the rest of their sample. The authors speculate that this slightly older kinematic age might be due to contamination from outliers. The higher velocity stars would have gained speed by means of ejection from multiple systems at formation skewing their kinematic age to slightly older than predicted by previous works.

Kirkpatrick et al. (2010) reported discoveries of new L and T dwarfs from a proper motion survey with spectroscopic follow-up. In that work, six new low gravity field brown dwarfs were reported, five red L dwarfs, three L subdwarfs, eight blue L dwarfs and several T dwarfs. Objects were followed up based on minimal color criteria therefore photometric biases of past studies should have been limited. The kinematics of the blue L dwarfs appear to be drawn from a relatively old population consistent with results described in this chapter. However, Kirkpatrick et al. (2010) also find that the five red L dwarfs lack low-surface gravity features and have kinematics consistent with an older Galactic population. The authors speculate that the unusually red and blue L dwarfs might be explained by the same phenomena. One possible scenario is presented that viewing angle determines the spectral appearance. This would be the case if clouds are not homogenously distributed in latitude or if properties such as grain size and cloud thickness vary in latitude. Such a hypothesis could be readily tested by measuring the rotational velocities (v_{rot}) of examples in each subsample to see if v_{rot} is smaller for red L dwarfs.

Table 2.11: New Proper Motion Measurements

Source Name	RA (J2000)	DEC (J2000)	SpT[a] (optical)	SpT (near-IR)	$\mu_\alpha cos(\delta)$ ($''$ yr^{-1})	μ_δ ($''$ yr^{-1})	Baseline (yrs)	Instrument
(1)	(2)	(3)	(4)	(5)	(6)	(7)	(8)	(9)
2MASS J00034227-2822410	00 03 42.27	-28 22 41.0	M7.5	—	0.257 ± 0.016	-0.145 ± 0.018	9.2	CPAPIR
2MASSI J0006205-172051	00 06 20.50	-17 20 50.6	L2.5	—	-0.032 ± 0.017	0.017 ± 0.018	9.5	CPAPIR
2MASS J00100009-2031122	00 10 00.09	-20 31 12.2	L0	—	0.100 ± 0.022	0.007 ± 0.023	9.1	CFIM
2MASSI J0013578-223520	00 13 57.79	-22 35 20.0	L4	—	0.055 ± 0.017	-0.051 ± 0.019	9.4	CPAPIR
2MASS J00145575-4844171	00 14 55.75	-48 44 17.1	L2.5	—	0.851 ± 0.012	0.289 ± 0.018	8.1	CPAPIR
2MASS J00165953-4056541	00 16 59.53	-40 56 54.1	L3.5	—	0.201 ± 0.014	0.032 ± 0.018	8.3	CPAPIR
EROS-MP J0032-4405	00 32 55.84	-44 05 05.8	L0	—	0.126 ± 0.015	-0.099 ± 0.021	8.4	CPAPIR
2MASS J00332386-1521309	00 33 23.86	-15 21 30.9	L4	—	0.291 ± 0.016	0.043 ± 0.017	8.3	CPAPIR
2MASS J00374306-5846229	00 37 43.06	-58 46 22.9	L0	—	0.049 ± 0.010	-0.051 ± 0.020	8.2	CPAPIR
SIPS J0050-1538	00 50 24.44	-15 38 18.4	L1	—	-0.229 ± 0.018	-0.494 ± 0.019	9.6	CPAPIR
2MASSW J0051107-154417	00 51 10.78	-15 44 16.9	L3.5	—	0.043 ± 0.015	-0.021 ± 0.016	9.4	CPAPIR
2MASS J00531899-3631102	00 53 18.99	-36 31 10.2	L3.5	—	0.018 ± 0.015	-0.085 ± 0.019	8.5	CPAPIR
SDSSp J005406.55-003101.8	00 54 06.55	-00 31 01.8	L1	—	0.200 ± 0.009	-0.160 ± 0.009	9.2	TIFKAM
2MASSI J0104075-005328	01 04 07.50	-00 53 28.3	L4.5	—	0.473 ± 0.018	-0.021 ± 0.018	9.2	CPAPIR
2MASS J01062285-5933185	01 06 22.85	-59 33 18.5	L0	—	0.046 ± 0.010	-0.198 ± 0.020	8.2	CPAPIR
2MASS J01071607-1517577	01 07 16.07	-15 17 57.7	M7	—	-0.031 ± 0.016	0.011 ± 0.017	9.5	CPAPIR
SDSSp J010752.33+004156.1	01 07 52.42	+00 41 56.3	L8	L5.5	0.612 ± 0.020	0.078 ± 0.020	5.1	CPAPIR
SSSPM J0109-4955	01 09 09.18	-49 54 53.2	—	L1	0.095 ± 0.013	0.168 ± 0.020	8.2	CPAPIR
2MASS J01165457-1357342	01 16 54.57	-13 57 34.2	M9	—	-0.026 ± 0.022	-0.110 ± 0.022	7.5	CPAPIR
2MASSI J0117474-340325	01 17 47.48	-34 03 25.8	L2	—	0.080 ± 0.017	-0.062 ± 0.020	8.9	CFIM
2MASS J01244599-5745379	01 24 45.99	-57 45 37.9	L0	—	-0.003 ± 0.010	0.018 ± 0.019	8.3	CPAPIR
2MASSI J0125369-343505	01 25 36.89	-34 35 04.9	L2	—	0.151 ± 0.016	0.036 ± 0.019	9.1	CPAPIR
2MASS J01303563-4445411	01 30 35.63	-44 45 41.1	M9	—	0.120 ± 0.014	-0.025 ± 0.020	8.3	CPAPIR
2MASS J01311838+3801554	01 31 18.38	+38 01 55.4	L4	—	0.373 ± 0.012	-0.031 ± 0.015	9.1	TIFKAM
2MASSW J0135358+120522	01 35 35.86	+12 05 21.6	L1.5	—	-0.042 ± 0.023	-0.422 ± 0.023	7.3	CPAPIR
2MASSW J0141032+180450	01 41 03.21	+18 04 50.2	L1	L4.5	0.403 ± 0.011	-0.045 ± 0.012	9.1	TIFKAM
2MASS J01411479-2417311	01 41 14.79	-24 17 31.1	M7.5	—	-0.161 ± 0.017	-0.303 ± 0.019	9.2	CPAPIR
2MASS J01415823-4633574	01 41 58.23	-46 33 57.4	L0	L0	0.104 ± 0.017	-0.026 ± 0.024	8.1	CFIM
2MASS J01443536-0716142	01 44 35.36	-07 16 14.2	L5	—	0.395 ± 0.018	-0.204 ± 0.018	9.2	CPAPIR
2MASS J01460119-4545263	01 46 01.19	-45 45 26.3	M9	—	0.121 ± 0.016	0.060 ± 0.023	7.3	CPAPIR
2MASSW J0147334+345311	01 47 33.44	+34 53 11.2	L0.5	—	0.037 ± 0.009	-0.055 ± 0.011	10.0	TIFKAM
2MASS J01550354+0950003	01 55 03.54	+09 50 00.3	L5	—	0.338 ± 0.023	-0.080 ± 0.023	7.3	CPAPIR
2MASS J02042212-3632308	02 04 22.12	-36 32 30.8	M9	—	0.193 ± 0.017	-0.034 ± 0.021	8.5	CPAPIR
2MASSW J0205034+125142	02 05 03.44	+12 51 42.2	L5	—	0.349 ± 0.011	-0.018 ± 0.011	9.2	TIFKAM

Continued on Next Page...

Table 2.11 – Continued

Source Name (1)	RA (J2000) (2)	DEC (J2000) (3)	SpT[1] (optical) (4)	SpT (near-IR) (5)	$\mu_\alpha cos(\delta)$ ($''$ yr^{-1}) (6)	μ_δ ($''$ yr^{-1}) (7)	Baseline (yrs) (8)	Instrument (9)
SDSS J020608.97+223559.2	02 06 08.80	+22 35 59.3	—	L5.5	0.341 ± 0.015	-0.062 ± 0.016	10.2	CPAPIR
SDSS J020735.60+135556.3	02 07 35.57	+13 55 56.4	L3	L3	0.260 ± 0.017	-0.161 ± 0.018	9.3	CPAPIR
2MASSW J0208183+254253	02 08 18.33	+25 42 53.3	L1	—	0.356 ± 0.010	-0.021 ± 0.011	10.0	TIFKAM
2MASSW J0208236+273740	02 08 23.63	+27 37 40.0	L5	—	0.217 ± 0.013	-0.110 ± 0.014	10.1	TIFKAM
2MASSW J0208549+250048	02 08 54.99	+25 00 48.8	L5	—	-0.022 ± 0.011	0.060 ± 0.012	10.1	TIFKAM
SDSS J021128.25+141003.8	02 11 28.27	+14 10 03.9	L1	—	-0.092 ± 0.010	-0.030 ± 0.010	9.2	TIFKAM
2MASSI J0218291-313322	02 18 29.13	-31 33 23.0	L3	—	-0.165 ± 0.015	-0.138 ± 0.018	9.0	CPAPIR
2MASS J02192196+0506306	02 19 21.96	+05 06 30.6	—	L1	0.190 ± 0.024	0.005 ± 0.024	7.4	CPAPIR
2MASS J02212859-6831400	02 21 28.46	-68 31 40.0	M8	—	0.046 ± 0.006	-0.006 ± 0.017	7.3	CPAPIR
2MASS J02215494-5412054	02 21 54.99	-54 12 05.4	M9	—	0.136 ± 0.010	-0.010 ± 0.017	7.4	CPAPIR
2MASS J02235464-5815067	02 23 54.46	-58 15 06.7	L0	—	0.134 ± 0.010	0.005 ± 0.019	7.4	CPAPIR
2MASS J02251947-5837295	02 25 18.81	-58 37 29.5	M9	—	0.085 ± 0.010	-0.030 ± 0.018	7.4	CPAPIR
2MASS J02271036-1624479	02 27 10.36	-16 24 47.9	L1	—	0.426 ± 0.016	-0.297 ± 0.017	7.0	CFIM
2MASS J02284243+1639329	02 28 42.43	+16 39 32.9	L0	—	0.422 ± 0.020	-0.412 ± 0.021	8.2	CPAPIR
2MASS J02284355-6325052	02 28 43.55	-63 25 05.2	—	L0	0.593 ± 0.010	0.458 ± 0.023	7.3	CPAPIR
2MASS J02301551+2704061	02 30 15.51	+27 04 06.1	L0	—	0.189 ± 0.008	-0.007 ± 0.010	9.1	TIFKAM
SDSS J023547.56-084919.8	02 35 47.56	-08 49 19.8	L2	—	-0.044 ± 0.013	0.013 ± 0.013	9.1	TIFKAM
SDSSp J023617.93+004855.0	02 36 17.94	+00 48 54.8	L6	L6.5	0.123 ± 0.012	-0.176 ± 0.012	7.2	TIFKAM
2MASSI J0239424-173547	02 39 42.45	-17 35 47.1	L0	—	0.042 ± 0.017	-0.095 ± 0.018	9.4	CPAPIR
2MASSI J0241536-124106	02 41 53.67	-12 41 06.9	L2	—	0.312 ± 0.016	-0.040 ± 0.017	9.4	CPAPIR
2MASSW J0242435+160739	02 42 43.55	+16 07 39.2	L1.5	—	0.152 ± 0.011	-0.210 ± 0.012	9.2	TIFKAM
2MASS J02435103-5432194	02 43 51.03	-54 32 19.4	M9	—	0.096 ± 0.011	-0.026 ± 0.019	8.2	CPAPIR
SDSS J024749.90-163112.6	02 47 49.78	-16 31 13.2	—	T2	0.313 ± 0.017	0.143 ± 0.017	9.3	CPAPIR
SDSS J025601.86+011047.2	02 56 01.89	+01 10 46.7	L0	—	0.025 ± 0.015	-0.068 ± 0.015	7.2	TIFKAM
2MASS J02572581-3105523	02 57 25.81	-31 05 52.3	L8	—	0.602 ± 0.018	0.320 ± 0.021	6.2	CPAPIR
2MASSI J0302012+135814	03 02 01.22	+13 58 14.2	L3	—	0.055 ± 0.015	-0.037 ± 0.016	10.3	CPAPIR
SDSSp J030321.24-000938.2	03 03 21.23	-00 09 37.8	L0	—	0.025 ± 0.017	-0.023 ± 0.017	9.2	CPAPIR
2MASSW J0306268+154514	03 06 26.84	+15 45 13.7	L6	—	0.212 ± 0.017	-0.071 ± 0.018	9.2	CPAPIR
2MASSW J0309088-194938	03 09 08.88	-19 49 38.7	L4.5	—	0.184 ± 0.016	-0.038 ± 0.017	9.2	CPAPIR
2MASS J03100053+0726506	03 10 00.53	+07 26 50.6	M7.5	—	0.539 ± 0.022	0.254 ± 0.022	7.3	CPAPIR
2MASS J03101401-2756452	03 10 14.01	-27 56 45.2	L5	—	-0.116 ± 0.016	-0.052 ± 0.018	9.2	CPAPIR
2MASSW J0310599+164816	03 10 59.86	+16 48 15.5	L8	L9	-0.706 ± 0.019	0.119 ± 0.020	8.3	CPAPIR
2MASS J03134443+0433165	03 13 44.43	+04 33 16.5	M7.5	—	-0.049 ± 0.022	0.006 ± 0.022	7.4	CPAPIR
2MASS J03140344+1603056	03 14 03.44	+16 03 05.6	L0	—	-0.241 ± 0.018	-0.076 ± 0.019	8.3	CPAPIR
2MASS J03144011-0450316	03 14 40.11	-04 50 31.6	M7.5	—	-0.068 ± 0.018	-0.119 ± 0.018	9.3	CPAPIR
2MASSI J0316451-284852	03 16 45.12	-28 48 52.1	L0	—	0.107 ± 0.017	-0.081 ± 0.019	9.2	CPAPIR

Continued on Next Page...

Table 2.11 – Continued

Source Name (1)	RA (J2000) (2)	DEC (J2000) (3)	SpT[1] (optical) (4)	SpT (near-IR) (5)	$\mu_\alpha cos(\delta)$ ($''$ yr^{-1}) (6)	μ_δ ($''$ yr^{-1}) (7)	Baseline (yrs) (8)	Instrument (9)
2MASS J03185403-3421292	03 18 54.03	-34 21 29.2	L7	—	0.365 ± 0.016	0.017 ± 0.019	9.1	CPAPIR
2MASS J03201720-1026124	03 20 17.20	-10 26 12.4	M8	—	0.013 ± 0.018	-0.100 ± 0.018	9.3	CPAPIR
2MASSW J0320284-044636	03 20 28.39	-04 46 35.8	—	L0.5	-0.267 ± 0.016	-0.533 ± 0.016	9.2	CPAPIR
2MASS J03231002-4631237	03 23 10.02	-46 31 23.7	L0	—	0.060 ± 0.013	-0.010 ± 0.019	7.5	CPAPIR
2MASS J03250136+2253039	03 25 01.36	+22 53 03.9	L3	—	0.405 ± 0.013	-0.146 ± 0.014	10.1	TIFKAM
SDSS J032553.17+042540.1	03 25 53.22	+04 25 40.6	—	T5.5	-0.183 ± 0.014	-0.099 ± 0.014	7.8	TIFKAM
2MASS J03264225-2102057	03 26 42.25	-21 02 05.7	L4	—	0.108 ± 0.014	-0.146 ± 0.015	9.0	CPAPIR
2MASS J03274091-3148156	03 27 40.91	-31 48 15.6	—	L3	0.038 ± 0.017	0.018 ± 0.020	9.1	CPAPIR
SDSSp J032817.38+003257.2	03 28 17.38	+00 32 57.2	L3	—	0.195 ± 0.013	0.033 ± 0.013	7.8	TIFKAM
SDSSp J033017.77+000047.8	03 30 17.74	+00 00 47.7	L0	—	-0.011 ± 0.018	-0.046 ± 0.018	9.3	CPAPIR
SDSSp J033035.13-002534.5	03 30 35.11	-00 25 34.6	L4	—	0.394 ± 0.015	-0.336 ± 0.015	9.2	CPAPIR
2MASS J03320043-2317496	03 32 00.43	-23 17 49.6	M8	—	-0.013 ± 0.020	-0.153 ± 0.022	7.3	CPAPIR
2MASS J03341218-4953322	03 34 12.04	-49 53 32.2	M9	—	2.308 ± 0.012	0.480 ± 0.019	7.4	CPAPIR
2MASS J03354535+0658058	03 35 45.35	+06 58 05.8	M8	—	0.029 ± 0.021	-0.333 ± 0.021	8.0	CPAPIR
2MASSW J0337036-175807	03 37 03.59	-17 58 07.9	L4.5	—	0.191 ± 0.031	0.115 ± 0.033	8.8	CFIM
2MASS J03400942-6724051	03 40 09.42	-67 24 05.1	L7	—	-0.318 ± 0.007	0.508 ± 0.018	8.9	CFIM
2MASS J03421621-6817321	03 42 16.21	-68 17 32.1	L2	—	0.064 ± 0.007	0.021 ± 0.018	9.2	CPAPIR
SDSS J035048.62-051812.8	03 50 48.61	-05 18 12.6	L1	—	0.012 ± 0.022	-0.028 ± 0.022	7.3	CPAPIR
SDSS J035104.37+481046.8	03 51 04.23	+48 10 47.7	—	T1	0.312 ± 0.019	-0.180 ± 0.029	7.9	TIFKAM
SDSS J035448.73-002742.1	03 54 48.55	-00 27 42.0	—	L2	-0.011 ± 0.022	-0.019 ± 0.022	7.3	CPAPIR
2MASS J03550477-1032415	03 55 04.77	-10 32 41.5	M8.5	—	0.046 ± 0.018	-0.044 ± 0.019	9.0	CPAPIR
2MASS J03552337+1133437	03 55 23.37	+11 33 43.7	L5	—	0.192 ± 0.017	-0.613 ± 0.017	7.2	CPAPIR
2MASSW J0355419+225702	03 55 41.91	+22 57 01.6	L3	—	0.146 ± 0.014	-0.025 ± 0.016	10.2	CPAPIR
SDSS J035721.11-064126.0	03 57 21.10	-06 41 26.0	L0	—	0.109 ± 0.012	0.008 ± 0.012	9.1	CPAPIR
DENIS-P J035726.9-441730	03 57 26.95	-44 17 30.5	L0	—	0.064 ± 0.013	-0.020 ± 0.019	8.4	CPAPIR
2MASS J03582255-4116060	03 58 22.55	-41 16 06.0	L5	—	0.051 ± 0.015	0.075 ± 0.020	8.1	CPAPIR
2MASS J04012977-4050448	04 01 29.77	-40 50 44.8	L0	—	-0.036 ± 0.015	-0.102 ± 0.020	8.4	CPAPIR
2MASS J04070752+1546457	04 07 07.52	+15 46 45.7	L3.5	—	0.049 ± 0.019	-0.044 ± 0.020	8.1	CPAPIR
2MASS J04070885+1514565	04 07 08.85	+15 14 56.5	—	T5	0.106 ± 0.016	-0.110 ± 0.017	8.0	TIFKAM
2MASS J04081032+0742494	04 08 10.32	+07 42 49.4	M8	—	0.162 ± 0.020	0.095 ± 0.020	8.1	CPAPIR
2MASSI J0408290-145033	04 08 29.05	-14 50 33.4	L2	L4.5	0.188 ± 0.017	-0.131 ± 0.018	9.4	CPAPIR
2MASSI J0409095+210439	04 09 09.50	+21 04 39.3	L3	—	0.094 ± 0.015	-0.145 ± 0.016	10.2	CPAPIR
SDSSp J041320.38-011424.9	04 13 20.39	-01 14 24.8	L0.5	—	0.070 ± 0.017	0.001 ± 0.017	9.2	CPAPIR
2MASS J04174743-2129191	04 17 47.43	-21 29 19.1	M8	—	0.072 ± 0.017	0.022 ± 0.018	9.2	CPAPIR
2MASS J04210718-6306022	04 21 07.18	-63 06 02.2	L4	—	0.146 ± 0.008	0.191 ± 0.018	9.2	CPAPIR
2MASS J04270723+0859027	04 27 07.23	+08 59 02.7	M8	—	-0.121 ± 0.021	-0.005 ± 0.021	8.1	CPAPIR

Continued on Next Page...

Table 2.11 – Continued

Source Name (1)	RA (J2000) (2)	DEC (J2000) (3)	SpT[1] (optical) (4)	SpT (near-IR) (5)	$\mu_\alpha cos(\delta)$ ($''$ yr^{-1}) (6)	μ_δ ($''$ yr^{-1}) (7)	Baseline (yrs) (8)	Instrument (9)
2MASSI J0428510-225323	04 28 50.96	-22 53 22.7	L0.5	—	0.113 ± 0.012	0.155 ± 0.013	8.8	CFIM
2MASS J04305157-0849007	04 30 51.57	-08 49 00.7	M8	—	-0.021 ± 0.017	-0.171 ± 0.018	9.3	CPAPIR
2MASS J04351455-1414468	04 35 14.55	-14 14 46.8	M8	—	0.009 ± 0.014	0.016 ± 0.014	8.3	CPAPIR
2MASS J04362767+1151243	04 36 27.67	+11 51 24.3	M9	—	0.117 ± 0.020	-0.009 ± 0.020	8.1	CPAPIR
2MASS J04362788-4114465	04 36 27.88	-41 14 46.5	M8	—	0.073 ± 0.012	0.013 ± 0.016	8.2	CPAPIR
2MASS J04365019-1803262	04 36 50.19	-18 03 26.2	M7	—	0.204 ± 0.017	-0.015 ± 0.018	9.1	CPAPIR
2MASSI J0439010-235308	04 39 01.01	-23 53 08.3	L6.5	—	-0.110 ± 0.015	-0.152 ± 0.016	8.3	CPAPIR
2MASSI J0443058-320209	04 43 05.81	-32 02 09.0	L5	—	-0.013 ± 0.015	0.211 ± 0.018	9.1	CPAPIR
2MASS J04433761+0002051	04 43 37.61	+00 02 05.1	M9	—	0.028 ± 0.014	-0.099 ± 0.014	8.4	CPAPIR
2MASS J04441479+0543573	04 44 14.79	+05 43 57.3	M8	—	0.095 ± 0.021	-0.006 ± 0.021	8.0	CPAPIR
2MASS J04451119-0602526	04 45 11.19	-06 02 52.6	M7	—	0.047 ± 0.017	0.007 ± 0.018	9.2	CPAPIR
2MASS J04453237-3642258	04 45 32.37	-36 42 25.8	M9	—	0.454 ± 0.018	-0.008 ± 0.023	7.2	CPAPIR
2MASSI J0445538-304820	04 45 53.87	-30 48 20.4	L2	—	0.183 ± 0.013	-0.393 ± 0.015	8.2	CPAPIR
2MASS J04474307-1936045	04 47 43.07	-19 36 04.5	—	L5	0.069 ± 0.022	0.088 ± 0.023	7.3	CPAPIR
2MASSI J0451009-340214	04 51 00.93	-34 02 15.0	L0.5	—	0.107 ± 0.017	0.138 ± 0.021	8.8	CFIM
2MASSI J0453264-175154	04 53 26.47	-17 51 54.3	L3	—	0.037 ± 0.017	-0.021 ± 0.018	9.4	CPAPIR
2MASS J04553267-2701493	04 55 32.67	-27 01 49.3	M9	—	0.078 ± 0.016	-0.119 ± 0.017	9.1	CPAPIR
2MASS J05002100+0330501	05 00 21.00	+03 30 50.1	L4	—	-0.002 ± 0.021	-0.349 ± 0.021	8.0	CPAPIR
2MASS J05012406-0010452	05 01 24.06	-00 10 45.2	L4	—	0.158 ± 0.014	-0.139 ± 0.014	8.5	CPAPIR
2MASSI J0502134+144236	05 02 13.45	+14 42 36.7	L0	—	0.060 ± 0.012	-0.022 ± 0.012	9.1	TIFKAM
2MASS J05084947-1647167	05 08 49.47	-16 47 16.7	M8	—	-0.197 ± 0.018	-0.362 ± 0.018	9.1	CPAPIR
2MASS J05103520-4208140	05 10 35.20	-42 08 14.0	—	T5	0.104 ± 0.015	0.580 ± 0.021	8.3	CPAPIR
2MASSI J0512063-294954	05 12 06.36	-29 49 54.0	L4.5	—	-0.028 ± 0.016	0.099 ± 0.018	9.1	CPAPIR
2MASS J05161597-3332046	05 16 15.97	-33 32 04.6	—	L3	0.059 ± 0.016	0.184 ± 0.019	9.1	CPAPIR
2MASS J05170548-4154413	05 17 05.48	-41 54 41.3	M9	—	0.089 ± 0.015	0.016 ± 0.021	8.2	CPAPIR
2MASS J05184616-2756457	05 18 46.16	-27 56 45.7	L0	—	0.020 ± 0.013	0.022 ± 0.014	8.2	CPAPIR
2MASS J05185995-2828372	05 18 59.95	-28 28 37.2	L7.5	T1	-0.065 ± 0.016	-0.282 ± 0.019	9.0	CPAPIR
2MASSI J0523382-140302	05 23 38.22	-14 03 02.2	L2.5	L5	0.090 ± 0.017	0.166 ± 0.017	9.0	CPAPIR
2MASS J05265973-5026216	05 26 59.73	-50 26 21.6	L3	—	0.008 ± 0.012	0.227 ± 0.020	8.2	CPAPIR
2MASS J05284435-3252228	05 28 44.35	-32 52 22.8	M8.5	—	-0.029 ± 0.016	0.066 ± 0.018	9.0	CPAPIR
2MASS J05345844-1511439	05 34 58.44	-15 11 43.9	M9	—	-0.115 ± 0.018	0.085 ± 0.018	9.0	CPAPIR
2MASS J05361998-1920396	05 36 19.98	-19 20 39.6	L1	—	0.017 ± 0.017	-0.024 ± 0.018	9.0	CPAPIR
2MASS J06020638+4043588	06 02 06.38	+40 43 58.8	—	T4.5	0.243 ± 0.011	-0.212 ± 0.015	8.0	TIFKAM
2MASS J06050196-2342270	06 05 01.96	-23 42 27.0	L0	—	-0.057 ± 0.017	0.082 ± 0.018	9.0	CPAPIR
2MASS J06085283-2753583	06 08 52.83	-27 53 58.3	M9.5	—	-0.013 ± 0.011	-0.002 ± 0.013	8.1	CPAPIR
2MASS J06160532-4557080	06 16 05.32	-45 57 08.0	L2	—	-0.057 ± 0.014	0.114 ± 0.020	8.2	CPAPIR

Continued on Next Page...

Table 2.11 – Continued

Source Name (1)	RA (J2000) (2)	DEC (J2000) (3)	SpT[1] (optical) (4)	SpT (near-IR) (5)	$\mu_\alpha cos(\delta)$ ($''$ yr^{-1}) (6)	μ_δ ($''$ yr^{-1}) (7)	Baseline (yrs) (8)	Instrument (9)
2MASS J06193544-5249367	06 19 35.44	-52 49 36.7	M9	—	0.057 ± 0.012	0.172 ± 0.020	8.2	CPAPIR
2MASS J06244595-4521548	06 24 45.95	-45 21 54.8	L5	—	-0.045 ± 0.011	0.370 ± 0.015	7.3	CPAPIR
SDSS J062621.22+002934.2	06 26 21.21	+00 29 34.1	L1	—	0.084 ± 0.015	-0.092 ± 0.015	8.0	TIFKAM
2MASS J06322402-5010349	06 32 24.02	-50 10 34.9	L3	—	-0.103 ± 0.013	-0.018 ± 0.021	8.2	CPAPIR
2MASS J06395596-7418446	06 39 55.96	-74 18 44.6	L5	—	0.000 ± 0.005	-0.002 ± 0.019	9.1	CPAPIR
2MASS J06411840-4322329	06 41 18.40	-43 22 32.9	L1.5	—	0.189 ± 0.013	0.613 ± 0.018	8.8	CPAPIR
2MASS J06524851-5741376	06 52 48.47	-57 41 37.6	M8	—	-0.007 ± 0.008	0.025 ± 0.015	7.3	CPAPIR
SDSS J065405.63+652805.4	06 54 05.64	+65 28 05.1	—	L6	-0.015 ± 0.006	0.030 ± 0.015	8.8	TIFKAM
2MASSW J0708213+295035	07 08 21.33	+29 50 35.0	L5	—	0.040 ± 0.014	-0.236 ± 0.016	10.0	CPAPIR
2MASSW J0717163+570543	07 17 16.26	+57 05 43.0	—	L6.5	-0.016 ± 0.009	0.046 ± 0.016	8.9	TIFKAM
2MASS J07193188-5051410	07 19 31.88	-50 51 41.0	L0	—	0.190 ± 0.013	-0.060 ± 0.020	7.9	CPAPIR
2MASS J07231462+5727081	07 23 14.62	+57 27 08.1	L1	—	0.062 ± 0.011	-0.238 ± 0.020	9.3	TIFKAM
2MASS J07290002-3954043	07 29 00.02	-39 54 04.3	—	T8	-0.578 ± 0.014	1.636 ± 0.018	8.9	CPAPIR
SDSS J073922.26+661503.5	07 39 22.03	+66 15 03.9	—	T1	0.180 ± 0.010	-0.077 ± 0.026	9.2	TIFKAM
SDSS J074007.30+200921.9	07 40 07.12	+20 09 21.6	—	L6	-0.185 ± 0.015	-0.111 ± 0.016	10.1	CPAPIR
2MASSW J0740096+321203	07 40 09.66	+32 12 03.2	L4.5	—	-0.029 ± 0.010	-0.084 ± 0.012	9.7	TIFKAM
SDSS J074149.15+235127.5	07 41 49.20	+23 51 27.5	—	T5	-0.243 ± 0.013	-0.143 ± 0.014	10.0	TIFKAM
SDSS J074201.41+205520.5	07 42 01.30	+20 55 19.8	—	T5	-0.316 ± 0.018	-0.255 ± 0.020	10.0	TIFKAM
2MASSI J0746425+200032	07 46 42.56	+20 00 32.1	L0.5	L1	-0.362 ± 0.012	-0.042 ± 0.013	9.2	CPAPIR
SDSS J074756.31+394732.9	07 47 56.31	+39 47 32.9	L0	—	0.052 ± 0.012	-0.057 ± 0.015	9.6	TIFKAM
SDSS J075259.43+413634.6	07 52 59.42	+41 36 34.4	L0	—	-0.014 ± 0.020	0.041 ± 0.027	10.1	TIFKAM
2MASSI J0753321+291711	07 53 32.17	+29 17 11.9	L2	—	-0.090 ± 0.012	-0.102 ± 0.013	9.8	TIFKAM
SDSS J075515.26+293445.4	07 55 15.28	+29 34 45.3	—	L3.5	-0.092 ± 0.019	-0.074 ± 0.022	10.3	TIFKAM
2MASSI J0755480+221218	07 55 47.95	+22 12 16.9	T6	T5	-0.034 ± 0.016	-0.248 ± 0.017	9.2	CPAPIR
2MASSI J0756252+124456	07 56 25.29	+12 44 56.0	L6	—	0.004 ± 0.015	-0.056 ± 0.016	10.2	CPAPIR
SDSS J075656.54+231458.5	07 56 56.31	+23 14 57.7	—	L3.5	0.158 ± 0.016	-0.156 ± 0.017	9.2	CPAPIR
SDSS J075840.33+324723.4	07 58 40.37	+32 47 24.5	—	T2	-0.191 ± 0.014	-0.349 ± 0.017	9.6	TIFKAM
2MASS J07592947+0323564	07 59 29.47	+03 23 56.4	M7	—	-0.052 ± 0.020	-0.003 ± 0.020	8.1	CPAPIR
2MASSW J0801405+462850	08 01 40.56	+46 28 49.8	L6.5	—	-0.200 ± 0.009	-0.335 ± 0.013	9.6	TIFKAM
2MASS J08041429+0330474	08 04 14.29	+03 30 47.4	M8.5	—	-0.006 ± 0.020	-0.013 ± 0.020	8.0	CPAPIR
SDSS J080531.84+481233.0	08 05 31.89	+48 12 33.0	L4	L9	-0.455 ± 0.012	0.054 ± 0.018	8.9	TIFKAM
SDSS J080959.01+443422.2	08 09 59.03	+44 34 21.6	—	L6	-0.198 ± 0.014	-0.214 ± 0.019	8.3	TIFKAM
2MASS J08151407+1030117	08 15 14.07	+10 30 11.7	M7	—	-0.059 ± 0.020	0.048 ± 0.020	7.9	CPAPIR
2MASS J08194602+1658539	08 19 46.02	+16 58 53.9	M9	—	-0.160 ± 0.016	-0.035 ± 0.017	9.4	TIFKAM
2MASSW J0820299+450031	08 20 29.96	+45 00 31.5	L5	—	-0.111 ± 0.009	-0.323 ± 0.012	9.6	TIFKAM
SDSS J082030.12+103737.0	08 20 30.13	+10 37 37.2	—	L9.5	-0.077 ± 0.017	-0.026 ± 0.017	7.8	TIFKAM

Continued on Next Page...

Table 2.11 – Continued

Source Name (1)	RA (J2000) (2)	DEC (J2000) (3)	SpT[1] (optical) (4)	SpT (near-IR) (5)	$\mu_\alpha cos(\delta)$ ($''$ yr^{-1}) (6)	μ_δ ($''$ yr^{-1}) (7)	Baseline (yrs) (8)	Instrument (9)
2MASS J08234818+2428577	08 23 48.18	+24 28 57.7	L3	—	-0.170 ± 0.014	0.062 ± 0.015	8.0	TIFKAM
2MASSW J0829066+145622	08 29 06.64	+14 56 22.5	L2	—	-0.048 ± 0.010	-0.244 ± 0.010	10.0	TIFKAM
2MASS J08294908-0012241	08 29 49.08	-00 12 24.1	M7	—	-0.197 ± 0.017	0.175 ± 0.017	9.1	CPAPIR
2MASSW J0829570+265510	08 29 57.07	+26 55 09.9	L6.5	—	-0.099 ± 0.015	-0.043 ± 0.017	10.0	CPAPIR
SDSS J083048.80+012831.1	08 30 48.78	+01 28 31.1	—	T4.5	0.236 ± 0.020	-0.312 ± 0.020	8.0	CPAPIR
2MASS J08315598+1025417	08 31 55.98	+10 25 41.7	M9	—	-0.049 ± 0.021	-0.184 ± 0.021	7.9	CPAPIR
2MASSW J0832045-012835	08 32 04.51	-01 28 36.0	L1.5	—	0.070 ± 0.015	0.003 ± 0.015	9.0	TIFKAM
SDSS J083506.16+195304.4	08 35 06.22	+19 53 05.0	—	L4.5	-0.158 ± 0.013	-0.108 ± 0.014	9.1	TIFKAM
2MASS J08352366+1029318	08 35 23.66	+10 29 31.8	M7	—	-0.050 ± 0.022	-0.179 ± 0.022	7.2	CPAPIR
2MASS J08355829+0548308	08 35 58.29	+05 48 30.8	L3	—	-0.099 ± 0.021	-0.020 ± 0.021	7.9	CPAPIR
2MASS J08391608+1253543	08 39 16.08	+12 53 54.3	M9	—	-0.044 ± 0.015	-0.127 ± 0.016	10.2	CPAPIR
2MASSI J0847287-153237	08 47 28.72	-15 32 37.2	L2	—	0.145 ± 0.012	-0.183 ± 0.013	8.1	CPAPIR
2MASS J08500174-1924184	08 50 01.74	-19 24 18.4	M8	—	-0.116 ± 0.017	0.045 ± 0.018	8.9	CPAPIR
SDSS J085116.20+181730.0	08 51 16.27	+18 17 30.2	—	L4.5	-0.195 ± 0.018	-0.050 ± 0.019	9.2	CPAPIR
SDSS J085234.90+472035.0	08 52 34.90	+47 20 35.9	—	L9.5	-0.069 ± 0.018	-0.418 ± 0.026	9.4	TIFKAM
2MASSI J0856479+223518	08 56 47.93	+22 35 18.2	L3	—	-0.208 ± 0.017	-0.006 ± 0.018	9.2	CPAPIR
2MASS J08572787-0332396	08 57 27.87	-03 32 39.6	M9.5	—	-0.150 ± 0.018	-0.056 ± 0.018	9.2	CPAPIR
SDSSp J085758.45+570851.4	08 57 58.49	+57 08 51.4	L8	L8	-0.413 ± 0.006	-0.349 ± 0.012	8.0	TIFKAM
SDSS J085834.42+325627.7	08 58 34.67	+32 56 27.5	—	T1	-0.760 ± 0.023	0.075 ± 0.023	9.7	TIFKAM
2MASSI J0859254-194926	08 59 25.47	-19 49 26.8	L6	—	-0.300 ± 0.013	-0.081 ± 0.014	8.1	CPAPIR
2MASS J08593854+6341355	08 59 38.54	+63 41 35.5	L0	—	-0.096 ± 0.019	-0.495 ± 0.042	8.3	TIFKAM
2MASS J08594029+1145325	08 59 40.29	+11 45 32.5	M8	—	-0.275 ± 0.021	-0.060 ± 0.021	7.9	CPAPIR
2MASS J09054654+5623117	09 05 46.54	+56 23 11.7	L5	—	-0.014 ± 0.017	0.089 ± 0.031	8.3	TIFKAM
SDSS J090900.73+652527.2	09 09 00.85	+65 25 27.5	—	T1	-0.217 ± 0.003	-0.138 ± 0.008	7.9	TIFKAM
DENIS-P J0909-0658	09 09 57.49	-06 58 18.6	L0	—	-0.210 ± 0.018	0.015 ± 0.019	9.0	CPAPIR
2MASSW J0913032+184150	09 13 03.20	+18 41 50.1	L3	—	0.032 ± 0.016	-0.187 ± 0.017	10.0	CPAPIR
2MASS J09153413+0422045	09 15 34.13	+04 22 04.5	L7	—	-0.109 ± 0.025	0.031 ± 0.025	6.9	CPAPIR
2MASS J09161504+2139512	09 16 15.04	+21 39 51.2	M9	—	-0.199 ± 0.017	-0.054 ± 0.018	10.3	TIFKAM
2MASSW J0918382+213406	09 18 38.15	+21 34 05.8	L2.5	—	0.330 ± 0.015	-0.156 ± 0.017	10.0	CPAPIR
2MASSW J0920122+351742	09 20 12.23	+35 17 42.9	L6.5	T0	-0.167 ± 0.009	-0.200 ± 0.010	9.7	TIFKAM
2MASS J09211410-2104446	09 21 14.10	-21 04 44.6	L2	—	0.244 ± 0.016	-0.908 ± 0.017	7.0	CPAPIR
2MASS J09221952-8010399	09 22 19.52	-80 10 39.9	L4	—	0.041 ± 0.004	-0.045 ± 0.022	8.1	CPAPIR
SDSS J092757.46+602746.3	09 27 57.41	+60 27 46.4	L1	—	0.003 ± 0.013	0.016 ± 0.025	9.3	TIFKAM
2MASS J09282562+4230545	09 28 25.62	+42 30 54.5	M8.5	—	-0.390 ± 0.019	-0.378 ± 0.025	9.2	TIFKAM
2MASSW J0928397-160312	09 28 39.72	-16 03 12.8	L2	—	-0.158 ± 0.017	0.034 ± 0.017	9.8	CPAPIR
SDSS J093109.56+032732.5	09 31 09.55	+03 27 33.1	—	L7.5	-0.612 ± 0.018	-0.131 ± 0.018	7.1	CPAPIR

Continued on Next Page...

Table 2.11 – Continued

Source Name (1)	RA (J2000) (2)	DEC (J2000) (3)	SpT[1] (optical) (4)	SpT (near-IR) (5)	$\mu_\alpha cos(\delta)$ ($''$ yr^{-1}) (6)	μ_δ ($''$ yr^{-1}) (7)	Baseline (yrs) (8)	Instrument (9)
2MASS J09312823+0528223	09 31 28.23	+05 28 22.3	M7	—	-0.142 ± 0.021	-0.204 ± 0.021	8.0	CPAPIR
2MASS J09342920-1352434	09 34 29.20	-13 52 43.4	M7	—	-0.238 ± 0.016	-0.127 ± 0.017	9.8	CPAPIR
2MASS J09352803-2934596	09 35 28.03	-29 34 59.6	L0	—	-0.023 ± 0.016	0.064 ± 0.018	8.9	CPAPIR
2MASS J09384022-2748184	09 38 40.22	-27 48 18.4	M8	—	-0.408 ± 0.017	-0.164 ± 0.020	7.9	CPAPIR
2MASS J09393548-2448279	09 39 35.48	-24 48 27.9	—	T8	0.592 ± 0.019	-1.064 ± 0.021	7.9	CPAPIR
2MASS J09424604+5531025	09 42 46.04	+55 31 02.5	M8	—	-0.066 ± 0.018	0.085 ± 0.032	9.3	TIFKAM
2MASS J09474477+0224327	09 47 44.77	+02 24 32.7	M8	—	-0.081 ± 0.020	-0.162 ± 0.020	8.0	CPAPIR
2MASS J09532126-1014205	09 53 21.26	-10 14 20.5	L0	—	-0.048 ± 0.019	-0.089 ± 0.019	9.0	CPAPIR
2MASSW J1004392-333518	10 04 39.29	-33 35 18.9	L4	—	0.366 ± 0.016	-0.340 ± 0.019	8.7	CPAPIR
SDSS J100711.74+193056.2	10 07 11.85	+19 30 56.3	—	L8	-0.263 ± 0.015	-0.018 ± 0.016	10.0	CPAPIR
2MASS J10073369-4555147	10 07 33.69	-45 55 14.7	—	T5	-0.758 ± 0.013	0.138 ± 0.019	7.9	CPAPIR
2MASS J10184314-1624273	10 18 43.14	-16 24 27.3	M7.5	—	0.053 ± 0.015	-0.017 ± 0.016	9.8	CPAPIR
2MASSW J1018588-290953	10 18 58.79	-29 09 53.5	L1	—	-0.319 ± 0.017	-0.086 ± 0.019	8.9	CPAPIR
2MASS J10213232-2044069	10 21 32.32	-20 44 06.9	M9	—	-0.312 ± 0.016	-0.051 ± 0.017	8.8	CPAPIR
2MASS J10220489+0200477	10 22 04.89	+02 00 47.7	M9	—	-0.178 ± 0.018	-0.394 ± 0.018	7.1	CPAPIR
SDSS J102552.43+321234.0	10 25 52.27	+32 12 34.9	—	L7.5	0.393 ± 0.011	-0.228 ± 0.013	8.5	TIFKAM
2MASS J10284042-1438439	10 28 40.42	-14 38 43.9	M7	—	0.024 ± 0.016	-0.162 ± 0.016	9.8	CPAPIR
2MASS J10321706+0501032	10 32 17.06	+05 01 03.2	M8.5	—	-0.032 ± 0.021	-0.012 ± 0.021	8.0	CPAPIR
SDSS J103321.92+400549.5	10 33 21.86	+40 05 49.9	—	L6	0.154 ± 0.013	-0.188 ± 0.018	9.1	TIFKAM
2MASSW J1036530-344138	10 36 53.05	-34 41 38.0	L6	—	-0.020 ± 0.015	-0.462 ± 0.019	8.8	CPAPIR
SDSS J103931.35+325625.5	10 39 31.37	+32 56 26.3	—	T1	0.031 ± 0.046	-0.023 ± 0.054	9.7	TIFKAM
2MASS J10430758+2225236	10 43 07.58	+22 25 23.6	L8	—	-0.117 ± 0.015	0.013 ± 0.016	9.1	CPAPIR
SDSSp J104325.10+000148.2	10 43 25.08	+00 01 48.2	L3	—	-0.161 ± 0.019	-0.156 ± 0.019	9.1	CPAPIR
SDSS J104335.08+121314.1	10 43 35.08	+12 13 14.9	—	L7	0.046 ± 0.017	-0.248 ± 0.018	9.2	CPAPIR
2MASS J10451718-2607249	10 45 17.18	-26 07 24.9	M8	—	-0.162 ± 0.017	-0.146 ± 0.019	8.9	CPAPIR
SDSS J104829.21+091937.8	10 48 29.26	+09 19 37.3	—	T2.5	-0.268 ± 0.020	0.241 ± 0.020	7.9	CPAPIR
SDSS J105213.51+442255.7	10 52 13.50	+44 22 55.9	—	T0.5	0.018 ± 0.017	-0.152 ± 0.024	9.6	TIFKAM
2MASS J10544168+1214084	10 54 41.68	+12 14 08.4	M7.5	—	0.103 ± 0.018	-0.080 ± 0.019	8.8	CPAPIR
DENIS-P J1058.7-1548	10 58 47.87	-15 48 17.2	L3	L3	-0.237 ± 0.015	0.014 ± 0.015	8.9	CPAPIR
2MASS J11000965+4957470	11 00 09.65	+49 57 47.0	L3.5	—	-0.133 ± 0.018	-0.151 ± 0.028	9.3	TIFKAM
2MASS J11020983-3430355	11 02 09.90	-34 30 35.5	M8.5	—	-0.033 ± 0.012	-0.024 ± 0.015	7.9	CPAPIR
2MASSW J1102337-235945	11 02 33.75	-23 59 46.4	L4.5	—	-0.238 ± 0.019	0.075 ± 0.020	8.0	CPAPIR
2MASSI J1104012+195921	11 04 01.27	+19 59 21.7	L4	—	0.080 ± 0.022	0.154 ± 0.023	7.7	CPAPIR
2MASS J11061197+2754225	11 06 11.97	+27 54 22.5	—	T2.5	-0.229 ± 0.019	-0.448 ± 0.021	7.8	CPAPIR
2MASS J11103321+5424028	11 10 33.21	+54 24 02.8	M7	—	-0.066 ± 0.009	-0.299 ± 0.016	8.4	TIFKAM
2MASS J11124910-2044315	11 12 49.10	-20 44 31.5	—	L0.5	0.001 ± 0.014	0.023 ± 0.015	8.9	CPAPIR

Continued on Next Page...

Table 2.11 – Continued

Source Name (1)	RA (J2000) (2)	DEC (J2000) (3)	SpT[1] (optical) (4)	SpT (near-IR) (5)	$\mu_\alpha cos(\delta)$ ($''$ yr^{-1}) (6)	μ_δ ($''$ yr^{-1}) (7)	Baseline (yrs) (8)	Instrument (9)
SDSS J111320.16+343057.9	11 13 20.09	+34 30 58.2	—	L3	0.108 ± 0.040	-0.025 ± 0.049	10.0	TIFKAM
2MASS J11145133-2618235	11 14 51.33	-26 18 23.5	—	T7.5	-3.011 ± 0.015	-0.391 ± 0.016	8.0	CPAPIR
2MASSI J1117369+360936	11 17 36.91	+36 09 35.9	L0	—	0.001 ± 0.019	-0.016 ± 0.023	9.2	TIFKAM
SDSS J112118.57+433246.5	11 21 18.58	+43 32 46.4	—	L7.5	-0.057 ± 0.024	0.026 ± 0.033	8.0	TIFKAM
2MASSW J1122362-391605	11 22 36.24	-39 16 05.4	L3	—	0.073 ± 0.012	-0.180 ± 0.015	8.0	CPAPIR
2MASS J11233605+1241222	11 23 36.05	+12 41 22.2	M7	—	-0.036 ± 0.017	0.009 ± 0.017	10.0	CPAPIR
2MASS J11240487+3808054	11 24 04.87	+38 08 05.4	M8.5	—	0.130 ± 0.021	-0.019 ± 0.027	10.0	TIFKAM
SDSS J112615.25+012048.2	11 26 15.28	+01 20 48.1	—	L6	-0.131 ± 0.022	0.042 ± 0.022	7.9	CPAPIR
2MASS J11304761-2210335	11 30 47.61	-22 10 33.5	M8	—	-0.126 ± 0.017	-0.232 ± 0.018	9.7	CPAPIR
2MASS J11345493+0022541	11 34 54.93	+00 22 54.1	M9	—	0.401 ± 0.021	-0.343 ± 0.021	7.9	CPAPIR
SDSS J113833.10+674040.3	11 38 33.08	+67 40 40.3	L0	—	0.024 ± 0.014	-0.127 ± 0.037	9.1	TIFKAM
2MASS J11391107+0841121	11 39 11.07	+08 41 12.1	M7.5	—	0.089 ± 0.021	-0.025 ± 0.022	7.9	CPAPIR
2MASS J11395113-3159214	11 39 51.16	-31 59 21.4	M9	—	-0.071 ± 0.014	-0.017 ± 0.016	7.1	CPAPIR
2MASS J11485427-2544404	11 48 54.27	-25 44 40.4	M8	—	0.147 ± 0.018	0.047 ± 0.020	7.9	CPAPIR
2MASS J11524266+2438079	11 52 42.66	+24 38 07.9	M9	—	-0.451 ± 0.032	0.036 ± 0.035	10.2	TIFKAM
2MASS J11543399+0135545	11 54 33.99	+01 35 54.5	M9	—	0.121 ± 0.022	-0.043 ± 0.022	7.9	CPAPIR
2MASS J11544223-3400390	11 54 42.23	-34 00 39.0	L0	—	-0.161 ± 0.013	0.004 ± 0.015	8.0	CPAPIR
2MASSW J1155395-372735	11 55 39.52	-37 27 35.0	L2	—	0.050 ± 0.012	-0.767 ± 0.015	7.9	CPAPIR
SDSS J115553.86+055957.5	11 55 53.89	+05 59 57.7	—	L7.5	-0.406 ± 0.022	-0.026 ± 0.022	7.9	CPAPIR
2MASS J11580269-2545369	11 58 02.69	-25 45 36.9	M8	—	-0.102 ± 0.019	-0.167 ± 0.021	7.8	CPAPIR
2MASS J11582484+1354456	11 58 24.84	+13 54 45.6	M9	—	-0.116 ± 0.017	0.168 ± 0.018	10.0	CPAPIR
2MASS J12022564-0629026	12 02 25.64	-06 29 02.6	M9	—	0.096 ± 0.019	-0.075 ± 0.019	9.0	CPAPIR
2MASS J12023666-0604054	12 02 36.66	-06 04 05.4	M8	—	0.088 ± 0.018	-0.034 ± 0.018	9.0	CPAPIR
SDSS J120602.51+281328.7	12 06 02.48	+28 13 29.3	—	T3	0.047 ± 0.014	-0.105 ± 0.016	9.7	TIFKAM
2MASS J12070374-3151298	12 07 03.74	-31 51 29.8	L3	—	-0.232 ± 0.016	-0.074 ± 0.019	8.8	CPAPIR
2MASS J12073804-3909050	12 07 38.04	-39 09 05.0	L4	—	-0.142 ± 0.011	0.031 ± 0.015	7.9	CPAPIR
2MASS J12095613-1004008	12 09 56.13	-10 04 00.8	—	T3	0.250 ± 0.019	-0.390 ± 0.019	9.0	CPAPIR
2MASS J12123389+0206280	12 12 33.89	+02 06 28.0	—	L1	0.065 ± 0.021	-0.141 ± 0.021	7.9	CPAPIR
2MASSI J1213033-043243	12 13 03.36	-04 32 43.7	L5	—	-0.388 ± 0.020	-0.013 ± 0.020	9.0	CPAPIR
SDSS J121440.95+631643.4	12 14 40.89	+63 16 43.4	—	T3.5	0.165 ± 0.030	-0.021 ± 0.068	7.9	TIFKAM
2MASS J12154432-3420591	12 15 44.32	-34 20 59.1	—	T4.5	-0.212 ± 0.017	-0.310 ± 0.021	7.8	CPAPIR
2MASS J12155348+0050498	12 15 53.48	+00 50 49.8	M8	—	0.220 ± 0.020	-0.398 ± 0.020	7.9	CPAPIR
2MASS J12162161+4456340	12 16 21.61	+44 56 34.0	L5	—	-0.035 ± 0.014	-0.004 ± 0.019	8.1	TIFKAM
SDSS J121659.17+300306.3	12 16 59.18	+30 03 05.4	—	L3.5	-0.021 ± 0.017	0.115 ± 0.019	10.1	TIFKAM
2MASS J12172935+0035326	12 17 29.35	+00 35 32.6	M7.5	—	0.078 ± 0.026	-0.001 ± 0.026	6.9	CPAPIR
2MASS J12185957-0550282	12 18 59.57	-05 50 28.2	M8.5	—	-0.279 ± 0.019	-0.036 ± 0.019	9.0	CPAPIR

Continued on Next Page...

Table 2.11 – Continued

Source Name (1)	RA (J2000) (2)	DEC (J2000) (3)	SpT[1] (optical) (4)	SpT (near-IR) (5)	$\mu_\alpha cos(\delta)$ ($''$ yr^{-1}) (6)	μ_δ ($''$ yr^{-1}) (7)	Baseline (yrs) (8)	Instrument (9)
SDSS J121951.45+312849.4	12 19 51.56	+31 28 49.7	—	L8	-0.250 ± 0.026	-0.017 ± 0.031	10.1	TIFKAM
2MASS J12215066-0843197	12 21 50.66	-08 43 19.7	M8	—	-0.192 ± 0.019	0.015 ± 0.019	9.0	CPAPIR
2MASS J12271545-0636458	12 27 15.45	-06 36 45.8	M9	—	-0.106 ± 0.019	-0.085 ± 0.019	9.0	CPAPIR
SDSS J122855.38+005044.1	12 28 55.38	+00 50 44.0	L0	—	-0.041 ± 0.021	-0.038 ± 0.021	7.9	CPAPIR
2MASS J12312141+4959234	12 31 21.41	+49 59 23.4	L2	—	-0.053 ± 0.019	-0.022 ± 0.030	9.2	TIFKAM
2MASS J12314753+0847331	12 31 47.53	+08 47 33.1	—	T5.5	-1.176 ± 0.021	-1.043 ± 0.021	7.8	CPAPIR
2MASS J12473570-1219518	12 47 35.70	-12 19 51.8	M8.5	—	0.036 ± 0.018	-0.223 ± 0.018	9.8	CPAPIR
SDSS J125011.65+392553.9	12 50 11.66	+39 25 58.2	—	T4	-0.015 ± 0.008	-0.828 ± 0.011	9.6	TIFKAM
2MASS J12522042-3149288	12 52 20.42	-31 49 28.8	M8	—	0.166 ± 0.016	-0.032 ± 0.019	8.8	CPAPIR
2MASSW J1300425+191235	13 00 42.55	+19 12 35.4	L1	L3	-0.820 ± 0.018	-1.244 ± 0.019	8.8	CPAPIR
2MASS J13015465-1510223	13 01 54.65	-15 10 22.3	L1	—	-0.086 ± 0.016	-0.075 ± 0.017	7.9	CPAPIR
2MASS J13023897+0351410	13 02 38.97	+03 51 41.0	M7.5	—	-0.039 ± 0.021	0.025 ± 0.021	7.9	CPAPIR
2MASS J13061727+3820296	13 06 17.27	+38 20 29.6	L1	—	-0.175 ± 0.027	-0.008 ± 0.035	8.3	TIFKAM
2MASS J13082507+0725512	13 08 25.07	+07 25 51.2	M9	—	0.259 ± 0.021	-0.416 ± 0.021	7.8	CPAPIR
SDSSp J131415.52-000848.1	13 14 15.51	-00 08 48.0	—	L3.5	-0.001 ± 0.023	0.073 ± 0.023	7.0	CPAPIR
2MASSI J1315309-264951	13 15 30.94	-26 49 51.3	L5.5	—	-0.682 ± 0.013	-0.282 ± 0.014	8.8	CPAPIR
2MASS J13204159+0957506	13 20 41.59	+09 57 50.6	M7.5	—	-0.236 ± 0.021	-0.129 ± 0.021	7.9	CPAPIR
DENIS-P J1323-1806	13 23 35.97	-18 06 37.9	L0	—	-0.097 ± 0.016	-0.024 ± 0.017	8.0	CPAPIR
2MASS J13235206+3014340	13 23 52.06	+30 14 34.0	M8.5	—	-0.695 ± 0.023	0.156 ± 0.027	8.1	TIFKAM
2MASSW J1326201-272937	13 26 20.09	-27 29 37.0	L5	—	-0.368 ± 0.014	-0.028 ± 0.016	8.0	CPAPIR
2MASS J13290099-4147133	13 29 00.99	-41 47 13.3	M9	—	0.231 ± 0.013	-0.280 ± 0.017	8.7	CPAPIR
2MASS J13373116+4938367	13 37 31.16	+49 38 36.7	L0	—	0.039 ± 0.016	0.049 ± 0.025	8.9	TIFKAM
2MASS J13411160-3052505	13 41 11.60	-30 52 50.5	L3	—	0.030 ± 0.013	-0.134 ± 0.015	7.9	CPAPIR
SDSS J134203.11+134022.2	13 42 03.11	+13 40 22.2	—	L5.5	0.000 ± 0.019	-0.027 ± 0.019	9.1	CPAPIR
2MASS J13435275-3851385	13 43 52.75	-38 51 38.5	M8	—	-0.044 ± 0.014	-0.016 ± 0.018	8.8	CPAPIR
DENIS-P J1347590-761005	13 47 59.11	-76 10 05.4	—	L0	0.203 ± 0.005	0.038 ± 0.020	7.9	CPAPIR
2MASS J13480100-0304328	13 48 01.00	-03 04 32.8	M7	—	0.191 ± 0.020	-0.408 ± 0.020	8.6	CPAPIR
2MASS J13571237+1428398	13 57 12.37	+14 28 39.8	—	L4	0.069 ± 0.052	-0.006 ± 0.053	8.3	TIFKAM
SDSS J135852.68+374711.9	13 58 52.69	+37 47 13.7	—	T4.5	-0.010 ± 0.013	-0.411 ± 0.016	10.0	TIFKAM
SDSS J135923.99+472843.2	13 59 24.03	+47 28 43.1	—	L8.5	-0.144 ± 0.010	0.034 ± 0.014	9.0	TIFKAM
2MASS J13595510-4034582	13 59 55.10	-40 34 58.2	L1	—	0.038 ± 0.011	-0.485 ± 0.015	7.9	CPAPIR
SDSS J140023.12+433822.3	14 00 23.20	+43 38 22.2	—	L7	-0.235 ± 0.020	0.012 ± 0.028	9.0	TIFKAM
2MASS J14022235+0648479	14 02 22.35	+06 48 47.9	M9	—	0.056 ± 0.021	-0.006 ± 0.021	7.8	CPAPIR
SDSS J140231.75+014830.3	14 02 31.75	+01 48 30.1	L1	—	-0.230 ± 0.018	0.015 ± 0.018	7.0	CPAPIR
SDSS J140255.66+080055.2	14 02 55.64	+08 00 55.3	—	T1	0.065 ± 0.021	-0.098 ± 0.022	7.8	CPAPIR
SDSS J140441.68+023550.1	14 04 41.67	+02 35 50.1	L1	—	0.072 ± 0.019	-0.226 ± 0.019	7.0	CPAPIR

Continued on Next Page...

Table 2.11 – Continued

Source Name (1)	RA (J2000) (2)	DEC (J2000) (3)	SpT[1] (optical) (4)	SpT (near-IR) (5)	$\mu_\alpha cos(\delta)$ ($''$ yr^{-1}) (6)	μ_δ ($''$ yr^{-1}) (7)	Baseline (yrs) (8)	Instrument (9)
2MASS J14090310-3357565	14 09 03.10	-33 57 56.5	L2	—	0.089 ± 0.012	0.047 ± 0.014	8.0	CPAPIR
2MASS J14122268+2354108	14 12 22.68	+23 54 10.8	M9	—	-0.175 ± 0.036	0.068 ± 0.039	8.1	TIFKAM
SDSS J141530.05+572428.7	14 15 30.03	+57 24 30.0	—	T3	0.043 ± 0.013	-0.345 ± 0.025	9.2	TIFKAM
SDSS J141659.78+500626.4	14 16 59.87	+50 06 25.8	—	L5.5	-0.297 ± 0.013	0.188 ± 0.021	8.1	TIFKAM
2MASS J14193867-3136519	14 19 38.67	-31 36 51.9	M7	—	-0.041 ± 0.018	0.028 ± 0.021	7.8	CPAPIR
SDSS J142227.25+221557.1	14 22 27.20	+22 15 57.5	—	L6.5	0.047 ± 0.019	-0.054 ± 0.020	7.9	CPAPIR
DENIS-P J142527.97-365023.4	14 25 27.98	-36 50 22.9	—	L5	-0.268 ± 0.015	-0.473 ± 0.019	8.5	CPAPIR
2MASS J14360977+2900350	14 36 09.77	+29 00 35.0	M8.5	—	-0.098 ± 0.018	0.068 ± 0.021	9.1	TIFKAM
2MASS J14384542+5559134	14 38 45.42	+55 59 13.4	M7	—	-0.062 ± 0.015	-0.059 ± 0.027	9.1	TIFKAM
2MASSW J1438549-130910	14 38 54.98	-13 09 10.3	L3	—	0.154 ± 0.016	-0.022 ± 0.017	9.0	CPAPIR
SDSS J143933.44+031759.2	14 39 33.43	+03 17 59.1	L1	—	-0.013 ± 0.021	0.030 ± 0.021	7.0	CPAPIR
SDSS J144016.20+002638.9	14 40 16.22	+00 26 39.0	L3	L1	-0.006 ± 0.021	0.004 ± 0.021	7.8	CPAPIR
2MASS J14410457+2719323	14 41 04.57	+27 19 32.3	M7	—	0.089 ± 0.030	-0.053 ± 0.034	9.1	TIFKAM
SDSS J144128.52+504600.4	14 41 28.46	+50 46 00.5	—	L3	0.077 ± 0.013	-0.109 ± 0.021	9.9	TIFKAM
DENIS-P J1441-0945, G 124-62B	14 41 37.16	-09 45 59.0	L0.5	—	-0.182 ± 0.016	-0.038 ± 0.016	8.0	CPAPIR
2MASSW J1448256+103159	14 48 25.63	+10 31 59.0	—	L3.5	0.262 ± 0.022	-0.120 ± 0.022	7.7	CPAPIR
2MASS J14532303+1543081	14 53 23.03	+15 43 08.1	M7.5	—	-0.011 ± 0.018	0.028 ± 0.018	8.9	TIFKAM
Gliese 570D	14 57 14.96	-21 21 47.7	T7	T7.5	1.028 ± 0.013	-1.688 ± 0.014	8.9	CPAPIR
2MASS J14582453+2839580	14 58 24.53	+28 39 58.0	M8	—	-0.109 ± 0.024	-0.432 ± 0.028	8.9	TIFKAM
2MASS J15004572+4219448	15 00 45.72	+42 19 44.8	M9	—	0.136 ± 0.011	-0.065 ± 0.015	8.2	TIFKAM
SDSS J150240.80+613815.5	15 02 40.82	+61 38 15.8	L1	—	-0.098 ± 0.010	0.036 ± 0.022	9.0	TIFKAM
2MASSW J1507476-162738	15 07 47.69	-16 27 38.6	L5	L5.5	-0.128 ± 0.014	-0.906 ± 0.015	8.9	CPAPIR
SDSS J151114.66+060742.9	15 11 14.66	+06 07 43.1	—	T0	-0.252 ± 0.021	-0.256 ± 0.021	7.0	CPAPIR
2MASS J15124058+3403501	15 12 40.58	+34 03 50.1	—	L1	0.228 ± 0.010	-0.010 ± 0.012	10.1	TIFKAM
SDSS J151506.11+443648.3	15 15 06.07	+44 36 48.3	—	L7.5	0.075 ± 0.019	-0.020 ± 0.027	8.9	TIFKAM
SDSS J151603.03+025928.9	15 16 03.03	+02 59 29.2	—	T0	-0.048 ± 0.022	-0.174 ± 0.022	7.7	CPAPIR
SDSS J151643.01+305344.4	15 16 43.06	+30 53 44.3	—	T0.5	-0.132 ± 0.021	0.004 ± 0.024	10.1	TIFKAM
SDSS J152039.82+354619.8	15 20 39.74	+35 46 21.0	—	T0	0.279 ± 0.023	-0.386 ± 0.028	8.2	TIFKAM
SDSS J152103.24+013142.7	15 21 03.27	+01 31 42.6	—	T2	-0.232 ± 0.018	0.085 ± 0.018	6.9	CPAPIR
SDSS J152531.32+581053.1	15 25 31.32	+58 10 52.5	—	L6.5	0.064 ± 0.015	0.044 ± 0.028	9.0	TIFKAM
2MASSI J1526140+204341	15 26 14.05	+20 43 41.4	L7	—	-0.207 ± 0.018	-0.362 ± 0.019	10.9	TIFKAM
ULAS J153108.89+060111.1	15 31 08.88	+06 01 11.2	L0	—	0.028 ± 0.025	-0.048 ± 0.025	8.0	TIFKAM
2MASS J15311344+1641282	15 31 13.44	+16 41 28.2	—	L1	-0.076 ± 0.025	0.040 ± 0.026	9.2	TIFKAM
SDSS J153417.05+161546.1AB	15 34 17.11	+16 15 46.3	—	T3.5	-0.066 ± 0.020	-0.052 ± 0.021	9.1	TIFKAM
SDSS J153453.33+121949.2	15 34 53.25	+12 19 49.5	—	L4	0.177 ± 0.020	-0.040 ± 0.021	9.1	TIFKAM
2MASS J15382417-1953116	15 38 24.17	-19 53 11.6	L6	—	0.032 ± 0.019	-0.061 ± 0.020	9.9	TIFKAM

Continued on Next Page...

Table 2.11 – Continued

Source Name (1)	RA (J2000) (2)	DEC (J2000) (3)	SpT[1] (optical) (4)	SpT (near-IR) (5)	$\mu_\alpha cos(\delta)$ ($''$ yr^{-1}) (6)	μ_δ ($''$ yr^{-1}) (7)	Baseline (yrs) (8)	Instrument (9)
2MASS J15392137+6502364	15 39 21.37	+65 02 36.4	—	L1	-0.038 ± 0.011	0.038 ± 0.025	9.0	TIFKAM
SDSS J154009.36+374230.3	15 40 09.42	+37 42 31.6	—	L9	-0.205 ± 0.016	-0.382 ± 0.020	8.1	TIFKAM
SDSS J154508.93+355527.3	15 45 09.01	+35 55 27.1	—	L7.5	-0.183 ± 0.016	0.063 ± 0.020	10.1	TIFKAM
SDSS J154727.23+033636.3	15 47 27.23	+03 36 36.1	L2	—	-0.062 ± 0.019	0.056 ± 0.019	6.9	CPAPIR
2MASS J15474719-2423493	15 47 47.19	-24 23 49.3	L0	—	-0.126 ± 0.014	-0.143 ± 0.015	7.9	CPAPIR
SDSS J154849.02+172235.4	15 48 49.12	+17 22 35.9	—	L5	-0.277 ± 0.019	-0.109 ± 0.019	9.2	TIFKAM
2MASS J15485834-1636018	15 48 58.34	-16 36 01.8	—	L2	-0.210 ± 0.016	-0.107 ± 0.017	9.8	CPAPIR
2MASS J15515237+0941148	15 51 52.37	+09 41 14.8	L2	—	-0.070 ± 0.022	-0.050 ± 0.022	8.0	TIFKAM
2MASSW J1553214+210907	15 53 21.42	+21 09 07.1	L5.5	—	-0.045 ± 0.015	0.114 ± 0.016	10.9	TIFKAM
2MASSW J1555157-095605	15 55 15.73	-09 56 05.5	L1	—	0.950 ± 0.015	-0.767 ± 0.015	8.0	CPAPIR
2MASS J16062665+6837268	16 06 26.65	+68 37 26.8	—	L2	-0.083 ± 0.008	0.043 ± 0.023	8.9	TIFKAM
SDSS J161626.46+221859.2	16 16 26.49	+22 18 59.1	—	L5	-0.073 ± 0.018	0.021 ± 0.019	9.9	TIFKAM
SDSS J161731.65+401859.7	16 17 31.68	+40 19 00.3	—	L4	-0.038 ± 0.014	-0.132 ± 0.019	10.0	TIFKAM
2MASS J16184503-1321297	16 18 45.03	-13 21 29.7	L0	—	-0.094 ± 0.015	-0.081 ± 0.015	7.9	CPAPIR
SDSS J162051.17+323732.1	16 20 51.16	+32 37 32.2	—	L6	0.015 ± 0.011	-0.033 ± 0.014	10.1	TIFKAM
SDSS J162255.27+115924.1	16 22 55.33	+11 59 23.8	—	L6	-0.128 ± 0.025	-0.012 ± 0.026	9.1	TIFKAM
SDSS J162838.77+230821.1	16 28 38.55	+23 08 24.1	—	T7	0.497 ± 0.020	-0.461 ± 0.021	10.9	TIFKAM
SDSS J163022.92+081822.0	16 30 22.95	+08 18 22.1	—	T5.5	-0.083 ± 0.018	-0.084 ± 0.019	6.8	CPAPIR
SDSS J163030.53+434404.0	16 30 30.54	+43 44 03.2	—	L7	-0.138 ± 0.020	0.052 ± 0.028	8.1	TIFKAM
2MASS J16304139+0938446	16 30 41.39	+09 38 44.6	L0	—	-0.058 ± 0.018	-0.069 ± 0.018	6.8	CPAPIR
SDSS J163359.23-064056.5	16 33 59.33	-06 40 55.2	—	L6	-0.232 ± 0.015	-0.195 ± 0.015	7.9	CPAPIR
2MASS J16452207+3004071	16 45 22.07	+30 04 07.1	L3	—	-0.065 ± 0.019	-0.065 ± 0.022	9.0	TIFKAM
2MASSW J1645221-131951	16 45 22.11	-13 19 51.6	L1.5	—	-0.352 ± 0.015	-0.801 ± 0.016	7.9	CPAPIR
2MASS J16490419+0444571	16 49 04.19	+04 44 57.1	M8	—	0.054 ± 0.023	0.083 ± 0.023	7.9	TIFKAM
SDSS J165329.69+623136.5	16 53 29.70	+62 31 36.4	L3	—	0.031 ± 0.016	-0.024 ± 0.035	8.0	TIFKAM
2MASSI J1656188+283506	16 56 18.85	+28 35 05.6	L4.5	—	0.011 ± 0.027	-0.027 ± 0.031	8.2	TIFKAM
DENIS-P J170548.38-051645.7	17 05 48.34	-05 16 46.2	—	L4	0.141 ± 0.015	-0.101 ± 0.015	8.0	CPAPIR
SDSS J171147.17+233130.5	17 11 47.16	+23 31 31.0	—	L3.5	0.010 ± 0.017	-0.085 ± 0.018	10.9	TIFKAM
SDSS J171714.10+652622.2	17 17 14.08	+65 26 22.1	L4	—	0.159 ± 0.007	-0.092 ± 0.016	8.9	TIFKAM
SDSS J172244.32+632946.8	17 22 44.32	+63 29 47.0	L0	—	0.013 ± 0.012	-0.038 ± 0.027	8.9	TIFKAM
SDSS J173101.41+531047.9	17 31 01.40	+53 10 47.6	—	L6	0.064 ± 0.011	0.162 ± 0.018	9.8	TIFKAM
2MASSW J1743415+212707	17 43 41.48	+21 27 06.9	L2.5	—	0.159 ± 0.018	0.233 ± 0.019	8.9	TIFKAM
2MASS J17461199+5034036	17 46 11.99	+50 34 03.6	L5	—	0.258 ± 0.018	0.025 ± 0.028	8.1	TIFKAM
2MASS J19285196-4356256	19 28 51.96	-43 56 25.6	L5	—	0.066 ± 0.012	-0.273 ± 0.016	6.9	CFIM
2MASS J19360187-5502322	19 36 01.87	-55 02 32.2	L5	—	0.169 ± 0.009	-0.298 ± 0.016	7.0	CPAPIR
2MASS J20025073-0521524	20 02 50.73	-05 21 52.4	L6	—	-0.102 ± 0.014	-0.110 ± 0.014	8.5	CPAPIR

Continued on Next Page...

Table 2.11 – Continued

Source Name (1)	RA (J2000) (2)	DEC (J2000) (3)	SpT[1] (optical) (4)	SpT (near-IR) (5)	$\mu_\alpha cos(\delta)$ ($''$ yr^{-1}) (6)	μ_δ ($''$ yr^{-1}) (7)	Baseline (yrs) (8)	Instrument (9)
2MASS J20343769+0827009	20 34 37.69	+08 27 00.9	L3	—	-0.096 ± 0.016	-0.489 ± 0.016	7.3	CFIM
2MASS J20360316+1051295	20 36 03.16	+10 51 29.5	L3	—	-0.132 ± 0.017	-0.184 ± 0.018	7.5	TIFKAM
2MASS J20414283-3506442	20 41 42.83	-35 06 44.2	L2	—	0.063 ± 0.010	-0.120 ± 0.012	9.3	CPAPIR
2MASSI J2107316-030733	21 07 31.69	-03 07 33.7	L0	—	0.143 ± 0.020	-0.009 ± 0.020	7.0	CFIM
2MASS J21075409-4544064	21 07 54.09	-45 44 06.4	L0	—	0.107 ± 0.014	-0.027 ± 0.020	8.1	CFIM
2MASSW J2130446-084520	21 30 44.64	-08 45 20.5	L1.5	—	0.346 ± 0.019	-0.044 ± 0.019	8.3	CFIM
SDSS J213240.36+102949.4	21 32 40.36	+10 29 49.4	—	L4.5	0.120 ± 0.018	-0.007 ± 0.019	7.5	TIFKAM
SDSS J213352.72+101841.0	21 33 52.74	+10 18 41.0	—	L5	-0.008 ± 0.012	-0.094 ± 0.012	7.4	TIFKAM
2MASS J21392676+0220226	21 39 26.76	+02 20 22.6	—	T1	0.507 ± 0.022	0.123 ± 0.022	6.1	CPAPIR
2MASS J21420580-3101162	21 42 05.80	-31 01 16.2	L3	—	0.060 ± 0.012	-0.095 ± 0.014	9.3	CPAPIR
2MASS J21481633+4003594	21 48 16.33	+40 03 59.4	L6.5	—	0.770 ± 0.018	0.456 ± 0.024	7.9	TIFKAM
2MASS J21501592-7520367	21 50 15.92	-75 20 36.7	L1	—	0.879 ± 0.005	-0.300 ± 0.019	7.2	CFIM
2MASS J21512543-2441000	21 51 25.43	-24 41 00.0	L3	—	0.278 ± 0.014	-0.021 ± 0.015	9.4	CPAPIR
2MASS J21542494-1023022	21 54 24.94	-10 23 02.2	—	T4.5	0.193 ± 0.012	0.037 ± 0.012	9.1	TIFKAM
2MASS J21543318+5942187	21 54 33.18	+59 42 18.7	—	T6	-0.182 ± 0.009	-0.445 ± 0.017	8.1	TIFKAM
2MASS J21574904-5534420	21 57 49.04	-55 34 42.0	L2	—	0.043 ± 0.011	-0.012 ± 0.019	7.2	CPAPIR
2MASS J21580457-1550098	21 58 04.57	-15 50 09.8	L4	—	0.057 ± 0.030	-0.035 ± 0.032	7.0	CFIM
2MASSW J2206450-421721	22 06 44.98	-42 17 20.8	L2	—	0.111 ± 0.013	-0.182 ± 0.018	9.0	CPAPIR
2MASS J22120703+3430351	22 12 07.03	+34 30 35.1	L5	—	0.160 ± 0.023	-0.232 ± 0.028	7.9	TIFKAM
2MASS J22134491-2136079	22 13 44.91	-21 36 07.9	L0	—	0.033 ± 0.017	-0.061 ± 0.019	8.1	CPAPIR
2MASSW J2224438-015852	22 24 43.81	-01 58 52.1	L4.5	L3.5	0.467 ± 0.015	-0.869 ± 0.015	9.1	TIFKAM
2MASSI J2238074+435317	22 38 07.42	+43 53 17.9	L1.5	—	0.324 ± 0.012	-0.132 ± 0.016	9.1	TIFKAM
SDSSp J224953.45+004404.2	22 49 53.45	+00 44 04.6	L3	L5	0.075 ± 0.018	0.026 ± 0.018	7.3	CPAPIR
2MASSI J2254519-284025	22 54 51.94	-28 40 25.3	L0.5	L0.5	0.000 ± 0.023	0.024 ± 0.026	7.2	CFIM
2MASS J22551861-5713056	22 55 18.61	-57 13 05.6	—	L5.5	-0.216 ± 0.011	-0.260 ± 0.020	8.2	CPAPIR
2MASS J23224684-3133231	23 22 46.88	-31 33 23.1	L0	—	-0.210 ± 0.017	-0.519 ± 0.020	7.0	CPAPIR
SDSS J232804.58-103845.7	23 28 04.59	-10 38 45.2	—	L3.5	-0.010 ± 0.015	-0.037 ± 0.015	9.2	CPAPIR
2MASS J23302258-0347189	23 30 22.58	-03 47 18.9	L1	—	0.223 ± 0.022	0.014 ± 0.022	8.9	CFIM
2MASS J23312378-4718274	23 31 23.78	-47 18 27.4	—	T5	0.104 ± 0.013	-0.049 ± 0.019	7.1	CPAPIR
2MASS J23440624-0733282	23 44 06.24	-07 33 28.2	L4.5	—	-0.013 ± 0.027	-0.064 ± 0.027	8.9	CFIM
2MASS J23453903+0055137	23 45 39.03	+00 55 13.7	L0	—	0.078 ± 0.039	-0.045 ± 0.039	7.1	CFIM

[1]SpT refers to the spectral type of the object.

Table 2.12: Full Astrometric Database

RA (J2000) (1)	DEC (J2000) (2)	Ref. (3)	2MASS J (mag) (4)	2MASS K_s (mag) (5)	$\mu_\alpha cos(\delta)$ ($''$ yr^{-1}) (6)	μ_δ ($''$ yr^{-1}) (7)	μ Ref. (8)	SpT (opt) (9)	SpT (IR) (10)	Distance (pc) (11)	V_{tan} (km s^{-1}) (12)	Note[r] (13)	Epoch (14)
00 00 13.54	+25 54 18.0	54	14.99 ± 0.10[c]	14.73 ± 0.06[c]	0.006 ± 0.019	0.130 ± 0.022	10	—	T4.5	11 ± 1	7 ± 1	—	1998.8
00 01 12.17	+15 35 35.5	54	15.42 ± 0.06[c]	13.56 ± 0.10[c]	0.150 ± 0.023	-0.169 ± 0.015	10	—	L4	29 ± 6	31 ± 7	—	2000.7
00 03 42.27	-28 22 41.0	20	13.07 ± 0.02	11.97 ± 0.03	0.257 ± 0.016	-0.145 ± 0.018	19	M7.5	—	26 ± 3	37 ± 4	VLMC	1998.9
00 04 34.84	-40 44 05.8	37	13.11 ± 0.02	11.40 ± 0.03	0.644 ± 0.003	-1.494 ± 0.002	23	L5	L4.5	13.0 ± 0.7[j]	100.4 ± 5.2	CB	1999.6
00 04 41.44	-20 58 29.8	45	12.40 ± 0.02	11.40 ± 0.02	0.826 ± 0.076	-0.009 ± 0.075	27	M8	—	18 ± 3	70 ± 14	—	1999.5
00 05 48.44	-21 57 19.6	86	13.27 ± 0.03	12.20 ± 0.03	0.703 ± 0.024	-0.119 ± 0.004	28	M9	—	23 ± 3	78 ± 11	—	1999.5
00 06 20.50	-17 20 50.6	43	15.66 ± 0.07	14.01 ± 0.05	-0.032 ± 0.017	0.017 ± 0.018	19	L2.5	—	43 ± 4	7 ± 4	—	1998.5
00 07 07.87	-24 58 04.2	86	13.12 ± 0.02	12.06 ± 0.02	0.189 ± 0.022	-0.051 ± 0.006	28	M7	—	30 ± 4	28 ± 5	—	1998.9
00 10 00.09	-20 31 12.2	20	14.13 ± 0.02	12.88 ± 0.03	0.117 ± 0.020	0.031 ± 0.017	10	L0	—	30 ± 2	17 ± 3	—	1998.6
00 13 57.79	-22 35 20.0	43	15.78 ± 0.07	14.04 ± 0.05	0.055 ± 0.017	-0.051 ± 0.019	19	L4	—	35 ± 4	12 ± 3	—	1998.6
00 14 55.75	-48 44 17.1	49	14.05 ± 0.04	12.72 ± 0.03	0.851 ± 0.012	0.289 ± 0.018	19	L2.5	—	21 ± 2	88 ± 7	—	1999.8
00 15 44.76	+35 16 02.6	47	13.88 ± 0.03	12.26 ± 0.02	0.083 ± 0.018	-0.246 ± 0.014	10	L2	—	21 ± 2	25 ± 2	—	1999.9
00 16 59.53	-40 56 54.1	49	15.32 ± 0.06	13.43 ± 0.04	0.201 ± 0.014	0.032 ± 0.018	19	L3.5	—	31 ± 3	30 ± 4	—	1999.6
00 19 11.65	+00 30 17.6	40	14.92 ± 0.04	13.57 ± 0.03	-0.029 ± 0.018	-0.025 ± 0.011	10	L1	—	38 ± 3	7 ± 3	—	2000.7
00 19 26.26	+46 14 07.8	19	12.60 ± 0.02	11.50 ± 0.01	0.14 ± 0.06	-0.10 ± 0.05	36	M8	—	20 ± 2	16 ± 6	—	1998.8
00 19 45.79	+52 13 17.9	19	12.79 ± 0.02	11.62 ± 0.02	0.27 ± 0.20	-0.10 ± 0.23	36	M9	—	19 ± 1	26 ± 17	—	1998.8
00 24 24.63	-01 58 20.1	42	11.99 ± 0.04	10.54 ± 0.02	-0.080 ± 0.004	0.133 ± 0.006	41	M9.5	—	11.8 ± 0.6[o]	8.7 ± 0.6	—	1998.7
00 25 03.65	+47 59 19.1	20	14.84 ± 0.04	12.90 ± 0.06	0.312 ± 0.039	-0.009 ± 0.044	14	L4	—	31 ± 6[ee]	46 ± 11	CB	1998.8
00 27 41.97	+05 03 41.7	89	16.19 ± 0.09	14.96 ± 0.12	0.0105 ± 0.0004	-0.0008 ± 0.0003	15	M9.5	—	72.5 ± 8.5[h]	3.6 ± 0.4	LG	2000.6
00 27 55.92	+22 19 32.8	57	10.61 ± 0.02	9.57 ± 0.02	0.40 ± 0.04	-0.17 ± 0.04	36	M8	—	10 ± 1[x]	21 ± 3	CB	1997.8
00 30 30.13	-14 50 33.3	47	16.53 ± 0.06[c]	14.51 ± 0.06[c]	0.245 ± 0.004	-0.028 ± 0.002	44	L7	—	26.7 ± 3.3[q]	31.2 ± 3.8	—	2000.8
00 30 43.84	+31 39 32.1	46	15.48 ± 0.05	14.03 ± 0.05	-0.049 ± 0.016	-0.057 ± 0.014	10	L2	—	43 ± 3	15 ± 3	—	1997.9
00 31 54.77	+06 49 46.3	56	12.82 ± 0.02	11.72 ± 0.02	0.27 ± 0.10	0.07 ± 0.06	36	M7	—	26 ± 3	35 ± 13	—	2000.5
00 32 05.09	+02 19 01.7	83	14.32 ± 0.03	12.80 ± 0.03	0.417 ± 0.017	-0.312 ± 0.013	10	L1.5	M9	27 ± 2	67 ± 5	—	2000.6
00 32 43.08	-22 37 27.2	43	15.39 ± 0.05	13.96 ± 0.05	0.115 ± 0.027	0.023 ± 0.015	10	L1	—	48 ± 3	27 ± 6	—	1998.7
00 32 55.84	-44 05 05.8	37	14.78 ± 0.04	13.27 ± 0.04	0.126 ± 0.015	-0.099 ± 0.021	19	L0	—	41 ± 5	31 ± 5	LG	1999.7
00 32 59.37	+14 10 37.1	32	16.83 ± 0.17	14.95 ± 0.11	0.273 ± 0.007	0.039 ± 0.004	44	—	L8	33.2 ± 5.9[q]	43.4 ± 7.7	—	2000.9
00 33 23.86	-15 21 30.9	35	15.29 ± 0.06	13.41 ± 0.04	0.291 ± 0.016	0.043 ± 0.017	19	L4	—	28 ± 6	38 ± 8	LG	1999.6
00 34 51.57	+05 23 05.0	13	15.54 ± 0.05	< 16.24	0.65 ± 0.06	0.21 ± 0.05	5	—	T6.5	14 ± 2	44 ± 7	—	2000.7
00 34 56.84	-07 06 01.3	43	15.53 ± 0.06	13.94 ± 0.07	0.2 ± 0.1	0.1 ± 0.1	24	L3	—	37 ± 3	40 ± 18	—	1998.8
00 36 16.17	+18 21 10.4	82	12.41 ± 0.06[c]	11.09 ± 0.06[c]	0.8991 ± 0.0006	0.120 ± 0.002	15	L3.5	L4	8.8 ± 0.1[h]	37.7 ± 0.3	—	2000.9
00 37 43.06	-58 46 22.9	74	15.37 ± 0.05	13.59 ± 0.05	0.049 ± 0.010	-0.051 ± 0.020	19	L0	—	54 ± 7	18 ± 5	LG	1999.8
00 38 43.98	+13 43 39.5	40	15.91 ± 0.07	14.76 ± 0.10	0.064 ± 0.016	-0.041 ± 0.008	10	L1	—	61 ± 4	22 ± 4	—	1997.8
00 39 18.91	+21 15 16.8	71	16.16 ± 0.03	16.87 ± 0.05	-0.4611 ± 0.0007	-0.3709 ± 0.0007	34	—	T7.5	11.1 ± 0.1[l]	31.2 ± 0.3	VLMC	1997.8
00 41 35.38	-56 21 12.7	57	11.96 ± 0.02	10.86 ± 0.02	0.08 ± 0.12	-0.09 ± 0.13	36	M8	—	15 ± 1	8 ± 9	—	1999.8
00 41 54.53	+13 41 35.1	40	14.45 ± 0.03	13.24 ± 0.03	-0.174 ± 0.024	-0.138 ± 0.036	10	L0	—	35 ± 2	37 ± 5	—	2000.8
00 45 21.43	+16 34 44.6	105	13.06 ± 0.02	11.37 ± 0.02	0.385 ± 0.017	-0.026 ± 0.012	10	L2	L3.5	14 ± 1	26 ± 2	LG	2000.9
00 46 48.41	+07 15 17.7	83	13.89 ± 0.03	12.55 ± 0.03	0.098 ± 0.022	-0.051 ± 0.010	10	L0	M9	27 ± 3	14 ± 3	—	2000.8
00 49 26.77	-06 35 46.7	19	13.34 ± 0.02	12.10 ± 0.02	-0.111 ± 0.008	-0.460 ± 0.030	9	M8.5	—	25 ± 2	57 ± 5	—	1998.8
00 50 19.94	-33 22 40.2	99	15.93 ± 0.07	15.24 ± 0.19	1.20 ± 0.11	0.90 ± 0.12	41	—	T7	8 ± 1	54 ± 8	—	1998.9
00 50 24.44	-15 38 18.4	25	13.78 ± 0.02	12.65 ± 0.03	-0.229 ± 0.018	-0.494 ± 0.019	19	L1	—	23 ± 3	59 ± 8	—	1998.5
00 51 10.78	-15 44 16.9	47	15.28 ± 0.05	13.47 ± 0.04	0.043 ± 0.015	-0.021 ± 0.016	19	L3.5	—	30 ± 3	7 ± 2	—	1998.5
00 52 54.68	-27 05 59.7	85	13.61 ± 0.03	12.54 ± 0.03	0.056 ± 0.005	0.090 ± 0.005	42	M8	—	22.2 ± 5.2[n]	11.2 ± 2.7	—	1998.9
00 53 18.99	-36 31 10.2	49	14.45 ± 0.03	12.94 ± 0.03	0.018 ± 0.015	-0.085 ± 0.019	19	L3.5	—	21 ± 2	9 ± 2	—	1999.6
00 54 06.55	-00 31 01.8	90	15.73 ± 0.05	14.38 ± 0.07	0.200 ± 0.009	-0.160 ± 0.009	19	L1	—	56 ± 4	68 ± 5	—	1998.7
00 58 42.53	-06 51 23.9	47	14.31 ± 0.03	12.90 ± 0.03	0.229 ± 0.028	-0.200 ± 0.024	17	L0	—	33 ± 2	47 ± 6	—	1998.8
01 02 51.00	-37 37 43.8	93	11.13 ± 0.02	10.07 ± 0.02	1.456 ± 0.003	0.262 ± 0.004	13	M8	—	12.2 ± 0.4[g]	85.6 ± 2.9	—	1999.6
01 03 32.03	+19 35 36.1	47	16.29 ± 0.08	14.15 ± 0.06	0.305 ± 0.017	0.035 ± 0.014	10	L6	—	23 ± 2	33 ± 4	—	1997.8

Continued on Next Page...

Table 2.12 – Continued

RA (J2000) (1)	DEC (J2000) (2)	Ref.[1] (3)	2MASS J[3] (mag) (4)	2MASS K_s[3] (mag) (5)	$\mu_\alpha cos(\delta)$ ($''$ yr^{-1}) (6)	μ_δ ($''$ yr^{-1}) (7)	μ Ref.[2] (8)	SpT (opt) (9)	SpT (IR) (10)	Distance[3] (pc) (11)	V_{tan} (km s^{-1}) (12)	Note[4] (13)	Epoch (14)
01 04 07.50	-00 53 28.3	3	16.53 ± 0.13	15.33 ± 0.18	0.473 ± 0.018	-0.021 ± 0.018	19	L4.5	—	44 ± 5	99 ± 11	—	1998.7
01 06 22.85	-59 33 18.5	74	14.33 ± 0.04	13.01 ± 0.04	0.046 ± 0.010	-0.198 ± 0.020	19	L0	—	33 ± 4	32 ± 5	—	1999.8
01 07 16.07	-15 17 57.7	20	13.34 ± 0.02	12.28 ± 0.02	-0.031 ± 0.016	0.011 ± 0.017	19	M7	—	33 ± 4	5 ± 3	—	1998.6
01 07 52.42	+00 41 56.3	32	15.82 ± 0.06	13.71 ± 0.04	0.628 ± 0.007	0.091 ± 0.004	44	L8	L5.5	15.6 ± 1.1[q]	46.9 ± 3.3	—	2000.7
01 09 09.18	-49 54 53.2	61	13.55 ± 0.02	12.45 ± 0.03	0.095 ± 0.013	0.168 ± 0.020	19	—	L1	20 ± 1	19 ± 2	—	1999.8
01 09 21.70	+29 49 25.5	57	12.91 ± 0.02	11.68 ± 0.02	1.014 ± 0.019	0.348 ± 0.019	29	M9.5	—	18 ± 1	93 ± 6	—	1997.8
01 09 51.17	-03 43 26.4	57	11.69 ± 0.02	10.43 ± 0.03	0.360 ± 0.002	0.018 ± 0.002	13	M9	—	9.6 ± 0.2[g]	16.4 ± 0.4	—	1998.7
01 16 54.57	-13 57 34.2	74	14.21 ± 0.03	12.97 ± 0.03	-0.026 ± 0.022	-0.110 ± 0.022	19	M9	—	35 ± 2	19 ± 4	—	2000.6
01 17 47.48	-34 03 25.8	19	15.18 ± 0.04	13.49 ± 0.04	0.080 ± 0.017	-0.062 ± 0.020	19	L2	—	38 ± 6	18 ± 4	—	1998.9
01 20 49.16	-07 41 03.6	57	12.99 ± 0.03	11.85 ± 0.02	-0.013 ± 0.019	-0.115 ± 0.019	29	M8	—	23 ± 4	13 ± 3	—	1998.8
01 23 11.25	-69 21 37.9	20	12.32 ± 0.02	11.32 ± 0.03	0.10 ± 0.11	-0.03 ± 0.07	36	M7.5	—	19 ± 2	10 ± 10	—	1998.8
01 23 59.05	-42 40 07.3	61	13.15 ± 0.02	12.04 ± 0.02	-0.145 ± 0.004	-0.229 ± 0.007	30	M8	L2.5	25 ± 2	32 ± 3	—	2000.6
01 24 45.99	-57 45 37.9	74	16.31 ± 0.11	14.32 ± 0.09	-0.003 ± 0.010	0.018 ± 0.019	19	L0	—	82 ± 10	7 ± 7	LG	1999.8
01 25 36.89	-34 35 04.9	43	15.52 ± 0.06	13.90 ± 0.05	0.151 ± 0.016	0.036 ± 0.019	19	L2	—	44 ± 3	32 ± 4	—	1998.9
01 27 39.17	+28 05 53.6	51	14.04 ± 0.03	12.86 ± 0.03	-0.1334 ± 0.0003	-0.1348 ± 0.0003	15	M8.5	—	32.8 ± 0.3[h]	29.5 ± 0.2	—	1997.8
01 28 26.64	-55 45 34.3	45	13.78 ± 0.03	12.34 ± 0.03	-0.249 ± 0.019	0.154 ± 0.019	22	—	L1	23 ± 1	31 ± 3	—	1999.8
01 30 35.63	-44 45 41.1	74	14.07 ± 0.03	12.87 ± 0.03	0.120 ± 0.014	-0.025 ± 0.020	19	M9	—	33 ± 2	19 ± 3	—	1999.8
01 31 18.38	+38 01 55.4	20	14.68 ± 0.03	13.05 ± 0.03	0.373 ± 0.012	-0.031 ± 0.015	19	L4	—	21 ± 4	37 ± 8	—	1998.8
01 33 32.48	-63 14 41.5	61	14.51 ± 0.04	13.70 ± 0.04	0.077 ± 0.008	-0.081 ± 0.009	30	—	L0	36 ± 2	19 ± 2	—	1999.9
01 35 35.86	+12 05 21.6	47	14.41 ± 0.03	12.92 ± 0.03	-0.042 ± 0.023	-0.422 ± 0.023	19	L1.5	—	28 ± 2	57 ± 5	—	2000.7
01 36 56.62	+09 33 47.3	1	13.46 ± 0.03	12.56 ± 0.02	1.241 ± 0.009	-0.004 ± 0.011	1	—	T2.5	6.0 ± 0.4	36 ± 2	—	2000.7
01 41 03.21	+18 04 50.2	105	13.88 ± 0.03	12.49 ± 0.03	0.403 ± 0.011	-0.045 ± 0.012	19	L1	L4.5	24 ± 2	46 ± 3	—	1998.8
01 41 14.79	-24 17 31.1	19	13.42 ± 0.02	12.30 ± 0.02	-0.161 ± 0.017	-0.303 ± 0.019	19	M7.5	—	31 ± 3	51 ± 6	—	1998.8
01 41 58.23	-46 33 57.4	48	14.83 ± 0.04	13.10 ± 0.03	0.104 ± 0.017	-0.026 ± 0.024	19	L0	L0	42 ± 5	21 ± 4	LG	1999.7
01 42 31.53	+05 23 28.5	110	15.91 ± 0.08	15.60 ± 0.26	0.56 ± 0.05	-0.29 ± 0.05	47	sdM8.5	—	65 ± —	194 ± —	—	2000.7
01 44 35.36	-07 16 14.2	59	14.19 ± 0.03	12.27 ± 0.02	0.395 ± 0.018	-0.204 ± 0.018	19	L5	—	12 ± 1	24 ± 2	—	1998.8
01 46 01.19	-45 45 26.3	74	14.40 ± 0.04	13.03 ± 0.03	0.121 ± 0.016	0.060 ± 0.023	19	M9	—	39 ± 2	25 ± 4	—	2000.8
01 46 31.92	+06 41 15.3	56	13.47 ± 0.02	12.35 ± 0.03	-0.079 ± 0.010	-0.249 ± 0.010	28	M7.5	—	32 ± 3	39 ± 4	—	2000.7
01 47 32.82	-49 54 47.8	74	13.06 ± 0.03	11.92 ± 0.02	-0.014 ± 0.001	-0.288 ± 0.026	16	M8	—	33 ± 6[ee]	45 ± 9	CB	1999.8
01 47 33.44	+34 53 11.2	46	14.95 ± 0.04	13.57 ± 0.04	0.037 ± 0.009	-0.055 ± 0.011	19	L0.5	—	41 ± 3	13 ± 2	—	1997.9
01 48 38.64	-30 24 39.6	19	12.30 ± 0.02	11.23 ± 0.02	-0.11 ± 0.10	0.10 ± 0.09	36	M7.5	—	18 ± 2	13 ± 9	—	1998.8
01 49 08.95	+29 56 13.1	46	13.45 ± 0.02	11.98 ± 0.02	0.1757 ± 0.0008	-0.4021 ± 0.0007	15	M9.5	—	22.5 ± 0.4[h]	46.8 ± 0.7	—	1997.8
01 51 41.55	+12 44 30.0	32	16.57 ± 0.13	15.18 ± 0.19	0.742 ± 0.004	-0.037 ± 0.002	44	—	T1	21.4 ± 1.6[q]	75.3 ± 5.5	—	1997.7
01 55 03.54	+09 50 00.3	46	14.83 ± 0.04	13.14 ± 0.04	0.338 ± 0.023	-0.080 ± 0.023	19	L5	—	17 ± 3	28 ± 5	—	2000.7
02 04 22.12	-36 32 30.8	61	13.27 ± 0.03	12.19 ± 0.03	0.193 ± 0.017	-0.034 ± 0.021	19	M9	—	23 ± 3	21 ± 3	—	1999.6
02 05 03.44	+12 51 42.2	47	15.68 ± 0.06	13.67 ± 0.04	0.349 ± 0.011	-0.018 ± 0.011	19	L5	—	22 ± 2	37 ± 3	—	1998.7
02 05 29.40	-11 59 29.6	26	14.59 ± 0.03	13.00 ± 0.03	0.4343 ± 0.0008	0.0549 ± 0.0008	15	L7	L5.5	19.8 ± 0.6[h]	41.0 ± 1.2	CB	2000.9
02 06 08.80	+22 35 59.3	18	16.44 ± 0.06[a]	15.08 ± 0.06[a]	0.341 ± 0.015	-0.062 ± 0.016	19	—	L5.5	39 ± 4	64 ± 6	—	1997.8
02 07 35.57	+13 55 56.4	40	15.39 ± 0.06[c]	13.84 ± 0.06[c]	0.260 ± 0.017	-0.161 ± 0.018	19	L3	L3	35 ± 3	51 ± 5	—	1998.7
02 07 42.84	+00 00 56.4	32	16.80 ± 0.16	< 15.41	0.155 ± 0.011	-0.017 ± 0.006	44	—	T4.5	29 ± 9[q]	21 ± 7	—	2000.6
02 08 18.33	+25 42 53.3	47	13.99 ± 0.03	12.59 ± 0.03	0.356 ± 0.010	-0.021 ± 0.011	19	L1	—	25 ± 2	42 ± 3	—	1997.8
02 08 23.63	+27 37 40.0	47	15.71 ± 0.06	13.87 ± 0.05	0.217 ± 0.013	-0.110 ± 0.014	19	L5	—	24 ± 2	28 ± 3	—	1997.8
02 08 54.99	+25 00 48.8	47	16.21 ± 0.09	14.41 ± 0.07	-0.022 ± 0.011	0.060 ± 0.012	19	L5	—	31 ± 3	9 ± 2	—	1997.8
02 11 28.27	+14 10 03.9	40	16.13 ± 0.08	15.01 ± 0.12	-0.092 ± 0.010	-0.030 ± 0.010	19	L1	—	67 ± 4	31 ± 4	—	1998.7
02 13 28.80	+44 44 45.3	19	13.49 ± 0.03	12.21 ± 0.02	-0.04 ± 0.06	-0.16 ± 0.06	36	L1.5	—	19 ± 1	15 ± 5	—	1998.8
02 15 08.02	-30 40 01.1	57	11.62 ± 0.03	10.54 ± 0.02	0.770 ± 0.018	-0.339 ± 0.019	28	M8	—	12 ± 1	49 ± 4	—	1999.6
02 18 29.13	-31 33 23.0	19	14.73 ± 0.04	13.15 ± 0.04	-0.165 ± 0.015	-0.138 ± 0.018	19	L3	—	26 ± 2	26 ± 3	—	1998.9
02 18 57.92	-06 17 49.9	57	12.85 ± 0.02	11.84 ± 0.03	0.367 ± 0.019	-0.097 ± 0.019	29	M8	—	23 ± 2	41 ± 4	—	2000.8
02 19 21.96	+05 06 30.6	21	14.97 ± 0.04	13.48 ± 0.04	0.190 ± 0.024	0.005 ± 0.024	19	—	L1	39 ± 5	36 ± 6	—	2000.7
02 19 28.07	-19 38 41.6	62	14.11 ± 0.03	12.91 ± 0.03	0.194 ± 0.004	-0.173 ± 0.006	31	L1	L2.5	26 ± 2	33 ± 2	—	2000.9

Continued on Next Page...

Table 2.12 – Continued

RA (J2000) (1)	DEC (J2000) (2)	Ref.[1] (3)	2MASS J[3] (mag) (4)	2MASS K_s[3] (mag) (5)	$\mu_\alpha cos(\delta)$ ($''$ yr^{-1}) (6)	μ_δ ($''$ yr^{-1}) (7)	μ Ref.[2] (8)	SpT (opt) (9)	SpT (IR) (10)	Distance[3] (pc) (11)	V_{tan} (km s^{-1}) (12)	Note[4] (13)	Epoch (14)
02 21 28.46	-68 31 40.0	74	13.97 ± 0.03	12.81 ± 0.04	0.046 ± 0.006	-0.006 ± 0.017	19	M8	—	36 ± 6	8 ± 2	LG	1999.9
02 21 54.99	-54 12 05.4	61	13.90 ± 0.03	12.67 ± 0.03	0.136 ± 0.010	-0.010 ± 0.017	19	M9	—	31 ± 4	20 ± 3	LG	1999.8
02 23 54.46	-58 15 06.7	74	15.07 ± 0.05	13.42 ± 0.04	0.134 ± 0.010	0.005 ± 0.019	19	L0	—	47 ± 6	30 ± 4	LG	1999.8
02 25 18.81	-58 37 29.5	74	13.74 ± 0.03	12.56 ± 0.03	0.085 ± 0.010	-0.030 ± 0.018	19	M9	—	28 ± 4	12 ± 2	LG	1999.8
02 27 10.36	-16 24 47.9	83	13.57 ± 0.02	12.14 ± 0.03	0.509 ± 0.016	-0.303 ± 0.010	16	L1	—	21 ± 1	58 ± 4	—	2000.8
02 28 11.01	+25 37 38.0	105	13.84 ± 0.03	12.47 ± 0.03	0.257 ± 0.014	-0.014 ± 0.017	10	L0	L0	26 ± 3	32 ± 4	—	1998.8
02 28 33.05	+18 11 09.7	19	13.23 ± 0.02	12.26 ± 0.02	0.182 ± 0.010	-0.086 ± 0.010	28	M7	—	32 ± 4	30 ± 4	—	1997.8
02 28 42.43	+16 39 32.9	105	13.17 ± 0.03	11.82 ± 0.02	0.422 ± 0.020	-0.412 ± 0.021	19	L0	—	19 ± 2	54 ± 7	—	1999.8
02 28 43.55	-63 25 05.2	45	13.56 ± 0.03	12.25 ± 0.03	0.593 ± 0.010	0.458 ± 0.023	19	—	L0	23 ± 3	82 ± 10	—	2000.8
02 30 15.51	+27 04 06.1	20	14.29 ± 0.03	12.99 ± 0.02	0.189 ± 0.008	-0.007 ± 0.010	19	L0	—	33 ± 4	29 ± 4	—	1998.8
02 35 47.56	-08 49 19.8	40	15.57 ± 0.06	14.19 ± 0.07	-0.044 ± 0.013	0.013 ± 0.013	19	L2	—	45 ± 3	10 ± 3	—	1998.8
02 35 59.93	-23 31 20.5	34	< 12.69	12.19 ± 0.08	0.085 ± 0.001	0.0130 ± 0.0008	34	L1	L1	21.3 ± 0.5[l]	8.6 ± 0.2	VLMC	1998.9
02 36 17.94	+00 48 54.8	32	16.10 ± 0.08	14.67 ± 0.09	0.123 ± 0.012	-0.176 ± 0.012	19	L6	L6.5	29 ± 3	30 ± 3	—	2000.7
02 39 42.45	-17 35 47.1	19	14.29 ± 0.03	13.04 ± 0.03	0.042 ± 0.017	-0.095 ± 0.018	19	L0	—	33 ± 2	16 ± 3	—	1998.6
02 40 29.50	+28 32 57.6	57	12.67 ± 0.02	11.63 ± 0.02	0.046 ± 0.019	-0.192 ± 0.019	29	M7.5	—	22 ± 2	21 ± 3	—	1997.9
02 41 53.67	-12 41 06.9	19	15.61 ± 0.07	13.93 ± 0.06	0.312 ± 0.016	-0.040 ± 0.017	19	L2	—	46 ± 7	68 ± 11	—	1998.6
02 42 43.55	+16 07 39.2	46	15.78 ± 0.05	14.35 ± 0.06	0.152 ± 0.011	-0.210 ± 0.012	19	L1.5	—	53 ± 4	66 ± 5	—	1998.7
02 43 13.71	-24 53 29.8	10	15.42 ± 0.06[c]	15.22 ± 0.06[c]	-0.288 ± 0.004	-0.208 ± 0.003	44	—	T6	10.7 ± 0.4[q]	18.0 ± 0.7	—	1998.9
02 43 51.03	-54 32 19.4	65	14.04 ± 0.03	12.78 ± 0.02	0.096 ± 0.011	-0.026 ± 0.019	19	M9	—	33 ± 2	15 ± 2	—	1999.8
02 47 49.78	-16 31 13.2	18	16.94 ± 0.06[a]	15.76 ± 0.06[a]	0.313 ± 0.017	0.143 ± 0.017	19	—	T2	28 ± 4	46 ± 7	—	1998.6
02 48 41.00	-16 51 21.6	57	12.55 ± 0.02	11.42 ± 0.02	0.021 ± 0.009	-0.273 ± 0.012	42	M8	—	16.8 ± 1.5[n]	21.8 ± 2.2	—	1998.6
02 51 13.27	+00 47 36.4	102	13.77 ± 0.03	12.68 ± 0.03	0.234 ± 0.007	0.040 ± 0.004	41	M7.5	—	60 ± 8[o]	67 ± 9	—	2000.7
02 51 14.90	-03 52 45.9	19	13.06 ± 0.03	11.66 ± 0.02	1.128 ± 0.013	-1.826 ± 0.020	10	L3	L1	12 ± 1	122 ± 11	—	1998.8
02 52 26.28	+00 56 22.3	102	13.13 ± 0.02	11.96 ± 0.02	-0.175 ± 0.007	-0.100 ± 0.005	41	M8	—	28.4 ± 2.4[o]	27.2 ± 2.5	—	2000.7
02 53 00.84	+16 52 53.2	97	8.39 ± 0.03	7.59 ± 0.05	3.404 ± 0.005	-3.807 ± 0.005	23	M7	—	3.84 ± 0.04[j]	92.9 ± 1.0	—	1999.8
02 55 03.57	-47 00 50.9	65	13.25 ± 0.03	11.56 ± 0.02	1.07 ± 0.11	-0.62 ± 0.11	36	L8	L9	5.2 ± 0.3	30 ± 3	—	1998.9
02 56 01.89	+01 10 46.7	40	16.21 ± 0.10	15.22 ± 0.18	0.025 ± 0.015	-0.068 ± 0.015	19	L0	—	79 ± 5	27 ± 6	—	2000.7
02 57 25.81	-31 05 52.3	49	14.67 ± 0.04	12.88 ± 0.03	0.602 ± 0.018	0.320 ± 0.021	19	L8	—	10 ± 1	31 ± 2	—	1999.6
03 02 01.22	+13 58 14.2	47	16.53 ± 0.12	14.63 ± 0.08	0.055 ± 0.015	-0.037 ± 0.016	19	L3	—	59 ± 5	19 ± 5	—	1997.8
03 03 21.23	-00 09 37.8	90	16.12 ± 0.07	14.88 ± 0.10	0.025 ± 0.017	-0.023 ± 0.017	19	L0	—	76 ± 5	12 ± 6	—	1998.7
03 06 26.84	+15 45 13.7	47	17.11 ± 0.18	15.13 ± 0.14	0.212 ± 0.017	-0.071 ± 0.018	19	L6	—	36 ± 6	38 ± 7	—	1998.9
03 09 08.88	-19 49 38.7	47	15.75 ± 0.06	14.06 ± 0.07	0.184 ± 0.016	-0.038 ± 0.017	19	L4.5	—	31 ± 3	27 ± 4	—	1998.9
03 10 00.53	+07 26 50.6	74	12.85 ± 0.02	11.78 ± 0.02	0.539 ± 0.022	0.254 ± 0.022	19	M7.5	—	24 ± 2	67 ± 7	—	2000.7
03 10 14.01	-27 56 45.2	20	15.80 ± 0.07	13.96 ± 0.06	-0.116 ± 0.016	-0.052 ± 0.018	19	L5	—	25 ± 2	15 ± 2	—	1998.9
03 10 59.86	+16 48 15.5	47	16.03 ± 0.08	14.31 ± 0.07	-0.706 ± 0.019	0.119 ± 0.020	19	L8	L9	19 ± 1	63 ± 4	—	1999.8
03 13 44.43	+04 33 16.5	74	13.67 ± 0.03	12.59 ± 0.02	-0.049 ± 0.022	0.006 ± 0.022	19	M7.5	—	35 ± 3	8 ± 4	—	2000.7
03 14 03.44	+16 03 05.6	83	12.53 ± 0.02	11.24 ± 0.02	-0.241 ± 0.018	-0.076 ± 0.019	19	L0	—	14 ± 1	17 ± 2	—	1999.7
03 14 40.11	-04 50 31.6	19	12.64 ± 0.02	11.60 ± 0.03	-0.068 ± 0.018	-0.119 ± 0.018	19	M7.5	—	22 ± 2	14 ± 2	—	1998.8
03 16 45.12	-28 48 52.1	19	14.57 ± 0.04	13.11 ± 0.03	0.107 ± 0.017	-0.081 ± 0.019	19	L0	—	37 ± 5	23 ± 4	—	1998.9
03 18 54.03	-34 21 29.2	49	15.57 ± 0.06	13.51 ± 0.04	0.365 ± 0.016	0.017 ± 0.019	19	L7	—	15 ± 1	25 ± 2	—	1998.9
03 20 17.20	-10 26 12.4	20	13.88 ± 0.03	12.69 ± 0.03	0.013 ± 0.018	-0.100 ± 0.018	19	M8	—	35 ± 3	17 ± 3	—	1998.8
03 20 28.39	-04 46 35.8	19	13.26 ± 0.02	12.13 ± 0.03	-0.267 ± 0.016	-0.533 ± 0.016	19	M8	L0.5	26 ± 5	75 ± 13	—	1998.7
03 20 59.65	+18 54 23.3	57	11.76 ± 0.02	10.64 ± 0.02	0.3493 ± 0.0005	-0.2557 ± 0.0006	15	M8	—	14.5 ± 0.1[h]	29.8 ± 0.3	—	1997.8
03 23 10.02	-46 31 23.7	74	15.39 ± 0.07	13.70 ± 0.05	0.060 ± 0.013	-0.010 ± 0.019	19	L0	—	54 ± 7	16 ± 4	LG	1999.6
03 25 01.36	+22 53 03.9	20	15.43 ± 0.05	13.77 ± 0.05	0.405 ± 0.013	-0.146 ± 0.014	19	L3	—	36 ± 3	73 ± 7	—	1997.8
03 25 53.22	+04 25 40.6	18	16.16 ± 0.06[a]	16.37 ± 0.06[a]	-0.183 ± 0.014	-0.099 ± 0.014	19	—	T5.5	19 ± 2	18 ± 3	—	2000.1
03 26 13.67	+29 50 15.2	46	15.48 ± 0.05	13.84 ± 0.05	-0.0188 ± 0.0008	0.0668 ± 0.0008	15	L3.5	—	32.3 ± 1.6[h]	10.6 ± 0.5	—	1997.9
03 26 42.25	-21 02 05.7	35	16.13 ± 0.09	13.92 ± 0.07	0.108 ± 0.014	-0.146 ± 0.015	19	L4	—	41 ± 4	35 ± 5	—	1998.9
03 27 40.91	-31 48 15.6	21	16.09 ± 0.09	14.15 ± 0.07	0.038 ± 0.017	0.018 ± 0.020	19	—	L3	48 ± 9	10 ± 4	—	1998.9
03 28 17.38	+00 32 57.2	90	15.99 ± 0.09	14.16 ± 0.08	0.195 ± 0.013	0.033 ± 0.013	19	L3	—	46 ± 4	43 ± 5	—	2000.1

Continued on Next Page...

Table 2.12 – Continued

RA (J2000) (1)	DEC (J2000) (2)	Ref.[1] (3)	2MASS J[3] (mag) (4)	2MASS K_s[3] (mag) (5)	$\mu_\alpha cos(\delta)$ ($''$ yr^{-1}) (6)	μ_δ ($''$ yr^{-1}) (7)	μ Ref.[2] (8)	SpT (opt) (9)	SpT (IR) (10)	Distance[3] (pc) (11)	V_{tan} (km s^{-1}) (12)	Note[4] (13)	Epoch (14)
03 28 34.63	+11 29 51.5	56	12.46 ± 0.02	11.33 ± 0.02	0.548 ± 0.010	0.247 ± 0.010	28	M8	—	18 ± 2	52 ± 4	—	2000.0
03 28 42.65	+23 02 05.1	47	16.69 ± 0.14	14.92 ± 0.11	0.013 ± 0.003	-0.060 ± 0.005	44	L8	L9.5	30.2 ± 3.9[q]	8.7 ± 1.3	—	1997.8
03 30 05.07	+24 05 28.1	57	12.38 ± 0.02	11.39 ± 0.02	0.175 ± 0.019	-0.050 ± 0.019	29	M7	—	21 ± 5	18 ± 5	—	1997.9
03 30 17.74	+00 00 47.7	90	16.52 ± 0.11	15.53 ± 0.18	-0.011 ± 0.018	-0.046 ± 0.018	19	L0	—	91 ± 11	20 ± 8	—	1998.7
03 30 35.11	-00 25 34.6	30	15.31 ± 0.05	13.84 ± 0.05	0.394 ± 0.015	-0.336 ± 0.015	19	L4	—	28 ± 3	69 ± 7	—	1998.7
03 31 30.25	-30 42 38.3	57	11.36 ± 0.02	10.26 ± 0.02	0.057 ± 0.001	-0.403 ± 0.006	2	M7.5	—	13.4 ± —[e]	26.0 ± —	—	1998.9
03 32 00.43	-23 17 49.6	74	13.61 ± 0.03	12.51 ± 0.03	-0.013 ± 0.020	-0.153 ± 0.022	19	M8	—	31 ± 3	23 ± 4	—	2000.8
03 34 12.04	-49 53 32.2	76	11.38 ± 0.02	10.39 ± 0.02	2.308 ± 0.012	0.480 ± 0.019	19	M9	—	10 ± 1	107 ± 7	—	1999.8
03 35 45.35	+06 58 05.8	74	13.41 ± 0.03	12.25 ± 0.02	0.029 ± 0.021	-0.333 ± 0.021	19	M8	—	28 ± 2	45 ± 5	—	2000.0
03 37 03.59	-17 58 07.9	47	15.62 ± 0.06	13.58 ± 0.04	0.191 ± 0.031	0.115 ± 0.033	19	L4.5	—	29 ± 3	31 ± 5	—	1998.9
03 39 35.21	-35 25 44.0	57	10.73 ± 0.02	9.55 ± 0.02	0.324 ± 0.008	0.296 ± 0.007	42	M9	—	5.0 ± 0.1[n]	10.4 ± 0.3	—	1998.9
03 40 09.42	-67 24 05.1	20	14.74 ± 0.03	12.93 ± 0.03	-0.318 ± 0.007	0.508 ± 0.018	19	L7	—	11 ± 3	32 ± 10	—	1998.8
03 42 16.21	-68 17 32.1	20	16.85 ± 0.14	14.54 ± 0.09	0.064 ± 0.007	0.021 ± 0.018	19	L2	—	81 ± 12	26 ± 5	—	1998.8
03 45 43.16	+25 40 23.3	50	14.00 ± 0.03	12.67 ± 0.02	-0.0960 ± 0.0003	-0.0357 ± 0.0004	15	L0	L1	27.0 ± 0.4[h]	13.1 ± 0.2	—	2000.0
03 48 07.72	-60 22 27.0	14	15.32 ± 0.05	15.60 ± 0.23	-0.28 ± 0.04	-0.72 ± 0.04	8	—	T7	9 ± 1	32 ± 5	—	1999.9
03 50 48.61	-05 18 12.6	40	16.33 ± 0.09	15.13 ± 0.13	0.012 ± 0.022	-0.028 ± 0.022	19	L1	—	73 ± 5	11 ± 8	—	2000.8
03 50 57.37	+18 18 06.9	57	12.97 ± 0.02	11.78 ± 0.02	0.193 ± 0.010	-0.024 ± 0.010	28	M8	—	23 ± 2	21 ± 2	—	1997.8
03 51 00.04	-00 52 45.2	22	11.30 ± 0.02	10.23 ± 0.02	0.0367 ± —	-0.5247 ± —	46	M7.5	—	14.7 ± 0.4[p]	36.6 ± 1.0	—	2000.8
03 51 04.23	+48 10 47.7	18	16.46 ± 0.06[a]	15.17 ± 0.06[a]	0.312 ± 0.019	-0.180 ± 0.029	19	—	T1	23 ± 2	39 ± 5	—	2000.0
03 52 10.86	+02 10 47.9	45	13.08 ± 0.03	11.96 ± 0.02	0.262 ± 0.025	0.373 ± 0.025	22	M9	L0	21 ± 1	45 ± 4	—	2000.1
03 54 01.35	+23 16 33.9	57	13.12 ± 0.02	12.00 ± 0.02	0.189 ± 0.019	-0.071 ± 0.019	28	M8.5	—	23 ± 2	20 ± 2	—	1997.8
03 54 48.55	-00 27 42.0	54	17.26 ± 0.06[c]	15.98 ± 0.06[c]	-0.011 ± 0.022	-0.019 ± 0.022	19	—	L2	98 ± 15	10 ± 11	—	2000.8
03 55 04.77	-10 32 41.5	19	13.08 ± 0.03	11.98 ± 0.02	0.046 ± 0.018	-0.044 ± 0.019	19	M8.5	—	23 ± 2	7 ± 2	—	1999.1
03 55 23.37	+11 33 43.7	83	14.05 ± 0.02	11.53 ± 0.02	0.192 ± 0.017	-0.613 ± 0.017	19	L5	—	8 ± 1	25 ± 5	LG	2000.0
03 55 41.91	+22 57 01.6	46	16.11 ± 0.08	14.28 ± 0.06	0.146 ± 0.014	-0.025 ± 0.016	19	L3	—	49 ± 4	34 ± 5	—	1997.8
03 57 21.10	-06 41 26.0	40	15.95 ± 0.08	14.60 ± 0.09	0.109 ± 0.012	0.008 ± 0.012	19	L0	—	70 ± 4	36 ± 5	—	1998.9
03 57 26.95	-44 17 30.5	5	14.37 ± 0.03	12.91 ± 0.03	0.064 ± 0.013	-0.020 ± 0.019	19	L0	—	22 ± 2[bb]	7 ± 2	CB	1999.7
03 58 22.55	-41 16 06.0	74	15.85 ± 0.09	13.84 ± 0.05	0.051 ± 0.015	0.075 ± 0.020	19	L5	—	24 ± 2	10 ± 2	—	2000.0
04 01 29.77	-40 50 44.8	74	14.53 ± 0.04	13.18 ± 0.03	-0.036 ± 0.015	-0.102 ± 0.020	19	L0	—	36 ± 4	19 ± 4	—	1999.6
04 07 07.52	+15 46 45.7	74	15.48 ± 0.06	13.56 ± 0.04	0.049 ± 0.019	-0.044 ± 0.020	19	L3.5	—	33 ± 3	10 ± 3	—	1999.9
04 07 08.85	+15 14 56.5	13	16.06 ± 0.09	15.92 ± 0.26	0.106 ± 0.016	-0.110 ± 0.017	19	—	T5	17 ± 2	12 ± 2	—	1999.9
04 08 10.32	+07 42 49.4	74	13.59 ± 0.02	12.42 ± 0.02	0.162 ± 0.020	0.095 ± 0.020	19	M8	—	31 ± 3	27 ± 4	—	1999.9
04 08 29.05	-14 50 33.4	105	14.22 ± 0.03	12.82 ± 0.02	0.188 ± 0.017	-0.131 ± 0.018	19	L2	L4.5	24 ± 2	26 ± 3	—	1998.7
04 09 09.50	+21 04 39.3	47	15.51 ± 0.05	13.85 ± 0.05	0.094 ± 0.015	-0.145 ± 0.016	19	L3	—	37 ± 3	30 ± 4	—	1997.8
04 13 20.39	-01 14 24.8	30	15.30 ± 0.05	14.14 ± 0.06	0.070 ± 0.017	0.001 ± 0.017	19	L0.5	—	49 ± 3	16 ± 4	—	1998.7
04 15 19.54	-09 35 06.6	10	15.67 ± 0.06[c]	15.68 ± 0.06[c]	2.193 ± 0.003	0.527 ± 0.002	44	T8	T8	5.7 ± 0.1[q]	61.4 ± 1.0	—	1998.9
04 17 37.45	-08 00 00.7	19	12.18 ± 0.03	11.09 ± 0.03	0.49 ± 0.09	-0.05 ± 0.09	36	M7.5	—	17 ± 2	40 ± 8	—	1998.9
04 17 47.43	-21 29 19.1	20	13.89 ± 0.03	12.67 ± 0.03	0.072 ± 0.017	0.022 ± 0.018	19	M8	—	35 ± 3	12 ± 3	—	1998.9
04 21 07.18	-63 06 02.2	20	15.57 ± 0.05	13.45 ± 0.04	0.146 ± 0.008	0.191 ± 0.018	19	L4	—	31 ± 3	36 ± 4	—	1998.8
04 23 48.58	-04 14 03.5	32	14.47 ± 0.03	12.93 ± 0.03	-0.323 ± 0.003	0.082 ± 0.002	44	L7.5	T0	15.2 ± 0.4[q]	24.0 ± 0.6	CB	1998.7
04 23 53.22	-00 06 58.7	19	13.65 ± 0.02	12.48 ± 0.03	-0.13 ± 0.16	-0.24 ± 0.15	9	M8.5	—	29 ± 2	38 ± 21	—	1998.7
04 27 07.23	+08 59 02.7	74	12.92 ± 0.03	11.73 ± 0.02	-0.121 ± 0.021	-0.005 ± 0.021	19	M8	—	23 ± 2	13 ± 2	—	1999.9
04 28 50.96	-22 53 22.7	43	13.51 ± 0.02	12.12 ± 0.03	0.113 ± 0.012	0.155 ± 0.013	19	L0.5	—	21 ± 1	19 ± 2	—	1998.9
04 29 18.42	-31 23 56.8	19	10.87 ± 0.02	9.77 ± 0.02	0.085 ± 0.004	0.102 ± 0.005	2	M7.5	—	15.2 ± —[e]	9.5 ± —	CB	1999.0
04 30 51.57	-08 49 00.7	19	12.90 ± 0.02	11.78 ± 0.02	-0.021 ± 0.017	-0.171 ± 0.018	19	M8	—	23 ± 2	19 ± 2	—	1998.8
04 35 14.55	-14 14 46.8	19	11.88 ± 0.03	9.95 ± 0.02	0.009 ± 0.014	0.016 ± 0.014	19	M8	—	14 ± 2	1 ± 1	LG	1998.9
04 35 16.12	-16 06 57.4	57	10.41 ± 0.03	9.35 ± 0.02	0.167 ± 0.013	0.313 ± 0.024	17	M7	—	9 ± 1	14 ± 2	—	1998.9
04 36 27.67	+11 51 24.3	19	13.87 ± 0.03	12.68 ± 0.02	0.117 ± 0.020	-0.009 ± 0.020	19	M9	—	29 ± 4	16 ± 4	—	1999.9
04 36 27.88	-41 14 46.5	57	13.10 ± 0.03	12.05 ± 0.03	0.073 ± 0.012	0.013 ± 0.016	19	M8	—	25 ± 4	9 ± 2	LG	1999.0
04 36 50.19	-18 03 26.2	20	13.65 ± 0.02	12.53 ± 0.02	0.204 ± 0.017	-0.015 ± 0.018	19	M7	—	39 ± 5	37 ± 5	—	1998.9

Continued on Next Page...

Table 2.12 – Continued

RA (J2000) (1)	DEC (J2000) (2)	Ref.[1] (3)	2MASS J[3] (mag) (4)	2MASS K_s[3] (mag) (5)	$\mu_\alpha cos(\delta)$ ($''$ yr^{-1}) (6)	μ_δ ($''$ yr^{-1}) (7)	μ Ref.[2] (8)	SpT (opt) (9)	SpT (IR) (10)	Distance[3] (pc) (11)	V_{tan} (km s^{-1}) (12)	Note[4] (13)	Epoch (14)
04 39 01.01	-23 53 08.3	19	14.41 ± 0.03	12.82 ± 0.02	-0.110 ± 0.015	-0.152 ± 0.016	19	L6.5	—	11 ± 1	10 ± 1	—	1998.9
04 40 23.25	-05 30 08.2	57	10.66 ± 0.02	9.55 ± 0.02	0.330 ± 0.038	0.133 ± 0.015	17	M7	—	10 ± 1	16 ± 3	—	1998.8
04 43 05.81	-32 02 09.0	43	15.27 ± 0.05	13.88 ± 0.06	-0.013 ± 0.015	0.211 ± 0.018	19	L5	—	24 ± 2	24 ± 3	—	1999.0
04 43 37.61	+00 02 05.1	40	12.51 ± 0.03	11.22 ± 0.02	0.028 ± 0.014	-0.099 ± 0.014	19	M9	—	16 ± 2	8 ± 2	LG	1998.8
04 44 14.79	+05 43 57.3	74	13.67 ± 0.02	12.52 ± 0.03	0.095 ± 0.021	-0.006 ± 0.021	19	M8	—	32 ± 3	14 ± 3	—	2000.1
04 45 11.19	-06 02 52.6	19	13.26 ± 0.03	12.22 ± 0.03	0.047 ± 0.017	0.007 ± 0.018	19	M7	—	33 ± 4	7 ± 3	—	1998.9
04 45 32.37	-36 42 25.8	19	13.36 ± 0.03	12.26 ± 0.03	0.454 ± 0.018	-0.008 ± 0.023	19	M9	—	23 ± 3	50 ± 7	—	2000.9
04 45 53.87	-30 48 20.4	19	13.39 ± 0.03	11.98 ± 0.02	0.183 ± 0.013	-0.393 ± 0.015	19	L2	—	17 ± 1	34 ± 3	—	1999.0
04 47 43.07	-19 36 04.5	21	15.97 ± 0.07	14.01 ± 0.05	0.069 ± 0.022	0.088 ± 0.023	19	—	L5	26 ± 5	14 ± 4	—	2000.8
04 51 00.93	-34 02 15.0	19	13.54 ± 0.02	12.29 ± 0.03	0.107 ± 0.017	0.138 ± 0.021	19	L0.5	—	22 ± 1	18 ± 2	—	1999.0
04 52 09.94	-22 45 08.4	110	15.52 ± 0.05	14.76 ± 0.11	0.433 ± 0.1	-0.575 ± 0.1	47	esdM8	—	66 ± —	235 ± —	—	1998.9
04 53 26.47	-17 51 54.3	19	15.14 ± 0.04	13.47 ± 0.04	0.037 ± 0.017	-0.021 ± 0.018	19	L3	—	31 ± 6	6 ± 3	—	1998.7
04 55 32.67	-27 01 49.3	19	14.43 ± 0.03	13.08 ± 0.04	0.078 ± 0.016	-0.119 ± 0.017	19	M9	—	39 ± 5	27 ± 5	—	1999.0
04 57 25.65	+68 09 17.7	56	13.25 ± 0.03	12.13 ± 0.03	0.066 ± 0.010	-0.193 ± 0.010	28	M8	—	26 ± 2	25 ± 2	—	1999.8
05 00 21.00	+03 30 50.1	83	13.67 ± 0.02	12.06 ± 0.02	-0.002 ± 0.021	-0.349 ± 0.021	19	L4	—	13 ± 1	22 ± 3	—	2000.1
05 01 24.06	-00 10 45.2	83	14.98 ± 0.04	12.96 ± 0.04	0.158 ± 0.014	-0.139 ± 0.014	19	L4	—	24 ± 5	24 ± 5	LG	1998.7
05 02 13.45	+14 42 36.7	21	14.27 ± 0.03	12.96 ± 0.03	0.060 ± 0.012	-0.022 ± 0.012	19	L0	—	32 ± 2	10 ± 2	—	1998.7
05 08 49.47	-16 47 16.7	19	13.69 ± 0.03	12.53 ± 0.03	-0.197 ± 0.018	-0.362 ± 0.018	19	M8	—	32 ± 3	64 ± 6	—	1999.0
05 10 35.20	-42 08 14.0	63	16.22 ± 0.09	16.00 ± 0.28	0.104 ± 0.015	0.580 ± 0.021	19	—	T5	18 ± 2	50 ± 6	—	1999.8
05 11 01.63	-46 06 01.5	61	13.89 ± 0.03	12.71 ± 0.03	0.067 ± 0.020	0.159 ± 0.021	27	M8.5	—	33 ± 2	27 ± 4	—	1999.8
05 12 06.36	-29 49 54.0	19	15.46 ± 0.06	13.29 ± 0.04	-0.028 ± 0.016	0.099 ± 0.018	19	L4.5	—	27 ± 3	13 ± 3	—	1999.0
05 16 09.45	-04 45 49.9	14	15.98 ± 0.08	15.49 ± 0.20	-0.27 ± 0.03	-0.21 ± 0.03	8	—	T5.5	12 ± 2	20 ± 3	—	1998.7
05 16 15.97	-33 32 04.6	21	15.88 ± 0.06	13.99 ± 0.05	0.059 ± 0.016	0.184 ± 0.019	19	—	L3	44 ± 8	40 ± 8	—	1999.0
05 17 05.48	-41 54 41.3	74	13.46 ± 0.02	12.27 ± 0.02	0.089 ± 0.015	0.016 ± 0.021	19	M9	—	25 ± 2	11 ± 2	—	1999.8
05 17 37.66	-33 49 02.7	57	12.00 ± 0.02	10.83 ± 0.02	0.428 ± 0.005	-0.306 ± 0.004	2	M8	—	17.1 ± —[e]	42.6 ± —	—	1999.0
05 18 46.16	-27 56 45.7	20	15.26 ± 0.04	13.62 ± 0.04	0.020 ± 0.013	0.022 ± 0.014	19	L0	—	51 ± 6	7 ± 3	LG	1999.0
05 18 59.95	-28 28 37.2	19	15.98 ± 0.10	14.16 ± 0.07	-0.065 ± 0.016	-0.282 ± 0.019	19	L7.5	T1	34 ± 6[u]	47 ± 9	CB	1999.0
05 23 38.22	-14 03 02.2	19	13.08 ± 0.02	11.64 ± 0.03	0.090 ± 0.017	0.166 ± 0.017	19	L2.5	L5	13 ± 1	12 ± 1	—	1999.0
05 26 43.48	-44 55 45.5	45	14.08 ± 0.03	12.71 ± 0.03	0.013 ± 0.014	-0.168 ± 0.014	22	M9.5	L1	31 ± 2	25 ± 3	—	1999.7
05 26 59.73	-50 26 21.6	74	15.41 ± 0.07	13.64 ± 0.05	0.008 ± 0.012	0.227 ± 0.020	19	L3	—	35 ± 3	38 ± 5	—	1999.9
05 28 44.35	-32 52 22.8	19	13.71 ± 0.03	12.61 ± 0.03	-0.029 ± 0.016	0.066 ± 0.018	19	M8.5	—	30 ± 2	10 ± 3	—	1999.0
05 32 53.46	+82 46 46.5	110	15.14 ± 0.06	14.90 ± 0.15	1.99 ± 0.13	-1.67 ± 0.11	47	sdL7	—	20 ± —	247 ± —	—	1999.2
05 34 58.44	-15 11 43.9	20	13.19 ± 0.03	11.97 ± 0.02	-0.115 ± 0.018	0.085 ± 0.018	19	M9	—	22 ± 1	15 ± 2	—	1999.0
05 36 19.98	-19 20 39.6	20	15.77 ± 0.08	13.85 ± 0.06	0.017 ± 0.017	-0.024 ± 0.018	19	L1	—	57 ± 7	8 ± 5	—	1999.0
05 38 10.10	-02 36 26.0	107	19.98 ± 0.06	19.60 ± 0.08	0.010 ± 0.004	0.005 ± 0.004	45	—	T6	80 ± 20	4 ± 2	YC	1998.8
05 39 24.74	+40 38 43.7	56	11.11 ± 0.02	10.04 ± 0.02	0.654 ± 0.010	-0.831 ± 0.010	28	M8	—	10 ± 1	49 ± 4	—	1998.9
05 39 52.00	-00 59 01.9	30	14.03 ± 0.03	12.53 ± 0.02	0.164 ± 0.002	0.316 ± 0.003	44	L5	L5	13.1 ± 0.4[q]	22.2 ± 0.7	—	1998.8
05 44 11.50	-24 33 01.8	20	12.53 ± 0.02	11.46 ± 0.02	0.14 ± 0.03	-0.69 ± 0.03	36	M8	—	19 ± 2	63 ± 6	—	1999.0
05 58 58.64	-29 03 36.0	110	14.89 ± 0.04	14.46 ± 0.08	0.37 ± 0.02	0.06 ± 0.02	47	esdM7	—	70 ± —	126 ± —	—	1999.7
05 59 19.14	-14 04 48.8	9	13.80 ± 0.02	13.58 ± 0.05	0.563 ± 0.001	-0.346 ± 0.001	15	T5	T4.5	10.2 ± 0.1[h]	32.1 ± 0.4	—	1999.0
06 00 33.75	-33 14 26.8	19	13.21 ± 0.03	12.01 ± 0.02	-0.015 ± 0.010	0.119 ± 0.011	9	M7.5	—	28 ± 3	16 ± 2	—	1999.1
06 02 06.38	+40 43 58.8	63	15.54 ± 0.07	15.17 ± 0.16	0.243 ± 0.011	-0.212 ± 0.015	19	—	T4.5	14 ± 2	21 ± 3	—	1999.8
06 02 30.45	+39 10 59.2	88	12.30 ± 0.02	10.87 ± 0.02	0.146 ± 0.010	-0.501 ± 0.010	28	L1	—	11 ± 1	28 ± 2	—	1998.8
06 05 01.96	-23 42 27.0	20	14.51 ± 0.04	13.15 ± 0.03	-0.057 ± 0.017	0.082 ± 0.018	19	L0	—	36 ± 4	17 ± 4	—	1999.0
06 08 02.32	-29 44 59.0	19	13.86 ± 0.03	12.69 ± 0.03	0.030 ± 0.020	0.100 ± 0.020	9	M8.5	—	32 ± 2	16 ± 3	—	1999.0
06 08 52.83	-27 53 58.3	19	13.60 ± 0.03	12.37 ± 0.03	-0.013 ± 0.011	-0.002 ± 0.013	19	M9	—	27 ± 4	2 ± 1	LG	1999.0
06 10 34.80	-21 52 00.0	72	< 14.20	< 14.30	-0.1370 ± 0.0006	-0.7141 ± 0.0009	34	—	T7	5.77 ± 0.04[l]	19.9 ± 0.1	VLMC	1999.0
06 15 49.34	-01 00 41.5	75	13.75 ± 0.03	12.54 ± 0.03	0.226 ± 0.012	-0.075 ± 0.014	35	L2	—	20 ± 3	22 ± 4	—	1998.7
06 16 05.32	-45 57 08.0	74	15.16 ± 0.04	13.60 ± 0.04	-0.057 ± 0.014	0.114 ± 0.020	19	L2	—	37 ± 3	22 ± 4	—	1999.9
06 19 12.94	-58 03 20.9	17	16.18 ± 0.10	14.14 ± 0.08	0.0141 ± 0.0008	0.0452 ± 0.0010	34	—	L1	45.5 ± 1.7[l]	10.2 ± 0.4	VLMC	1999.9

Continued on Next Page...

Table 2.12 – Continued

RA (J2000) (1)	DEC (J2000) (2)	Ref.[1] (3)	2MASS J[3] (mag) (4)	2MASS K_s[3] (mag) (5)	$\mu_\alpha cos(\delta)$ ($''$ yr^{-1}) (6)	μ_δ ($''$ yr^{-1}) (7)	μ Ref.[2] (8)	SpT (opt) (9)	SpT (IR) (10)	Distance[3] (pc) (11)	V_{tan} (km s^{-1}) (12)	Note[4] (13)	Epoch (14)
06 19 35.44	-52 49 36.7	74	13.63 ± 0.03	12.45 ± 0.03	0.057 ± 0.012	0.172 ± 0.020	19	M9	—	27 ± 2	23 ± 3	—	1999.9
06 24 45.95	-45 21 54.8	83	14.48 ± 0.03	12.60 ± 0.03	-0.045 ± 0.011	0.370 ± 0.015	19	L5	—	13 ± 2	24 ± 4	—	1999.9
06 26 21.21	+00 29 34.1	40	15.93 ± 0.09	14.86 ± 0.12	0.084 ± 0.015	-0.092 ± 0.015	19	L1	—	61 ± 4	36 ± 5	—	1999.9
06 32 24.02	-50 10 34.9	74	15.02 ± 0.04	13.34 ± 0.03	-0.103 ± 0.013	-0.018 ± 0.021	19	L3	—	30 ± 3	15 ± 2	—	1999.9
06 39 55.96	-74 18 44.6	20	15.80 ± 0.11	14.04 ± 0.08	0.000 ± 0.005	-0.002 ± 0.019	19	L5	—	26 ± 2	0 ± 2	—	1998.9
06 41 18.40	-43 22 32.9	83	13.75 ± 0.03	12.45 ± 0.03	0.189 ± 0.013	0.613 ± 0.018	19	L1.5	—	21 ± 1	64 ± 5	—	1999.3
06 44 14.39	-28 41 41.7	19	13.87 ± 0.03	12.71 ± 0.03	0.155 ± 0.011	-0.036 ± 0.011	9	M8	—	34 ± 3	26 ± 3	—	1999.1
06 49 21.40	+43 45 33.1	69	15.92 ± 1.20	14.29 ± 0.11	-0.035 ± 0.007	-0.049 ± 0.006	34	—	L4	44.6 ± 1.7[l]	12.7 ± 1.4	VLMC	1998.8
06 52 19.77	-25 34 50.5	75	12.76 ± 0.02	11.52 ± 0.02	-0.233 ± 0.005	0.086 ± 0.003	35	L0	—	16 ± 1	19 ± 1	—	1999.1
06 52 30.73	+47 10 34.8	19	13.51 ± 0.02	11.69 ± 0.02	-0.05 ± 0.03	0.12 ± 0.05	36	L4.5	—	11 ± 1	7 ± 3	—	1998.8
06 52 48.47	-57 41 37.6	74	13.63 ± 0.03	12.45 ± 0.02	-0.007 ± 0.008	0.025 ± 0.015	19	M8	—	31 ± 5	4 ± 2	LG	1999.9
06 54 05.64	+65 28 05.1	18	16.22 ± 0.06[a]	14.62 ± 0.06[a]	-0.015 ± 0.006	0.030 ± 0.015	19	—	L6	29 ± 5	5 ± 2	—	1999.1
06 57 25.47	-40 19 13.4	19	12.73 ± 0.02	11.67 ± 0.02	-0.220 ± 0.030	0.026 ± 0.011	9	M7.5	—	23 ± 2	24 ± 4	—	1999.1
06 57 55.76	+40 29 42.0	19	13.30 ± 0.02	12.25 ± 0.02	0.001 ± 0.010	-0.276 ± 0.010	28	M8	—	27 ± 2	35 ± 3	—	1998.8
07 00 36.64	+31 57 26.6	98	12.92 ± 0.02	11.32 ± 0.02	0.130 ± 0.001	-0.546 ± 0.001	40	L3.5	—	12.2 ± 0.3[m]	32.4 ± 0.8	CB	1998.2
07 07 53.27	-49 00 50.3	61	13.23 ± 0.03	12.11 ± 0.03	-0.010 ± 0.005	0.391 ± 0.007	42	M8	—	18.8 ± 1.6[n]	34.9 ± 3.0	—	2000.2
07 08 21.33	+29 50 35.0	47	16.72 ± 0.12	14.77 ± 0.09	0.040 ± 0.014	-0.236 ± 0.016	19	L5	—	36 ± 3	41 ± 5	—	1998.1
07 14 03.94	+37 02 45.9	56	11.98 ± 0.02	10.84 ± 0.02	-0.11 ± 0.03	-0.17 ± 0.03	36	M8	—	15 ± 1	14 ± 2	—	1999.9
07 16 47.90	-06 30 36.9	75	13.90 ± 0.04	12.57 ± 0.04	-0.016 ± 0.013	0.121 ± 0.005	35	L1	—	24 ± 3	14 ± 2	—	2000.2
07 17 16.26	+57 05 43.0	105	14.64 ± 0.03	12.95 ± 0.03	-0.016 ± 0.009	0.046 ± 0.016	19	—	L6.5	12 ± 1	3 ± 1	—	1999.0
07 19 31.88	-50 51 41.0	83	14.09 ± 0.03	12.77 ± 0.03	0.190 ± 0.013	-0.060 ± 0.020	19	L0	—	30 ± 2	28 ± 3	—	2000.2
07 23 14.62	+57 27 08.1	83	13.97 ± 0.03	12.61 ± 0.03	0.062 ± 0.011	-0.238 ± 0.020	19	L1	—	25 ± 3	29 ± 4	—	1999.0
07 27 18.24	+17 10 01.2	10	15.51 ± 0.06[c]	15.81 ± 0.06[c]	1.046 ± 0.004	-0.767 ± 0.003	44	T8	T7	9.1 ± 0.2[q]	55.8 ± 1.2	—	1997.8
07 29 00.02	-39 54 04.3	63	15.92 ± 0.08	< 15.29	-0.578 ± 0.014	1.636 ± 0.018	19	—	T8	6 ± 1	45 ± 10	—	1999.1
07 39 22.03	+66 15 03.9	18	16.94 ± 0.06[a]	16.02 ± 0.06[a]	0.180 ± 0.010	-0.077 ± 0.026	19	—	T1	34 ± 4	31 ± 5	—	1999.1
07 39 43.86	+13 05 07.0	56	13.91 ± 0.10	12.77 ± 0.05	-0.069 ± 0.010	-0.145 ± 0.010	28	M8	—	36 ± 3	28 ± 3	—	1997.8
07 40 07.12	+20 09 21.6	54	16.81 ± 0.06[c]	15.14 ± 0.06[c]	-0.185 ± 0.015	-0.111 ± 0.016	19	—	L6	36 ± 10	37 ± 10	—	1997.9
07 40 09.66	+32 12 03.2	47	16.19 ± 0.09	14.22 ± 0.06	-0.029 ± 0.010	-0.084 ± 0.012	19	L4.5	—	38 ± 4	16 ± 3	—	1998.2
07 41 06.81	+17 38 45.9	57	12.01 ± 0.02	10.94 ± 0.02	-0.198 ± 0.010	-0.506 ± 0.010	28	M7	—	18 ± 2	46 ± 6	—	1997.8
07 41 49.20	+23 51 27.5	54	16.14 ± 0.06[c]	16.02 ± 0.10[c]	-0.243 ± 0.013	-0.143 ± 0.014	19	—	T5	18 ± 2	24 ± 3	—	1997.9
07 42 01.30	+20 55 19.8	54	15.87 ± 0.06[c]	15.96 ± 0.06[c]	-0.316 ± 0.018	-0.255 ± 0.020	19	—	T5	18 ± 2	34 ± 4	—	1997.9
07 46 42.56	+20 00 32.1	82	11.76 ± 0.02	10.47 ± 0.02	-0.3740 ± 0.0003	-0.0579 ± 0.0007	15	L0.5	L1	12.21 ± 0.04[h]	21.9 ± 0.1	CB	1997.9
07 47 56.31	+39 47 32.9	40	15.08 ± 0.04	13.72 ± 0.05	0.052 ± 0.012	-0.057 ± 0.015	19	L0	—	47 ± 3	17 ± 3	—	1998.3
07 51 16.45	-25 30 43.2	75	13.16 ± 0.02	11.99 ± 0.02	-0.885 ± 0.003	0.142 ± 0.005	35	L2.5	—	14 ± 1	58 ± 5	—	1999.1
07 52 23.90	+16 12 15.7	57	10.88 ± 0.02	9.85 ± 0.02	0.182 ± 0.010	-0.359 ± 0.010	28	M7	—	10 ± 1	20 ± 2	—	1997.8
07 52 59.42	+41 36 34.4	40	16.36 ± 0.13	< 15.19	-0.014 ± 0.020	0.041 ± 0.027	19	L0	—	84 ± 10	17 ± 11	—	1998.3
07 53 32.17	+29 17 11.9	47	15.52 ± 0.05	13.85 ± 0.04	-0.090 ± 0.012	-0.102 ± 0.013	19	L2	—	44 ± 3	28 ± 3	—	1998.1
07 55 15.28	+29 34 45.3	54	16.83 ± 0.06[c]	15.36 ± 0.06[c]	-0.092 ± 0.019	-0.074 ± 0.022	19	—	L3.5	62 ± 24	35 ± 15	—	1998.1
07 55 47.95	+22 12 16.9	10	15.73 ± 0.06[c]	15.98 ± 0.06[c]	-0.034 ± 0.016	-0.248 ± 0.017	19	T6	T5	18 ± 2	21 ± 2	—	1998.8
07 56 25.29	+12 44 56.0	47	16.66 ± 0.14	14.73 ± 0.12	0.004 ± 0.015	-0.056 ± 0.016	19	L6	—	30 ± 3	8 ± 2	—	1997.8
07 56 56.31	+23 14 57.7	54	16.92 ± 0.06[c]	15.04 ± 0.06[c]	0.158 ± 0.016	-0.156 ± 0.017	19	—	L3.5	65 ± 12	68 ± 14	—	1998.8
07 58 40.37	+32 47 24.5	54	14.99 ± 0.06[c]	13.82 ± 0.06[c]	-0.191 ± 0.014	-0.349 ± 0.017	19	—	T2	11 ± 1	22 ± 1	—	1998.3
07 59 29.47	+03 23 56.4	74	13.88 ± 0.03	12.70 ± 0.02	-0.052 ± 0.020	-0.003 ± 0.020	19	M7	—	42 ± 5	11 ± 4	—	2000.0
08 01 40.56	+46 28 49.8	47	16.35 ± 0.06[c]	14.61 ± 0.06[c]	-0.200 ± 0.009	-0.335 ± 0.013	19	L6.5	—	26 ± 2	48 ± 4	—	1998.3
08 04 05.80	+61 53 33.6	56	12.74 ± 0.02	11.45 ± 0.02	-0.05 ± 0.02	-0.63 ± 0.04	36	M9	—	18 ± 2	54 ± 8	—	1999.0
08 04 14.29	+03 30 47.4	74	13.69 ± 0.03	12.44 ± 0.02	-0.006 ± 0.020	-0.013 ± 0.020	19	M8.5	—	30 ± 2	2 ± 3	—	2000.1
08 05 31.89	+48 12 33.0	40	14.74 ± 0.06[c]	13.55 ± 0.06[c]	-0.455 ± 0.012	0.054 ± 0.018	19	L4	L9	15 ± 3[ii]	32 ± 6	CB-UBL	1999.0
08 07 26.07	+32 13 10.1	105	12.17 ± 0.02	11.05 ± 0.03	-0.356 ± 0.010	-0.248 ± 0.010	28	M8	—	16 ± 1	33 ± 3	—	1999.8
08 09 59.03	+44 34 21.6	54	16.51 ± 0.06[c]	14.34 ± 0.06[c]	-0.198 ± 0.014	-0.214 ± 0.019	19	—	L6	25 ± 5	35 ± 7	—	2000.0
08 10 58.65	+14 20 39.0	33	12.73 ± 0.02	11.59 ± 0.02	-0.034 ± 0.019	-0.128 ± 0.019	29	M8	—	21 ± 2	13 ± 2	—	1997.8

Continued on Next Page...

Table 2.12 – Continued

RA (J2000) (1)	DEC (J2000) (2)	Ref.[1] (3)	2MASS J[3] (mag) (4)	2MASS K_s[3] (mag) (5)	$\mu_\alpha cos(\delta)$ ($''$ yr^{-1}) (6)	μ_δ ($''$ yr^{-1}) (7)	μ Ref.[2] (8)	SpT (opt) (9)	SpT (IR) (10)	Distance[3] (pc) (11)	V_{tan} (km s^{-1}) (12)	Note[4] (13)	Epoch (14)
08 12 31.70	-24 44 42.3	75	13.82 ± 0.03	12.39 ± 0.02	0.096 ± 0.004	-0.165 ± 0.006	35	L2.5	—	19 ± 3	17 ± 3	—	1999.1
08 15 14.07	+10 30 11.7	74	12.42 ± 0.02	11.33 ± 0.02	-0.059 ± 0.020	0.048 ± 0.020	19	M7	—	22 ± 3	8 ± 2	—	2000.1
08 18 58.04	+23 33 52.2	33	12.18 ± 0.02	11.15 ± 0.02	0.263 ± 0.010	-0.314 ± 0.010	28	M7	—	19 ± 2	37 ± 4	—	1998.0
08 19 46.02	+16 58 53.9	19	13.79 ± 0.02	12.62 ± 0.02	-0.160 ± 0.016	-0.035 ± 0.017	19	M9	—	29 ± 4	23 ± 4	—	1998.9
08 20 29.96	+45 00 31.5	47	16.28 ± 0.11	14.22 ± 0.07	-0.111 ± 0.009	-0.323 ± 0.012	19	L5	—	28 ± 3	46 ± 4	—	1998.3
08 20 30.13	+10 37 37.2	18	17.20 ± 0.06[a]	15.57 ± 0.06[a]	-0.077 ± 0.017	-0.026 ± 0.017	19	—	L9.5	30 ± 5	11 ± 3	—	2000.1
08 23 03.13	-49 12 01.2	75	13.55 ± 0.03	12.06 ± 0.02	-0.137 ± 0.004	0.017 ± 0.001	35	L1.5	—	19 ± 1	12 ± 1	—	2000.2
08 23 48.18	+24 28 57.7	83	14.99 ± 0.04	13.38 ± 0.03	-0.170 ± 0.014	0.062 ± 0.015	19	L3	—	29 ± 3	25 ± 3	—	1999.9
08 25 19.68	+21 15 52.1	47	15.10 ± 0.03	13.03 ± 0.03	-0.510 ± 0.002	-0.288 ± 0.002	15	L7.5	L6	10.7 ± 0.1[h]	29.6 ± 0.3	—	1998.0
08 28 34.19	-13 09 19.8	75	12.80 ± 0.03	11.30 ± 0.02	-0.547 ± 0.018	0.078 ± 0.010	35	L1	—	14 ± 2	38 ± 5	—	1999.3
08 29 06.64	+14 56 22.5	47	14.75 ± 0.03	13.17 ± 0.03	-0.048 ± 0.010	-0.244 ± 0.010	19	L2	—	31 ± 2	36 ± 3	—	1997.9
08 29 32.44	-02 38 54.3	19	13.93 ± 0.03	12.79 ± 0.04	0.004 ± 0.006	-0.003 ± 0.006	9	M8	—	36 ± 3	1 ± 1	—	1999.0
08 29 49.08	-00 12 24.1	19	13.49 ± 0.03	12.47 ± 0.03	-0.197 ± 0.017	0.175 ± 0.017	19	M7	—	36 ± 9	45 ± 12	—	1999.0
08 29 57.07	+26 55 09.9	47	17.11 ± 0.19	14.96 ± 0.10	-0.099 ± 0.015	-0.043 ± 0.017	19	L6.5	—	31 ± 3	16 ± 3	—	1998.1
08 30 08.25	+48 28 48.2	32	15.44 ± 0.05	13.68 ± 0.04	-1.006 ± 0.006	-0.770 ± 0.005	44	L8	L9	13.1 ± 0.6[q]	78.6 ± 3.6	—	1999.0
08 30 32.56	+09 47 15.3	57	11.89 ± 0.02	10.76 ± 0.02	-0.500 ± 0.003	-0.449 ± 0.004	12	M7.5	—	16.7 ± 1.3[f]	53.3 ± 4.1	—	2000.2
08 30 48.78	+01 28 31.1	54	16.25 ± 0.06[c]	16.29 ± 0.10[c]	0.236 ± 0.020	-0.312 ± 0.020	19	—	T4.5	23 ± 3	43 ± 6	—	2000.1
08 31 55.98	+10 25 41.7	74	13.62 ± 0.03	12.45 ± 0.03	-0.049 ± 0.021	-0.184 ± 0.021	19	M9	—	27 ± 2	24 ± 3	—	2000.2
08 32 04.51	-01 28 36.0	47	14.13 ± 0.03	12.71 ± 0.03	0.070 ± 0.015	0.003 ± 0.015	19	L1.5	—	25 ± 2	8 ± 2	—	1998.9
08 35 06.22	+19 53 05.0	18	16.07 ± 0.06[a]	14.45 ± 0.06[a]	-0.158 ± 0.013	-0.108 ± 0.014	19	—	L4.5	36 ± 4	32 ± 4	—	1998.8
08 35 23.66	+10 29 31.8	74	13.14 ± 0.02	12.05 ± 0.02	-0.050 ± 0.022	-0.179 ± 0.022	19	M7	—	30 ± 4	27 ± 4	—	2000.9
08 35 42.56	-08 19 23.7	19	13.17 ± 0.02	11.14 ± 0.02	-0.53 ± 0.03	0.30 ± 0.03	36	L5	—	7 ± 1	20 ± 2	—	1999.1
08 35 58.29	+05 48 30.8	83	14.53 ± 0.04	13.17 ± 0.03	-0.099 ± 0.021	-0.020 ± 0.021	19	L3	—	24 ± 4	11 ± 3	—	2000.1
08 37 17.18	-00 00 17.9	55	17.10 ± 0.21	< 15.67	-0.015 ± 0.008	-0.172 ± 0.017	44	T0	T1	30 ± 14[q]	24 ± 12	—	—
08 39 16.08	+12 53 54.3	19	13.75 ± 0.02	12.59 ± 0.02	-0.044 ± 0.015	-0.127 ± 0.016	19	M9	—	28 ± 2	18 ± 2	—	1997.9
08 47 28.72	-15 32 37.2	19	13.51 ± 0.03	12.06 ± 0.02	0.145 ± 0.012	-0.183 ± 0.013	19	L2	—	17 ± 1	19 ± 2	—	1999.1
08 50 01.74	-19 24 18.4	19	12.77 ± 0.02	11.63 ± 0.02	-0.116 ± 0.017	0.045 ± 0.018	19	M8	—	21 ± 2	13 ± 2	—	1999.1
08 50 35.93	+10 57 15.6	46	16.47 ± 0.11	14.47 ± 0.07	-0.145 ± 0.002	-0.008 ± 0.002	15	L6	—	25.6 ± 2.3[h]	17.5 ± 1.6	CB	1997.9
08 51 16.27	+18 17 30.2	18	16.81 ± 0.06[a]	15.01 ± 0.06[a]	-0.195 ± 0.018	-0.050 ± 0.019	19	—	L4.5	50 ± 16	48 ± 15	—	1998.8
08 52 34.90	+47 20 35.9	54	16.30 ± 0.06[c]	14.61 ± 0.06[c]	-0.069 ± 0.018	-0.418 ± 0.026	19	—	L9.5	19 ± 2	38 ± 5	—	1998.9
08 53 36.19	-03 29 32.1	51	11.21 ± 0.03	9.94 ± 0.02	-0.5096 ± 0.0008	-0.2004 ± 0.0003	33	M9	—	8.5 ± 0.1[k]	22.1 ± 0.3	—	1999.0
08 56 47.93	+22 35 18.2	19	15.68 ± 0.07	13.95 ± 0.05	-0.208 ± 0.017	-0.006 ± 0.018	19	L3	—	35 ± 7[s]	34 ± 8	CB	1998.8
08 57 27.87	-03 32 39.6	19	14.37 ± 0.03	13.04 ± 0.03	-0.150 ± 0.018	-0.056 ± 0.018	19	M9.5	—	36 ± 2	27 ± 4	—	1998.9
08 57 58.49	+57 08 51.4	32	15.04 ± 0.04	12.96 ± 0.03	-0.413 ± 0.006	-0.349 ± 0.012	19	L8	L8	10 ± 1	25 ± 2	—	1999.9
08 58 34.67	+32 56 27.5	18	16.52 ± 0.06[a]	14.69 ± 0.06[a]	-0.760 ± 0.023	0.075 ± 0.023	19	—	T1	18 ± 1	66 ± 3	—	1998.2
08 59 25.47	-19 49 26.8	19	15.53 ± 0.05	13.75 ± 0.06	-0.300 ± 0.013	-0.081 ± 0.014	19	L6	—	19 ± 2	28 ± 3	—	1999.1
08 59 38.54	+63 41 35.5	83	13.70 ± 0.03	12.39 ± 0.03	-0.096 ± 0.019	-0.495 ± 0.042	19	L0	—	25 ± 3	59 ± 9	—	2000.0
08 59 40.29	+11 45 32.5	74	12.74 ± 0.03	11.49 ± 0.02	-0.275 ± 0.021	-0.060 ± 0.021	19	M8	—	21 ± 2	28 ± 3	—	2000.1
09 02 14.59	-06 42 09.9	19	13.70 ± 0.03	12.69 ± 0.03	0.014 ± 0.010	-0.039 ± 0.009	9	M7	—	40 ± 5	8 ± 2	—	1999.1
09 03 35.14	-06 37 33.6	19	13.67 ± 0.03	12.63 ± 0.03	-0.073 ± 0.007	0.013 ± 0.006	9	M7	—	39 ± 5	14 ± 2	—	1999.1
09 05 46.54	+56 23 11.7	74	15.40 ± 0.05	13.73 ± 0.04	-0.014 ± 0.017	0.089 ± 0.031	19	L5	—	23 ± 4	10 ± 4	—	2000.0
09 08 38.03	+50 32 08.8	19	14.53 ± 0.06[c]	12.93 ± 0.06[c]	-0.395 ± 0.026	-0.478 ± 0.015	10	L5	L9	16 ± 1	46 ± 4	—	1999.2
09 09 00.85	+65 25 27.5	18	16.00 ± 0.06[a]	15.16 ± 0.06[a]	-0.217 ± 0.003	-0.138 ± 0.008	19	—	T1	23 ± 1	28 ± 1	—	2000.0
09 09 57.49	-06 58 18.6	27	13.89 ± 0.02	12.54 ± 0.03	-0.210 ± 0.018	0.015 ± 0.019	19	L0	—	27 ± 2	27 ± 3	—	1999.0
09 11 12.97	+74 01 08.1	83	12.92 ± 0.03	11.75 ± 0.03	-0.20 ± 0.04	-0.17 ± 0.04	36	L0	—	17 ± 1	21 ± 4	—	2000.2
09 12 14.69	+14 59 39.6	104	15.51 ± 0.08	14.04 ± 0.06	-0.524 ± 0.001	0.2451 ± 0.0005	34	L8	T0	20.5 ± 0.4[l]	56.2 ± 1.1	CB	1997.9
09 13 03.20	+18 41 50.1	46	15.97 ± 0.06	14.28 ± 0.05	0.032 ± 0.016	-0.187 ± 0.017	19	L3	—	46 ± 4	41 ± 5	—	1998.0
09 13 04.43	-07 33 04.2	19	13.40 ± 0.02	12.14 ± 0.03	-0.050 ± 0.050	-0.200 ± 0.050	9	M9	—	24 ± 2	24 ± 6	—	1999.1
09 15 34.13	+04 22 04.5	83	14.55 ± 0.03	13.01 ± 0.04	-0.109 ± 0.025	0.031 ± 0.025	19	L7	—	15 ± 3[ee]	8 ± 2	CB	2001.1

Continued on Next Page...

Table 2.12 – Continued

RA (J2000) (1)	DEC (J2000) (2)	Ref.[1] (3)	2MASS J[3] (mag) (4)	2MASS K_s[3] (mag) (5)	$\mu_\alpha cos(\delta)$ ($''$ yr^{-1}) (6)	μ_δ ($''$ yr^{-1}) (7)	μ Ref.[2] (8)	SpT (opt) (9)	SpT (IR) (10)	Distance[3] (pc) (11)	V_{tan} (km s^{-1}) (12)	Note[4] (13)	Epoch (14)
09 16 15.04	+21 39 51.2	19	13.22 ± 0.02	12.07 ± 0.03	-0.199 ± 0.017	-0.054 ± 0.018	19	M9	—	22 ± 3	22 ± 3	—	1998.0
09 18 38.15	+21 34 05.8	46	15.66 ± 0.06	13.90 ± 0.04	0.330 ± 0.015	-0.156 ± 0.017	19	L2.5	—	43 ± 4	75 ± 7	—	1998.0
09 20 12.23	+35 17 42.9	47	15.63 ± 0.06	13.98 ± 0.06	-0.167 ± 0.009	-0.200 ± 0.010	19	L6.5	T0	21 ± 3[u]	26 ± 4	CB	1998.2
09 21 14.10	-21 04 44.6	83	12.78 ± 0.02	11.69 ± 0.02	0.244 ± 0.016	-0.908 ± 0.017	19	L2	—	12 ± 1	56 ± 4	UBL	2000.2
09 22 19.52	-80 10 39.9	83	15.28 ± 0.05	13.68 ± 0.05	0.041 ± 0.004	-0.045 ± 0.022	19	L4	—	27 ± 6	8 ± 3	—	2000.0
09 26 15.37	+58 47 21.2	32	15.90 ± 0.07	15.45 ± 0.19	-0.19 ± 0.25	-0.23 ± 0.27	4	—	T4.5	38 ± 7[u]	54 ± 55	CB	2000.2
09 27 57.41	+60 27 46.4	40	15.52 ± 0.06	14.23 ± 0.06	0.003 ± 0.013	0.016 ± 0.025	19	L1	—	51 ± 7	4 ± 6	—	1999.0
09 28 25.62	+42 30 54.5	105	13.08 ± 0.03	11.94 ± 0.02	-0.390 ± 0.019	-0.378 ± 0.025	19	M8.5	—	23 ± 3	58 ± 9	—	1999.1
09 28 39.72	-16 03 12.8	47	15.32 ± 0.04	13.62 ± 0.05	-0.158 ± 0.017	0.034 ± 0.017	19	L2	—	40 ± 3	31 ± 4	—	1998.2
09 31 09.55	+03 27 33.1	54	16.75 ± 0.10[c]	15.65 ± 0.10[c]	-0.612 ± 0.018	-0.131 ± 0.018	19	—	L7.5	36 ± 8	108 ± 23	UBL	2000.1
09 31 28.23	+05 28 22.3	74	12.86 ± 0.03	11.80 ± 0.02	-0.142 ± 0.021	-0.204 ± 0.021	19	M7	—	27 ± 3	31 ± 5	—	2000.1
09 34 29.20	-13 52 43.4	19	13.04 ± 0.03	12.01 ± 0.03	-0.238 ± 0.016	-0.127 ± 0.017	19	M7	—	29 ± 7	37 ± 10	—	1998.2
09 35 28.03	-29 34 59.6	83	14.04 ± 0.03	12.82 ± 0.03	-0.023 ± 0.016	0.064 ± 0.018	19	L0	—	29 ± 2	9 ± 3	—	1999.2
09 37 34.87	+29 31 40.9	10	14.58 ± 0.06[c]	15.51 ± 0.12[c]	0.973 ± 0.005	-1.298 ± 0.006	44	d/sdT6	T6	6.1 ± 0.1[q]	47.2 ± 1.1	—	2000.3
09 38 40.22	-27 48 18.4	74	13.00 ± 0.03	11.93 ± 0.02	-0.408 ± 0.017	-0.164 ± 0.020	19	M8	—	23 ± 4	49 ± 9	—	2000.1
09 39 35.48	-24 48 27.9	99	15.98 ± 0.11	< 16.56	0.592 ± 0.019	-1.064 ± 0.021	19	—	T8	10 ± 2	57 ± 12	—	2000.1
09 42 46.04	+55 31 02.5	74	12.92 ± 0.02	11.80 ± 0.02	-0.066 ± 0.018	0.085 ± 0.032	19	M8	—	23 ± 8	12 ± 5	—	1999.0
09 44 02.79	+31 31 32.8	47	15.50 ± 0.05	14.01 ± 0.04	0.043 ± 0.016	-0.033 ± 0.013	10	L2	—	43 ± 3	11 ± 3	—	1998.2
09 47 44.77	+02 24 32.7	74	13.17 ± 0.03	12.08 ± 0.03	-0.081 ± 0.020	-0.162 ± 0.020	19	M8	—	25 ± 4	22 ± 4	—	2000.1
09 49 08.60	-15 45 48.5	99	16.15 ± 0.12	15.23 ± 0.17	-0.10 ± 0.04	0.00 ± 0.06	41	—	T2	22 ± 1	10 ± 4	—	2000.2
09 49 22.23	+08 06 45.0	57	12.31 ± 0.02	11.21 ± 0.03	0.06 ± 0.03	-0.90 ± 0.02	36	M8.5	—	16 ± 1	67 ± 5	—	2000.2
09 51 05.49	+35 58 02.1	47	17.23 ± 0.21	15.14 ± 0.13	-0.100 ± 0.007	-0.161 ± 0.009	44	L6	—	62 ± 36[q]	56 ± 33	VLMC	1998.2
09 53 21.26	-10 14 20.5	20	13.47 ± 0.03	12.14 ± 0.02	-0.048 ± 0.019	-0.089 ± 0.019	19	L0	—	22 ± 1	11 ± 2	—	1999.1
10 03 19.18	-01 05 07.9	77	12.33 ± 0.02	11.24 ± 0.02	-0.490 ± 0.019	0.022 ± 0.019	29	M7	—	21 ± 2	49 ± 6	—	1999.1
10 04 20.66	+50 22 59.6	81	14.83 ± 0.05	12.78 ± 0.03	-0.133 ± 0.040	-0.185 ± 0.015	10	L2	—	32 ± 2	35 ± 5	VLMC	1999.1
10 04 39.29	-33 35 18.9	36	14.48 ± 0.04	12.92 ± 0.02	0.366 ± 0.016	-0.340 ± 0.019	19	L4	—	19 ± 2	45 ± 5	—	1999.3
10 06 31.97	-16 53 26.6	84	12.04 ± 0.02	10.99 ± 0.02	-0.28 ± 0.09	0.18 ± 0.08	36	M7.5	—	16 ± 2	26 ± 8	—	1998.3
10 07 11.85	+19 30 56.3	18	16.90 ± 0.10[a]	15.16 ± 0.06[a]	-0.263 ± 0.015	-0.018 ± 0.016	19	—	L8	27 ± 5	34 ± 6	—	1998.1
10 07 33.69	-45 55 14.7	63	15.65 ± 0.07	15.56 ± 0.23	-0.758 ± 0.013	0.138 ± 0.019	19	—	T5	15 ± 2	53 ± 7	—	2000.1
10 10 14.80	-04 06 49.9	19	15.51 ± 0.06	13.62 ± 0.05	-0.321 ± 0.016	0.020 ± 0.013	10	L6	—	18 ± 2	27 ± 3	—	1999.0
10 11 00.24	+42 45 03.5	102	13.36 ± 0.03	12.32 ± 0.02	-0.134 ± 0.006	-0.149 ± 0.006	41	M7.5	—	33.0 ± 3.2[o]	31.4 ± 3.2	—	1999.1
10 13 07.35	-13 56 20.4	110	14.59 ± 0.04	14.35 ± 0.08	0.066 ± 0.007	-1.026 ± 0.004	47	sdM9.5	—	30 ± —	147 ± —	—	1999.1
10 16 34.70	+27 51 49.7	66	11.99 ± 0.02	10.96 ± 0.02	-0.089 ± 0.019	-0.502 ± 0.019	29	M8	—	14 ± 1	35 ± 3	—	1998.2
10 17 07.54	+13 08 39.8	19	14.10 ± 0.02	12.71 ± 0.02	0.061 ± 0.022	-0.094 ± 0.012	10	L2	L1	33 ± 5[hh]	17 ± 4	CB	1997.9
10 18 43.14	-16 24 27.3	19	13.74 ± 0.03	12.69 ± 0.03	0.053 ± 0.015	-0.017 ± 0.016	19	M7.5	—	36 ± 4	10 ± 3	—	1998.2
10 18 58.79	-29 09 53.5	36	14.21 ± 0.03	12.80 ± 0.02	-0.319 ± 0.017	-0.086 ± 0.019	19	L1	—	28 ± 2	44 ± 4	—	1999.2
10 21 09.69	-03 04 19.7	55	16.25 ± 0.09	15.13 ± 0.17	-0.171 ± 0.003	-0.066 ± 0.003	43	T4	T3	29.1 ± 4.0[o]	25.2 ± 2.4	CB	1998.9
10 21 27.42	+50 55 04.3	102	13.39 ± 0.02	12.26 ± 0.02	-0.378 ± 0.002	0.056 ± 0.001	41	M7	—	27.5 ± 4.7[o]	49.9 ± 8.5	—	1999.0
10 21 32.32	-20 44 06.9	76	13.19 ± 0.02	12.07 ± 0.03	-0.312 ± 0.016	-0.051 ± 0.017	19	M9	—	22 ± 1	33 ± 3	—	1999.3
10 22 04.89	+02 00 47.7	83	14.10 ± 0.03	12.90 ± 0.03	-0.173 ± 0.018	-0.398 ± 0.016	10	M9	—	34 ± 4	69 ± 10	LG	2000.1
10 22 14.89	+41 14 26.6	104	14.90 ± 0.04	13.61 ± 0.04	-0.1202 ± 0.0006	-0.1386 ± 0.0005	34	L0	—	39.0 ± 1.1[l]	33.9 ± 0.9	VLMC	1998.3
10 22 48.21	+58 25 45.3	83	13.50 ± 0.03	12.16 ± 0.03	-0.36 ± 0.10	-0.78 ± 0.09	36	L1	—	20 ± 1	81 ± 9	—	2000.1
10 24 09.97	+18 15 53.3	33	12.28 ± 0.02	11.24 ± 0.02	-0.144 ± 0.019	-0.070 ± 0.019	29	M8	—	16 ± 1	13 ± 2	—	1998.1
10 25 52.27	+32 12 34.9	18	17.04 ± 0.10[a]	15.18 ± 0.06[a]	0.393 ± 0.011	-0.228 ± 0.013	19	—	L7.5	29 ± 10	63 ± 23	—	1999.4
10 28 40.42	-14 38 43.9	20	13.06 ± 0.03	12.03 ± 0.02	0.024 ± 0.016	-0.162 ± 0.016	19	M7	—	30 ± 4	23 ± 4	—	1998.2
10 29 21.65	+16 26 52.6	47	14.29 ± 0.03	12.62 ± 0.02	0.359 ± 0.015	-0.348 ± 0.017	10	L2.5	—	23 ± 2	55 ± 5	—	1997.9
10 32 17.06	+05 01 03.2	74	13.67 ± 0.04	12.54 ± 0.02	-0.032 ± 0.021	-0.012 ± 0.021	19	M8.5	—	29 ± 2	5 ± 3	—	2000.1
10 33 21.86	+40 05 49.9	18	16.88 ± 0.06[a]	15.63 ± 0.10[a]	0.154 ± 0.013	-0.188 ± 0.018	19	—	L6	45 ± 8	53 ± 10	UBL	1999.2
10 35 24.55	+25 07 45.0	47	14.76 ± 0.03	13.29 ± 0.03	-0.181 ± 0.017	-0.272 ± 0.023	10	L1	—	36 ± 2	55 ± 5	—	1998.2
10 36 53.05	-34 41 38.0	36	15.62 ± 0.05	13.80 ± 0.04	-0.020 ± 0.015	-0.462 ± 0.019	19	L6	—	20 ± 2	43 ± 4	—	1999.2

Continued on Next Page...

Table 2.12 – Continued

RA (J2000) (1)	DEC (J2000) (2)	Ref.[1] (3)	2MASS J[3] (mag) (4)	2MASS K_s[3] (mag) (5)	$\mu_\alpha cos(\delta)$ ($''$ yr^{-1}) (6)	μ_δ ($''$ yr^{-1}) (7)	μ Ref.[2] (8)	SpT (opt) (9)	SpT (IR) (10)	Distance[3] (pc) (11)	V_{tan} (km s^{-1}) (12)	Note[4] (13)	Epoch (14)
10 39 31.37	+32 56 26.3	18	16.35 ± 0.06[a]	14.98 ± 0.06[a]	0.031 ± 0.046	-0.023 ± 0.054	19	—	T1	21 ± 1	4 ± 5	—	1998.2
10 43 07.58	+22 25 23.6	20	15.97 ± 0.07	13.99 ± 0.04	-0.14 ± 0.00	-0.02 ± 0.00	36	L8	—	16 ± 1	11 ± 1	—	1998.1
10 43 25.08	+00 01 48.2	90	15.94 ± 0.08	14.47 ± 0.10	-0.161 ± 0.019	-0.156 ± 0.019	19	L3	—	45 ± 4	48 ± 6	—	1999.0
10 43 35.08	+12 13 14.9	18	15.96 ± 0.06[a]	14.22 ± 0.06[a]	0.046 ± 0.017	-0.248 ± 0.018	19	—	L7	20 ± 3	24 ± 4	—	1998.9
10 44 09.42	+04 29 37.6	54	15.98 ± 0.06[c]	14.34 ± 0.06[c]	-0.002 ± 0.012	0.094 ± 0.010	10	—	L7	21 ± 2	10 ± 1	—	2000.1
10 45 17.18	-26 07 24.9	36	12.79 ± 0.02	11.63 ± 0.02	-0.162 ± 0.017	-0.146 ± 0.019	19	M8	—	21 ± 2	22 ± 3	—	1999.2
10 45 24.00	-01 49 57.6	36	13.16 ± 0.02	11.78 ± 0.02	-0.495 ± 0.018	0.012 ± 0.012	10	L1	—	17 ± 1	40 ± 3	—	1999.1
10 47 31.09	-18 15 57.4	65	14.20 ± 0.03	12.89 ± 0.03	-0.347 ± 0.017	0.054 ± 0.014	10	L2.5	—	22 ± 2	37 ± 4	—	1998.3
10 47 53.85	+21 24 23.4	7	15.82 ± 0.06	< 16.41	-1.714 ± 0.007	-0.489 ± 0.004	44	T7	T6.5	10.6 ± 0.4[q]	86.5 ± 3.5	—	1998.1
10 48 14.63	-39 56 06.2	28	9.54 ± 0.02	8.45 ± 0.02	-1.175 ± 0.005	-0.993 ± 0.005	13	M9	—	4.00 ± 0.03[g]	29.2 ± 0.2	—	1999.3
10 48 27.88	-52 54 18.0	75	14.02 ± 0.03	12.67 ± 0.03	-0.179 ± 0.009	0.033 ± 0.017	35	L1.5	—	24 ± 3	20 ± 3	—	1999.4
10 48 29.26	+09 19 37.3	18	16.61 ± 0.06[a]	15.82 ± 0.06[a]	-0.268 ± 0.020	0.241 ± 0.020	19	—	T2.5	27 ± 2	46 ± 4	—	2000.2
10 48 42.81	+01 11 58.0	40	12.92 ± 0.02	11.62 ± 0.02	-0.442 ± 0.013	-0.209 ± 0.012	10	L1	L4	15 ± 1	36 ± 3	—	2000.1
10 51 19.00	+56 13 08.6	83	13.24 ± 0.03	11.91 ± 0.02	-0.231 ± 0.034	-0.288 ± 0.014	10	L2	—	15 ± 1	27 ± 3	—	1999.9
10 52 13.50	+44 22 55.9	18	16.07 ± 0.06[a]	14.44 ± 0.06[a]	0.018 ± 0.017	-0.152 ± 0.024	19	—	T0.5	17 ± 1	12 ± 2	—	1998.3
10 54 41.68	+12 14 08.4	19	12.46 ± 0.02	11.45 ± 0.02	0.103 ± 0.018	-0.080 ± 0.019	19	M7.5	—	20 ± 2	12 ± 2	—	1999.2
10 55 47.33	+08 08 42.7	74	12.55 ± 0.03	11.37 ± 0.02	-0.35 ± 0.02	-0.10 ± 0.03	36	M8	—	19 ± 2	33 ± 3	—	2000.2
10 58 47.87	-15 48 17.2	26	14.16 ± 0.04	12.53 ± 0.03	-0.2529 ± 0.0005	0.0414 ± 0.0004	15	L3	L3	17.3 ± 0.3[h]	21.1 ± 0.4	—	1998.2
10 59 51.38	-21 13 08.2	19	14.56 ± 0.04	13.21 ± 0.03	0.134 ± 0.017	-0.158 ± 0.014	10	L1	—	33 ± 2	32 ± 3	—	1998.4
11 00 09.65	+49 57 47.0	74	15.28 ± 0.04	13.47 ± 0.03	-0.133 ± 0.018	-0.151 ± 0.028	19	L3.5	—	30 ± 6	29 ± 7	—	1999.0
11 02 09.90	-34 30 35.5	94	13.03 ± 0.02	11.89 ± 0.02	-0.033 ± 0.012	-0.024 ± 0.015	19	M8.5	—	22 ± 3	4 ± 2	LG	1999.2
11 02 33.75	-23 59 46.4	47	16.72 ± 0.16	14.59 ± 0.10	-0.238 ± 0.019	0.075 ± 0.020	19	L4.5	—	48 ± 5	57 ± 7	—	2000.1
11 04 01.27	+19 59 21.7	19	14.38 ± 0.03	12.95 ± 0.03	0.075 ± 0.015	0.139 ± 0.020	19	L4	—	18 ± 2	14 ± 2	—	2000.3
11 06 11.97	+27 54 22.5	63	14.82 ± 0.04	13.80 ± 0.05	-0.229 ± 0.019	-0.448 ± 0.021	19	—	T2.5	11 ± 1	26 ± 2	—	2000.3
11 08 30.81	+68 30 16.9	33	13.12 ± 0.02	11.58 ± 0.02	-0.25 ± 0.04	-0.21 ± 0.04	36	L1	—	17 ± 1	26 ± 4	—	1999.2
11 10 10.01	+01 16 13.0	32	16.34 ± 0.12	< 15.13	-0.243 ± 0.021	-0.238 ± 0.018	10	—	T5.5	11 ± 1	17 ± 2	—	2000.1
11 10 33.21	+54 24 02.8	74	12.97 ± 0.03	11.91 ± 0.02	-0.066 ± 0.009	-0.299 ± 0.016	19	M7	—	28 ± 7	41 ± 10	—	1999.9
11 12 25.67	+35 48 13.1	47	14.58 ± 0.03	12.72 ± 0.03	-0.2486 ± 0.0007	-0.1513 ± 0.0007	34	L4.5	—	21.7 ± 0.4[l]	30.0 ± 0.6	CB	1998.4
11 12 49.10	-20 44 31.5	44	14.92 ± 0.04	13.47 ± 0.04	0.001 ± 0.014	0.023 ± 0.015	19	—	L0.5	41 ± 11	4 ± 3	—	1998.3
11 13 16.94	-00 02 46.7	40	15.08 ± 0.04	13.80 ± 0.05	0.042 ± 0.022	0.006 ± 0.013	10	L0	—	47 ± 3	9 ± 5	—	1999.0
11 13 20.09	+34 30 58.2	18	17.04 ± 0.06[a]	15.38 ± 0.06[a]	0.108 ± 0.040	-0.025 ± 0.049	19	—	L3	75 ± 13	40 ± 16	—	1998.4
11 14 51.33	-26 18 23.5	99	15.86 ± 0.08	< 16.11	-3.03 ± 0.04	-0.36 ± 0.04	41	—	T7.5	10 ± 2	140 ± 22	—	1999.2
11 17 36.91	+36 09 35.9	19	14.27 ± 0.03	12.96 ± 0.03	0.001 ± 0.019	-0.016 ± 0.023	19	L0	—	32 ± 8	2 ± 4	—	1999.1
11 21 18.58	+43 32 46.4	18	17.19 ± 0.10[a]	16.15 ± 0.08[a]	-0.057 ± 0.024	0.026 ± 0.033	19	—	L7.5	46 ± 6	14 ± 6	UBL	2000.3
11 21 49.24	-13 13 08.4	33	11.93 ± 0.02	10.74 ± 0.02	-0.4650 ± 0.0007	-0.0503 ± 0.0007	33	M8.5	—	14.3 ± 0.4[k]	31.7 ± 1.0	CB	1998.3
11 22 08.26	-35 12 36.3	99	15.02 ± 0.04	14.38 ± 0.07	-0.15 ± 0.04	-0.25 ± 0.03	41	—	T2	15 ± 1	20 ± 2	—	1999.2
11 22 36.24	-39 16 05.4	36	15.71 ± 0.06	13.88 ± 0.05	0.073 ± 0.012	-0.180 ± 0.015	19	L3	—	41 ± 4	37 ± 4	—	1999.3
11 23 36.05	+12 41 22.2	19	14.00 ± 0.02	12.81 ± 0.02	-0.036 ± 0.017	0.009 ± 0.017	19	M7	—	46 ± 5	8 ± 4	—	1998.0
11 23 55.64	+41 22 28.6	47	16.07 ± 0.08	14.34 ± 0.06	-0.110 ± 0.025	-0.060 ± 0.013	10	L2.5	—	52 ± 4	31 ± 6	—	1998.3
11 24 04.87	+38 08 05.4	19	12.71 ± 0.02	11.57 ± 0.03	0.130 ± 0.021	-0.019 ± 0.027	19	M8.5	—	19 ± 3	12 ± 3	—	1998.3
11 26 15.28	+01 20 48.1	54	16.82 ± 0.06[c]	15.07 ± 0.06[c]	-0.131 ± 0.022	0.042 ± 0.022	19	—	L6	35 ± 3	23 ± 4	—	2000.1
11 26 39.91	-50 03 55.0	31	14.00 ± 0.03	12.83 ± 0.03	-1.570 ± 0.004	0.438 ± 0.011	20	L4.5	L9	14 ± 1	106 ± 11	UBL	1999.4
11 27 53.46	+74 11 07.6	33	13.02 ± 0.04	11.95 ± 0.03	-0.016 ± 0.019	-0.030 ± 0.019	29	M8	—	34 ± 6[w]	5 ± 3	CB	2000.3
11 28 25.57	+78 31 01.6	56	13.38 ± 0.02	12.37 ± 0.02	-0.008 ± 0.010	-0.271 ± 0.010	28	M7	—	34 ± 9	44 ± 11	—	1999.2
11 30 47.61	-22 10 33.5	19	13.80 ± 0.03	12.73 ± 0.03	-0.126 ± 0.017	-0.232 ± 0.018	19	M8	—	34 ± 3	43 ± 5	—	1998.3
11 34 54.93	+00 22 54.1	40	12.85 ± 0.02	11.67 ± 0.02	0.401 ± 0.021	-0.343 ± 0.021	19	M9	—	19 ± 1	47 ± 4	—	2000.2
11 38 33.08	+67 40 40.3	40	15.22 ± 0.04	13.95 ± 0.05	0.024 ± 0.014	-0.127 ± 0.037	19	L0	—	50 ± 6	31 ± 9	—	1999.2
11 39 11.07	+08 41 12.1	74	12.92 ± 0.03	11.84 ± 0.02	0.089 ± 0.021	-0.025 ± 0.022	19	M7.5	—	25 ± 2	11 ± 3	—	2000.2
11 39 51.16	-31 59 21.4	36	12.69 ± 0.03	11.50 ± 0.02	-0.071 ± 0.014	-0.017 ± 0.016	19	M9	—	18 ± 2	6 ± 1	LG	2000.0
11 41 44.06	-22 32 15.6	19	12.63 ± 0.02	11.57 ± 0.02	-0.141 ± 0.019	0.400 ± 0.019	29	M7.5	—	22 ± 2	44 ± 5	—	1998.4

Continued on Next Page...

Table 2.12 – Continued

RA (J2000) (1)	DEC (J2000) (2)	Ref.[1] (3)	2MASS J[3] (mag) (4)	2MASS K_s[3] (mag) (5)	$\mu_\alpha cos(\delta)$ ($''$ yr^{-1}) (6)	μ_δ ($''$ yr^{-1}) (7)	μ Ref.[2] (8)	SpT (opt) (9)	SpT (IR) (10)	Distance[3] (pc) (11)	V_{tan} (km s^{-1}) (12)	Note[4] (13)	Epoch (14)
11 45 57.14	+23 17 29.7	46	15.39 ± 0.05	13.95 ± 0.06	0.155 ± 0.016	-0.056 ± 0.006	10	L1.5	—	44 ± 3	35 ± 4	—	1999.3
11 46 34.49	+22 30 52.7	46	14.17 ± 0.03	12.59 ± 0.03	0.0320 ± 0.0005	0.0905 ± 0.0005	15	L3	—	27.2 ± 0.6[h]	12.4 ± 0.3	CB	1999.3
11 46 57.91	-39 14 14.4	45	13.64 ± 0.02	12.49 ± 0.03	-0.292 ± 0.012	0.004 ± 0.010	27	M8	—	31 ± 3	44 ± 4	—	2000.1
11 47 04.79	+14 20 09.5	56	13.27 ± 0.02	12.27 ± 0.02	-0.340 ± 0.010	0.133 ± 0.010	28	M7	—	33 ± 4	56 ± 7	—	1998.0
11 48 04.23	+02 54 05.7	40	16.11 ± 0.10	15.20 ± 0.21	0.026 ± 0.025	-0.041 ± 0.010	10	L0	—	75 ± 5	17 ± 6	—	2000.1
11 48 05.02	+02 03 50.9	40	15.52 ± 0.07	14.51 ± 0.12	0.237 ± 0.026	-0.322 ± 0.013	10	L1	—	51 ± 3	96 ± 8	—	2000.1
11 48 54.27	-25 44 40.4	36	13.40 ± 0.02	12.17 ± 0.03	0.147 ± 0.018	0.047 ± 0.020	19	M8	—	28 ± 2	21 ± 3	—	2000.2
11 52 42.66	+24 38 07.9	19	13.03 ± 0.02	11.78 ± 0.02	-0.451 ± 0.032	0.036 ± 0.035	19	M9	—	21 ± 3	44 ± 6	—	1998.2
11 53 39.66	+50 32 09.2	83	14.19 ± 0.03	12.85 ± 0.03	0.084 ± 0.023	0.060 ± 0.011	10	L1	—	27 ± 4	13 ± 3	—	1999.0
11 54 33.99	+01 35 54.5	27	13.16 ± 0.03	11.99 ± 0.02	0.121 ± 0.022	-0.043 ± 0.022	19	M9	—	22 ± 3	13 ± 3	—	2000.1
11 54 42.23	-34 00 39.0	5	14.20 ± 0.03	12.85 ± 0.03	-0.161 ± 0.013	0.004 ± 0.015	19	L0	—	31 ± 2	24 ± 2	—	1999.2
11 55 00.87	+23 07 05.8	46	15.85 ± 0.09	14.08 ± 0.05	0.026 ± 0.025	0.038 ± 0.021	10	L4	—	36 ± 4	8 ± 4	—	1999.2
11 55 39.52	-37 27 35.0	36	12.81 ± 0.02	11.46 ± 0.02	0.050 ± 0.012	-0.767 ± 0.015	19	L2	—	13 ± 1	46 ± 4	—	1999.3
11 55 42.86	-22 24 58.6	57	10.93 ± 0.02	9.88 ± 0.02	-0.340 ± 0.083	-0.142 ± 0.035	17	M7.5	—	10 ± 1	17 ± 5	—	1999.3
11 55 53.89	+05 59 57.7	54	15.78 ± 0.06[c]	14.11 ± 0.06[c]	-0.406 ± 0.022	-0.026 ± 0.022	19	—	L7.5	18 ± 1	35 ± 3	—	2000.2
11 57 48.09	-48 44 42.8	75	14.01 ± 0.03	12.79 ± 0.03	-0.052 ± 0.016	0.001 ± 0.001	35	L0.5	—	27 ± 3	7 ± 2	—	1999.4
11 58 02.69	-25 45 36.9	19	13.58 ± 0.03	12.43 ± 0.02	-0.102 ± 0.019	-0.167 ± 0.021	19	M8	—	30 ± 2	28 ± 4	—	2000.2
11 58 24.84	+13 54 45.6	19	13.93 ± 0.02	12.76 ± 0.02	-0.116 ± 0.017	0.168 ± 0.018	19	M9	—	31 ± 2	30 ± 3	—	1998.0
11 59 38.50	+00 57 26.8	65	14.08 ± 0.03	12.81 ± 0.03	0.012 ± 0.023	0.007 ± 0.017	10	L0	—	30 ± 2	2 ± 3	—	2000.1
12 00 32.92	+20 48 51.3	57	12.86 ± 0.02	11.86 ± 0.02	-0.159 ± 0.019	0.232 ± 0.019	29	M7	—	26 ± 3	35 ± 5	—	1999.4
12 02 25.64	-06 29 02.6	19	13.74 ± 0.03	12.59 ± 0.03	0.096 ± 0.019	-0.075 ± 0.019	19	M9	—	28 ± 2	16 ± 3	—	1999.1
12 02 36.66	-06 04 05.4	19	14.01 ± 0.03	12.82 ± 0.03	0.088 ± 0.018	-0.034 ± 0.018	19	M8	—	36 ± 3	16 ± 3	—	1999.1
12 03 58.12	+00 15 50.0	30	14.01 ± 0.03	12.48 ± 0.02	-1.209 ± 0.018	-0.261 ± 0.015	10	L3	—	19 ± 2	109 ± 10	—	2000.1
12 04 30.36	+32 12 59.5	19	13.82 ± 0.04	12.52 ± 0.03	0.091 ± 0.038	-0.018 ± 0.019	10	L0	M9	26 ± 2	12 ± 5	—	2000.3
12 06 02.48	+28 13 29.3	18	16.33 ± 0.06[a]	15.91 ± 0.06[a]	0.047 ± 0.014	-0.105 ± 0.016	19	—	T3	26 ± 2	14 ± 2	—	1998.2
12 07 03.74	-31 51 29.8	74	15.85 ± 0.07	14.00 ± 0.06	-0.232 ± 0.016	-0.074 ± 0.019	19	L3	—	43 ± 8	50 ± 10	—	1999.2
12 07 33.46	-39 32 53.9	36	13.00 ± 0.03	11.95 ± 0.03	-0.063 ± 0.002	-0.023 ± 0.003	21	M8	—	54.0 ± 3.0[i]	17.1 ± 1.0	CB-LG-YC	1999.3
12 07 33.50	-39 32 54.4	16	—	16.93 ± 0.11	-0.063 ± 0.002	-0.023 ± 0.003	21	—	L5	54.0 ± 3.0[i]	17.1 ± 1.0	CB	1999.3
12 07 38.04	-39 09 05.0	83	14.69 ± 0.04	13.24 ± 0.04	-0.142 ± 0.011	0.031 ± 0.015	19	L4	—	21 ± 2	14 ± 2	—	1999.3
12 07 47.17	+02 44 24.9	40	15.56 ± 0.06[c]	14.28 ± 0.06[c]	-0.498 ± 0.018	0.138 ± 0.019	10	L8	T0	16 ± 1	39 ± 3	—	2000.1
12 09 56.13	-10 04 00.8	13	15.91 ± 0.07	15.06 ± 0.14	0.250 ± 0.019	-0.390 ± 0.019	19	—	T3	18 ± 1	39 ± 4	—	1999.1
12 12 33.89	+02 06 28.0	21	16.13 ± 0.13	14.19 ± 0.09	0.065 ± 0.021	-0.141 ± 0.021	19	—	L1	67 ± 9	49 ± 9	—	2000.2
12 13 03.36	-04 32 43.7	19	14.68 ± 0.04	13.01 ± 0.03	-0.354 ± 0.016	-0.012 ± 0.012	10	L5	—	16 ± 1	27 ± 3	—	1999.1
12 14 40.89	+63 16 43.4	18	16.29 ± 0.06[a]	15.66 ± 0.06[a]	0.165 ± 0.030	-0.021 ± 0.068	19	—	T3.5	21 ± 4	17 ± 4	—	2000.0
12 15 44.32	-34 20 59.1	63	16.24 ± 0.13	< 16.32	-0.212 ± 0.017	-0.310 ± 0.021	19	—	T4.5	23 ± 3	42 ± 5	—	2000.2
12 15 53.48	+00 50 49.8	74	13.49 ± 0.03	12.38 ± 0.03	0.220 ± 0.020	-0.398 ± 0.020	19	M8	—	29 ± 5	63 ± 11	—	2000.2
12 16 21.61	+44 56 34.0	20	16.35 ± 0.10	15.02 ± 0.12	-0.035 ± 0.014	-0.004 ± 0.019	19	L5	—	41 ± 7	7 ± 3	—	2000.2
12 16 59.18	+30 03 05.4	18	17.01 ± 0.10[a]	15.60 ± 0.06[a]	-0.021 ± 0.017	0.115 ± 0.019	19	—	L3.5	67 ± 26	38 ± 16	—	1998.2
12 17 11.10	-03 11 13.1	7	15.86 ± 0.06	< 15.89	-1.054 ± 0.002	0.076 ± 0.002	43	T7	T7.5	11.0 ± 0.3[o]	55.2 ± 1.4	—	1999.1
12 17 29.35	+00 35 32.6	19	13.09 ± 0.02	12.05 ± 0.02	0.078 ± 0.026	-0.001 ± 0.026	19	M7.5	—	27 ± 3	10 ± 3	—	2001.1
12 18 59.57	-05 50 28.2	19	14.05 ± 0.03	12.78 ± 0.03	-0.279 ± 0.019	-0.036 ± 0.019	19	M8.5	—	35 ± 3	47 ± 5	—	1999.1
12 19 51.56	+31 28 49.7	18	16.00 ± 0.06[a]	14.31 ± 0.06[a]	-0.250 ± 0.026	-0.017 ± 0.031	19	—	L8	19 ± 2	22 ± 3	—	1998.2
12 21 27.70	+02 57 19.8	83	13.17 ± 0.02	11.95 ± 0.03	-0.115 ± 0.030	-0.018 ± 0.027	10	L0	—	19 ± 1	11 ± 3	—	2000.2
12 21 50.66	-08 43 19.7	20	13.52 ± 0.03	12.50 ± 0.02	-0.192 ± 0.019	0.015 ± 0.019	19	M8	—	30 ± 2	27 ± 3	—	1999.1
12 24 52.22	-12 38 35.2	33	12.57 ± 0.02	11.35 ± 0.03	-0.262 ± 0.011	-0.187 ± 0.011	42	M9	—	17.5 ± 1.2[n]	26.6 ± 2.0	—	1998.2
12 25 54.32	-27 39 46.6	7	15.26 ± 0.05	15.07 ± 0.15	0.385 ± 0.002	-0.628 ± 0.003	43	T6	T6	13.3 ± 0.4[o]	46.5 ± 1.7	CB	1998.5
12 27 05.06	-04 47 20.7	110	15.50 ± 0.05	14.92 ± 0.12	0.41 ± 0.02	0.24 ± 0.01	47	esdM7.5	—	65 ± —	148 ± —	—	1999.0
12 27 15.45	-06 36 45.8	19	14.20 ± 0.03	12.88 ± 0.04	-0.106 ± 0.019	-0.085 ± 0.019	19	M9	—	34 ± 2	22 ± 3	—	1999.1
12 28 15.23	-15 47 34.2	26	14.38 ± 0.03	12.77 ± 0.03	0.134 ± 0.001	-0.180 ± 0.001	15	L5	L6	20.2 ± 0.8[h]	21.5 ± 0.8	CB	1998.2
12 28 55.38	+00 50 44.0	40	15.61 ± 0.06	14.16 ± 0.08	-0.041 ± 0.021	-0.038 ± 0.021	19	L0	—	60 ± 4	16 ± 6	—	2000.2

Continued on Next Page...

Table 2.12 – Continued

RA (J2000) (1)	DEC (J2000) (2)	Ref.[1] (3)	2MASS J[3] (mag) (4)	2MASS K_s[3] (mag) (5)	$\mu_\alpha cos(\delta)$ ($''$ yr^{-1}) (6)	μ_δ ($''$ yr^{-1}) (7)	μ Ref.[2] (8)	SpT (opt) (9)	SpT (IR) (10)	Distance[3] (pc) (11)	V_{tan} (km s^{-1}) (12)	Note[4] (13)	Epoch (14)
12 31 21.41	+49 59 23.4	20	14.62 ± 0.04	13.14 ± 0.03	-0.053 ± 0.019	-0.022 ± 0.030	19	L2	—	29 ± 4	8 ± 3	—	1999.1
12 31 47.53	+08 47 33.1	13	15.42 ± 0.06[c]	15.35 ± 0.06[c]	-1.176 ± 0.021	-1.043 ± 0.021	19	—	T5.5	12 ± 1	87 ± 11	—	2000.2
12 32 18.27	-09 51 50.2	83	13.73 ± 0.03	12.55 ± 0.03	-0.156 ± 0.013	-0.101 ± 0.017	10	L0	—	25 ± 2	22 ± 2	—	2000.2
12 37 39.19	+65 26 14.8	7	16.05 ± 0.09	< 16.06	-1.002 ± 0.008	-0.525 ± 0.006	44	T7	T6.5	10.4 ± 0.5[q]	55.8 ± 2.8	—	1999.2
12 39 27.27	+55 15 37.1	47	14.71 ± 0.03	12.79 ± 0.03	0.161 ± 0.029	0.038 ± 0.006	10	L5	—	21 ± 1[y]	17 ± 3	CB	1999.1
12 46 46.78	+40 27 15.0	47	15.09 ± 0.05	13.28 ± 0.04	0.145 ± 0.012	-0.079 ± 0.017	10	L4	—	25 ± 3	20 ± 3	—	2000.3
12 46 51.76	+31 48 10.4	33	12.23 ± 0.02	11.21 ± 0.02	-0.792 ± 0.019	0.050 ± 0.019	29	M7.5	—	18 ± 2	68 ± 7	—	1998.2
12 47 35.70	-12 19 51.8	19	13.89 ± 0.03	12.72 ± 0.03	0.036 ± 0.018	-0.223 ± 0.018	19	M8.5	—	33 ± 2	35 ± 4	—	1998.2
12 50 11.66	+39 25 58.2	18	16.37 ± 0.06[a]	15.99 ± 0.06[a]	-0.015 ± 0.008	-0.828 ± 0.011	19	—	T4	23 ± 2	89 ± 10	—	1998.3
12 52 20.42	-31 49 28.8	74	13.66 ± 0.03	12.56 ± 0.03	0.166 ± 0.016	-0.032 ± 0.019	19	M8	—	32 ± 3	25 ± 3	—	1999.2
12 53 10.92	-57 09 24.8	75	13.45 ± 0.02	12.05 ± 0.02	-1.575 ± 0.005	-0.434 ± 0.014	35	L0.5	—	21 ± 3	162 ± 20	—	2000.2
12 53 12.40	+40 34 03.8	52	12.19 ± 0.02	11.16 ± 0.02	0.24 ± 0.08	-0.61 ± 0.09	36	M7.5	—	17 ± 2	54 ± 10	—	1998.3
12 54 53.93	-01 22 47.4	55	14.89 ± 0.04	13.84 ± 0.05	-0.479 ± 0.002	0.130 ± 0.003	15	T2	T2	11.8 ± 0.3[h]	27.7 ± 0.6	—	1999.1
12 56 56.88	+01 46 16.3	83	14.48 ± 0.03	12.79 ± 0.03	-0.183 ± 0.013	-0.017 ± 0.018	10	L2	—	27 ± 4	24 ± 4	—	2000.2
12 57 37.26	-01 13 36.0	32	15.94 ± 0.08	14.12 ± 0.07	0.081 ± 0.020	-0.003 ± 0.011	10	L4	L5	37 ± 4	14 ± 4	—	1999.1
13 00 42.55	+19 12 35.4	33	12.72 ± 0.02	11.62 ± 0.02	-0.820 ± 0.018	-1.244 ± 0.019	19	L1	L3	14 ± 1	99 ± 7	UBL	1999.2
13 01 54.65	-15 10 22.3	83	14.54 ± 0.04	13.10 ± 0.03	-0.069 ± 0.012	-0.074 ± 0.016	10	L1	—	32 ± 2	16 ± 2	—	1999.3
13 02 38.97	+03 51 41.0	74	13.93 ± 0.03	12.77 ± 0.03	-0.039 ± 0.021	0.025 ± 0.021	19	M7.5	—	39 ± 4	9 ± 4	—	2000.2
13 05 40.19	-25 41 05.9	87	13.41 ± 0.03	11.75 ± 0.02	-0.285 ± 0.001	0.011 ± 0.001	15	L2	L3	18.7 ± 0.7[h]	25.2 ± 0.9	CB	1998.4
13 05 41.06	+20 46 39.4	19	15.20 ± 0.05	13.37 ± 0.04	-0.023 ± 0.017	0.073 ± 0.027	10	L4	—	27 ± 5	10 ± 4	—	1999.2
13 06 17.27	+38 20 29.6	83	14.63 ± 0.03	13.22 ± 0.04	-0.175 ± 0.027	-0.008 ± 0.035	19	L1	—	34 ± 4	28 ± 6	—	2000.0
13 08 25.07	+07 25 51.2	74	13.19 ± 0.03	12.00 ± 0.03	0.259 ± 0.021	-0.416 ± 0.021	19	M9	—	22 ± 1	51 ± 4	—	2000.2
13 09 21.85	-23 30 35.0	19	11.79 ± 0.02	10.67 ± 0.02	0.027 ± 0.002	-0.419 ± 0.030	11	M8	—	13 ± 1	26 ± 3	—	1998.3
13 11 39.21	+80 32 21.9	33	12.76 ± 0.02	11.68 ± 0.02	-0.068 ± 0.019	-0.348 ± 0.019	29	M8	—	29 ± 5[cc]	49 ± 9	CB	2000.1
13 12 07.07	+39 37 44.5	20	14.17 ± 0.03	12.95 ± 0.02	-0.097 ± 0.023	0.013 ± 0.018	10	L0	—	31 ± 4	14 ± 4	—	1998.3
13 14 15.51	-00 08 48.0	32	16.66 ± 0.06[c]	15.36 ± 0.06[c]	-0.001 ± 0.023	0.073 ± 0.023	19	—	L3.5	57 ± 16	20 ± 8	—	2001.0
13 15 30.94	-26 49 51.3	39	15.20 ± 0.05	13.46 ± 0.04	-0.678 ± 0.016	-0.280 ± 0.015	10	L5.5	—	18 ± 2	64 ± 6	—	1998.4
13 20 41.59	+09 57 50.6	74	13.73 ± 0.03	12.61 ± 0.03	-0.236 ± 0.021	-0.129 ± 0.021	19	M7.5	—	36 ± 3	45 ± 6	—	2000.2
13 20 44.27	+04 09 04.5	83	15.25 ± 0.05	13.62 ± 0.05	-0.483 ± 0.019	0.211 ± 0.017	10	L3	—	33 ± 3	82 ± 8	—	2000.2
13 23 35.97	-18 06 37.9	65	14.90 ± 0.04	13.66 ± 0.05	-0.087 ± 0.015	-0.022 ± 0.019	10	L0	—	43 ± 3	18 ± 3	—	1999.2
13 23 52.06	+30 14 34.0	20	13.64 ± 0.02	12.55 ± 0.02	-0.695 ± 0.023	0.156 ± 0.027	19	M8.5	—	30 ± 4	100 ± 15	—	2000.3
13 24 35.59	+63 58 28.4	63	15.60 ± 0.07	14.06 ± 0.06	-0.343 ± 0.064	-0.260 ± 0.048	32	—	T2	13 ± 1	26 ± 6	—	2000.2
13 26 20.09	-27 29 37.0	36	15.85 ± 0.07	13.85 ± 0.05	-0.364 ± 0.016	-0.016 ± 0.014	10	L5	—	24 ± 2	41 ± 4	—	1999.2
13 26 29.81	-00 38 31.4	30	16.37 ± 0.06[c]	14.17 ± 0.06[c]	-0.226 ± 0.008	-0.107 ± 0.006	44	L8	L5.5	20.0 ± 2.6[q]	23.8 ± 3.2	—	1999.1
13 28 55.03	+21 14 48.6	46	16.19 ± 0.11	14.27 ± 0.08	0.219 ± 0.002	-0.428 ± 0.002	15	L5	—	32.3 ± 4.0[h]	73.6 ± 9.0	—	1999.4
13 29 00.99	-41 47 13.3	36	13.65 ± 0.02	12.27 ± 0.02	0.231 ± 0.013	-0.280 ± 0.017	19	M9	—	27 ± 2	47 ± 4	—	1999.4
13 30 02.32	-04 53 20.2	19	13.34 ± 0.03	12.24 ± 0.03	-0.079 ± 0.009	-0.007 ± 0.009	9	M8	—	27 ± 2	10 ± 1	—	1999.1
13 31 33.10	+34 07 58.3	83	14.33 ± 0.03	12.89 ± 0.02	-0.353 ± 0.019	-0.169 ± 0.018	10	L0	—	33 ± 2	62 ± 5	—	2000.3
13 31 48.94	-01 16 50.0	40	15.48 ± 0.06[c]	14.12 ± 0.06[c]	-0.407 ± 0.019	-1.030 ± 0.014	10	L6	L8	23 ± 2	119 ± 11	UBL	1999.1
13 32 24.42	-04 41 12.6	19	12.37 ± 0.03	11.28 ± 0.02	0.08 ± 0.09	0.05 ± 0.08	36	M7.5	—	19 ± 2	9 ± 9	—	1999.1
13 32 28.63	+26 35 07.9	47	16.08 ± 0.09	14.35 ± 0.08	-0.152 ± 0.012	0.041 ± 0.017	10	L2	—	57 ± 4	42 ± 5	—	1997.5
13 34 06.23	+19 40 35.1	46	15.48 ± 0.06	14.00 ± 0.05	-0.058 ± 0.012	0.098 ± 0.016	10	L1.5	—	46 ± 3	25 ± 4	—	1997.4
13 36 40.62	+37 43 23.0	20	14.41 ± 0.03	13.10 ± 0.02	-0.200 ± 0.009	-0.060 ± 0.014	10	L1	—	30 ± 2	30 ± 2	—	1998.3
13 37 31.16	+49 38 36.7	20	13.77 ± 0.03	12.58 ± 0.03	0.039 ± 0.016	0.049 ± 0.025	19	L0	—	26 ± 3	8 ± 3	—	1999.4
13 38 26.15	+41 40 34.2	47	14.22 ± 0.03	12.77 ± 0.02	-0.153 ± 0.024	-0.311 ± 0.025	10	L2.5	—	22 ± 2	37 ± 4	—	1998.3
13 38 49.44	+04 37 31.5	83	14.16 ± 0.03	12.74 ± 0.03	0.112 ± 0.014	-0.224 ± 0.013	10	L1	—	27 ± 2	32 ± 3	—	2000.2
13 39 26.51	-17 55 05.3	19	13.47 ± 0.03	12.32 ± 0.03	-0.190 ± 0.020	-0.070 ± 0.020	9	M7.5	—	31 ± 3	30 ± 4	—	1999.3
13 41 11.60	-30 52 50.5	83	14.61 ± 0.03	13.08 ± 0.03	0.030 ± 0.013	-0.134 ± 0.015	19	L3	—	24 ± 2	16 ± 2	—	1999.3
13 42 03.11	+13 40 22.2	18	17.03 ± 0.06[a]	15.16 ± 0.06[a]	0.000 ± 0.019	-0.027 ± 0.019	19	—	L5.5	40 ± 4	5 ± 4	—	1999.0
13 42 23.62	+17 51 55.8	46	16.14 ± 0.08	14.59 ± 0.09	-0.070 ± 0.011	-0.002 ± 0.008	10	L2.5	—	54 ± 4	18 ± 3	—	1999.0

Continued on Next Page...

Table 2.12 – Continued

RA (J2000) (1)	DEC (J2000) (2)	Ref.[1] (3)	2MASS J[3] (mag) (4)	2MASS K_s[3] (mag) (5)	$\mu_\alpha cos(\delta)$ ($''$ yr^{-1}) (6)	μ_δ ($''$ yr^{-1}) (7)	μ Ref.[2] (8)	SpT (opt) (9)	SpT (IR) (10)	Distance[3] (pc) (11)	V_{tan} (km s^{-1}) (12)	Note[4] (13)	Epoch (14)
13 43 16.70	+39 45 08.7	47	16.16 ± 0.07	14.15 ± 0.05	-0.343 ± 0.031	0.116 ± 0.025	10	L5	—	27 ± 2	47 ± 6	—	1998.3
13 43 52.75	-38 51 38.5	74	13.83 ± 0.03	12.71 ± 0.02	-0.044 ± 0.014	-0.016 ± 0.018	19	M8	—	34 ± 3	8 ± 2	—	1999.3
13 46 46.34	-00 31 50.1	103	16.00 ± 0.10	15.77 ± 0.27	-0.503 ± 0.003	-0.114 ± 0.002	43	T7	T6.5	14.6 ± 0.5[o]	35.8 ± 1.4	—	2001.1
13 47 59.11	-76 10 05.4	45	13.79 ± 0.03	12.55 ± 0.03	0.203 ± 0.005	0.038 ± 0.020	19	—	L0	26 ± 3	25 ± 3	—	2000.2
13 47 59.11	-76 10 05.4	75	13.79 ± 0.03	12.55 ± 0.03	0.203 ± 0.005	0.038 ± 0.020	19	L0	—	26 ± 3	25 ± 3	—	2000.2
13 48 01.00	-03 04 32.8	74	12.74 ± 0.03	11.66 ± 0.03	0.191 ± 0.020	-0.408 ± 0.020	19	M7	—	25 ± 3	54 ± 7	—	1999.5
13 48 45.91	+03 53 54.5	83	14.63 ± 0.03	13.23 ± 0.04	0.207 ± 0.023	-0.356 ± 0.011	10	L1	—	34 ± 4	66 ± 9	—	2000.2
13 56 41.48	+43 42 58.7	84	11.71 ± 0.02	10.65 ± 0.02	-0.46 ± 0.07	0.07 ± 0.07	36	M7	—	16 ± 2	34 ± 7	—	1999.3
13 57 12.37	+14 28 39.8	21	15.58 ± 0.06	13.88 ± 0.04	0.069 ± 0.052	-0.006 ± 0.053	19	—	L4	32 ± 13	10 ± 9	—	2000.0
13 57 14.97	-14 38 52.9	77	12.87 ± 0.03	11.74 ± 0.03	-0.038 ± 0.010	-0.106 ± 0.009	9	M7	—	27 ± 3	14 ± 2	—	1998.3
13 58 52.69	+37 47 13.7	18	16.43 ± 0.06[a]	16.57 ± 0.10[a]	-0.010 ± 0.013	-0.411 ± 0.016	19	—	T4.5	26 ± 12	51 ± 24	—	1998.3
13 59 24.03	+47 28 43.1	54	17.11 ± 0.06[c]	15.35 ± 0.06[c]	-0.144 ± 0.010	0.034 ± 0.014	19	—	L8.5	28 ± 3	20 ± 2	—	1999.3
13 59 55.10	-40 34 58.2	83	13.65 ± 0.03	12.57 ± 0.03	0.038 ± 0.011	-0.485 ± 0.015	19	L1	—	21 ± 1	49 ± 4	—	1999.3
14 00 23.20	+43 38 22.2	18	16.30 ± 0.06[a]	14.49 ± 0.06[a]	-0.235 ± 0.020	0.012 ± 0.028	19	—	L7	23 ± 7	26 ± 8	—	1999.3
14 02 22.35	+06 48 47.9	74	13.72 ± 0.03	12.51 ± 0.03	0.056 ± 0.021	-0.006 ± 0.021	19	M9	—	28 ± 2	8 ± 3	—	2000.2
14 02 31.75	+01 48 30.1	40	15.45 ± 0.06	14.18 ± 0.07	-0.232 ± 0.014	0.008 ± 0.011	10	L1	—	49 ± 3	54 ± 5	—	2000.2
14 02 55.64	+08 00 55.3	18	17.04 ± 0.06[a]	15.70 ± 0.06[a]	0.065 ± 0.021	-0.098 ± 0.022	19	—	T1	29 ± 1	16 ± 3	—	2000.2
14 03 22.32	+30 07 54.7	33	12.68 ± 0.02	11.60 ± 0.02	-0.81 ± 0.03	0.00 ± 0.07	36	M8.5	—	19 ± 1	73 ± 6	—	1999.3
14 04 41.67	+02 35 50.1	40	15.60 ± 0.06	14.53 ± 0.10	0.054 ± 0.017	-0.248 ± 0.013	10	L1	—	53 ± 3	63 ± 5	—	2000.2
14 04 44.95	+46 34 29.7	20	14.34 ± 0.03	13.06 ± 0.03	-0.231 ± 0.030	0.143 ± 0.026	10	L0	—	33 ± 4	43 ± 7	—	1999.3
14 04 49.41	-31 59 32.9	63	15.58 ± 0.06	14.54 ± 0.10	-0.349 ± 0.030	0.032 ± 0.003	32	—	T2.5	15 ± 1	25 ± 3	—	2001.1
14 07 53.61	+12 41 09.9	83	15.38 ± 0.06	13.60 ± 0.04	-0.312 ± 0.019	0.082 ± 0.019	10	L5	—	21 ± 2	33 ± 4	—	2000.0
14 09 03.10	-33 57 56.5	49	14.25 ± 0.03	12.87 ± 0.03	0.089 ± 0.012	0.047 ± 0.014	19	L2	—	24 ± 2	12 ± 2	—	1999.3
14 11 17.35	+39 36 36.3	47	14.64 ± 0.03	13.24 ± 0.04	-0.911 ± 0.015	0.137 ± 0.016	10	L1.5	—	32 ± 2	138 ± 10	—	2000.3
14 11 21.31	-21 19 50.3	19	12.44 ± 0.02	11.33 ± 0.02	0.0 ± 0.2	0.1 ± 0.2	25	M9	—	16 ± 1	7 ± 7	—	1998.4
14 12 22.68	+23 54 10.8	20	13.73 ± 0.03	12.65 ± 0.02	-0.175 ± 0.036	0.068 ± 0.039	19	M9	—	29 ± 4	26 ± 6	—	2000.2
14 12 24.49	+16 33 11.5	47	13.89 ± 0.03	12.52 ± 0.03	0.029 ± 0.016	-0.080 ± 0.030	10	L0.5	—	25 ± 2	10 ± 4	—	2000.0
14 13 59.81	-04 57 48.3	19	13.41 ± 0.03	12.24 ± 0.03	-0.190 ± 0.050	-0.060 ± 0.040	9	M8	—	28 ± 2	27 ± 7	—	1999.1
14 15 30.03	+57 24 30.0	18	16.72 ± 0.06[a]	15.49 ± 0.06[a]	0.043 ± 0.013	-0.345 ± 0.025	19	—	T3	22 ± 7	36 ± 12	—	1999.1
14 16 59.87	+50 06 25.8	18	16.94 ± 0.06[a]	15.38 ± 0.06[a]	-0.297 ± 0.013	0.188 ± 0.021	19	—	L5.5	44 ± 31	74 ± 51	—	2000.2
14 19 38.67	-31 36 51.9	74	13.49 ± 0.02	12.35 ± 0.02	-0.041 ± 0.018	0.028 ± 0.021	19	M7	—	36 ± 4	8 ± 3	—	2000.3
14 21 18.73	-16 18 20.1	36	12.76 ± 0.02	11.67 ± 0.03	-0.230 ± 0.020	-0.070 ± 0.020	9	M7.5	—	23 ± 2	26 ± 3	—	1998.3
14 21 31.45	+18 27 40.7	33	13.23 ± 0.02	11.94 ± 0.02	-0.75 ± 0.04	-0.17 ± 0.03	36	L0	—	20 ± 1	73 ± 6	—	1999.3
14 22 27.20	+22 15 57.5	18	17.01 ± 0.06[a]	15.67 ± 0.06[a]	0.047 ± 0.019	-0.054 ± 0.020	19	—	L6.5	42 ± 14	14 ± 6	UBL	2000.2
14 24 39.09	+09 17 10.4	2	15.69 ± 0.08	14.17 ± 0.10	-0.2182 ± —	-0.1260 ± —	46	L4	L3	31.5 ± 2.5[p]	37.7 ± 3.0	VLMC	2000.3
14 25 05.03	+71 02 09.6	110	14.83 ± 0.04	14.34 ± 0.096	-0.62 ± —	-0.17 ± —	47	sdM8	—	65 ± —	197 ± —	—	1999.4
14 25 27.98	-36 50 22.9	44	13.75 ± 0.03	11.81 ± 0.03	-0.268 ± 0.015	-0.473 ± 0.019	19	—	L5	9 ± 1	24 ± 2	—	1999.6
14 26 31.61	+15 57 01.2	33	12.91 ± 0.02	11.73 ± 0.02	0.108 ± 0.019	-0.056 ± 0.019	29	M9	—	26 ± 5[cc]	15 ± 4	CB	1998.1
14 28 31.32	+59 23 35.4	74	14.78 ± 0.04	13.27 ± 0.03	-0.25 ± 0.17	-0.09 ± 0.15	36	L4	—	22 ± 2	28 ± 18	—	2000.1
14 28 43.23	+33 10 39.1	57	11.99 ± 0.02	10.74 ± 0.02	-0.3457 ± 0.0002	-0.7079 ± 0.0004	33	M9	—	11.0 ± 0.2[k]	41.2 ± 0.6	—	2000.2
14 29 50.80	+33 30 11.0	95	< 16.88	< 16.99	-0.003 ± —	-0.100 ± —	38	T5	T4.5	32 ± 13	15 ± 8	—	—
14 30 43.58	+29 15 40.5	105	14.27 ± 0.03	12.77 ± 0.03	-0.185 ± 0.020	0.142 ± 0.016	10	L2	L0.5	29 ± 2[hh]	33 ± 3	CB	1999.2
14 30 55.89	+00 13 52.3	40	16.29 ± 0.11	14.98 ± 0.13	0.058 ± 0.024	-0.036 ± 0.012	10	L0	—	82 ± 5	26 ± 9	—	2000.3
14 32 11.75	-00 59 00.6	54	17.12 ± 0.10[c]	15.49 ± 0.10[c]	-0.009 ± 0.020	-0.032 ± 0.017	10	—	L4.5	58 ± 6	9 ± 5	—	1999.2
14 34 58.19	-23 35 57.2	15	12.93 ± 0.02	11.87 ± 0.03	-0.306 ± 0.030	0.051 ± 0.005	11	M7	—	27 ± 3	40 ± 6	—	1998.4
14 35 17.20	-00 46 13.0	40	16.48 ± 0.10	15.32 ± 0.18	0.022 ± 0.009	0.010 ± 0.006	44	L0	—	102 ± 74[q]	12 ± 10	—	1999.3
14 35 35.72	-00 43 47.1	40	16.53 ± 0.06[c]	15.15 ± 0.06[c]	0.022 ± 0.005	-0.105 ± 0.009	44	L3	L2.5	62 ± 26[q]	32 ± 13	—	1999.3
14 36 09.77	+29 00 35.0	19	13.30 ± 0.02	12.17 ± 0.02	-0.098 ± 0.018	0.068 ± 0.021	19	M8.5	—	25 ± 4	14 ± 3	—	1999.2
14 38 08.29	+64 08 36.3	19	12.99 ± 0.02	11.65 ± 0.02	0.64 ± 0.06	-0.20 ± 0.04	36	M9.5	—	18 ± 1	58 ± 6	—	2000.2
14 38 45.42	+55 59 13.4	19	13.09 ± 0.02	12.03 ± 0.02	-0.062 ± 0.015	-0.059 ± 0.027	19	M7	—	30 ± 7	12 ± 4	—	1999.3

Continued on Next Page...

Table 2.12 – Continued

RA (J2000) (1)	DEC (J2000) (2)	Ref.[1] (3)	2MASS J[3] (mag) (4)	2MASS K_s[3] (mag) (5)	$\mu_\alpha cos(\delta)$ ($''$ yr^{-1}) (6)	μ_δ ($''$ yr^{-1}) (7)	μ Ref.[2] (8)	SpT (opt) (9)	SpT (IR) (10)	Distance[3] (pc) (11)	V_{tan} (km s^{-1}) (12)	Note[4] (13)	Epoch (14)
14 38 54.98	-13 09 10.3	47	15.49 ± 0.06	13.86 ± 0.05	0.161 ± 0.022	-0.017 ± 0.016	10	L3	—	37 ± 7	28 ± 6	—	1998.2
14 39 00.31	+18 39 38.8	110	13.19 ± 0.03	12.48 ± 0.03	-0.03 ± —	-1.22 ± —	47	sdM7	—	35 ± —	208 ± —	—	2000.2
14 39 28.36	+19 29 14.9	46	12.76 ± 0.02	11.55 ± 0.02	-1.2298 ± 0.0007	0.407 ± 0.002	15	L1	—	14.4 ± 0.1[h]	88.2 ± 0.6	—	1997.4
14 39 33.43	+03 17 59.1	40	15.99 ± 0.10	14.81 ± 0.13	-0.006 ± 0.021	0.019 ± 0.016	10	L1	—	63 ± 4	6 ± 5	—	2000.3
14 39 40.92	+18 26 36.9	46	16.22 ± 0.10	14.54 ± 0.10	-0.013 ± 0.018	0.001 ± 0.025	10	L1	—	70 ± 5	4 ± 6	—	1997.4
14 40 01.80	+00 21 45.7	30	15.95 ± 0.08	14.60 ± 0.09	-0.074 ± 0.018	0.037 ± 0.018	10	L1	—	62 ± 4	24 ± 5	—	2000.3
14 40 16.22	+00 26 39.0	40	16.05 ± 0.06[c]	14.67 ± 0.06[c]	-0.006 ± 0.021	0.004 ± 0.021	19	L3	L1	48 ± 4	2 ± 5	—	2000.3
14 40 22.93	+13 39 23.0	20	12.40 ± 0.02	11.34 ± 0.02	-0.146 ± 0.010	-0.340 ± 0.010	28	M8	—	18 ± 1	28 ± 2	—	1998.3
14 41 04.57	+27 19 32.3	20	12.99 ± 0.02	11.98 ± 0.02	0.089 ± 0.030	-0.053 ± 0.034	19	M7	—	29 ± 7	14 ± 5	—	1999.2
14 41 28.46	+50 46 00.5	18	16.98 ± 0.06[a]	15.21 ± 0.06[a]	0.077 ± 0.013	-0.109 ± 0.021	19	—	L3	73 ± 13	46 ± 11	—	1998.5
14 41 37.16	-09 45 59.0	65	14.02 ± 0.03	12.66 ± 0.03	-0.198 ± 0.003	-0.016 ± 0.004	12	L0.5	—	27.5 ± 2.7[f]	25.9 ± 2.6	CB	1999.2
14 42 21.75	+66 03 19.8	38	11.51 ± 0.03	10.33 ± 0.07	-0.311 ± 0.011	-0.059 ± 0.012	34	—	L0	9.9 ± 1.3[l]	14.8 ± 2.0	VLMC	1999.3
14 44 20.67	-20 19 22.3	110	12.50 ± 0.03	11.91 ± 0.03	-2.919 ± 0.009	-1.950 ± 0.005	47	d/sdM9	—	20 ± —	333 ± —	—	1998.3
14 46 00.61	+00 24 51.9	32	15.89 ± 0.08	13.94 ± 0.05	0.180 ± 0.007	-0.066 ± 0.004	44	L6	L5	22.0 ± 1.6[q]	19.9 ± 1.6	—	2000.3
14 48 03.37	+15 54 14.9	19	12.48 ± 0.02	11.48 ± 0.02	-0.536 ± 0.019	0.118 ± 0.019	29	M7	—	22 ± 3	58 ± 7	—	1998.3
14 48 25.63	+10 31 59.0	105	14.56 ± 0.03	12.68 ± 0.03	0.262 ± 0.022	-0.120 ± 0.022	19	—	L3.5	22 ± 2	30 ± 4	—	2000.3
14 49 37.84	+23 55 37.8	47	15.82 ± 0.08	14.31 ± 0.09	0.050 ± 0.013	0.027 ± 0.024	10	L0	—	64 ± 4[y]	17 ± 5	CB	1997.4
14 50 16.00	+23 54 41.8	79	< 13.90	< 12.30	0.1447 ± 0.0008	0.0324 ± 0.0007	34	—	L4	17.9 ± 0.3[l]	12.6 ± 0.2	CB	1999.3
14 50 16.00	+23 54 41.8	79	< 14.20	< 12.60	0.1447 ± 0.0008	0.0324 ± 0.0007	34	—	L4	17.9 ± 0.3[l]	12.6 ± 0.2	CB	1999.3
14 53 23.03	+15 43 08.1	20	13.26 ± 0.02	12.21 ± 0.03	-0.011 ± 0.018	0.028 ± 0.018	19	M7.5	—	28 ± 6	4 ± 3	—	1999.4
14 54 07.97	-66 04 47.6	75	13.06 ± 0.02	11.72 ± 0.03	0.525 ± 0.004	-0.376 ± 0.004	35	L3.5	—	11 ± 2	33 ± 6	—	2000.2
14 56 01.35	-27 47 37.4	19	13.25 ± 0.03	12.19 ± 0.02	-0.244 ± 0.008	-0.784 ± 0.027	16	M9	—	23 ± 1	89 ± 7	—	2001.1
14 56 38.31	-28 09 47.3	19	9.97 ± 0.03	8.93 ± 0.03	-0.485 ± 0.004	-0.846 ± 0.003	13	M7	—	6.9 ± 0.2[g]	31.8 ± 0.7	—	1998.5
14 57 14.96	-21 21 47.7	8	15.32 ± 0.05	15.24 ± 0.16	1.034 ± 0.002	-1.726 ± 0.001	34	T7	T7.5	5.9 ± 0.1[l]	56.4 ± 0.6	VLMC	1998.4
14 57 39.65	+45 17 16.7	33	13.12 ± 0.02	11.93 ± 0.02	-0.191 ± 0.019	0.100 ± 0.019	29	M9	—	22 ± 1	22 ± 2	—	1999.2
14 58 24.53	+28 39 58.0	74	13.08 ± 0.02	11.85 ± 0.02	-0.109 ± 0.024	-0.432 ± 0.028	19	M8	—	24 ± 4	51 ± 9	—	1999.4
15 00 45.72	+42 19 44.8	74	13.78 ± 0.03	12.65 ± 0.02	0.136 ± 0.011	-0.065 ± 0.015	19	M9	—	29 ± 4	21 ± 3	—	2000.1
15 01 08.18	+22 50 02.0	102	11.87 ± 0.02	10.71 ± 0.02	-0.0246 ± 0.0003	-0.0579 ± 0.0004	15	M9	—	10.6 ± 0.1[h]	3.2 ± 0.0	—	2000.2
15 02 40.82	+61 38 15.8	40	16.35 ± 0.12	15.39 ± 0.21	-0.098 ± 0.010	0.036 ± 0.022	19	L1	—	74 ± 10	37 ± 6	—	1999.3
15 03 19.61	+25 25 19.6	11	13.82 ± 0.06[c]	14.11 ± 0.06[c]	0.009 ± 0.017	0.021 ± 0.018	10	T6	T5	7 ± 1	1 ± 1	—	1999.4
15 04 16.21	-23 55 56.4	57	12.01 ± 0.03	11.03 ± 0.03	-0.305 ± 0.029	-0.119 ± 0.011	17	M7.5	—	16 ± 2	25 ± 3	—	1998.5
15 06 54.41	+13 21 06.0	33	13.37 ± 0.02	11.74 ± 0.02	-1.087 ± 0.013	0.014 ± 0.011	10	L3	—	14 ± 1	71 ± 6	—	1999.2
15 07 27.79	-20 00 43.1	19	11.71 ± 0.02	10.66 ± 0.02	0.104 ± 0.003	-0.071 ± 0.002	2	M7.5	—	22.8 ± —[e]	13.6 ± —	—	1998.4
15 07 47.69	-16 27 38.6	82	12.83 ± 0.03	11.31 ± 0.03	-0.161 ± 0.002	-0.8885 ± 0.0006	15	L5	L5.5	7.33 ± 0.03[h]	31.4 ± 0.1	—	1998.3
15 10 16.85	-02 41 07.8	36	12.61 ± 0.02	11.35 ± 0.02	-0.405 ± 0.012	0.024 ± 0.006	41	M9	—	16.6 ± 1.3[o]	32.0 ± 2.7	—	1999.2
15 10 47.61	-28 18 23.4	36	14.01 ± 0.03	12.79 ± 0.03	0.1 ± 0.2	0.1 ± 0.2	25	M9	—	32 ± 2	14 ± 15	—	1999.2
15 10 47.86	-28 18 17.4	36	12.84 ± 0.03	11.69 ± 0.03	-0.10 ± 0.18	0.00 ± 0.30	36	M9	—	19 ± 1	9 ± 16	—	1999.2
15 11 14.66	+06 07 43.1	18	16.01 ± 0.06[a]	14.51 ± 0.06[a]	-0.252 ± 0.021	-0.256 ± 0.021	19	—	T0	18 ± 3	30 ± 5	—	2000.3
15 12 33.29	-10 32 41.4	74	13.16 ± 0.03	12.02 ± 0.03	-0.040 ± 0.020	-0.037 ± 0.019	9	M8	—	25 ± 2	6 ± 2	—	1999.2
15 12 40.58	+34 03 50.1	21	15.04 ± 0.04	13.43 ± 0.04	0.228 ± 0.010	-0.010 ± 0.012	19	—	L1	41 ± 11	44 ± 12	—	1998.2
15 15 00.83	+48 47 41.6	105	14.11 ± 0.03	12.50 ± 0.02	-0.950 ± 0.021	1.471 ± 0.021	10	L6	L6	11 ± 1	89 ± 8	—	2000.2
15 15 06.07	+44 36 48.3	18	16.69 ± 0.06[a]	14.88 ± 0.06[a]	0.075 ± 0.019	-0.020 ± 0.027	19	—	L7.5	25 ± 11	9 ± 5	—	1999.4
15 16 03.03	+02 59 29.2	54	17.06 ± 0.10[c]	15.34 ± 0.10[c]	-0.048 ± 0.022	-0.174 ± 0.022	19	—	T0	26 ± 1	22 ± 3	—	2000.3
15 16 43.06	+30 53 44.3	18	16.97 ± 0.06[a]	15.10 ± 0.06[a]	-0.132 ± 0.021	0.004 ± 0.024	19	—	T0.5	23 ± 3	14 ± 3	—	1998.2
15 20 02.24	-44 22 41.9	45	13.55 ± 0.04	12.27 ± 0.03	-0.63 ± 0.03	-0.37 ± 0.02	6	—	L1.5	19 ± 1[v]	66 ± 5	CB	1999.4
15 20 02.24	-44 22 41.9	45	14.70 ± 0.07	13.22 ± 0.04	-0.63 ± 0.03	-0.37 ± 0.02	6	—	L4.5	19 ± 2[v]	66 ± 7	CB	1999.4
15 20 39.74	+35 46 21.0	18	15.65 ± 0.06[a]	14.01 ± 0.06[a]	0.279 ± 0.023	-0.386 ± 0.028	19	—	T0	14 ± 2	32 ± 4	—	2000.1
15 21 01.03	+50 53 23.0	19	12.01 ± 0.02	10.92 ± 0.02	0.07 ± 0.06	-0.21 ± 0.08	36	M7.5	—	16 ± 2	17 ± 7	—	1998.5
15 21 03.27	+01 31 42.6	54	16.27 ± 0.06[c]	15.43 ± 0.06[c]	-0.212 ± 0.019	0.084 ± 0.017	10	—	T2	24 ± 2	26 ± 3	—	2000.3

Continued on Next Page...

Table 2.12 – Continued

RA (J2000) (1)	DEC (J2000) (2)	Ref.[1] (3)	2MASS J[3] (mag) (4)	2MASS K_s[3] (mag) (5)	$\mu_\alpha cos(\delta)$ ($''$ yr^{-1}) (6)	μ_δ ($''$ yr^{-1}) (7)	μ Ref.[2] (8)	SpT (opt) (9)	SpT (IR) (10)	Distance[3] (pc) (11)	V_{tan} (km s^{-1}) (12)	Note[4] (13)	Epoch (14)
15 23 06.57	-23 47 52.6	45	14.20 ± 0.03	12.90 ± 0.03	0.159 ± 0.013	0.308 ± 0.012	22	—	L2.5	22 ± 2	36 ± 3	—	1998.4
15 23 22.63	+30 14 56.2	47	16.06 ± 0.10	14.35 ± 0.07	0.1258 ± 0.0006	-0.1765 ± 0.0008	34	L8	L8	18.6 ± 0.4[l]	19.1 ± 1.2	VLMC	2000.1
15 25 31.32	+58 10 52.5	54	17.04 ± 0.10[c]	15.46 ± 0.10[c]	0.064 ± 0.015	0.044 ± 0.028	19	—	L6.5	39 ± 13	14 ± 6	—	1999.3
15 26 14.05	+20 43 41.4	47	15.59 ± 0.06	13.92 ± 0.05	-0.207 ± 0.018	-0.362 ± 0.019	19	L7	—	18 ± 3	35 ± 6	—	1997.5
15 31 08.88	+06 01 11.2	45	16.17 ± 0.19[b]	14.40 ± 0.21[b]	0.028 ± 0.025	-0.048 ± 0.025	19	L0	—	77 ± 9	20 ± 10	—	2000.3
15 31 13.45	+16 41 28.2	21	15.58 ± 0.06	13.80 ± 0.05	-0.076 ± 0.025	0.040 ± 0.026	19	—	L1	52 ± 14	21 ± 8	—	1999.1
15 34 17.11	+16 15 46.3	18	16.86 ± 0.06[a]	15.99 ± 0.06[a]	-0.066 ± 0.020	-0.052 ± 0.021	19	—	T3.5	36 ± 5[aa]	14 ± 4	CB	1999.2
15 34 49.84	-29 52 27.4	10	14.88 ± 0.06[c]	15.03 ± 0.06[c]	0.0959 ± 0.0008	-0.251 ± 0.002	43	T6	T5.5	13.6 ± 0.2[o]	17.3 ± 0.4	CB	1998.5
15 34 53.25	+12 19 49.5	18	15.40 ± 0.06[a]	13.73 ± 0.06[a]	0.177 ± 0.020	-0.040 ± 0.021	19	—	L4	29 ± 17	25 ± 15	—	1999.2
15 34 57.04	-14 18 48.6	36	11.38 ± 0.02	10.31 ± 0.02	-0.915 ± 0.003	-0.311 ± 0.001	2	M7	—	11.1 ± —[e]	50.8 ± —	—	1998.3
15 38 24.17	-19 53 11.6	74	15.93 ± 0.06	14.00 ± 0.05	0.032 ± 0.019	-0.061 ± 0.020	19	L6	—	21 ± 8	7 ± 3	—	1998.4
15 39 21.37	+65 02 36.4	21	14.60 ± 0.04	13.20 ± 0.04	-0.038 ± 0.011	0.038 ± 0.025	19	—	L1	33 ± 9	8 ± 4	—	1999.3
15 39 41.89	-05 20 42.8	44	13.92 ± 0.03	12.58 ± 0.03	0.599 ± 0.014	0.117 ± 0.015	10	L4	L2	15 ± 1	43 ± 4	—	1999.2
15 39 44.42	+74 37 27.3	74	12.93 ± 0.02	11.73 ± 0.02	-0.04 ± 0.08	0.06 ± 0.09	36	M9	—	20 ± 1	6 ± 9	—	1999.3
15 40 09.42	+37 42 31.6	18	16.49 ± 0.06[a]	14.65 ± 0.06[a]	-0.205 ± 0.016	-0.382 ± 0.020	19	—	L9	20 ± 5	41 ± 10	—	2000.3
15 45 09.01	+35 55 27.1	18	17.12 ± 0.06[a]	15.31 ± 0.06[a]	-0.183 ± 0.016	0.063 ± 0.020	19	—	L7.5	31 ± 4	28 ± 5	—	1998.2
15 46 05.40	+37 49 45.8	33	12.44 ± 0.02	11.41 ± 0.02	-0.020 ± 0.019	-0.120 ± 0.019	29	M7.5	—	20 ± 2	11 ± 2	—	2000.3
15 46 27.18	-33 25 11.1	10	15.63 ± 0.05	15.49 ± 0.18	0.121 ± 0.002	0.190 ± 0.002	43	—	T5.5	11.4 ± 0.2[o]	12.1 ± 0.4	—	1998.5
15 47 27.23	+03 36 36.1	40	16.08 ± 0.07	14.27 ± 0.07	-0.063 ± 0.013	0.052 ± 0.017	10	L2	—	57 ± 4	22 ± 4	—	2000.3
15 47 47.19	-24 23 49.3	83	13.97 ± 0.03	12.74 ± 0.03	-0.133 ± 0.015	-0.122 ± 0.016	10	L0	—	28 ± 3	24 ± 4	—	1999.3
15 48 49.12	+17 22 35.9	18	16.22 ± 0.06[a]	14.53 ± 0.06[a]	-0.277 ± 0.019	-0.109 ± 0.019	19	—	L5	33 ± 6	46 ± 9	—	1999.1
15 48 58.34	-16 36 01.8	45	13.89 ± 0.03	12.64 ± 0.03	-0.210 ± 0.016	-0.107 ± 0.017	19	—	L2	21 ± 3	23 ± 4	—	1998.3
15 49 12.09	-35 39 03.9	73	— [d]	13.10 ± 0.10[d]	-0.027 ± 0.003	-0.014 ± 0.001	39	—	L1.5	140 ± 25	20 ± 4	YC-VLMC	1998.6
15 50 08.45	+14 55 18.0	20	14.78 ± 0.04	13.26 ± 0.04	0.105 ± 0.019	-0.127 ± 0.013	10	L2	—	31 ± 5	24 ± 4	—	1999.1
15 51 06.62	+64 57 04.7	33	12.89 ± 0.02	11.72 ± 0.02	-0.220 ± 0.019	0.010 ± 0.019	29	M8	—	22 ± 2	23 ± 3	—	1999.4
15 51 52.37	+09 41 14.8	74	16.32 ± 0.11	14.31 ± 0.06	-0.070 ± 0.022	-0.050 ± 0.022	19	L2	—	64 ± 10	26 ± 8	LG	2000.3
15 52 59.06	+29 48 48.5	105	13.48 ± 0.03	12.02 ± 0.03	-0.157 ± 0.020	-0.051 ± 0.020	10	—	L1	20 ± 1	16 ± 2	—	2000.1
15 53 02.28	+15 32 36.9	10	15.66 ± 0.06[c]	15.82 ± 0.06[c]	-0.402 ± 0.017	0.171 ± 0.016	10	—	T7	12 ± 2[u]	25 ± 4	CB	1998.1
15 53 19.93	+14 00 33.7	33	13.05 ± 0.02	11.82 ± 0.02	-0.659 ± 0.019	0.072 ± 0.019	29	M9	—	20 ± 1	64 ± 5	—	1998.1
15 53 21.42	+21 09 07.1	46	16.70 ± 0.16	14.68 ± 0.11	-0.045 ± 0.015	0.114 ± 0.016	19	L5.5	—	32 ± 6	19 ± 4	—	1997.4
15 55 15.73	-09 56 05.5	36	12.56 ± 0.02	11.44 ± 0.02	0.950 ± 0.015	-0.767 ± 0.015	19	L1	—	13 ± 1	75 ± 5	—	1999.2
15 55 26.14	+00 17 20.4	40	14.95 ± 0.04	13.82 ± 0.06	-0.234 ± 0.018	-0.041 ± 0.018	10	L0	—	44 ± 3	50 ± 5	—	2000.3
16 00 05.48	+17 08 32.8	47	16.05 ± 0.09	14.68 ± 0.11	-0.009 ± 0.015	0.015 ± 0.021	10	L1.5	—	61 ± 4[y]	5 ± 6	CB	1997.5
16 06 26.65	+68 37 26.8	21	14.91 ± 0.04	13.43 ± 0.04	-0.083 ± 0.008	0.043 ± 0.023	19	—	L2	33 ± 10	15 ± 5	—	1999.4
16 07 31.23	-04 42 09.1	36	11.90 ± 0.02	10.72 ± 0.03	0.028 ± 0.002	-0.461 ± 0.029	17	M8	—	14 ± 1	31 ± 3	—	1999.2
16 10 29.00	-00 40 53.0	110	12.91 ± 0.02	12.02 ± 0.03	-1.25 ± 0.06	-1.18 ± 0.06	47	d/sdM7	—	16 ± —	111 ± —	—	1999.2
16 14 20.48	+00 46 43.4	40	16.23 ± 0.10	14.85 ± 0.11	-0.057 ± 0.021	-0.031 ± 0.021	10	L2	—	61 ± 5	19 ± 6	—	2000.3
16 15 04.13	+13 40 07.9	63	16.35 ± 0.09	< 15.86	0.315 ± 0.033	-0.362 ± 0.038	32	—	T6	13 ± 2	30 ± 5	—	1999.1
16 15 42.45	+05 46 40.0	74	12.88 ± 0.02	11.74 ± 0.02	0.11 ± 0.06	-0.12 ± 0.07	36	M9	—	19 ± 1	15 ± 6	—	2000.5
16 15 44.16	+35 59 00.5	47	14.54 ± 0.03	12.94 ± 0.03	-0.017 ± 0.012	-0.512 ± 0.015	10	L3	—	24 ± 2	58 ± 5	—	1998.3
16 16 26.49	+22 18 59.1	54	17.66 ± 0.06[c]	15.69 ± 0.06[c]	-0.073 ± 0.018	0.021 ± 0.019	19	—	L5	56 ± 38	20 ± 15	—	1998.4
16 17 31.68	+40 19 00.3	18	16.96 ± 0.06[a]	14.88 ± 0.06[a]	-0.038 ± 0.014	-0.132 ± 0.019	19	—	L4	59 ± 12	39 ± 9	—	1998.3
16 18 45.03	-13 21 29.7	49	14.25 ± 0.02	12.92 ± 0.03	-0.101 ± 0.015	-0.062 ± 0.015	10	L0	—	32 ± 4	18 ± 3	—	1999.3
16 19 28.30	+00 50 11.8	40	14.39 ± 0.04	13.19 ± 0.04	0.074 ± 0.016	-0.088 ± 0.017	10	L2	—	26 ± 2	14 ± 2	—	2000.4
16 20 26.14	-04 16 31.5	104	15.28 ± 0.05	13.60 ± 0.04	-0.417 ± 0.002	-0.023 ± 0.002	34	L2.5	—	30.3 ± 2.4[l]	60.1 ± 4.8	VLMC	2000.4
16 20 51.16	+32 37 32.2	18	17.31 ± 0.08[a]	15.43 ± 0.06[a]	0.015 ± 0.011	-0.033 ± 0.014	19	—	L6	41 ± 7	7 ± 3	—	1998.3
16 22 55.33	+11 59 23.8	18	17.03 ± 0.10[a]	15.49 ± 0.06[a]	-0.128 ± 0.025	-0.012 ± 0.026	19	—	L6	43 ± 23	26 ± 15	—	1999.2
16 24 14.36	+00 29 15.8	96	15.49 ± 0.05	< 15.52	-0.373 ± 0.002	-0.009 ± 0.002	43	—	T6	11.0 ± 0.1[o]	19.5 ± 0.3	—	1999.3
16 26 20.34	+39 25 19.0	110	14.43 ± 0.04	14.44 ± 0.08	-1.35 ± 0.10	0.24 ± 0.10	47	sdL4	—	20 ± —	120 ± —	—	1998.3
16 27 27.94	+81 05 07.5	33	13.03 ± 0.02	11.88 ± 0.02	-0.209 ± 0.019	0.338 ± 0.019	29	M9	—	21 ± 1	39 ± 3	—	1999.3

Continued on Next Page...

Table 2.12 – Continued

RA (J2000) (1)	DEC (J2000) (2)	Ref.[1] (3)	2MASS J[3] (mag) (4)	2MASS K_s[3] (mag) (5)	$\mu_\alpha cos(\delta)$ ($''$ yr^{-1}) (6)	μ_δ ($''$ yr^{-1}) (7)	μ Ref.[2] (8)	SpT (opt) (9)	SpT (IR) (10)	Distance[3] (pc) (11)	V_{tan} (km s^{-1}) (12)	Note[4] (13)	Epoch (14)
16 28 38.55	+23 08 24.1	18	16.57 ± 0.06[a]	16.59 ± 0.06[a]	0.497 ± 0.020	-0.461 ± 0.021	19	—	T7	14 ± 4	45 ± 12	—	1997.4
16 30 22.95	+08 18 22.1	18	16.46 ± 0.06[a]	16.30 ± 0.06[a]	-0.083 ± 0.018	-0.084 ± 0.019	19	—	T5.5	18 ± 2	10 ± 2	—	2000.4
16 30 30.54	+43 44 03.2	54	16.62 ± 0.06[c]	14.72 ± 0.06[c]	-0.138 ± 0.020	0.052 ± 0.028	19	—	L7	25 ± 12	18 ± 9	—	2000.2
16 30 41.39	+09 38 44.6	83	14.87 ± 0.03	13.30 ± 0.04	-0.064 ± 0.015	-0.056 ± 0.014	10	L0	—	43 ± 5	17 ± 4	—	2000.4
16 30 49.99	+00 51 01.0	40	16.00 ± 0.08	14.62 ± 0.08	-0.080 ± 0.015	-0.139 ± 0.018	10	L1	—	63 ± 4	48 ± 6	—	2000.4
16 32 29.11	+19 04 40.7	46	15.87 ± 0.07	14.00 ± 0.05	0.293 ± 0.001	-0.054 ± 0.001	15	L8	L8	15.2 ± 0.5[h]	21.5 ± 0.7	—	1997.4
16 33 59.33	-06 40 55.2	18	16.14 ± 0.06[a]	14.57 ± 0.06[a]	-0.232 ± 0.015	-0.195 ± 0.015	19	—	L6	28 ± 3	40 ± 4	—	1999.3
16 35 19.19	+42 23 05.3	33	12.88 ± 0.03	11.79 ± 0.02	-0.073 ± 0.019	-0.010 ± 0.019	29	M8	—	22 ± 2	8 ± 2	—	1998.4
16 40 31.97	+12 31 06.9	110	15.95 ± 0.08	< 15.499	-0.75 ± 0.06	-0.33 ± 0.06	47	d/sdM9	—	75 ± —	292 ± —	—	1997.6
16 45 22.07	+30 04 07.1	20	15.19 ± 0.04	13.59 ± 0.04	-0.065 ± 0.019	-0.065 ± 0.022	19	L3	—	32 ± 6	14 ± 4	—	1999.4
16 45 22.11	-13 19 51.6	36	12.45 ± 0.03	11.15 ± 0.03	-0.364 ± 0.018	-0.804 ± 0.016	10	L1.5	—	12 ± 1	48 ± 4	—	1999.3
16 49 04.19	+04 44 57.1	74	12.96 ± 0.03	11.88 ± 0.02	0.054 ± 0.023	0.083 ± 0.023	19	M8	—	23 ± 4	11 ± 3	—	2000.4
16 53 29.70	+62 31 36.4	40	15.09 ± 0.05	< 14.07	0.031 ± 0.016	-0.024 ± 0.035	19	L3	—	31 ± 5	6 ± 4	—	2000.3
16 56 18.85	+28 35 05.6	47	< 16.95	15.22 ± 0.15	0.011 ± 0.027	-0.027 ± 0.031	19	L4.5	—	54 ± 11	7 ± 8	—	2000.2
16 57 34.54	+10 54 23.3	83	14.15 ± 0.04	12.80 ± 0.03	-0.084 ± 0.017	-0.061 ± 0.021	10	L2	—	23 ± 2	11 ± 2	—	2000.4
16 58 03.80	+70 27 01.5	33	13.29 ± 0.02	11.92 ± 0.02	-0.1468 ± 0.0007	-0.3133 ± 0.0009	15	L1	—	18.6 ± 0.2[h]	30.4 ± 0.4	—	2000.2
17 05 48.34	-05 16 46.2	44	13.31 ± 0.03	12.03 ± 0.02	0.129 ± 0.014	-0.103 ± 0.015	10	—	L4	11 ± 1	9 ± 1	—	1999.2
17 07 18.30	+64 39 33.1	57	12.54 ± 0.02	11.38 ± 0.02	0.226 ± 0.019	-0.091 ± 0.019	29	M9	—	16 ± 1	19 ± 2	—	2000.2
17 07 23.43	-05 58 24.9	67	13.96 ± 0.11	12.20 ± 0.08	0.100 ± 0.008	0.003 ± 0.005	22	—	L3	15 ± 1[dd]	7 ± 1	CB	1999.3
17 07 33.34	+43 01 30.4	19	13.97 ± 0.03	12.62 ± 0.03	-0.200 ± 0.022	-0.022 ± 0.014	10	L0.5	—	26 ± 2	25 ± 3	—	1999.4
17 11 13.53	+23 26 33.3	20	14.50 ± 0.03	13.06 ± 0.03	-0.053 ± 0.011	-0.036 ± 0.016	10	L0	—	36 ± 4	11 ± 3	—	1997.5
17 11 45.73	+22 32 04.4	47	17.09 ± 0.18	14.73 ± 0.10	0.031 ± 0.007	-0.005 ± 0.004	44	L6.5	—	30.2 ± 4.5[q]	4.5 ± 1.2	—	1997.5
17 11 47.16	+23 31 31.0	18	16.96 ± 0.06[a]	15.29 ± 0.06[a]	0.010 ± 0.017	-0.085 ± 0.018	19	—	L3.5	66 ± 37	27 ± 16	—	1997.5
17 17 14.08	+65 26 22.1	40	14.95 ± 0.04	13.18 ± 0.03	0.159 ± 0.007	-0.092 ± 0.016	19	L4	—	24 ± 5	21 ± 4	—	1999.4
17 21 03.90	+33 44 16.0	19	13.63 ± 0.02	12.49 ± 0.02	-1.854 ± 0.017	0.602 ± 0.017	10	L3	—	16 ± 1	144 ± 13	UBL	1998.3
17 22 44.32	+63 29 47.0	40	15.37 ± 0.05	14.08 ± 0.07	0.013 ± 0.012	-0.038 ± 0.027	19	L0	—	53 ± 6	10 ± 7	—	1999.4
17 26 00.07	+15 38 19.0	47	15.67 ± 0.07	13.66 ± 0.05	-0.031 ± 0.013	-0.048 ± 0.014	10	L2	—	47 ± 4	13 ± 3	—	1997.5
17 28 11.50	+39 48 59.3	47	15.99 ± 0.08	13.91 ± 0.05	0.037 ± 0.006	-0.026 ± 0.005	44	L7	—	24.1 ± 1.9[q]	5.1 ± 0.9	CB	1998.4
17 28 22.17	+58 45 09.5	40	16.40 ± 0.16	< 15.15	0.024 ± 0.013	0.102 ± 0.012	10	L1	—	76 ± 5	38 ± 5	—	1999.3
17 31 01.40	+53 10 47.6	18	16.46 ± 0.06[a]	14.81 ± 0.06[a]	0.064 ± 0.011	0.162 ± 0.018	19	—	L6	31 ± 16	26 ± 14	—	1998.5
17 31 29.74	+27 21 23.3	83	12.09 ± 0.03	10.91 ± 0.02	-0.082 ± 0.015	-0.240 ± 0.017	10	L0	—	12 ± 1	14 ± 1	—	2000.3
17 33 18.93	+46 33 59.3	33	13.24 ± 0.02	11.89 ± 0.02	0.044 ± 0.019	-0.257 ± 0.019	29	M9.5	—	21 ± 1	26 ± 2	—	1998.4
17 33 42.27	-16 54 50.0	75	13.53 ± 0.05	12.35 ± 0.03	0.081 ± 0.011	-0.048 ± 0.014	35	L0.5	—	22 ± 3	10 ± 2	—	1998.3
17 35 12.96	+26 34 47.5	74	11.25 ± 0.03	10.16 ± 0.02	0.19 ± 0.08	-0.32 ± 0.09	36	M7.5	—	11 ± 1[z]	19 ± 6	CB	2000.3
17 43 41.48	+21 27 06.9	47	15.83 ± 0.09	14.32 ± 0.10	0.159 ± 0.018	0.233 ± 0.019	19	L2.5	—	47 ± 8	63 ± 11	—	1999.5
17 45 34.66	-16 40 53.8	75	13.65 ± 0.03	12.40 ± 0.02	0.116 ± 0.099	-0.111 ± 0.095	35	L1.5	—	20 ± 3	15 ± 13	—	1998.3
17 46 11.99	+50 34 03.6	74	15.10 ± 0.06	13.53 ± 0.04	0.258 ± 0.018	0.025 ± 0.028	19	L5	—	21 ± 4	25 ± 5	—	2000.2
17 50 12.91	+44 24 04.3	33	12.80 ± 0.02	11.77 ± 0.02	-0.018 ± 0.019	0.151 ± 0.019	29	M7.5	—	31 ± 6[ff]	22 ± 5	CB	1998.4
17 50 23.85	+42 22 37.3	54	16.33 ± 0.06[c]	15.26 ± 0.06[c]	-0.044 ± 0.016	0.095 ± 0.014	10	—	T2	22 ± 1	11 ± 2	—	1998.4
17 50 24.84	-00 16 15.1	45	13.29 ± 0.02	11.85 ± 0.02	-0.440 ± 0.043	0.218 ± 0.041	22	—	L5.5	9 ± 1	20 ± 3	—	1999.2
17 50 32.93	+17 59 04.2	32	16.34 ± 0.10	15.48 ± 0.19	0.178 ± 0.007	0.100 ± 0.005	44	—	T3.5	27.6 ± 3.5[q]	26.7 ± 3.5	—	1999.2
17 53 45.18	-65 59 55.9	83	14.10 ± 0.03	12.42 ± 0.03	0.01 ± 0.15	-0.36 ± 0.09	36	L4	—	16 ± 3	27 ± 9	—	2000.3
17 56 56.20	-48 05 09.6	75	13.41 ± 0.02	12.19 ± 0.02	0.078 ± 0.008	0.050 ± 0.009	35	L0	—	22 ± 3	10 ± 1	—	2000.6
17 57 15.39	+70 42 01.1	33	11.45 ± 0.02	10.40 ± 0.02	0.01 ± 0.04	0.34 ± 0.09	36	M7.5	—	12 ± 1	20 ± 6	—	1999.4
17 58 05.45	+46 33 09.9	54	16.17 ± 0.06[c]	15.99 ± 0.06[c]	0.026 ± 0.015	0.594 ± 0.016	10	—	T6.5	12 ± 2	34 ± 4	—	1998.4
18 07 15.93	+50 15 31.6	19	12.93 ± 0.02	11.60 ± 0.03	0.035 ± 0.019	-0.126 ± 0.014	10	L1.5	L1	14 ± 1	9 ± 1	—	2000.3
18 26 11.31	+30 14 20.1	56	11.66 ± 0.02	10.81 ± 0.02	-2.280 ± 0.010	-0.684 ± 0.010	28	M8.5	—	12 ± 1	132 ± 9	—	1998.3
18 28 35.72	-48 49 04.6	13	15.18 ± 0.06	15.18 ± 0.14	0.25 ± 0.07	0.21 ± 0.07	5	—	T5.5	11 ± 1	17 ± 4	—	2000.8
18 35 37.90	+32 59 54.5	19	10.27 ± 0.02	9.17 ± 0.02	-0.075 ± 0.010	-0.743 ± 0.010	28	M8.5	—	6.2 ± 0.4	22 ± 2	—	1998.3
18 41 08.61	+31 17 27.9	47	16.16 ± 0.09	14.22 ± 0.07	0.059 ± 0.003	0.042 ± 0.003	44	L4	—	42.4 ± 3.4[q]	14.6 ± 1.4	—	1998.3

Continued on Next Page...

Table 2.12 – Continued

RA (J2000) (1)	DEC (J2000) (2)	Ref.[1] (3)	2MASS J[3] (mag) (4)	2MASS K_s[3] (mag) (5)	$\mu_\alpha cos(\delta)$ ($''$ yr^{-1}) (6)	μ_δ ($''$ yr^{-1}) (7)	μ Ref.[2] (8)	SpT (opt) (9)	SpT (IR) (10)	Distance[3] (pc) (11)	V_{tan} (km s^{-1}) (12)	Note[4] (13)	Epoch (14)
18 43 22.13	+40 40 20.9	84	11.31 ± 0.02	10.31 ± 0.02	-0.1187 ± 0.0004	0.5940 ± 0.0004	33	M8	—	14.1 ± 0.2[k]	40.6 ± 0.5	—	1999.3
18 45 05.00	-63 57 48.0	4	13.26 ± 0.02	13.69 ± 0.02	2.592 ± 0.002	0.617 ± 0.003	23	—	T6	3.85 ± 0.02[j]	48.7 ± 0.2	VLMC	2000.4
18 45 05.41	-63 57 47.5	109	9.54 ± 0.02	8.51 ± 0.02	2.592 ± 0.002	0.617 ± 0.003	23	M8.5	—	3.85 ± 0.02[j]	48.7 ± 0.2	CB	2000.4
18 45 18.89	+38 53 24.8	74	12.21 ± 0.02	11.05 ± 0.02	0.22 ± 0.09	0.34 ± 0.10	36	M8	—	16 ± 1	32 ± 8	—	2000.3
19 01 06.01	+47 18 13.6	13	15.86 ± 0.07	15.64 ± 0.29	-0.11 ± 0.02	-0.36 ± 0.02	5	—	T5	15 ± 2	27 ± 4	—	1998.5
19 09 08.21	-19 37 47.9	75	14.52 ± 0.03	12.92 ± 0.00	0.054 ± 0.015	0.148 ± 0.030	35	L1	—	32 ± 4	24 ± 6	—	1999.5
19 16 57.62	+05 09 02.2	57	9.91 ± 0.03	8.77 ± 0.02	-0.576 ± 0.013	-1.363 ± 0.015	42	M8	—	6.2 ± 0.1[n]	43.7 ± 1.1	—	1999.6
19 28 51.96	-43 56 25.6	83	15.20 ± 0.04	13.46 ± 0.04	0.066 ± 0.012	-0.273 ± 0.016	19	L5	—	20 ± 2	27 ± 3	—	2000.8
19 29 40.99	-43 10 36.9	110	14.79 ± 0.03	14.09 ± 0.07	-0.019 ± 0.011	-0.865 ± 0.008	47	sdM7	—	73 ± —	301 ± —	—	2000.6
19 36 01.87	-55 02 32.2	83	14.49 ± 0.04	13.05 ± 0.03	0.169 ± 0.009	-0.298 ± 0.016	19	L5	—	17 ± 3	27 ± 5	—	1999.6
19 56 15.42	-17 54 25.2	45	13.75 ± 0.03	12.65 ± 0.03	-0.157 ± 0.015	0.093 ± 0.015	22	M8	L0	33 ± 3	29 ± 3	—	1999.4
20 00 48.41	-75 23 07.0	74	12.73 ± 0.03	11.51 ± 0.03	-0.22 ± 0.06	-0.26 ± 0.06	36	M9	—	18 ± 2	29 ± 7	LG	2000.5
20 02 50.73	-05 21 52.4	20	15.32 ± 0.05	13.42 ± 0.04	-0.098 ± 0.013	-0.105 ± 0.014	10	L6	—	16 ± 1	11 ± 1	—	1998.8
20 04 06.22	+17 04 11.7	60	—	< 13.00	-0.3941 ± 0.0006	-0.4064 ± 0.0006	34	—	L4.5	17.7 ± 0.2[l]	47.4 ± 0.6	VLMC	2000.4
20 04 53.69	-14 16 23.1	19	13.13 ± 0.02	12.05 ± 0.03	0.534 ± 0.018	0.056 ± 0.017	9	M7.5	—	28 ± 3	70 ± 7	—	1998.4
20 14 03.59	-20 16 21.7	19	12.54 ± 0.02	11.45 ± 0.03	0.025 ± 0.011	-0.124 ± 0.012	9	M7.5	—	21 ± 2	12 ± 2	—	1998.4
20 19 26.95	-25 02 44.1	19	13.68 ± 0.03	12.44 ± 0.02	-0.130 ± 0.020	-0.090 ± 0.020	9	M8	—	32 ± 3	24 ± 4	—	1998.6
20 26 15.84	-29 43 12.4	20	14.80 ± 0.03	13.36 ± 0.03	0.043 ± 0.019	-0.348 ± 0.015	10	L1	—	36 ± 5	60 ± 8	—	1998.6
20 28 20.35	+00 52 26.5	40	14.30 ± 0.04	12.79 ± 0.03	0.114 ± 0.014	0.007 ± 0.015	10	L3	—	21 ± 2	11 ± 2	—	2000.5
20 34 37.69	+08 27 00.9	83	14.46 ± 0.03	13.08 ± 0.03	-0.077 ± 0.015	-0.468 ± 0.015	10	L3	—	23 ± 2	51 ± 5	—	2000.4
20 36 03.16	+10 51 29.5	83	13.95 ± 0.03	12.45 ± 0.03	-0.115 ± 0.014	-0.168 ± 0.014	10	L3	—	18 ± 2	17 ± 2	—	2000.4
20 36 21.61	+51 00 05.3	110	13.61 ± 0.03	12.94 ± 0.03	1.04 ± —	-0.20 ± —	47	sdM7.5	—	18 ± —	90 ± —	—	2000.4
20 37 07.15	-11 37 56.9	19	12.27 ± 0.03	11.26 ± 0.02	-0.01 ± 0.11	-0.41 ± 0.06	36	M8	—	17 ± 1	33 ± 5	—	1998.8
20 39 13.14	-11 26 53.1	19	13.79 ± 0.03	12.68 ± 0.03	0.064 ± 0.011	-0.105 ± 0.011	9	M8	—	34 ± 3	20 ± 2	—	1998.8
20 41 42.83	-35 06 44.2	20	14.89 ± 0.03	13.40 ± 0.04	0.063 ± 0.010	-0.120 ± 0.012	19	L2	—	33 ± 5	21 ± 4	—	1998.7
20 45 02.38	-63 32 06.6	74	12.62 ± 0.03	11.21 ± 0.02	0.097 ± 0.008	-0.201 ± 0.017	17	M9	—	17 ± 1	18 ± 2	—	2000.5
20 47 31.76	-08 08 20.1	19	13.63 ± 0.03	12.59 ± 0.03	0.1 ± 0.3	-0.2 ± 0.3	9	M7	—	39 ± 5	41 ± 55	—	1998.8
20 49 19.72	-19 44 32.4	33	12.85 ± 0.02	11.79 ± 0.02	0.193 ± 0.019	-0.260 ± 0.019	29	M7.5	—	24 ± 2	37 ± 4	—	1998.5
20 54 35.85	+15 19 04.3	47	16.37 ± 0.13	14.98 ± 0.14	-0.045 ± 0.018	-0.082 ± 0.018	10	L1	—	75 ± 10	33 ± 8	—	2000.4
20 57 15.38	+17 15 15.4	47	15.97 ± 0.09	14.50 ± 0.07	0.090 ± 0.016	0.066 ± 0.015	10	L1.5	—	58 ± 4	31 ± 5	—	2000.8
20 57 54.09	-02 52 30.2	19	13.12 ± 0.02	11.72 ± 0.03	0.01 ± 0.02	-0.08 ± 0.02	36	L1.5	L1.5	16 ± 1	6 ± 2	—	1998.7
21 01 15.44	+17 56 58.6	47	16.85 ± 0.17	14.89 ± 0.12	0.144 ± 0.003	-0.151 ± 0.003	44	L7.5	—	33.2 ± 3.8[q]	32.8 ± 3.8	CB	2000.3
21 04 14.91	-10 37 36.9	19	13.84 ± 0.03	12.37 ± 0.02	0.614 ± 0.016	-0.281 ± 0.015	10	L3	—	17 ± 2	55 ± 5	—	1998.8
21 07 31.69	-03 07 33.7	19	14.20 ± 0.03	12.88 ± 0.03	0.170 ± 0.018	-0.010 ± 0.013	10	L0	—	31 ± 2	25 ± 3	—	2000.7
21 07 54.09	-45 44 06.4	83	14.92 ± 0.03	13.38 ± 0.03	0.107 ± 0.014	-0.027 ± 0.020	19	L0	—	43 ± 5	23 ± 4	—	1999.6
21 18 58.97	+26 13 46.1	70	18.13 ± 0.55	16.21 ± 0.10	0.133 ± 0.001	0.0092 ± 0.0008	34	—	L7.5	40.8 ± 1.8[l]	25.8 ± 1.1	VLMC	1997.8
21 24 13.87	+00 59 59.9	54	16.15 ± 0.06[c]	15.97 ± 0.06[c]	0.202 ± 0.014	0.287 ± 0.014	10	—	T5	18 ± 2	29 ± 4	—	2000.6
21 30 44.64	-08 45 20.5	49	14.14 ± 0.03	12.82 ± 0.03	0.360 ± 0.013	-0.031 ± 0.014	10	L1.5	—	25 ± 2	43 ± 3	—	1999.4
21 32 11.45	+13 41 58.4	20	15.80 ± 0.06	13.84 ± 0.06	-0.055 ± 0.009	-0.395 ± 0.009	37	L6	—	28 ± 4[gg]	53 ± 8	CB	1998.7
21 32 40.36	+10 29 49.4	18	16.51 ± 0.06[a]	14.80 ± 0.06[a]	0.120 ± 0.018	-0.007 ± 0.019	19	—	L4.5	44 ± 9	25 ± 6	—	2000.3
21 33 52.74	+10 18 41.0	18	17.05 ± 0.06[a]	15.65 ± 0.06[a]	-0.008 ± 0.012	-0.094 ± 0.012	19	—	L5	55 ± 10	25 ± 5	—	2000.5
21 37 10.44	+14 50 47.5	83	14.13 ± 0.03	12.82 ± 0.03	-0.138 ± 0.014	-0.122 ± 0.017	10	L2	—	23 ± 2	20 ± 2	—	2000.5
21 37 37.42	+08 08 46.3	83	14.77 ± 0.03	13.02 ± 0.03	0.705 ± 0.021	0.102 ± 0.019	10	L4	—	22 ± 4	74 ± 15	—	2000.5
21 39 26.76	+02 20 22.6	21	15.26 ± 0.05	13.58 ± 0.05	0.507 ± 0.022	0.123 ± 0.022	19	—	T1	11.0 ± 0.3	27 ± 1	—	2000.5
21 40 29.31	+16 25 18.3	33	12.94 ± 0.03	11.83 ± 0.03	-0.008 ± 0.019	-0.102 ± 0.019	29	M8.5	—	26 ± 4[w]	12 ± 3	CB	1998.7
21 40 46.54	+01 12 59.4	40	15.89 ± 0.08	14.42 ± 0.08	-0.078 ± 0.020	-0.164 ± 0.022	10	L3	—	44 ± 4	38 ± 6	—	2000.5
21 42 05.80	-31 01 16.2	58	15.84 ± 0.07	13.97 ± 0.05	0.060 ± 0.012	-0.095 ± 0.014	19	L3	—	43 ± 4	23 ± 3	—	1998.7
21 44 28.47	+14 46 07.7	64	15.86 ± 0.03	15.12 ± 0.03	0.230 ± 0.004	-0.111 ± 0.003	34	—	T2.5	18.2 ± 1.2[l]	22.1 ± 1.5	VLMC	1998.7
21 48 16.33	+40 03 59.4	108	14.15 ± 0.03	11.77 ± 0.02	0.770 ± 0.018	0.456 ± 0.024	19	L6.5	—	7 ± 1	30 ± 5	—	2000.4

Continued on Next Page...

Table 2.12 – Continued

RA (J2000) (1)	DEC (J2000) (2)	Ref.[1] (3)	2MASS J[3] (mag) (4)	2MASS K_s[3] (mag) (5)	$\mu_\alpha cos(\delta)$ ($''$ yr^{-1}) (6)	μ_δ ($''$ yr^{-1}) (7)	μ Ref.[2] (8)	SpT (opt) (9)	SpT (IR) (10)	Distance[3] (pc) (11)	V_{tan} (km s^{-1}) (12)	Note[4] (13)	Epoch (14)
21 50 15.92	-75 20 36.7	83	14.06 ± 0.03	12.67 ± 0.03	0.980 ± 0.048	-0.281 ± 0.014	16	L1	—	26 ± 3	125 ± 18	—	2000.6
21 51 25.43	-24 41 00.0	58	15.75 ± 0.08	13.65 ± 0.05	0.278 ± 0.014	-0.021 ± 0.015	19	L3	—	41 ± 4	55 ± 6	—	1998.5
21 51 38.39	-48 53 54.2	29	15.73 ± 0.07	15.43 ± 0.18	0.52 ± 0.07	-0.22 ± 0.04	18	—	T4	17 ± 2	47 ± 8	—	1999.7
21 52 26.09	+09 37 57.5	83	15.19 ± 0.03	13.34 ± 0.03	0.294 ± 0.019	0.170 ± 0.017	10	L6	—	24 ± 5[ee]	39 ± 8	CB	2000.8
21 54 24.94	-10 23 02.2	63	16.43 ± 0.12	< 17.05	0.193 ± 0.012	0.037 ± 0.012	19	—	T4.5	33 ± 4	30 ± 4	—	1998.8
21 54 33.18	+59 42 18.7	63	15.66 ± 0.07	< 15.34	-0.182 ± 0.009	-0.445 ± 0.017	19	—	T6	10 ± 1	23 ± 3	—	1999.8
21 57 49.04	-55 34 42.0	83	14.26 ± 0.03	13.00 ± 0.03	0.043 ± 0.011	-0.012 ± 0.019	19	L2	—	25 ± 2	5 ± 1	—	2000.8
21 58 04.57	-15 50 09.8	49	15.04 ± 0.04	13.19 ± 0.04	0.070 ± 0.011	-0.033 ± 0.015	10	L4	—	25 ± 5	9 ± 2	—	2000.8
22 00 02.01	-30 38 32.7	44	13.44 ± 0.03	12.20 ± 0.03	0.3 ± 0.1	-0.1 ± 0.1	25	M9	—	35 ± 2[t]	44 ± 17	CB	1999.6
22 00 02.01	-30 38 32.7	44	14.36 ± 0.10	13.09 ± 0.10	0.210 ± 0.048	-0.064 ± 0.021	22	—	L0	35 ± 2[t]	37 ± 9	CB	1999.6
22 04 10.52	-56 46 57.7	92	12.29 ± 0.02	11.35 ± 0.02	3.9600 ± 0.0006	-2.5388 ± 0.0004	34	—	T1	3.6 ± 0.1[l]	80.9 ± 2.0	VLMC	1999.9
22 04 10.52	-56 46 57.7	92	13.23 ± 0.02	13.53 ± 0.02	3.9600 ± 0.0006	-2.5388 ± 0.0004	34	—	T6	3.6 ± 0.1[l]	80.9 ± 2.0	VLMC	1999.9
22 06 22.80	-20 47 05.8	33	12.37 ± 0.02	11.32 ± 0.03	0.019 ± 0.007	-0.031 ± 0.005	12	M8	—	26.7 ± 2.4[f]	4.5 ± 0.6	CB	1998.5
22 06 44.98	-42 17 20.8	47	15.56 ± 0.07	13.61 ± 0.06	0.111 ± 0.013	-0.182 ± 0.018	19	L2	—	45 ± 3	45 ± 5	—	1998.9
22 08 13.63	+29 21 21.5	47	15.80 ± 0.09	14.15 ± 0.07	0.111 ± 0.014	-0.011 ± 0.014	10	L2	—	50 ± 4	27 ± 4	—	1997.8
22 12 07.03	+34 30 35.1	74	16.32 ± 0.10	14.37 ± 0.07	0.160 ± 0.023	-0.232 ± 0.028	19	L5	—	30 ± 11	41 ± 15	—	2000.4
22 13 44.91	-21 36 07.9	20	15.38 ± 0.04	13.76 ± 0.04	0.060 ± 0.011	-0.063 ± 0.017	10	L0	—	54 ± 7	22 ± 5	LG	1998.5
22 14 50.70	-13 19 59.0	19	13.46 ± 0.03	12.32 ± 0.03	0.255 ± 0.015	-0.263 ± 0.015	9	M7.5	—	32 ± 3	55 ± 6	—	1998.4
22 24 43.81	-01 58 52.1	47	14.02 ± 0.06[c]	12.02 ± 0.06[c]	0.457 ± 0.002	-0.871 ± 0.001	15	L4.5	L3.5	11.4 ± 0.1[h]	52.9 ± 0.7	—	1998.8
22 26 44.40	-75 03 42.5	57	12.35 ± 0.02	11.25 ± 0.02	0.048 ± 0.019	0.014 ± 0.019	29	M8	—	17 ± 1	4 ± 2	—	1999.9
22 28 28.89	-43 10 26.2	14	15.66 ± 0.07	15.30 ± 0.21	0.03 ± 0.08	-0.31 ± 0.03	8	—	T6	10 ± 1	15 ± 2	—	1998.9
22 35 49.05	+18 40 29.8	33	12.39 ± 0.02	11.37 ± 0.02	0.326 ± 0.019	0.042 ± 0.019	29	M7	—	22 ± 3	34 ± 5	—	1997.8
22 37 32.55	+39 22 39.8	53	13.34 ± 0.02	12.18 ± 0.02	0.022 ± 0.002	-0.341 ± 0.002	34	M9.5	—	18.9 ± 0.7[l]	30.6 ± 1.1	—	1998.8
22 38 07.42	+43 53 17.9	19	13.84 ± 0.03	12.52 ± 0.03	0.324 ± 0.012	-0.132 ± 0.016	19	L1.5	—	22 ± 2	36 ± 3	—	1998.8
22 42 53.17	+25 42 57.3	35	14.81 ± 0.04	13.05 ± 0.03	0.409 ± 0.015	-0.045 ± 0.016	10	L3	—	27 ± 2	52 ± 5	—	1998.8
22 43 16.96	-59 32 20.6	45	14.07 ± 0.03	12.84 ± 0.03	-0.016 ± 0.024	-0.243 ± 0.023	22	—	L0	29 ± 4	34 ± 5	—	2000.8
22 44 31.67	+20 43 43.3	23	16.47 ± 0.06[c]	13.93 ± 0.06[c]	0.252 ± 0.014	-0.214 ± 0.011	10	L6.5	L7.5	19 ± 2	30 ± 3	—	1997.8
22 49 53.45	+00 44 04.6	32	16.41 ± 0.06[c]	14.41 ± 0.06[c]	0.075 ± 0.018	0.026 ± 0.018	19	L3	L5	56 ± 5	21 ± 5	—	2000.6
22 52 01.51	-18 15 59.4	19	13.52 ± 0.03	12.37 ± 0.02	0.081 ± 0.015	-0.382 ± 0.016	9	M8.5	—	28 ± 2	52 ± 4	—	2000.6
22 52 10.73	-17 30 13.4	44	14.31 ± 0.03	12.90 ± 0.02	0.405 ± 0.020	0.154 ± 0.020	10	—	L7.5	14 ± 3[ee]	28 ± 7	CB	1999.5
22 54 18.92	+31 23 49.8	10	15.26 ± 0.06[c]	14.95 ± 0.06[c]	0.068 ± 0.015	0.201 ± 0.011	10	—	T4	14 ± 2	14 ± 2	—	1998.5
22 54 51.94	-28 40 25.3	19	14.13 ± 0.02	12.96 ± 0.02	0.008 ± 0.019	0.052 ± 0.030	10	L0.5	L0.5	29 ± 2	7 ± 4	—	2000.6
22 55 18.61	-57 13 05.6	45	14.08 ± 0.03	12.58 ± 0.03	-0.216 ± 0.011	-0.260 ± 0.020	19	—	L5.5	12 ± 1	20 ± 2	—	1999.9
22 55 29.07	-00 34 33.6	90	15.65 ± 0.06	14.44 ± 0.08	-0.036 ± 0.001	-0.176 ± 0.003	44	L0	—	62 ± 10[q]	53 ± 9	—	1999.6
22 59 13.88	-00 51 58.1	40	16.36 ± 0.10	14.65 ± 0.09	0.084 ± 0.017	0.068 ± 0.017	10	L2	—	65 ± 5	33 ± 6	—	2000.7
23 06 29.28	-05 02 28.5	33	11.35 ± 0.02	10.30 ± 0.02	0.922 ± 0.002	-0.472 ± 0.003	12	M8	—	12.1 ± 0.4[f]	59.5 ± 1.9	—	1998.7
23 10 18.46	-17 59 09.0	62	14.38 ± 0.03	12.97 ± 0.03	0.024 ± 0.017	-0.246 ± 0.013	31	L0	L1	34 ± 4	40 ± 5	—	1998.5
23 21 12.54	-13 26 28.2	45	14.50 ± 0.03	13.14 ± 0.03	0.550 ± 0.036	-0.171 ± 0.036	22	—	L1	32 ± 2	87 ± 8	—	1999.5
23 22 46.88	-31 33 23.1	74	13.58 ± 0.03	12.32 ± 0.02	-0.210 ± 0.017	-0.519 ± 0.020	19	L0	—	23 ± 3	62 ± 8	—	1999.6
23 25 45.30	+42 51 48.8	20	15.49 ± 0.05	13.76 ± 0.05	0.00 ± 0.22	-0.28 ± 0.10	36	L8	—	14 ± 1	19 ± 7	—	1998.8
23 28 04.59	-10 38 45.2	18	16.89 ± 0.06[a]	15.24 ± 0.06[a]	-0.010 ± 0.015	-0.037 ± 0.015	19	—	L3.5	64 ± 6	12 ± 5	—	1998.8
23 30 22.58	-03 47 18.9	20	14.48 ± 0.03	13.12 ± 0.03	0.232 ± 0.017	0.032 ± 0.014	10	L1	—	31 ± 4	35 ± 5	—	1998.8
23 31 01.61	-04 06 19.3	33	12.94 ± 0.02	11.95 ± 0.03	0.401 ± 0.019	-0.231 ± 0.019	29	M8	—	26 ± 1[w]	58 ± 3	CB	1998.8
23 31 21.74	-27 49 50.0	57	11.65 ± 0.02	10.65 ± 0.03	0.077 ± 0.002	0.760 ± 0.001	12	M7.5	—	14.5 ± 0.4[f]	52.4 ± 1.6	—	1999.4
23 31 23.78	-47 18 27.4	13	15.66 ± 0.07	15.39 ± 0.20	0.104 ± 0.013	-0.049 ± 0.019	19	—	T5	13 ± 2	7 ± 1	—	2000.8
23 34 39.45	+19 33 04.1	33	12.78 ± 0.02	11.62 ± 0.02	-0.236 ± 0.019	-0.117 ± 0.019	29	M8	—	21 ± 2	26 ± 3	—	1997.8
23 36 43.95	+21 53 38.8	57	12.71 ± 0.02	11.72 ± 0.02	0.203 ± -0.037	0.024 ± 0.019	29	M7	—	25 ± 3	46 ± 6	—	2000.4
23 37 14.91	-08 38 08.4	22	12.19 ± 0.03	11.19 ± 0.02	0.248 ± 0.019	0.017 ± 0.019	29	M7	—	20 ± 2	24 ± 3	—	1998.8
23 39 10.25	+13 52 28.4	10	16.08 ± 0.06[c]	16.07 ± 0.06[c]	0.30 ± 0.15	-0.77 ± 0.12	4	—	T5	18 ± 2	73 ± 13	—	2000.9

Continued on Next Page...

Table 2.12 – Continued

RA (J2000) (1)	DEC (J2000) (2)	Ref.[1] (3)	2MASS J[3] (mag) (4)	2MASS K_s[3] (mag) (5)	$\mu_\alpha cos(\delta)$ ($''$ yr^{-1}) (6)	μ_δ ($''$ yr^{-1}) (7)	μ Ref.[2] (8)	SpT (opt) (9)	SpT (IR) (10)	Distance[3] (pc) (11)	V_{tan} (km s^{-1}) (12)	Note[4] (13)	Epoch (14)
23 44 06.24	-07 33 28.2	49	14.80 ± 0.04	13.23 ± 0.03	0.021 ± 0.017	-0.051 ± 0.008	10	L4.5	—	20 ± 2	5 ± 1	—	1998.8
23 45 39.03	+00 55 13.7	83	13.77 ± 0.03	12.58 ± 0.03	0.101 ± 0.019	-0.034 ± 0.014	10	L0	—	26 ± 2	13 ± 2	—	2000.6
23 46 45.99	+11 29 09.4	74	12.80 ± 0.02	11.61 ± 0.02	-0.40 ± 0.07	-0.07 ± 0.06	36	M9	—	18 ± 1	36 ± 7	—	2000.7
23 46 54.71	-31 53 53.2	25	13.28 ± 0.02	12.20 ± 0.03	0.460 ± 0.030	-0.458 ± 0.030	16	M8	—	27 ± 2	83 ± 9	—	1999.0
23 47 36.80	+27 02 06.8	33	13.19 ± 0.02	11.98 ± 0.02	0.313 ± 0.019	0.033 ± 0.019	29	M9	—	22 ± 1	33 ± 3	—	1998.0
23 49 48.99	+12 24 38.6	33	12.60 ± 0.02	11.56 ± 0.02	0.018 ± 0.019	-0.209 ± 0.019	29	M8	—	20 ± 2	20 ± 2	—	1998.7
23 51 50.44	-25 37 36.7	61	12.47 ± 0.03	11.27 ± 0.03	0.387 ± 0.021	0.163 ± 0.009	17	M8	—	18 ± 2	36 ± 4	—	1998.9
23 53 59.46	-08 33 31.1	77	13.03 ± 0.03	11.93 ± 0.03	-0.6 ± 0.2	0.0 ± 0.2	9	M8.5	—	22 ± 2	61 ± 22	—	1998.8
23 56 54.77	-15 53 11.1	10	15.76 ± 0.06[c]	15.62 ± 0.06[c]	-0.443 ± 0.002	-0.600 ± 0.002	44	—	T5.5	14.5 ± 0.7[q]	51.3 ± 2.6	—	1998.5

Continued on Next Page...

Table 2.12 – Continued

RA (J2000) (1)	DEC (J2000) (2)	Ref.[1] (3)	2MASS J[3] (mag) (4)	2MASS K_s[3] (mag) (5)	$\mu_\alpha cos(\delta)$ ($''$ yr^{-1}) (6)	μ_δ ($''$ yr^{-1}) (7)	μ Ref.[2] (8)	SpT (opt) (9)	SpT (IR) (10)	Distance[3] (pc) (11)	V_{tan} (km s^{-1}) (12)	Note[4] (13)	Epoch (14)

Continued on Next Page...

[1]Discovery Reference Key:1 = Artigau et al. (2006) 2 = Becklin & Zuckerman (1988) 3 = Berriman et al. (2003) 4 = Biller et al. (2006) 5 = Bouy et al. (2003) 6 = Burgasser et al. (2004) 6B = Burgasser (2004a) 7 = Burgasser et al. (1999) 8 = Burgasser et al. (2000a) 9 = Burgasser et al. (2000c) 10 = Burgasser et al. (2002a) 11 = Burgasser et al. (2003b) 12 = Burgasser et al. (2003a) 13 = Burgasser et al. (2004) 14 = Burgasser et al. (2003d) 15 = Ruiz et al. (2001) 16 = Chauvin et al. (2004) 17 = Chauvin et al. (2005a) 18 = Chiu et al. (2006) 19 = Cruz et al. (2003) 20 = Cruz et al. (2007) 21 = Cruz et al. (in prep) 22 = Cruz & Reid (2002) 23 = Dahn et al. (2002) 24 = Deacon & Hambly (2007) 25 = Deacon et al. (2005) 26 = Delfosse et al. (1997) 27 = Delfosse et al. (1999) 28 = Delfosse et al. (2001) 29 = Ellis et al. (2005) 30 = Fan et al. (2000) 31 = Folkes et al. (2007) 32 = Geballe et al. (2002) 33 = Gizis et al. (2000b) 34 = Gizis et al. (2001b) 35 = Gizis et al. (2003) 36 = Gizis (2002) 37 = EROS Collaboration et al. (1999) 38 = Golimowski et al. (2004b) 39 = Hall (2002) 40 = Hawley et al. (2002) 41 = Henry et al. (2004) 42 = Irwin et al. (1991) 43 = Kendall et al. (2003) 44 = Kendall et al. (2004) 45 = Kendall et al. (2007) 46 = Kirkpatrick et al. (1999) 48 = Kirkpatrick et al. (2006) 49 = Kirkpatrick et al. (in prep) 50 = Kirkpatrick et al. (1997) 51 = Kirkpatrick et al. (1991) 52 = Kirkpatrick et al. (1993) 53 = Kirkpatrick et al. (2001b) 54 = Knapp et al. (2004) 55 = Leggett et al. (2000) 56 = Lépine et al. (2002) 57 = Luyten (1995) 58 = Liebert & Gizis (2006) 59 = Liebert et al. (2003) 60 = Liu et al. (2002) 61 = Lodieu et al. (2005) 62 = Lodieu et al. (2002) 63 = Looper et al. (2007) 64 = Luhman et al. (2007) 65 = Martín et al. (1999) 66 = Martin et al. (1994) 67 = McElwain & Burgasser (2006) 68 = Ménard et al. (2002) 69 = Metchev & Hillenbrand (2004) 70 = Metchev & Hillenbrand (2006) 71 = Mugrauer et al. (2006) 72 = Nakajima et al. (1995) 73 = Neuhäuser et al. (2005) 74 = Paper 10 75 = Phan-Bao et al. (2008) 76 = Phan-Bao et al. (2006) 77 = Phan-Bao et al. (2001) 78 = Phan-Bao et al. (2003) 79 = Potter et al. (2002) 80 = Probst & Liebert (1983) 81 = Rebolo et al. (1998) 82 = Reid et al. (2000) 83 = Reid et al. (in prep) 84 = Reid & Cruz (2002) 85 = Reid & Gilmore (1981) 86 = Reylé & Robin (2004) 87 = Ruiz et al. (1997) 88 = Salim et al. (2003) 89 = Schneider et al. (1991) 90 = Schneider et al. (2002) 91 = Scholz & Meusinger (2002) 92 = Scholz et al. (2003) 93 = Scholz et al. (2000) 94 = Scholz et al. (2005) 95 = Stern et al. (2007) 96 = Strauss et al. (1999) 97 = Teegarden et al. (2003) 98 = Thorstensen & Kirkpatrick (2003) 99 = Tinney et al. (2005) 100 = Tinney et al. (1993) 101 = Tinney et al. (1998) 102 = Tinney et al. (1993) 103 = Tsvetanov et al. (2000) 104 = Wilson et al. (2001) 105 = Wilson et al. (2003) 106 = Wilson (2002) 107 = Zapatero Osorio et al. (2002) 108 = Looper et al. (2008b) 109 = Hambly et al. (2004)

[2]PM reference 1 = Artigau et al. (2006) 2 = Bartlett (2007) 3 = Burgasser (2004a) 4 = Burgasser et al. (2003b) 5 = Burgasser et al. (2004) 6 = Burgasser et al. (2007a) 7 = Burgasser et al. (2008c) 8 = Burgasser et al. (2003d) 9 = Caballero (2007) 10 = Jameson et al. (2008a) 11 = Ruiz et al. (2001) 12 = Costa et al. (2006) 13 = Costa et al. (2005) 14 = Cruz et al. (2007) 15 = Dahn et al. (2002) 16 = Deacon et al. (2005) 17 = Deacon & Hambly (2007) 18 = Ellis et al. (2005) 19 = Faherty et al. 2008 20 = Folkes et al. (2007) 21 = Gizis et al. (2007) 22 = Hambly et al. (2001) 23 = Henry et al. (2006) 24 = Kendall et al. (2003) 25 = Kendall et al. (2004) 27

Table 2.12 – Continued

RA (J2000) (1)	DEC (J2000) (2)	Ref.[1] (3)	2MASS J[3] (mag) (4)	2MASS K_s[3] (mag) (5)	$\mu_\alpha cos(\delta)$ ($''$ yr^{-1}) (6)	μ_δ ($''$ yr^{-1}) (7)	μ Ref.[2] (8)	SpT (opt) (9)	SpT (IR) (10)	Distance[3] (pc) (11)	V_{tan} (km s^{-1}) (12)	Note[4] (13)	Epoch (14)

= Kendall et al. (2007) 28 = Lépine et al. (2002) 29 = Luyten (1995) 30 = Lodieu et al. (2005) 31 = Lodieu et al. (2002) 32 = Looper et al. (2007) 33 = Monet et al. (1992) 34 = Perryman et al. (1997) 35 = Phan-Bao et al. (2008) 36 = Schmidt et al. (2007) 37 = Siegler et al. (2007) 38 = Stern et al. (2007) 39 = Teixeira et al. (2000) 40 = Thorstensen & Kirkpatrick (2003) 41 = Tinney et al. (2005) 42 = Tinney (1996) 43 = Tinney et al. (2003) 44 = Vrba et al. (2004) 45 = Zapatero Osorio et al. (2007) 46 = van Altena et al. (1995)

[3]Key for distance and photometry footnotes: a = Chiu et al. 2006 MKO photometry converted to 2MASS b = Kendall et al. 2007 MKO photometry converted to 2MASS c = Knapp et al. 2004 MKO photometry converted to 2MASS d = Lodieu et al. 2007 MKO photometry converted to 2MASS e = Parallax from Bartlett (2007) f = Parallax from Costa et al. (2006) g = Parallax from Costa et al. (2005) h = Parallax from Dahn et al. (2002) i = Parallax from Gizis et al. (2007) j = Parallax from Henry et al. (2006) k = Parallax from Monet et al. (1992) l = Parallax from Perryman et al. (1997) m = Parallax from Thorstensen & Kirkpatrick (2003) n = Parallax from Tinney (1996) o = Parallax from Tinney et al. (2003) p = Parallax from van Altena et al. (1995) q = Parallax from Vrba et al. (2004) s = Binary Distance from Bouy et al. (2003) t = Binary Distance from Burgasser & McElwain (2006) u = Binary Distance from Burgasser et al. (2006b) v = Binary Distance from Burgasser et al. (2007a) w = Binary Distance from Close et al. (2003) x = Binary Distance from Forveille et al. (2005) y = Binary Distance from Kirkpatrick et al. (2000) z = Binary Distance from Law et al. (2006) aa = Binary Distance from Liu et al. (2006) bb = Binary Distance from Martín et al. (2005) cc = Binary Distance from Martín et al. (2006) dd = Binary Distance from McElwain & Burgasser (2006) ee = Binary Distance from Reid et al. (2006) ff = Binary Distance from Siegler et al. (2003) gg = Binary Distance from Siegler et al. (2007) hh = Binary Distance from vlmbinaries.org ii = Binary Distance from Burgasser (2007)

[4]VLMC is a wide, very low mass companion, UBL is an Unusually Blue L dwarf, LG is a low surface-gravity dwarf, YC is a dwarf linked to a young cluster, CB is a close binary unresolved in 2MASS

Chapter 3

Wide Common Proper Motion Pairs

Once the astrometric catalog described in chapter one was complete, it was possible to begin cross-checking the astrometry of individual brown dwarfs to those of nearby stars in order to search for widely spaced common proper motion companions. The majority of brown dwarf companions had been discovered to date serendipitously or by vicinity to a nearby object on the sky. The lack of proper motion measurements for the majority of brown dwarfs precluded the most basic search for a wide companion.

In this chapter I describe the results of a cross-correlation of the BDKP catalog to the Hipparcos and Lepine-Shara Proper Motion North (LSPM-N) catalog and the subsequent discovery of a number of wide stellar-brown dwarf pairs. This chapter is a reprinting of a paper, of which I am the primary author, published in the Astronomical Journal with co-authors Adam J Burgasser, Andrew A. West, John J. Bochanski, Michael M. Shara, Frederick M. Walter, and Kelle L. Cruz.

3.1 Introduction

Ultracool dwarfs (UCDs) comprise the late-type M, L, and T dwarf spectral classifications (e.g., Kirkpatrick, 2005, and references therein) and include brown dwarfs–objects that do not support stable hydrogen fusion (Kumar 1962; Hayashi & Nakano 1963). UCDs sample the low-mass extremum of star formation processes and are abundant in nearly every Galactic environment. The low temperatures and high pressures in the photospheres of UCDs give rise to abundant molecular species, whose complex chemistry and opacities result in highly-structured spectral energy distributions (SEDs). Disentangling the

physical characteristics—mass, age, surface gravity, metallicity, atmospheric properties, etc.— that modulate these spectral features is a critical step for testing theoretical models. However, individual characterization of Galactic brown dwarfs is challenging because their thermal evolution leads to a degeneracy between mass, age, and physical properties derived from observables such as luminosity and effective temperature (T_{eff}). While spectral analyses can constrain physical properties for some systems (e.g. Burgasser et al. 2006a; Saumon et al. 2007; Warren et al. 2007; Cushing et al. 2008), calibration of these techniques requires detailed studies of well-understood benchmark systems.

One useful group of UCD benchmarks are those which are resolved companions to nearby, well-characterized stars. Assuming coevality, the physical properties of the primary, such as metallicity and age—which are extremely difficult to measure for low-mass stars—can be applied to the companion. In particular, independent age determinations are critical to break the mass/age/observable degeneracy for the brown dwarf companion. Despite the apparent scarcity of wide UCD companions to nearby stars (∼2-3%; Gizis et al. 2001a, Lafrenière et al. 2008), several have been identified and used to calibrate spectral analysis techniques (e.g., Burgasser et al. 2006a; Saumon et al. 2007), as well as to critically test atmospheric (e.g., Leggett et al. 2008) and structure/evolutionary models (e.g., Mohanty et al. 2004; Dupuy et al. 2008). The frequency and characteristics of widely-separated stellar-UCD pairs also puts important constraints on the star formation processes and the subsequent dynamical evolution of stellar systems (e.g., Burgasser et al. 2003c; Close et al. 2003, 2007; Allen 2007; Luhman et al. 2009). However, the known population of UCD companions remains small and does not yet fully sample the range of ages, masses and metallicities found among unassociated field sources.

In the past decade, multiplicity surveys focused on the field UCD population have distinguished two classes:

- Roughly 10-20% of the field UCDs are found to be closely-separated ($\rho < 20$ AU), near-equal mass, small total mass (M_{tot} <0.2) UCD-UCD multiples (e.g. Bouy et al. 2003, Close et al. 2003, Burgasser et al. 2003c, Ahmic et al. 2007, Reid et al. 2008a)

- A smaller fraction are found to be widely-separated ($\rho > 100$AU) from a much more massive stellar companion (e.g. Kirkpatrick et al. 2001a, Wilson et al. 2001, Allen et al. 2005)

In the first case, the typically tight separations for UCD binaries is well-established (e.g. Allen et. al 2007), and early studies by Burgasser et al. (2003c), and Close et al. (2003) identified a maximum separation limit/minimum

binding energy for field UCD-UCD pairs of $E_b \sim 2\times10^{42}$ erg. However, the recent discovery of a number of young UCD systems (ages <10 Myr) and a handful of field systems that are more widely-separated ($\rho > 100$ AU) and more weakly bound ($E_b << 10^{42}$ erg), questions whether separation limits can be considered constraints for formation models or if wide UCD binaries are a normal (albeit rare) mechanism of UCD formation (Kraus et al. 2005, 2006, Konopacky et al. 2007, Luhman et al. 2009, and Allers et al. 2009, Artigau et al. 2007, Billères et al. 2005, Phan-Bao et al. 2005, Caballero 2007, Radigan et al. 2009).

In contrast, systems in the second category ($\rho >> 100$ AU) have binding energies that are several orders of magnitude smaller than the minimum set for UCD-UCD pairs. Burgasser et al. (2005) noted a higher binary frequency among UCDs that are widely-separated from a stellar primary, suggesting the need for higher masses or an angular momentum sink in multibody interactions to form these systems. Recent work by Whitworth & Stamatellos (2006) suggests that for a low-mass primary fragment formed in the cooler outer parts of a circumstellar disk ($\rho > 100$ AU), and spinning at a fast enough rate, H_2 dissociation is likely to trigger a Secondary Fragmentation phase, thereby potentially giving rise to a closely-separated (a$\sim$5 AU ($m_{system}/0.1M_\odot$) UCD binary.

Current observational evidence suggests that widely-separated stellar companions exist out to distances of $\sim$0.1pc (Latham et al. 1984; Weinberg et al. 1987). Beyond this separation, perturbations from passing stars and giant molecular clouds will likely disrupt the companions over the lifetime of the Galaxy. Separations of stellar-UCD and, especially, UCD-UCD multiples appear to fall well below the perturbation limit, suggesting dynamical sculpting occurs only in the natal environment (Burgasser et al. 2003c; Close et al. 2007). However, the current sample of such systems is far from complete. In large part this is due to the challenge of covering a large area of the sky, and ascertaining evidence for companionship between two objects. For stars, common proper motions have been the standard characteristic for identifying co-moving objects at large angular separations (van Biesbroeck (1961, 1944); Luyten 1979; Lépine et al. 2002). Historically, optical proper motion catalogs lacked the depth to detect late-type M, L, and T dwarfs. In addition, the recent discovery of UCDs has largely precluded astrometric measurements due to short temporal baselines, making an extensive common proper motion search difficult. In the past few years, large UCD proper motion samples (e.g., Jameson et al. 2008a; Casewell et al. 2008; Faherty et al. 2009) and near-IR proper motion surveys have become available (e.g., Deacon et al. 2005; Deacon & Hambly 2007; Deacon et al. 2009), making it possible to perform a

search in the reverse direction: using the UCD proper motion to find a stellar companion.

In this study, we used a proper motion catalog of UCDs from Faherty et al. (2009) (hereafter, the BDKP catalog) to conduct a common proper motion search for main sequence companions to Hipparcos (Perryman et al. 1997) or LSPM-N (Lépine et al. 2002) catalog stars. We have uncovered nine systems, six of which have been briefly noted in the literature and three of which are presented here for the first time. In section 2 we discuss our target list, the criteria for companionship and the reliability of our matches. In section 3 we discuss follow-up photometry as well as optical and near-IR spectroscopy of our candidate systems. In section 4 we apply age diagnostic tests to the primaries and secondaries and calculate masses of the UCD secondaries. In section 5 we explore the stability of the nine systems as well as multiplicity and formation mechanisms for a large sample of UCD field companions. We summarize our results in section 6.

3.2 Wide Companion Discovery

3.2.1 Initial Target List and Selection Criteria

We began an astrometric search for common proper motion candidates to UCDs using the BDKP catalog (Faherty et al. 2009) of 842 late-type M, L, and T dwarfs. The catalog is composed of 570 L and T dwarfs (all of which can be found on the DwarfArchives compendium[1]) and 272 M7-M9 dwarfs drawn from the literature. Objects span spectral types from M7-T8 and cover a wide range of magnitudes, distances, and proper motions.

To avoid a large number of chance alignments with slowly moving objects, we only considered the 681 UCDs in the BDKP catalog with proper motion $>$ 100 mas yr^{-1}. We compared the positions and motions of the UCDs to stars in the Hipparcos (Perryman et al. 1997) and LSPM-N (Lépine et al. 2002) catalogs. An angular separation of up to 10 arcminutes and a proper motion match criterion of better than 2σ in both RA and DEC were required between the system components. The average uncertainty for objects in the BDKP catalog is 15 mas yr^{-1} so we typically required an agreement in proper motion $<$ 30 mas yr^{-1} between the stellar companion and UCD.

We also used distances to further rule out chance alignment pairs. All of the UCDs listed in the BDKP catalog have photometric distance estimates based on the Cruz et al. (2003) relation for M7-L5 dwarfs or the Burgasser (2007) relation for L6-T8 dwarfs. All of the stellar candidate companions

[1]http://dwarfarchives.org

had either photometric distances of their own (Lépine 2005) or had parallax measurements from the Hipparcos catalog. We required a distance agreement of better than 2σ, which generally meant < 10 pc difference.

3.2.2 New Candidate Companion Systems

After selecting by angular separation, proper motion, and distance we were left with 30 possible wide common proper motion pairs with a Hipparcos or LSPM-N star. Twenty-one of these were previously known systems and are listed in Table 3.1 and not discussed at length within this study. Six systems with UCD components: 2MASS J0003-2822, 2MASS J0025+4759, SDSS J0041+1341, SDSS J0207+1355, 2MASS J1320+0957, and 2MASS J1320+0409, have been previously reported in the literature but not studied in detail (Cruz et al. 2003, Pinfield et al. 2006, Jameson et al. 2008a, Deacon et al. 2009). Three systems with UCD components 2MASS J1200+2048, 2MASS J1416+5006, and SDSS J1758+4633, are reported here for the first time. These nine systems are summarized in Table 3.2.

3.2.3 Reliability of Common Proper Motion Candidates

To quantify the probability that our pairs might be chance alignments, we ran a Monte Carlo simulation of all stars in the LSPM-N and Hipparcos catalogs that shared a common proper motion, but not necessarily distance or position, with our UCDs (to within 2σ). We assumed that high proper motion objects are rare so we can accurately sample the observed proper motion distributions in the LSPM-N and Hipparcos catalogs. For computational purposes we created a simulation grid that was equal in angular size to the area covered by the catalogs.

LSPM-N is over 99% complete at high galactic latitudes and over 90% complete at low galactic latitudes so we assume an area of half the sky for this survey. Hipparcos is an all-sky catalog and depending on galactic latitude and spectral type, complete to V$\sim$7.3-9.0. The resolution of each grid point was set to be the angular separation between the pairs discussed in Table 3.2. Our simulation drew N stars (where N is the number of stars with matching proper motions) and placed them randomly in the grid. The number of times two stars fell in the same grid region (or within the observed pair separation) was determined. We iterated each simulation 10000, 100000 or 1000000 times, depending on the iterations required to produce a chance alignment. The ratio of matches to trials provided a probability for random association, as listed in Table 3.3. The simulations are based solely on the distributions of proper motions in empirical data and do not account for the spatial distribution

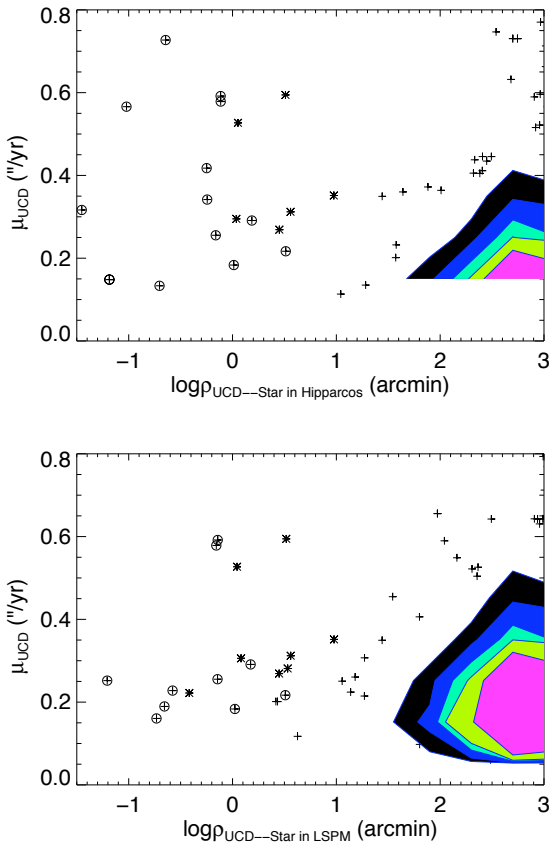

Figure 3.1: Proper motion vs. separation of the known and potential common proper motion pairs of Hipparcos stars (left panel) and LSPM-North stars (right panel) to UCDs in the BDKP catalog moving faster than 100 mas yr^{-1}. We required a proper motion component match of 2σ between star and UCD. There was no distance requirement between potential pairs applied in this plot. Objects marked by circles are previously published wide ultracool dwarf pairs. Objects marked by asterisks are wide ultracool pairs discussed in this paper. In the right plot, we rejected two objects within the 10 arc-minute radius because their photometric distances were greater than 3σ from the UCD. The contours in each plot represent densities of 75, 200, 500, 750, and 2000 objects.

of the stars on the sky or any models of Galactic structure, both of which would likely decrease the probability of chance alignment. We found that the likelihood that any of the nine systems in Table 3.2 is a chance coincidence is $<$ 0.01%. Figure 3.1 illustrates the reliability of the new common proper motion pairs. We investigated the spatial distribution of these matches and found no preferred direction indicating that the matches are indeed randomly selected. Only two objects within a 10 arcminute separation did not have matching distances (see the LSPM-N matches in the right panel of Figure 3.1).

Lépine & Bongiorno (2007) performed a similar proper motion reliability check by comparing the entire LSPM-N catalog to the Hipparcos catalog. They used over 4000 known Hipparcos stars that had a wide LSPM-N companion and then simulated chance alignments in those fields by moving from 1 to 5 degrees away from the known pair and evaluating any additional systems that shared the same proper motion. They derived the following relation which is globally applicable for any pair of co-moving stars with μ $>$0.15$''$/yr and tests whether a common proper motion system has $>$50% probability of being physically associated:

$$\Delta\theta\Delta\mu < (\mu/0.15)^{3.8} \tag{3.1}$$

where $\Delta\theta$ is the angular separation (in $''$), μ is the mean total proper motion of the pair in $''$ yr^{-1}, and $\Delta\mu$ is the magnitude of the difference between the proper motion vectors in $''$ yr^{-1}.

We have used this relation as a second reliability check on each of our pairs and find that the nine systems from Table 3.2 pass this criterion.

Table 3.1: Information on Wide Companions

Name (1)	SpT (primary) (2)	SpT (secondary) (3)	$\rho_{star-UCD}$ ($''$) (4)	$\rho_{star-UCD}$ (AU) (5)	$\rho_{UCD-UCD}$[1] ($''$) (6)	$\rho_{UCD-UCD}$[1] (AU) (7)	Lower Age[2] (Gyr) (8)	Upper Age[2] (Gyr) (9)	Mass ($M_{\odot}$)[3] (primary) (10)	Mass ($M_{\odot}$)[4] (secondary) (11)	Ref (12)
TWA 5[7]	M1.5	M8	2	100	<0.15	<8	0.01	0.3	0.40	0.02	3
GQ Lup[7]	K7	L1.5	0.7	103	<0.4	<71	3	3	0.70	0.02	20
G203-50[7]	M4.5	L5	6.4	135	<0.18	<11	1	5	0.15	0.07	32
LHS 5166	dM4.5	L4	8.43	160	<1	<24	2.6	8	0.21	0.07	25
GJ 1001[7]	M4	L4.5+L4.5	18.6	180	0.09	0.8	1	10	0.25	0.07	17,4,6
eta Tel[7]	A0V	L1	4.2	190	<0.15	<7	0.08	0.02	2.08	0.20	8,37
GSC 08047-00232[7]	K3	M9.5	3.2	200	<0.1	<7	0.01	0.04	0.50	0.02	16,19
GG Tau[7]	K7+M0.5+M5+	M7	1.5	210	<0.1	<14	0.01	0.02	1.10	0.04	5
2MASS J0551-4434	M8.5	L0	2.2	220	<1	<62	0.1	10	0.07	0.06	23
LP 213-67[7]	M6.5	M8+L0	14	230	0.12	3	—	—	0.10	0.18[5]	9,15
GJ 1048	K2	L1	11.9	250	<1	<26	0.6	2	0.84	0.07	10
HD 65216 [7]	G5	M7+L2	7	253	0.17	6	3	6	0.94	0.09	31
AB Pic[7]	K2	L1	5.5	275	<0.1	<6	∼0.03	∼0.03	0.70	0.01	21,38
G196-3	M2.5	L2	16.2	300	<1	<2 0	0.06	0.3	0.30	0.04	2
BD+13 1727	K5	M8	10.5	380	<1	<45	—	—	1.20	—	28
Wolf 940	M4	T8.5	32	400	<1	<62	3.5	6	0.20	0.03	35
V1428 Aql[6]	M3	M8	75	400	<1	<6	—	—	0.40	—	1
Denis-P J1347-7610	M0	L0	16.8	418	<1	<62	0.2	1.4	0.60	—	33
LP 655-23	M4	M8	20	450	<1	<29	1	8	0.26	0.09	30
LP 261-75	M4.5	L6	13	450	<1	<60	0.1	0.2	0.22	0.02	27
HD 3651	K0	T7.5	43	480	<1	<44	0.7	4.7	0.80	0.03	29
HD 203030	G8	L7.5	11	487	<1	<51	0.13	0.4	0.97	0.02	26
G216-7[7]	M3.5+M3.5	M9.5	33.6	634	<0.3	<6	1	10	1.00	0.07	11
HN Peg[7]	G0	T2.5	43	795	<0.4	<5.5	0.1	0.5	1.09	0.02	29
Gl 337[7]	G8+K1	L8+L8/T	43	880	0.53	10.9	0.6	3.4	1.74	0.04	12,24
Gl 618.1	M0	L2.5	35	1090	<1	<38	0.5	12	0.67	0.06	12
eps Indi[7]	K5	T1+T6	402	1460	0.62	2.2	0.8	2	0.67	0.04	13
G124-62[7]	dM4.5e	L1+L1	44	1496	0.42	14.3	0.5	0.8	0.21	0.07	22
Gl 570[7]	K4+M1.5+M3	T7	258	1500	<0.1	<0.6	2	5	0.95	0.05	7
LEHPM 494	M6.0	M9.5	78	1800	<1	<62	2	10	0.10	0.08	30
Gl 417[7]	G0+G0	L4.5+L6	90	2000	0.07	1.5	0.08	0.3	0.94	0.04	11,14
APMPM J2354-3316	DA+M4	M8.5	8	2200	<1	<62	1.8	1.8	0.65	0.10	18
HD 89744	F7	L0	63	2460	<1	<40	1.5	3	1.40	0.07	12
Gl 584	G1+G3	L8	194	3600	<1	<20	1	2.5	1.10	0.06	31
2MASS J0126-5022	M6.5	M8	82	5100	<1	<62	0.2	2	0.10	0.09	34
2MASS J1258+4013	M7	M6	63	6700	<1	<104	1	5	0.11	0.09	36
HD 221356[7]	F8	M8+L3	452	11900	0.57	15	5.5	8	1.02	0.09	30

Continued on Next Page...

Table 3.1 – Continued

Name	SpT (primary)	SpT (secondary)	$\rho_{star-UCD}$ ($''$)	$\rho_{star-UCD}$ (AU)	$\rho_{UCD-UCD}$[1] ($''$)	$\rho_{UCD-UCD}$[1] (AU)	Lower Age[2] (Gyr)	Upper Age[2] (Gyr)	Mass ($M_{\odot}$)[3] (primary)	Mass ($M_{\odot}$)[4] (secondary)	Ref[8]
(1)	(2)	(3)	(4)	(5)	(6)	(7)	(8)	(9)	(10)	(11)	(12)

[1]UCD-UCD separation estimated from the discovery paper or assumed to be $1''$, a limit which comes from the 2MASS images (Skrutskie et al. 2006)

[2]Ages come from the cited discovery paper

[3]Mass of the primary estimated from the mass-luminosity relation in Allen's Astrophysical Quantities (Cox 2000) or Reid & Hawley (2005) (for M stars) unless otherwise noted

[4]Mass of the secondary estimated from the discovery paper

[5]The mass of the primary in this system in less than the combined mass of the two components which make up the secondary

[6]aka VB 10

[7]These systems are used in the multiplicity analysis along with 2MASS J0025+4759 and 2MASS J1200+2048 as the UCD secondary has been targeted with HST or AO to resolve a closely separated (<20AU) pair

[8]Refs: 1= van Biesbroeck (1944) 2 = Rebolo et al. (1998) 3 = Lowrance et al. (1999) 4 = Kirkpatrick et al. (1999) 5 = White et al. (1999) 6 = Martin et al. (1999) 7 = Burgasser et al. (2000a) 8 = Lowrance et al. (2000) 9 = Gizis et al. (2000a) 10 = Gizis et al. (2001b) 11 = Kirkpatrick et al. (2001a) 12 = Wilson et al. (2001) 13 = Scholz et al. (2003) 14 = Bouy et al. (2003) 15 = Close et al. (2003) 16 = Neuhäuser & Guenther (2004) 17 = Golimowski et al. (2004a) 18 = Scholz et al. (2004) 19 = Chauvin et al. (2005a) 20 = Neuhäuser et al. (2005) 21 = Chauvin et al. (2005b) 22 = Seifahrt et al. (2005a) 23 = Billères et al. (2005) 24 = Burgasser et al. (2005) 25 = Seifahrt et al. (2005b) 26 = Metchev & Hillenbrand (2006) 27 = Reid & Walkowicz (2006) 28 = Cruz et al. (2007) 29 = Luhman et al. (2007) 30 = Caballero (2007) 31 = Mugrauer et al. (2007) 32 = Radigan et al. (2008) 33 = Phan-Bao et al. (2008) 34 = Artigau et al. (2009) 35 = Burningham et al. (2009) 36 = Radigan et al. (2009) 37 = Ortega et al. (2002) 38 = Song et al. (2003)

3.3 Observations

3.3.1 Optical Spectroscopy with SMARTS

R-C Spectrograph

Optical spectra for six of the primaries were obtained with the R-C spectrograph on the CTIO SMARTS 1.5m telescope over several nights in the fall of 2008 and winter of 2009. Table 3.4 provides details of our observations. The R-C is a slit spectrograph, with a 300″ long slit oriented east-west. We employed various spectral setups that covered either the red or blue part of the spectrum (see Table 3.4 for details). The detector is a Loral 1K CCD with 1199 pixels in the direction of the dispersion. All spectra were acquired through queue observing with time allocated through the SMARTS consortium. The conditions for these observations were moderate with an average seeing of 1.0 - 1.2 ″. Targets were observed through a 110μm (2.0″) wide slit. Three images of each target were obtained and accompanied by a wavelength calibration exposure of a Ne-Ar or Th-Ar arc lamp. A spectro-photometric standard, either Feige 110 or LTT 4364, was observed each night for flux calibration. Images were bias-subtracted, trimmed, and flattened, then co-added using a median filter. Spectra were extracted using IDL routines that fit a Gaussian in the spatial dimension at each column in the CCD. The net counts at each pixel are the integrated counts in the Gaussian, less the interpolated background fit to either side of the spectrum.

Echelle Spectrograph

High dispersion spectra of three of the primaries (Table 3.4) were obtained with the bench-echelle spectrograph on the CTIO SMARTS 1.5m telescope over three nights in the fall of 2008 and winter of 2009. Formerly mounted at the Cassegrain focus of the Blanco 4m telescope, the echelle spectrograph is fiber-fed from the 1.5m and uses a 31.6 line/mm echelle and a 226 line/mm cross disperser feeding a 2K SITE CCD detector. Our observations employed a 60 μm slit which corresponds to a 2 pixel resolution of R$\sim$40,000. All spectra were acquired through queue observing. The conditions for these observations were moderate with an average seeing of 1.0 - 1.2 ″. A quartz lamp exposure at the start of the night was obtained for flat fielding. Three images of 1500 s were obtained for each target followed by a wavelength calibration exposure of Th-Ar. The data were reduced using IDL routines. We median filtered and co-added the flat field and science spectra for each target. Using the quartz lamp trace we extracted individual spectra, and then divided by the extracted flat field spectra. The Th-Ar spectra were cross-correlated against a template

Table 3.2. Astrometric Information on the Companion Candidates

Name	Ref	μ_α $''_{\rm yr}{}^{-1}$	μ_δ $''_{\rm yr}{}^{-1}$	SpT Opt	SpT IR	Dist pc	ρ arcsec	ρ AU
(1)	(2)	(3)	(4)	(5)	(6)	(7)	(8)	(9)
2MASSJ0003-2822	2	0.257 ± 0.016	-0.145 ± 0.018	M8	M8	26 ± 3		
G 266-33		0.280 ± 0.001	-0.1431 ± 0.0007	G8		$39.5^{+1.8}_{-1.6}$	66	2610
2MASSJ0025+4759AB	2	0.312 ± 0.039	-0.009 ± 0.044	L4+L4[a]	—	31 ± 6[a]		
G 171-58		0.2743 ± 0.0007	0.0112 ± 0.0009	F8		$42.2^{+2.0}_{-1.8}$	218	9202
SDSSJ0041+1341	3,9	-0.174 ± 0.024	-0.138 ± 0.036	L0	—	31 ± 6		
NLTT 2274		-0.201 ± 0.013	-0.178 ± 0.013	M4	M4	21 ± 8	23	483
SDSSJ0207+1355	3,7	0.260 ± 0.017	-0.161 ± 0.018	L2	L2	35 ± 5		
G 73-26		0.262 ± 0.013	-0.186 ± 0.013	M2		26 ± 10	73	2774
2MASSJ1200+2048	5	-0.159 ± 0.019	0.232 ± 0.019	M7	—	26 ± 3		
G 121-42		-0.157 ± 0.013	0.241 ± 0.013	M4		30^{+14}_{-7}	204	5916
2MASSJ1320+0957	6,7	-0.236 ± 0.021	-0.129 ± 0.021	M8	—	36 ± 3		
G 63-23		-0.250 ± 0.002	-0.144 ± 0.002	K5		$38.1^{+2.6}_{-2.3}$	169	6445
2MASSJ1320+0409	6,8	-0.483 ± 0.019	0.211 ± 0.017	L3	—	33 ± 3		
G 62-33		-0.507 ± 0.001	0.202 ± 0.0009	K2		$30.5^{+1.0}_{-1.0}$	66	2010
SDSSJ1416+5006	1	-0.297 ± 0.013	0.188 ± 0.021	—	L4	44 ± 31		
G 200-28		-0.3003 ± 0.0007	0.1861 ± 0.0007	G5		$45.1^{+1.6}_{-1.5}$	570	25734
SDSSJ1758+4633	4	0.026 ± 0.015	0.594 ± 0.016	—	T6.5	12 ± 2		
G 204-39		-0.017 ± 0.002	0.575 ± 0.002	M3		$13.6^{+0.3}_{-0.3}$	198	2685

References. — 1 = Chiu et al. (2006) 2 = Cruz et al. (2007) 3 = Hawley et al. (2002) 4 = Knapp et al. (2004) 5 = Gizis et al. (2000b) 6 = Reid et al. (2008b) 7 = Deacon et al. 2009 8 = Pinfield et al. (2006) 9 = Jameson et al. (2008a)

[a]This L4+L4 distance is reported in Reid et al. (2006)

Table 3.3. Reliability of the Common Proper Motion Pairs

Name	Num Match[a] LSPM-N	% Chance Alignment LSPM-N	Num Match[a] Hipparcos	% Chance Alignment Hipparcos
(1)	(2)	(3)	(4)	
2MASS J0003-2822	259	0.01	63	0.01
2MASS J0025+4759	283	0.85	68	0.02
SDSS J0041+1341	2336	0.44	294	<0.01
SDSS J0207+1355	230	0.04	49	<0.01
2MASS J1200+2048	55	0.07	15	<0.01
2MASS J1320+0957	418	1.03	73	0.02
2MASS J1320+0409	11	<0.01	6	<0.01
SDSS J1416+5006	40	0.12	13	0.01
SDSS J1758+4633	2	<0.01	3	<0.01

[a]These columns tabulate the number of stars in the entire Hipparcos or LSPM-N catalog that had matching proper motion components to the UCD at the 2σ level

Table 3.4. Details of SMARTS Observations

Name	Instrument	Exposure Time (s)	Date	Airmass	Grating
(1)	(2)	(3)	(4)	(5)	(6)
G 266-33	R-C Spec	2100	12 November 2008	1.001	47/II
G 266-33	R-C Spec	1800	30 November 2008	1.313	26/Ia
G 266-33	Echelle	1500	20 April 2009	1.370	—
NLTT 2274	R-C Spec	2700	29 September 2008	1.571	47/Ib
NLTT 2274	R-C Spec	1800	24 October 2008	1.387	26/Ia
NLTT 2274	R-C Spec	2700	17 November 2008	1.413	26/Ia
G 73-26	R-C Spec	1800	17 September 2008	1.883	47/Ib
G 73-26	R-C Spec	1800	02 October 2008	1.812	26/Ia
G 73-26	R-C Spec	1800	16 November 2008	1.438	47/Ib
G 73-26	R-C Spec	2700	26 November 2008	1.393	47/II
G 121-42	R-C Spec	1500	25 December 2008	2.026	32/I
G 121-42	R-C Spec	1800	25 January 2009	1.766	26/Ia
G 121-42	R-C Spec	1500	25 December 2009	1.420	47/Ib
G 121-42	R-C Spec	1200	25 December 2009	1.827	47/II
G 63-23	Echelle	1800	14 November 2008	1.013	—
G 63-23	R-C Spec	1800	29 January 2009	1.647	26/Ia
G 63-23	R-C Spec	1200	14 February 2009	1.669	47/Ib
G 63-23	R-C Spec	3600	24 February 2009	1.306	47/II
G 62-33	R-C Spec	1200	29 January 2009	1.637	26/Ia
G 62-33	R-C Spec	1200	14 February 2009	1.660	47/Ib
G 62-33	Echelle	1500	21 February 2009	1.262	—
G 62-33	R-C Spec	1800	24 February 2009	1.223	47/II

Note. — Grating 26/Ia covers 3700-5400 Å at 4.4 Å spectral resolution, Gratings 47/Ib and 47/II cover 5600-6950 Å at 3.1 Å spectral resolution

Table 3.5. Details of KPNO Observations

Name	Instrument	Exposure Time (s)	Date
(1)	(2)	(3)	(4)
G 62-33	Echelle	915	26,27 June 2009
G 63-23	Echelle	500	27 June 20009
G 200-28	Echelle	900	25 June 2009
G 171-58	Echelle	900	25 June 2009

spectrum to determine the pixel shifts. The wavelength stability of the system is better than 0.5 km s^{-1} over the course of half a year. The extracted spectra were linearized using the wavelength solution. Our detection equivalent width for atomic absorption features, in a 1 hour exposure at V∼9, is 3 mÅ.

3.3.2 KPNO Echelle Spectroscopy

High dispersion spectra of four of the primaries (Table 3.5) were obtained with the KPNO 4.0m echelle spectrograph during the nights of 2008 June 25-29 (UT). We used the 58.5 echelle grating, the 226-1 cross-disperser in second order, and the $CuSO_4$ filter to obtain spectra between about 3700 and 5000Å. The weather conditions for these observations were poor with an average seeing of 1-2 ″. The rapidly changing sky conditions precluded precise focussing, and required hand-guiding. We observed with a 1 ″ slit and a 9.73 ″ decker. A ThAr lamp spectrum was obtained at each telescope position for wavelength calibration. At the start of the night, we observed the pflat lamp though a 15 ″ decker. Data extraction used conventional techniques. The bias was subtracted from the science frame which was then divided by the lengthened flat. Targets were self-traced during extraction and the background was estimated from the region above and below the target on the slit. For the primary G 62-33, a weighted sum of the two spectra taken on 2008 June 26 and 27 was used to improve S/N. The reciprocal dispersion in the order containing Ca II K&H is 0.05A/pixel and the nominal instrumental resolution is R∼33,000.

We followed the technique used by Linsky et al. (1979) to directly measure R'_{HK} from the echelle data. First we normalized the spectrum by scaling it to a flux-calibrated low-dispersion spectrum. This removed any residual instrumental signature remaining after flattening the spectrum. Then we scaled to an absolute surface flux using Linsky's calibration of Willstrop (1965) pho-

tometry in the 3925-3975Å bandpass. This calibration uses Johnson $V-R$ colors so we converted the $B-V$ colors to Cousins $V-R_C$, and then used the transformation in Bessell (1979) to convert to $V-R$. We measured the flux between the K_1 and H_1 minima and interpolated the photospheric contribution to the flux between them using the data in Linsky et al. (1979). R'_{HK} is the net surface flux normalized to σT^4_{eff}.

We verified the technique by measuring R'_{HK} for 5 calibration stars: ξ Boo A,B, 61 Cyg A,B, and HD 128165. With the exception of ξ Boo B which was high by$\sim$50%, all measurements agreed with published values to within 10-20%. We note that Hϵ is seen prominently in emission in the spectrum of ξ Boo B, so the star was likely flaring. Examination of chromospheric emission levels in Baliunas et al. (1995) shows that variations of 10-50% are common over the course of stellar magnetic cycles. We also measured the solar (twilight sky) spectrum and calculated the solar $\log(R'_{HK}) = -4.8^{+0.2}_{-0.3}$.

3.3.3 Optical Spectroscopy with MagE

Optical spectra for five of the primaries and three of the UCD secondaries were obtained with the Magellan Echellette Spectrograph (MAGE; Marshall et al. 2008) on the 6.5m Clay Telescope at Las Campanas Observatory over several nights in October 2008, November 2008, and January 2009. Table 3.6 lists the details of our observations. MagE is a cross–dispersed optical spectrograph, covering 3,000 to 10,000 Å at medium resolution ($R \sim 4,100$). Our observations employed a $0.7''$ slit aligned at the parallactic angle, and the chip was unbinned. These observations were made under clear conditions with an average seeing of $\sim 0.7''$. The targets were first acquired with the MagE finder camera using an R filter. For the primaries we used 5-30s exposures for the brightest targets and 100-120s exposures for the faintest. For the UCD secondaries we used 1200-2400s. A ThAr lamp spectrum was obtained at each telescope position for wavelength calibration and the spectrophotometric standard GD 108 was observed during each run for flux calibration purposes. Ten Xe-flash and Quartz lamp flats as well as twilight flats were taken at the start of each evening for pixel response calibration. The data were reduced using a preliminary version of the MagE Spectral Extractor pipeline (MASE; Bochanski et al., in prep) which incorporates flat fielding, sky subtraction and flux calibration IDL routines.

3.3.4 Near-Infrared Spectroscopy with SPEX

Near-IR spectra for two of the primaries and three of the UCD secondaries were obtained with the SpeX spectrograph mounted on the 3m NASA In-

Table 3.6. Details of MagE Observations

Name	Exposure Time (s)	Date	Airmass
(1)	(2)	(3)	(4)
G 266-33	5	25 November 2008	1.227
2MASS J0003-2822	1200	25 November 2008	1.266
NLTT 2274	100	07 October 2008	1.443
2MASS J0041+1341	1500	07 October 2008	1.464
G 73-26	120	25 November 2008	1.463
2MASS J0207+1355	2400	08 October 2008	1.376
G 121-42	100	07 March 2009	1.111
G 62-33	10	11 January 2009	2.038
G 63-23	30	11 January 2009	2.264

Table 3.7. Details of SpeX Observations

Name	Exposure Time (s)	Date	Airmass	Calibration Star
(1)	(2)	(3)	(4)	(5)
2MASS J0003-2822	450	09 December 2008	1.499	HD 220455
2MASS J0025+4759	510	09 December 2008	1.186	HD 1561
NLTT 2274	360	09 December 2008	1.006	HD 6457
G 73-26	360	15 December 2008	1.070	BD+18 337A
2MASS J0207+1355	510	10 December 2008	1.037	V* Vz ari

frared Telescope Facility (IRTF) over several nights in December 2008. The conditions of this run were variable with patchy clouds and average seeing (0.8 -1.0 $''$ at J). Table 3.7 lists the details of our observations. We operated in prism mode with the 0.8$''$ slit aligned at the parallactic angle and obtained low-resolution ($\lambda/\Delta\ \lambda \sim$90) near-infrared spectral data spanning 0.7 - 2.5 μm . Each target was first acquired in the guider camera. Exposure times varied from 120s to 150s depending on the brightness of the target. Six images were obtained for each object in an ABBA dither pattern along the slit. An A0V star was observed immediately after each target at a similar airmass for flux calibration and telluric correction. Internal flat-field and Ar arc lamp exposures were acquired for pixel response and wavelength calibration, respectively. All data were reduced using SpeXtool version 3.3 (Vacca et al. 2003, Cushing et al. 2004) using standard settings.

Table 3.8. Details of ANDICAM Observations

Name	Date (s)	Number of Images	Band
(1)	(2)	(3)	(4)
G 62-33	16 February 2009 – 9 April 2009	54	*B*
G 62-33	16 February 2009 – 26 March 2009	30	*V*
G 62-33	27 March 2009 – 9 April 2009	24	*I*
G 63-23	10 February 2009 – 3 April 2009	32	*V*
G 63-23	10 February 2009 – 3 April 2009	32	*I*
G 121-42	10 February 2009 – 31 May 2009	46	*V*
G 121-42	10 February 2009 – 31 May 2009	46	*I*
G 73-26	4 December 2008 – 31 January 2009	31	*V*
G 73-26	4 December 2008 – 31 January 2009	31	*I*

3.3.5 Photometric Follow-Up

Optical photometry for four of the primaries (Table 3.8) was obtained with the ANDICAM dual channel photometer on the CTIO SMARTS 1.3m telescope over several months in the winter of 2008 and spring of 2009. The ANDICAM optical detector is a Fairchild 447 2048×2048 CCD and was used in 2×2 binning mode, yielding a nominal plate scale of 0.369 arcsec pixel^{-1}. The ∼6.2 arcmin field of view allowed between 3-7 reference stars for photometric comparison in each image. All data were taken by service (or queue) observing in I, V, and/or B bands and nightly conditions varied. Domeflats were taken at the start of each night and science frames were flat-fielded and trimmed using standard IRAF tasks prior to delivery. Differential photometry was performed using IDL routines which utilized a 9 pixel aperture and a background annulus evaluated between 19 and 36 pixels from the target.

3.4 Characterizing the Systems

Nearby solar-type stars are generally well-characterized with spectral type, metallicity, activity, radial velocity, distance, rotation, and other measureable diagnostic parameters. As such, these companions serve to constrain the properties of the UCD counterparts. The primaries discussed in this paper range in spectral type from F8-M4 and are all within 50 pc of the Sun. We combined the data available for them in the literature with follow-up spectroscopy and photometry with the primary goal of obtaining an age. For the bright primaries, we used standard and template spectra provided within the IDL package the

Hammer (Covey et al. 2007)[2] as well as spectral standards from the Stony Brook/SMARTS Spectral Standards Library[3] to characterize the stars. For the fainter secondaries we used the M dwarf templates from Bochanski et al. (2007b); the L dwarf standards from Kirkpatrick et al. (1999) and Kirkpatrick et al. (2000), or data available from the SpeX Prism Libraries[4] to characterize each source.

3.4.1 Age-Dating The Systems

There are a number of age-dating techniques for solar analogs that can constrain ages to within a few Gyrs (Mamajek & Hillenbrand 2008, Lachaume et al. 1999). The techniques employed in this study were as follows:

- Gyrochronology: The ages of field stars are determined based on their rotational rates. Barnes (2007) derived a color-dependent version of the Skumanich (1972) law basing the timescale for stellar rotational decay on the Sun. For the systems for which we have rotation periods, we derive gyro ages using the Mamajek & Hillenbrand (2008) reformulation of Barnes' (2007) formula. The Mamajek & Hillenbrand gyro ages are typically about a factor of two larger than those derived using Barnes' coefficients.

- X-ray emission: Coronal activity as traced by X-ray emission is an age diagnostic, as magnetic activity declines as a star spins down over time (e.g. Fleming et al. 1995).

- Ca II H & K lines: The R'_{HK} index measures the amount of chromospheric emission that arises in the cores of the Ca II H & K lines and has been observed to decay with age (Wilson 1963; Skumanich 1972; Soderblom 1983; Soderblom et al. 1991). Mamajek & Hillenbrand (2008) recently revised the R'_{HK} activity relation for F7-K2 dwarfs (0.5<B-V<0.9 mag) and defined the following age:

$$\log \tau_1 = -38.053 - 17.912 \log R'_{HK} - 1.6675 \log(R'_{HK})^2 \qquad (3.2)$$

  where τ_1 is in years[5].

[2]http://www.cfa.harvard.edu/∼kcovey/thehammer.html

[3]http://www.astro.sunysb.edu/fwalter/SMARTS/spstds.html

[4]http://www.browndwarfs.org/spexprism/

[5]Mamajek & Hillenbrand (2008) also define a τ_2 age inferred from converting the chromospheric activity levels to a rotation period via the Rossby number and then converting the rotation period to an age using the revised gyrochronology relation. We convert τ_1 into

- Lithium abundances: Li is depleted in stellar cores early in the life of solar-type stars, so it is commonly used as an age indicator. A comparison of Li abundances to stars in clusters with well-determined ages is likely the most appropriate usage of Li as an age diagnostic. However, as in the case with nearly all other age diagnostics, there is a large scatter in the observed EW(Li) even in coeval clusters. For field-aged stars there are few to no clusters with well-determined ages to compare to. Therefore, for older stars, one can use the Pavlenko & Magazzu (1996) NLTE curve of growth, to obtain a logarithmic depletion of Li from cosmic abundances (log N(Li)=3.3) and use the models of Pinsonneault et al. (1990) to convert this depletion into an age.

- Theoretical isochrones: Ages can be determined directly by placing stars on a theoretical HR diagram, using the observed T_{eff}, M_V, and [Fe/H] (Nordström et al. 2004).

- Kinematics: While individual space motions can not be used to date objects, general information can be obtained from U, V, W velocity distribution. Studies such as Eggen (1989) and Leggett (1992) have defined velocity ranges that would indicate membership in the young or old part of the galaxy. Eggen & Iben (1989) define a U-V criterion (called the "Eggen box") for the young disk as roughly -50 km s^{-1} < U < +20 km s^{-1} and -30 km s^{-1} < V< 0 km s^{-1} (where the convention of U positive toward the Galactic center is used). While the age associated with membership in the young or old part of the Galaxy is uncertain, Eggen (1989); Eggen & Iben (1989) roughly define the transition between the two populations as 2-3 Gyr based on the kinematic analysis of well defined cluster members (Hyades, Pleiades, NGC 752 etc.). Admittedly, individual kinematics are a very poor age diagnostic tool and any use of space motion to age date a star needs to be viewed with caution and complimented with much more robust diagnostics. Therefore, throughout the text we use kinematics primarily as a secondary check on other more reliable age diagnostics.

- Metallicity: While metallicity is an important physical property of any stellar system, it is not a reliable age indicator. Nordström et al. (2004) construct an age-metallicity diagram for field stars, but as indicated in Figure 27 of that paper the scatter is quite large. We cite metallicity values throughout this section as being suggestive of an older or younger

τ_2 ages in this text using Table 13 from the Mamajek & Hillenbrand (2008) study as these are thought to be the more representative ages.

age; but as with kinematics we refrain from placing a significant weight on it in our analysis.

There are also a number of age-dating techniques for UCDs:

- Lithium absorption: In fully convective low-mass stars and higher mass brown dwarfs, primordial Li rapidly decays with age due to core fusion. Dantona & Mazzitelli (1985), Burrows et al. (1989), and Ushomirsky et al. (1998) have shown that for masses under 0.06 $M_\odot$ and ages $\gtrsim$ 500 Myr the maximum central temperature is below what is required for Lithium-burning. This mass can be converted to an age for a given spectral type using theoretical models such as Burrows et al. (1997).

- Hα activity: West et al. (2008) suggest activity lifetimes for M0-M7 dwarfs based on Hα equivalent width and vertical distance from the Galactic Disk Plane.

- Surface gravity features: Allers et al. (2007), Kirkpatrick et al. (2008), and Cruz et al. (2009) have shown that the presence of weak alkali spectral features, and enhanced metal oxide absorption in UCDs are best explained by lower surface gravities, implying typical ages $<$ 100 Myr.

- $J - K_s$ color: Kirkpatrick et al. (2008), Jameson et al. (2008b), and Faherty et al. (2009) have all shown that $J - K_s$ color can be used as a rough indicator of age within the UCD population. Faherty et al. (2009) combined this with v_{tan} and found that high v_{tan} objects ($v_{tan} > 100$ km s^{-1}) tended to be unusually blue for their spectral type and were considered to be older than the field population while low v_{tan} objects ($v_{tan} < 10$ km s^{-1}) tended to be unusually red for their spectral type and were concluded to be younger than the field population (note that this metric is only indicative of an older or younger age and does not provide a direct mapping to age (however, see Jameson et al. 2008b).

Age dating is fraught with large uncertainties, and some methods listed above are more reliable than others. The analysis that follows gives details on individual systems. In Tables 3.9 and 3.10 we tabulate the observational properties of the primaries and secondaries separately to permit comparison of the age diagnostics. In Table 3.11 we provide our adopted ages for the systems. While we have already discussed the reliability of the common proper motion companionship in section 2, confirming similarities in the ages of the components of each system establishes the more important criterion of coevality.

Table 3.9. Details of the Primaries

Name	SpT	[Fe/H]	$\log(R'_{HK})$	U	V	W	W_λ(Li) (Å)	W_λ(Hα) ($L_\odot$)	$L_{H\alpha}/L_{bol}$ (Å)	Mass ($M_\odot$)	P_{rot} (days)	Member?	Age (Gyr)	Ref
(1)	(2)	(3)	(4)	(5)	(6)	(7)	(8)	(9)	(10)	(11)	(12)	(13)	(14)	(15)
G 266-33	G8	0.07, 0.097	-4.55	-32	-47	-20	<0.004	-1.20±0.09	—	0.94	—	—	0.9-1.4	1, 2,3,4,11,12
G 171-58	F8	0.22	-4.81	-48	-26	-4	—	—	—	1.15	—	—	1.8-3.5	1,4,5,11
NLTT 2274	M4	—	—	—	—	—	<0.03	>0.10	<-5.20	0.20	—	—	4.5-10	9,12
G 73-26	M2	—	—	-44	-88	68	<0.04	>0.40	<-4.41	0.44	39.6±0.6	—	3-4	9,12
G 121-42	M4	—	—	—	—	—	<0.40	>0.20	<-4.71	0.20	47.0±0.9	—	4-5	9,10,12
G 62-33	K2	-0.18,0.15	-4.77	-73	-21	21	<0.004	-1.0±0.10	—	0.85	—	—	3.3-5.1	1,4,6,11,12
G 63-23	K5	—	-4.49	-20	-50	6	<0.006	-0.80±0.05	—	0.67	—	—	0.5-3	4,11,12
G 200-28	G5	-0.16	<-5.00	-72	-40	-35	—	—	—	1.01	—	—	7-12	1,4,11
G 204-39	M3	—	—	-35	8	8	—	-0.215	—	0.36	—	Hyad SC	0.5-3	4,7,8,11

Note. — References: 1=Holmberg et al. (2008) 2=Rocha-Pinto & Maciel (1998) 3=Henry et al. (1996) 4= Gontcharov (2006) 5=Pourbaix et al. (2005) 6=Ibukiyama & Arimoto (2002) 7=Gizis et al. (2002) 8=Eggen (1993, 1990) 9=Lépine et al. (2002) 10=van Altena et al. (1995) 11=Perryman et al. (1997) 12=This paper

Table 3.10. Details of the UCD Secondaries

Name	SpT	log(L_{bol}) ($L_\odot$)	W_λ(Hα) (Å)	log($L_{H\alpha}/L_{bol}$)	W_λ(Li) (Å)	$J-K_s$	Age (Gyr)	Mass ($M_\odot$)	References
(1)	(2)	(3)	(4)	(5)	(6)	(7)	(8)		
2MASS J0003-2822	M8	[-2.85,-2.93]	9.0±0.08	-4.27	<0.18	1.096±0.035	0.1-1	0.100-0.103	4
2MASS J0025+4759	L4/L4	[-3.57,-3.69]	<0.10	—	10.0±1.0	1.938±0.069	0.1-0.5	0.045-0.065[a]	1,2,4
2MASS J0025+4759	L4/L4	[-3.57,-3.69]	<0.10	—	10.0±1.0	1.938±0.069	0.1-0.5	0.080-0.083[b]	1,2,4
SDSS J0041+1341	L0	[-3.53,-3.85]	2.2±0.10	—	<0.40	1.218±0.042	2-8	0.081-0.083	4
SDSS J0207+1355	L3	[-3.78,-3.95]	<0.20	—	<0.30	1.550±0.085	2-8	0.079-0.081	4
2MASS J1200+2048	M7	[-2.86,-3.42]	2.9	<-5.44	<0.7	1.001±0.030	5-7	0.085-0.103	3,4
2MASS J1320+0409	L3	[-3.85,-3.94]	<0.80	—	<1.0	1.625±0.065	2-8	0.079-0.081	4
2MASS J1320+0957	M8	[-3.12,-3.23]	<0.40	<-5.74	<0.30	1.117±0.039	1-8	0.083-0.093	4
SDSS J1416+5006	L4	[-4.20,-4.31]	—	—	—	1.560±0.085	—	0.077-0.078	4
SDSS J1758+4633	T6.5	[-5.12,-5.24]	—	—	—	0.180±0.085	0.5-1.5	0.020-0.035	4

[a]Calculated using the age from diagnostics of the secondary

[b]Calculated using the age from diagnostics of the primary

Note. — References: 1= Reid et al. (2006) 2=Cruz et al. (2007) 3=Reid & Cruz 2002 4=This paper

3.4.2 Hipparcos Pairs

G 266-33 with 2MASS J00034227-2822410

G 266-33 lies just over 1.1 arcminutes from 2MASS J0003-2822 and the possibility of companionship between them was first noted in Cruz et al. (2007). Based on our MagE spectrum, this primary is a G8 dwarf. Henry et al. (1996) report Ca II H & K emission with a log R'_{HK} value of -4.55. Using the Mamajek & Hillenbrand (2008) relation for chromospheric activity places the age of this star in the range τ_2=0.9-1.4 Gyr. The U, V velocities fall into the Eggen Box supporting an age of <2 Gyr. There are two metallicity measurements for G 266-33: Holmberg et al. (2008) report [Fe/H]=0.07 and Rocha-Pinto & Maciel (1998) report [Fe/H]=0.097. The slightly metal-rich value for G 266-33 suggests a younger field age in agreement with the chromospheric and kinematic diagnostics. The absence of Lithium absorption in the optical spectrum (W_λ (Li) <4 mÅ, logN(Li)<-2.5) is consistent with an age older than 600 Myr. Based on this compilation of diagnostics the age range for G 266-33 is consistent with 0.9-1.4 Gyr.

The secondary, 2MASS J0003-2822, is classified as an M8 dwarf based on a MagE spectrum and has very strong Hα emission, shown in Figure 3.2. The measured Hα equivalent width is 9.0±0.08 Å and the Hβ, Hδ, and Hγ lines are also seen in emission. For comparison, West et al. (2008) examined 735 M8 dwarfs with Hα measurements, and only 25% of objects in that sample have stronger Hα emission than 2MASS J0003-2822. Combining the equivalent width of Hα with the χ parameter from Walkowicz et al. (2004) gives a log($L_{H\alpha}/L_{bol}$) of -4.26. Comparing this with other active late-type M dwarfs in West et al. (2009), we find that 2MASS J0003-2822 is similar to the most active M7 objects (there were no M8 dwarfs for comparison). The age determined from the age-activity relation in the West et al. (2009) study would place this object (if it were an M7) as younger than 1 Gyr. The MagE spectrum for 2MASS J0003-2822 does not display any low-gravity features (e.g., weak Na, strong VO) and is thus likely older than 0.1 Gyr (Kirkpatrick et al. 2008).

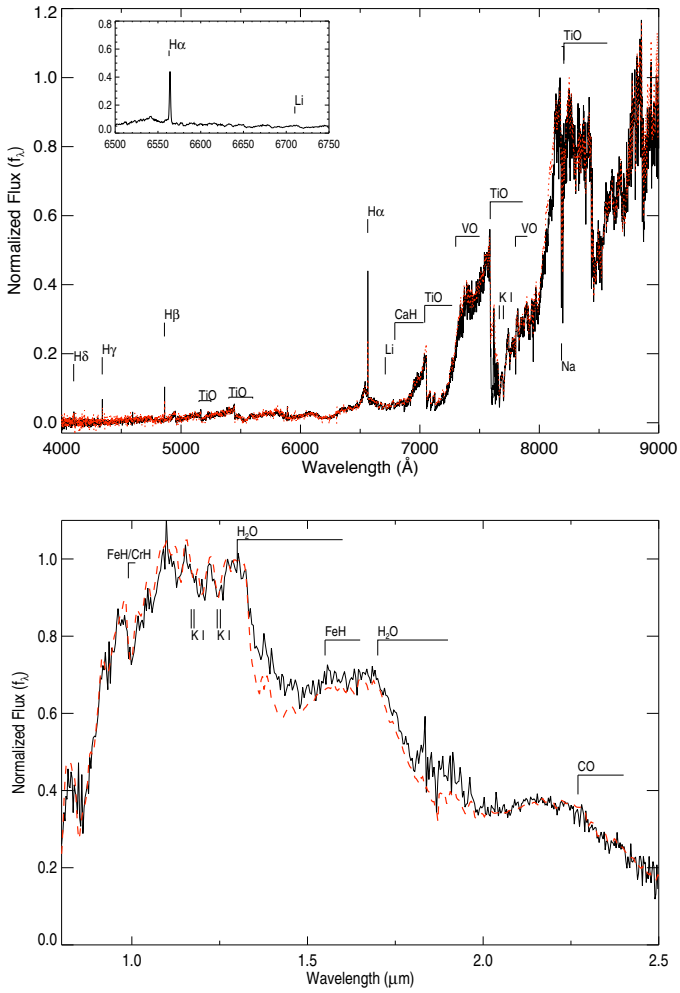

Figure 3.2: The optical spectrum of the secondary 2MASSJ0003-2822 using MagE (top plot) and IR spectrum using SpeX (bottom plot). Top: Over-plotted is the template for an active M8 from Bochanski et al. (2007b) (dotted line) normalized at 8350 Å. The inset shows strong Hα (6563 Å) emission and a lack of Li (6708 Å) absorption. Bottom: Over-plotted is the M8 optical standard VB 10 from the SpeX prism library (dotted line).

The $J - K_s$ color for 2MASS J0003-2822 is normal for its spectral type. However the Hipparcos distance would indicate that its absolute magnitude is overluminous by a factor of 1.5 for an M8. This indicates, as noted in Cruz et al. (2007), that 2MASS J0003-2822 is a potential near-equal luminosity unresolved binary which might affect the activity and age calculated from the West et al. (2009) relation (c.f. Silvestri et al. 2006).

Based on the consistent age diagnostics of the primary and the secondary, an age of 0.9-1.4 Gyr is adopted for the system.

G 171-58 with 2MASS J00250365+4759191AB

G 171-58 is an F8 star and lies 3.6 arcminutes from the L4+L4 close (separation 0.33″or ∼10 AU) binary dwarf 2MASS J0025+4759. The possibility for companionship with G 171-58 was noted by Reid et al. (2006) and Cruz et al. (2007). G 171-58 is itself a spectroscopic binary (Latham et al. 2002) resolved in Hipparcos images with a separation of ∼ 200 mas and an orbital period of just under 1 yr. Holmberg et al. (2008) measure [Fe/H]=0.22, and their age–metallicity relation suggests an age < 2 Gyr. In this same study, an age of 0.2 Gyr with an upper limit of 1.5 Gyr was estimated based on theoretical isochrones calculated from the T_{eff}, M_v, and [Fe/H] values. The U, V velocities for G 171-58 fall into the Eggen box which also indicate an age < 2 Gyr.

The echelle spectrum of G171-58 shows clear K_2 maxima surrounding a central absorption core but the fairly low S/N coupled with the large magnitude of the photospheric contribution between the K_1 minima makes a direct measurement of R'_{HK} problematic. Instead, we undertook a differential analysis with respect to the F8 standard HD 187691, which has a measured $\log(R'_{HK})$=-5.05 (Mamajek & Hillenbrand 2008). We normalized the spectra in the Ca II line wings and subtracted the spectrum of the standard. We convert the excess emission, seen in both the H and K lines, to surface flux, and add to this the $\log(R'_{HK})$=-5.05 we had subtracted. We find that $\log(R'_{HK})$=$-4.81^{+.03}_{-.08}$ for G 171-58, corresponding to τ_2=$2.2^{+1.3}_{-0.4}$ Gyr.

2MASS J0025+4759 is resolved into two near-equal mass components by Reid et al. (2006). The combined spectrum exhibits Lithium absorption with an equivalent width of 10±2 Å (Cruz et al. 2007) as seen in Figure 3.3, indicating component masses of at most ∼0.06$M_\odot$. For an L4 spectral type at the bolometric luminosity calculated from the Hipparcos distance (see Table 3.10) , this lead to an age upper limit of ∼0.5 Gyr for 2MASS J0025+4759 based on the evolutionary models of Burrows et al. (1997). The J-K_s color for 2MASS J0025+4759 is normal for its spectral type. Despite the presence of Li absorption, the spectrum for this L4 companion does not display any low surface gravity features. Therefore the age of this secondary is consistent with the range of 0.1-0.5 Gyr which is somewhat younger than indicated by the chromospheric activity of the primary.

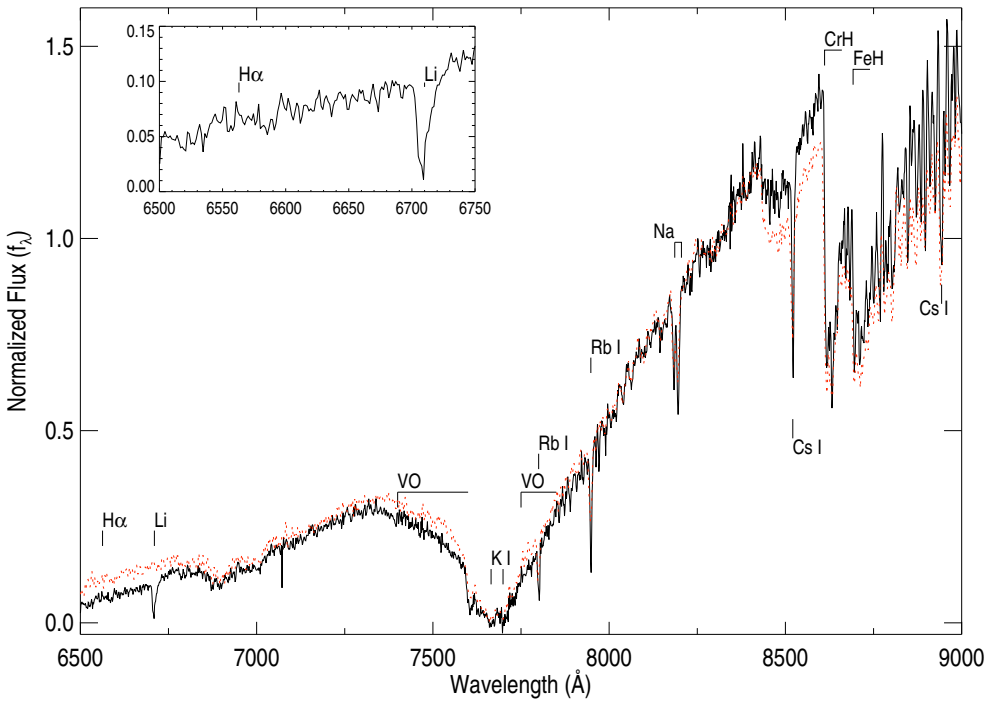

Figure 3.3: The optical spectrum of the secondary 2MASS J0025+4759 using published CTIO 4m data taken 2003 April 23 (Cruz et al. 2007). The inset shows a lack of Hα (6563 Å) emission but strong Li (6708 Å) absorption. As a reference, the LRIS optical spectrum of the standard L4 2MASSW J1155+2307 from Kirkpatrick et al. (2000) is over-plotted and normalized between 8240-8260 Å (dotted line).

We find a significant discrepancy between the age of the primary and secondary in this system. 2MASS J0025+4759 is likely younger than 0.5 Gyr and G 171-58 is likely older than 1.8 Gyr therefore we cannot adopt a suitable system age. Rather we note the inconsistency in age diagnostics and calculate a mass for 2MASS J0025+4759 from the best age range of both the primary and the secondary.

G 62-33 with 2MASS J13204427+0409045

G 62-33 is a K2 dwarf based on the MagE spectrum. The absence of Li absorption (W_λ(Li) $<$ 4 mÅ, logN(Li)$<$-2.9) in the optical spectrum indicates that this object is older than $\sim$ 1 Gyr. The U, V velocities fall outside of the Eggen box indicating an age $>$2 Gyr. The metallicity for G 62-33 provides an upper bound on the age. Holmberg et al. (2008) determine [Fe/H]=0.15,

and Ibukiyama & Arimoto (2002) determine [Fe/H]=-0.18. The majority of stars on the age-metallicity relation in Nordström et al. (2004) that lie between these two values are younger than 6 Gyr.

The photometric data for G 62-33 shows that the star is clearly variable with peak-to-peak amplitudes increasing from 0.2 mag at I to 0.4 mag at B. However, we were unable to recover a unique period from the data which would have provided a gyro age. A characteristic period from minimum to minimum is about 5 days for the first month of data, but this decreases to about 2-3 days during the last month. The changes in variability amplitude with wavelength are consistent with a spotted surface and the apparent period change may be due to a rapid evolution of the spot structures.

We calculated $\log(R'_{HK}) = -4.77^{+0.05}_{-0.07}$ from the echelle data, where the uncertainties are dominated by uncertainties in the positions of the minima. Comparison of the R-C data with three other K2 dwarfs observed at the same resolution with the R-C spectrograph, HD 22049, HD 4628, and HD 144628, independently showed that the emission strength lies between those of HD 22049 ($\log(R'_{HK})$=-4.51, τ_2=0.8 Gyr) and HD 4628 ($\log(R'_{HK})$=-4.87, τ_2=5.4 Gyr). Although the 0.94 $B-V$ color of G 62-33 is slightly outside the quoted $B-V$=0.92 limit for the Mamajek & Hillenbrand (2008) chromospheric/age relation, an extrapolation yields τ_2=4.2±0.9 Gyr, consistent with the other age diagnostics.

The L3 companion 2MASS J1320+0409 lies 1.1 arcminutes away from the primary. The spectrum used to type this UCD has a very low signal to noise and leads to a ±2 spectral type uncertainty. However, unless this is an unresolved binary, the absolute magnitude calculated from the Hipparcos measurement is consistent with an L3 dwarf. This object has a normal $J-K_s$ color for an L3. It is difficult to ascertain whether the spectrum demonstrates low surface gravity features, or Hα due to the low S/N. Hence, no firm constraint of the age of the secondary can be made, but its photometric color suggests a middle-aged dwarf.

Since the age of the secondary is unconstrained, we adopt a system age of 3.3-5.1 Gyr based on the chromospheric activity of the primary.

G 63-23 with 2MASS J13204159+0957506

Based on a MagE spectrum, we classify G 63-23 as a K5 dwarf. We place a 2σ limit on the Li absorption equivalent width in our echelle spectrum of $<$ 6 mÅ which corresponds to log N(Li)<-0.12 and a lower limit for the age of ∼1 Gyr. There is no metallicity measurement to aid in constraining the age but the U, V velocities fall outside of the Eggen box indicating an age >2 Gyr. The photometric data for G 62-33 shows no significant periodic or

quasi-periodic variability therefore gyrochronology can not be used.

From the echelle data of G 63-23, we determined log (R'_{HK})= $-4.49^{+0.02}_{-0.03}$. At this spectral type, it is probably not wise to extrapolate the Mamajek & Hillenbrand (2008) age relation. Rather, we bound the age by comparing the activity level of G 63-23 with the K5 dwarfs ξ Boo B and 61 Cyg A. Barnes (2007) find gyrochronology ages for these two systems of $\sim$0.2 Gyr and $\sim$2 Gyr respectively and G 63-23 shows chromospheric activity between them albeit much closer to the level of the older star 61 Cyg A. Using the coefficients in Mamajek & Hillenbrand (2008) revises the age of 61 Cyg A to 4 Gyr. Assuming a Skumanich (1972)-like power-law decay of activity between 0.3 and 4 Gyr, we find a likely age of G 63-23 of 1.2$\pm$0.4 Gyr. Therefore we conservatively date this system as 1-3 Gyr which is roughly consistent with the Li and kinematic indications.

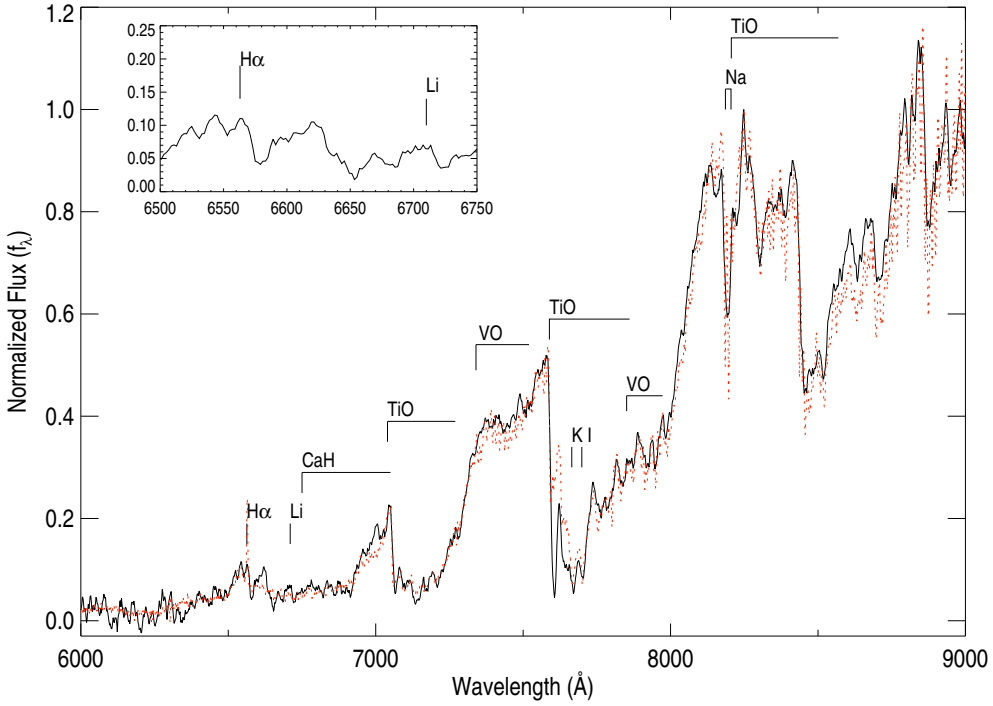

Figure 3.4: The optical spectrum of the secondary 2MASS J1320+0957 using published CTIO 4m data taken 2003 April 20 (Cruz et al. 2007). Over-plotted is the template for an M8 from Bochanski et al. (2007b) normalized at 8350 Å (dotted line). The inset shows the region that contains Hα (6563 Å) emission and Li (6708 Å) absorption neither of which are detected.

2MASS J1320+0957 is an M8 dwarf that lies 2.8 arcminutes from G 63-23. The J-K_s color and v_{tan} values for this object are normal for an M8. We have re-examined a published spectrum from Cruz et al. (2003) and find a lack of Hα emission ($W_\lambda(H\alpha) < 300$ mÅ) as seen in Figure 3.4. West et al. (2008) find that M7 dwarfs are active for $8.0\pm^{0.5}_{1.0}$ Gyr. M dwarf activity increases with decreasing temperature through M7 dwarfs where, for the most part, all nearby objects show Hα activity. However, it is not clear that this trend continues at the cooler temperatures of M8 dwarfs and beyond where the photospheres become increasingly neutral (Mohanty et al. 2002; Gelino et al. 2002). So the lack of Hα activity does not necessarily indicate that 2MASS J1320+0957 is old for its spectral type. As a result we can only assume a field M dwarf age range of 1-8 Gyr (Faherty et al. 2009) for this M8 dwarf.

A system age of 1-3 Gyr is adopted for the G 63-23 and 2MASS J1320+0957 system based on the more reliable activity diagnostics of the primary. However, while the kinematics and distance estimates for this system are in good agreement, we are concerned of the age discrepancy between an Hα inactive M dwarf and a chromospherically active K dwarf.

G 200-28 with SDSS J141659.78+500626.4

The primary in this system is a G5 star and it lies 9.5 arcminutes from the L5.5 dwarf SDSS J1416+5006. Holmberg et al. (2008) determine a value for [Fe/H] of -0.16, indicating a field age in the range of 1-5 Gyr. They further determined an age range of 7-12 Gyr based on theoretical isochrones. The kinematics of G 200-28 place this primary outside of the Eggen box for the young thin disk, in agreement with an age >2 Gyr. There is no available measurement of Li absorption for this primary to aid in the age diagnosis.

We obtained an echelle spectrum of the Ca II H&K region but despite fairly good S/N, the Ca II emission cores are not clearly evident. The Ca II line profiles are similar to those of the twilight sky, with deep central reversals. We place a limit of $R'_{HK} < -5.0$, suggesting $\tau_2 > 6$ Gyr. G 200-28 appears older than the Sun.

Therefore, based on the available diagnostics we adopt the theoretical isochrone estimated age range for G 200-28 of 7-12 Gyr.

SDSS J1416+5006 is classified as an L5.5 dwarf by Chiu et al. (2006). It has a spectral-type uncertainty of ±2 based on a low signal to noise SpeX prism spectrum. We have reanalyzed these data and deduce that an L4+/-1 is more likely. The $J-K_s$ color of 1.56±0.09 for SDSS J1416+5006 is 0.18 magnitudes bluer than a normal L4 or L5 dwarf (Faherty et al. 2009) although the near-IR spectrum appears normal. The blue near-IR color for its spectral type would indicate that SDSS J1416+5006 is likely to be older than the average UCD

field population (> 5 Gyr) or it is metal poor. However, the photometric uncertainty of this color does not allow a conclusive age constraint.

A system age of 7-12 Gyr is adopted for this system from the isochrone analysis of the primary.

G 204-39 with SDSS J175805.46+463311.9

The primary of this system is an M3 star that lies 3.3 arcminutes from the T6.5 dwarf SDSS J1758+4633. This primary is sufficiently late that solar-analog age/activity and age/rotation relations are not applicable, so we turn instead to the M dwarf age/activity relations examined by West et al. (2008). Gizis et al. (2002) measure an Hα absorption equivalent width of -0.215 Å. Due to the cool atmospheres of M dwarfs, Hα absorption is a sign of enhanced atmospheric heating and an indicator of magnetic activity. However, the absorption phase likely represents the end of the active life of an M dwarf (Walkowicz & Hawley 2009) indicating that G 204-39 is only weakly active.

It is also listed in the ROSAT All-Sky Faint Source Catalog (Voges et al. 2000) with a count rate of 2.53×10^{-2} cts s^{-1}, HR1=-0.58±0.18 and HR2=-1.0±0.27. We used the count rate/flux relation from Schmitt et al. (1995) to estimate the X-ray flux as 1.32×10^{-16} W m^{-2}. The bolometric luminosity is calculated from the Hipparcos distance and combined with L_x yields $\log(L_x/L_{bol})$=-5.3 which is slightly lower than the typical values for active M dwarfs ($\log(L_x/L_{bol})$ >-4; Fleming et al. 1995) . Comparing to X-ray datasets of Hyades and Pleiades members where typical $\log(L_x/L_{bol})$ values are >-4.5 for objects with similar colors, G 204-39 appears to be older. These measurements suggest that G 204-39 may be at the tail end of its active life, which West et al. (2008) find to be 2.0±0.5 Gyr for M3 dwarfs. Eggen (1990, 1993) list G 204-39 as a member of the Hyades supercluster based on its proper motion and luminosity. Age estimates for this supercluster span a relatively broad range (e.g., Chereul & Grenon 2001 cite 0.5 to more than 2-3 Gyr) but since it is not a coeval sample (e.g. Famaey et al. 2008, 2007, 2005), it is not a useful age indicator. The kinematics of G 204-39 do not indicate membership in the Hyades co-eval cluster and the chromospheric activity level discussed above further confirms that this object is likely older then ∼0.6Gyr.

The secondary of this system is the only T dwarf in our sample, and its properties have been studied in detail by Burgasser et al. (2006a) (hereafter BBK06) through a comparison of empirically-calibrated model spectral indices. BBK06 find T_{eff} = 960–1000 K and log g = 4.7–4.9 (cgs) for SDSS J1758+4633, consistent with an age of 0.3-0.9 Gyr and at the low end of age estimates for the Hyades supercluster. As companionship with a Hipparcos star provides a precise distance determination for SDSS J1758+4633, we

re-examined its properties as a check of the results of BBK06. We first determined the luminosity of this source using the method described in Burgasser et al. (2008c), by iteratively integrating its absolute flux-calibrated spectral energy distribution over the range 0.3–1000 μm. Near-infrared spectral data from BBK06 were used to calculate the 0.9–2.4 μm flux, after calibrating the data to JHK photometry from Knapp et al. (2004). The 2.4–9.3 μm flux was determined by piece-wise flux-calibrating a T_{eff}=1000 K, log g = 5.0 cgs spectral model from Burrows et al. (2005) with mid-infrared photometry obtained with the *Spitzer Space Telescope* Infrared Array Camera (IRAC; Fazio et al. 2004; program GTO-40198). Apparent magnitudes of [3.6] = 14.88±0.04, [4.5] = 13.91±0.03, [5.8] = 13.64±0.10 and [8.0] = 13.15±0.04 were measured for SDSS J1758+4633 from basic calibrated data (version S18.5.0) using IRAF PHOT and standard calibration methods for aperture photometry (Reach et al. 2005). Short- and long-wavelength fluxes were computed using a combination of spectral models and blackbody fluxes calibrated to the ends of the near-infrared and mid-infrared data. This procedure provided a luminosity measurement of $\log(L_{bol}/L_{\odot})$ = -5.18±0.06, where the uncertainty includes astrometric and photometric uncertainties from the near-infrared and mid-infrared data, and systematic uncertainties in the luminosity calculation method (Burgasser et al. 2008b).

Combining just the luminosity measurement of the secondary, the age of the Hyades supercluster, and evolutionary models from Burrows et al. (1997), we derive an independent constraint on the T_{eff} and log g of SDSS J1758+4633 as shown in Figure 3.5. At the lower end of the age range, our analysis indicates T_{eff} = 860–930 K, log g = 4.7 cgs and M = 0.02 $M_{\odot}$ for this source; at the upper end we find T_{eff} = 910–1030 K, log g = 5.25 cgs and M = 0.05 $M_{\odot}$. Note that the T_{eff} estimates are broadly consistent with the $H-[4.6]$ = 2.29±0.04 color of this source (Warren et al. 2007). Importantly, the T_{eff}/log g phase space constrained by the luminosity and age do not overlap with the seemingly tighter constraints provided by the BBK06 analysis.

Examination of the absolute spectral fluxes of SDSS J1758+4633 appear to favor the luminosity analysis (Figure 3.6); spectral models from Burrows et al. (2005) tied to these constraints provide a closer match to the observed fluxes than models tied to the BBK06 constraints. However, if the systematic uncertainties estimated for the BBK06 method are included (ΔT_{eff} = 50 K and Δlog g = 0.1 cgs), there is reasonable overlap in T_{eff} and log g constraints over the range 0.5–1.5 Gyr. This somewhat younger age is consistent with enhanced K-band flux in the spectrum of SDSS J1758+4633, indicative of reduced H_2 opacity (see BBK06). However, it is also possible that this system is somewhat metal-rich, as indicated by comparison of CaH2+CaH3 and TiO5 for G 204-39

to other M3 dwarfs in West et al. (2008) (G 204-39 has (CaH2+CaH3)/TiO5 of 2.45 where the range for M3 dwarfs was from 2.25-2.55). Regardless, the activity level of the primary is consistent with the 0.5-1.5 Gyr age computed for the T dwarf, so we adopt this slightly younger age for the system.

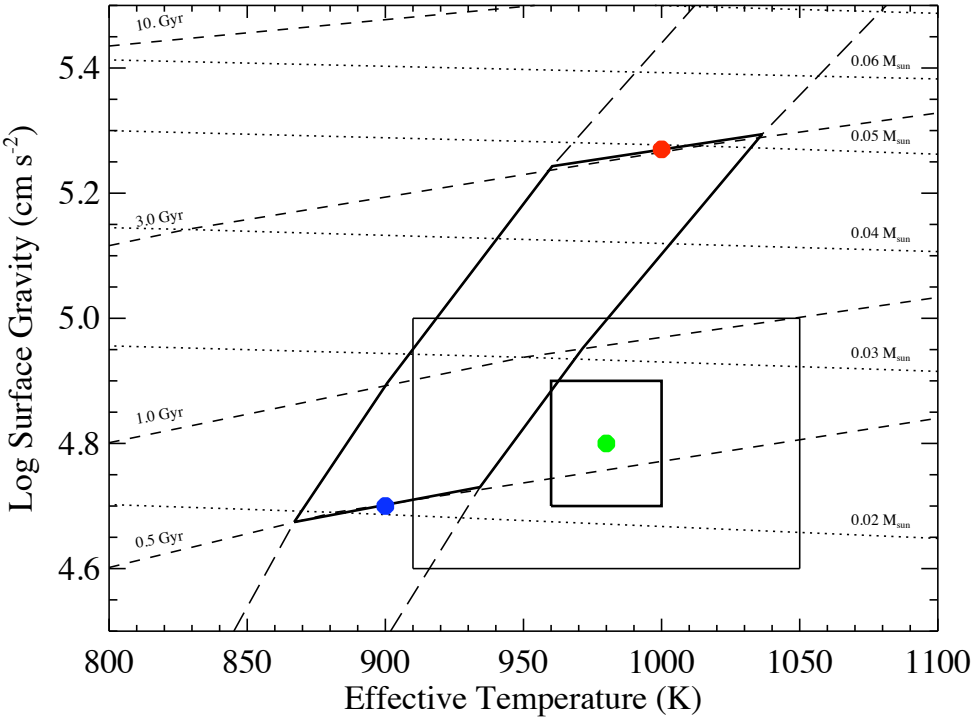

Figure 3.5: Effective temperature and surface gravity constraints for SDSS J1758+4633, based on the measured luminosity of the source (vertical long dashed lines), the estimated age of the system (0.5–3 Gyr leftmost parallelogram), and the spectral index analysis of BBK06 (boxes to right; inner box indicates quoted parameter range, outer box indicates additional systematic uncertainties). Labeled isochrone and isomass lines based on the evolutionary models of Burrows et al. (1997) are indicated by short-dashed and dotted lines, respectively. The green, red and blue circles correspond to spectral models shown in Figure 3.6.

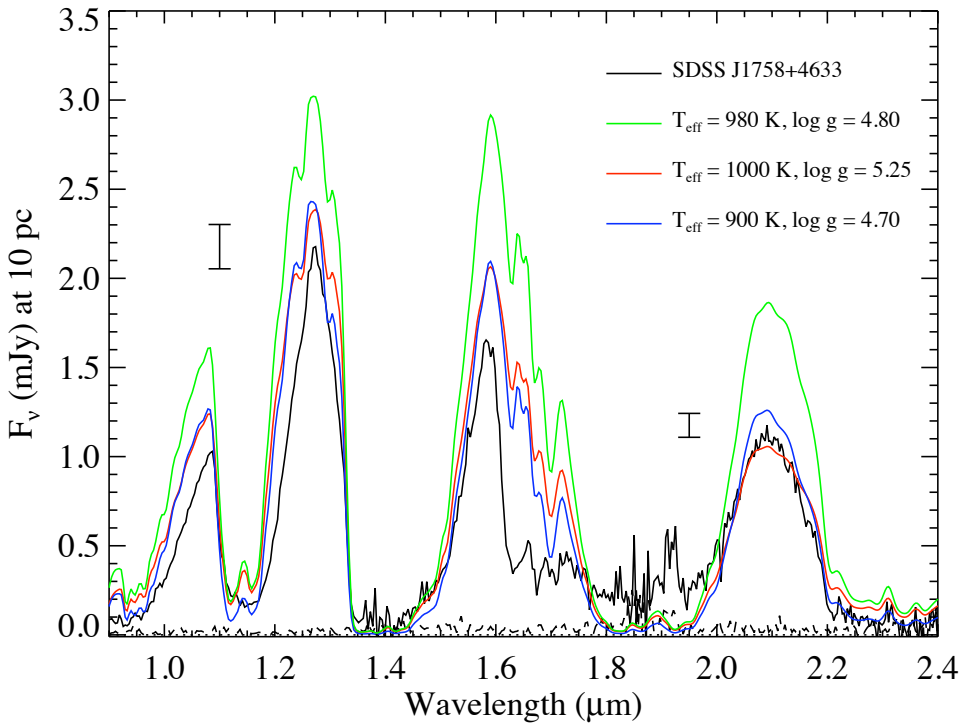

Figure 3.6: Comparison of observed absolute near-infrared spectral fluxes (F_ν at 10 pc) of SDSS J1758+4633 (black line; dashed line shows uncertainties) to solar-metallicity spectral models from Burrows et al. (2005) chosen from the T_{eff}/log g phase space constraint in Figure 3.5. The green line shows T_{eff} = 900 K and log g = 4.80 cgs, based on spectral index constraints from BBK06; red and blue lines shows T_{eff} = 1000 K and log g = 5.25 cgs and T_{eff} = 1000 K and log g = 4.70 cgs based on the luminosity/age constraints presented here.

3.4.3 LSPM-N Pairs

NLTT 2274 with SDSS J004154.54+134135.5

Jameson et al. (2008a) first noted this system as a potential wide pair due to its close separation (23″) and well matched proper motion components. Based on a MagE spectrum, we classify NLTT 2274 as an M4 dwarf (Figure 3.7). The 2MASS J band relation from Golimowski et al. (2009) was used to calculate a spectro-photometric distance of 21±8 pc. This is in statistical agreement with the companion which has an estimated spectro-photometric distance of 31±6 pc.

There is an absence of both Lithium absorption (W_λ(Li) $<$ 30 mÅ) and Hα emission (W_λ(Hα) $<$ 100 mÅ) in the optical spectrum of NLTT 2274. According to West et al. (2008), M4 objects remain active for $4.5^{+0.5}_{-1.0}$Gyr so we use this as a lower bound on the age. There is no radial velocity measurement available for this primary nor is there a defined metallicity relation for M dwarfs to further constrain the age.

SDSS J0041+1341 was first identified in Hawley et al. (2002) and classified as an L0 from a low signal to noise spectrum. We re-observed this object with MagE and confirm the L0 spectral type (Figure 3.8). Hα emission was detected with an equivalent width of 2.2 Å. There is an absence of Li absorption (W_λ(Li) $<$ 400 mÅ) in the optical spectrum indicating a mass $>$ 0.06 $M_\odot$ and a corresponding age $>$ 0.5 Gyr. SDSS J0041+1341 does not show any low-gravity features, such as weak Na or strong VO, indicating that it is older than 0.1 Gyr. The J-K_s color and v_{tan} values are both normal indicating it is a middle aged L dwarf (2-8 Gyr).

The age-activity relations applicable to G and K dwarfs become more complicated in the late-type M and L dwarf regime. As stars become fully convective ($\sim$ 0.35 $M_\odot$), the solar-type dynamo (Parker 1993, 1955; Thompson et al. 2003) can no longer produce magnetic fields because the radiative-convective boundary (the tachocline) is not present to help generate and preserve the field. However, the observed activity level of mid to late-type M dwarfs, which are beyond the fully convective boundary, remains high suggesting that a turbulent dynamo might be an alternate magnetic field source (Durney et al. 1993). Indeed, recent MHD simulations have produced large-scale magnetic fields in fully convective stars (Browning 2008). But while late-type M dwarfs are nearly all active, only a small fraction of L dwarfs have measured Hα (West et al. 2004); therefore these cooler objects mark a sharp change in activity. Gizis et al. (2000b) and Schmidt et al. (2007) investigated whether active L dwarfs are likely to be younger than inactive L dwarfs at the same spectral type but their results were inconclusive. It is likely that the drop in emission at the M/L transition is reflective of ineffective chromospheric heating as the photospheres become neutral (Mohanty et al. 2002; Gelino et al. 2002; Reiners & Basri 2008). This inactive M + active L system presents an interesting case for studying how the well-established age/activity relation for M dwarfs might break down at the cooler L dwarf temperatures. Although we can not at this time rule out a binary interaction with an equal-magnitude or fainter companion as suggested for the active T dwarf 2MASSW J1237+6526 (Burgasser et al. 2000b), SDSS J0041+1341 could demonstrate that an early type L dwarf can remain active at least through the activity lifetime of an M4 dwarf. If the relationship between youth and Hα emission breaks down for L

dwarfs, activity metrics for these objects may prove to be poor indicators of age.

An age range of 4.5- 8 Gyr is adopted for the NLTT 2274 and SDSS J0041+1341 system based on the activity level of the primary and the upper age bound for normal field L dwarfs.

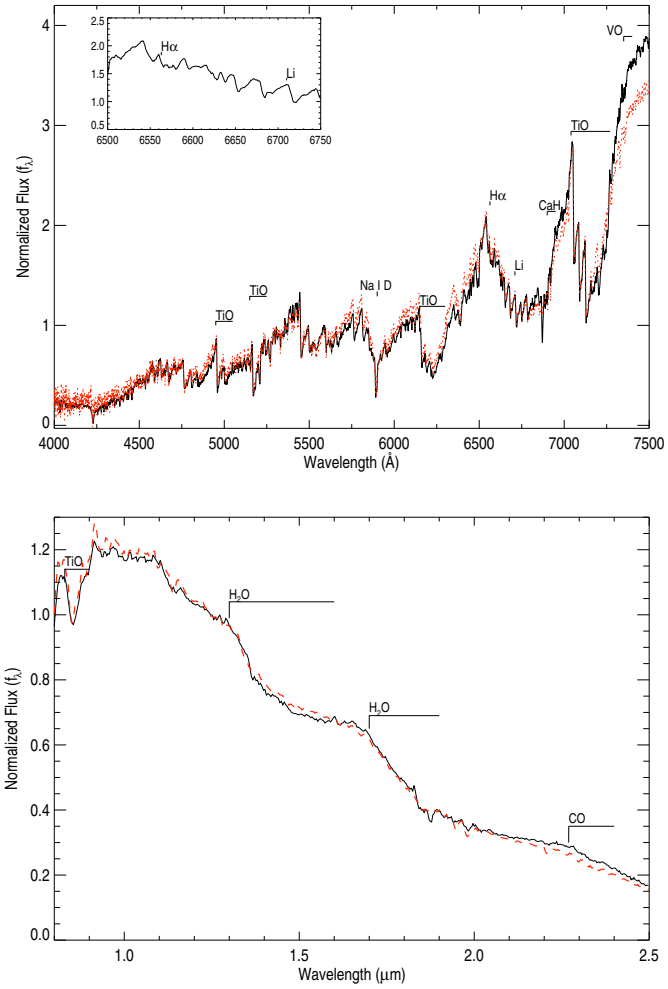

Figure 3.7: The optical spectrum of the primary NLTT 2274 using MagE (top plot) and IR spectrum using SpeX (bottom plot). Top: Over-plotted is the template for an inactive M4 from Bochanski et al. (2007b) (dotted line) normalized at 7400 Å. The inset shows a lack of both Hα (6563 Å) emission and Li (6708 Å) absorption. Bottom: Over-plotted is the M4 optical standard LP 508-14 (Burgasser et al. 2004) obtained from the SpeX Prism Library (dotted line).

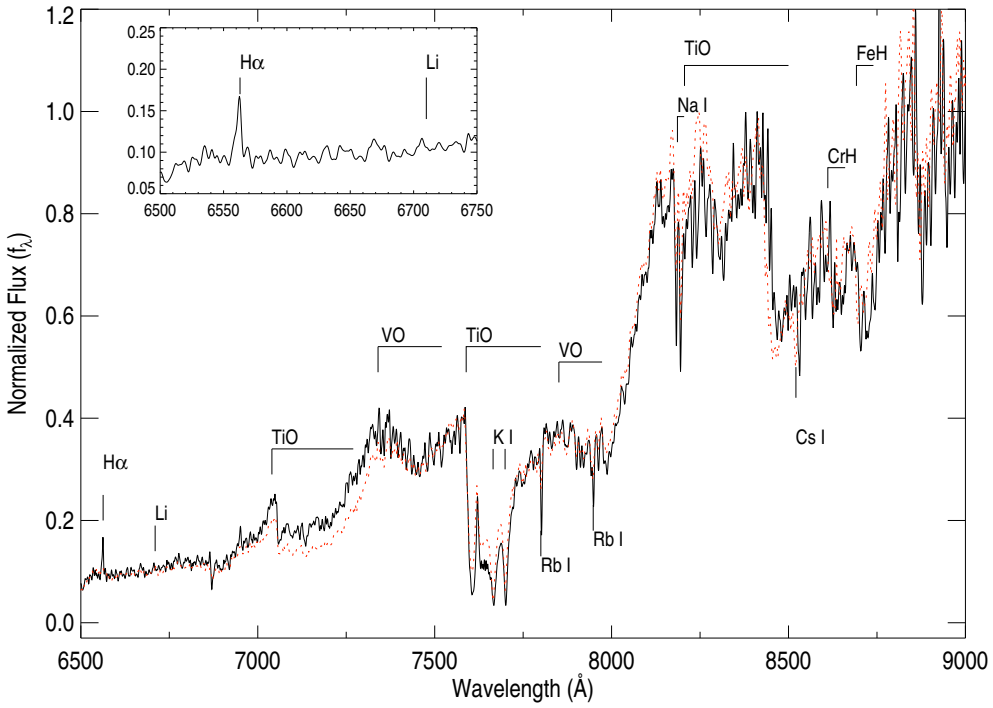

Figure 3.8: The optical spectrum of the secondary 2MASS J0041+1341 using MagE. Over-plotted is the optical standard L0 dwarf 2MASP J0345+2540, from Kirkpatrick et al. (2000) with spectra normalized at 8350 Å (dotted line). The inset shows strong Hα (6563 Å) emission but no Li (6708 Å) absorption.

G 73-26 with SDSS J020735.60+135556.3

Based on our MagE spectrum, G 73-26 is an M2 dwarf (Figure 3.9). The 2MASS J band relation from Golimowski et al. (2009) yields a spectro-photometric distance of 26±10 pc. This is in statistical agreement with the L3 companion which has an estimated spectro-photometric distance of 35±5 pc. There is an absence of both Li absorption (W_λ(Li) < 40 mÅ) and Hα emission (W_λ(Hα) < -400 mÅ) in the optical spectrum. West et al. (2008) determine that the active life of M2 stars ends at 1.2±0.4 Gyr placing a weak lower bound on the age. A radial velocity (RV) of -107±13 km s^{-1} was obtained for G 73-26 from an LDSS-3 spectrum. Combining the photometric distance and available proper motion values with the RV yields (U, V, W)=(-44,-89,68) km s^{-1} placing this object outside the Eggen box, favoring an age > 2 Gyr.

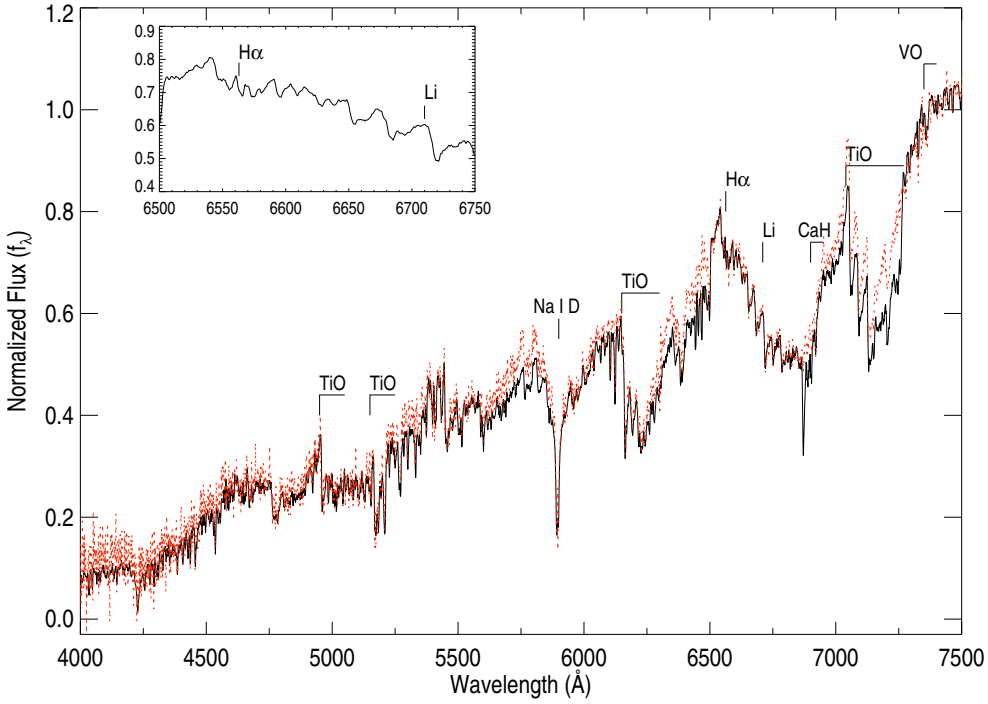

Figure 3.9: The optical spectrum of the primary LSPM J0207+1355 using MagE. Over-plotted is the template for an inactive M2 from Bochanski et al. (2007b) normalized at 7400 Å (dotted line). The inset shows a lack of both Hα (6563 Å) emission and Li (6708 Å) absorption.

The V and I band modulation are small for G 73-26 and a shortest string analysis (Dworetsky 1983) yields a likely period between 37 and 39 days. A sinusoidal fit to the V-band data yields a period of 39.6 $\pm$0.9 days with a semi-amplitude of 0.007$\pm$0.0007 mag and an I band period of 39.6 $\pm$0.6 days with a semi-amplitude of 0.006$\pm$0.0003 mag. The resultant gyro age is 3.4$\pm$0.5 Gyr, using the Mamajek & Hillenbrand (2008) coefficients, which is consistent with an inactive M2 dwarf.

SDSS J0207+1355 was first identified as an L3 in Hawley et al. (2002) and our MagE spectrum confirms this classification (Figure 3.10). There is an absence of both Li absorption (W_λ(Li) $<$ 200 mÅ) and Hα emission (W_λ(Hα) $<$ 300 mÅ) in the optical spectrum. The J-K_s color is normal for an L3 implying a field age in the range of 2-8 Gyr.

We adopt an age range of 3-4 Gyr for this system based on the rotation and activity level of the primary.

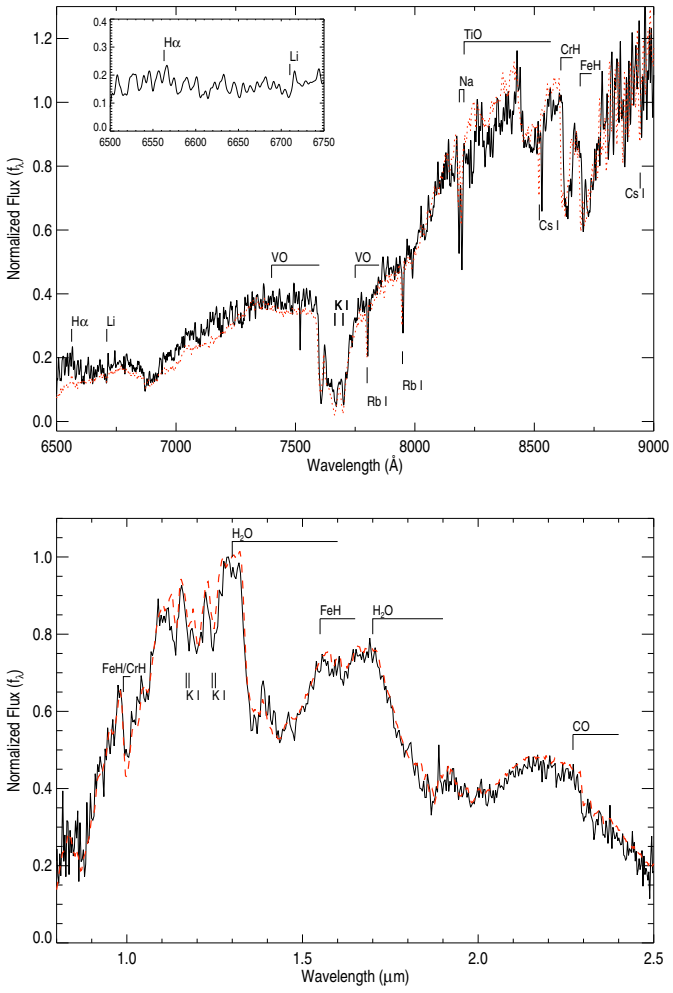

Figure 3.10: The optical spectrum of the secondary 2MASSJ0207+1355 using MagE (top plot) and IR spectrum using SpeX (bottom plot). Top: Over-plotted is Kelu-1, the L2 optical standard from Kirkpatrick et al. (1999), normalized between 8240-8260 Å(dotted line). The inset shows a lack of both Hα (6563 Å) emission and Li (6708 Å) absorption. Bottom: Over-plotted is the L2 spectrum of SSSPM 0829-1309 (Burgasser et al. 2007a) from the SpeX prism library (dotted line).

G 121-42 with 2MASS J12003292+2048513

From its optical spectra we infer that G121-42 is an M4 dwarf. There is a parallax measurement available which provides a distance of 32^{+14}_{-7} pc (van Altena et al. 1995). The optical spectrum of G 121-42 lacks both Li absorption (W_λ(Li) $<$ 400 mÅ) and Hα emission (W_λ(Hα) $<$ 200 mÅ). West et al. (2008)

determine that the active life of M4 stars ends at $4.5^{+0.5}_{-1.0}$Gyr placing a lower bound on the age of the system. The photometric data shows clear long term sinusoidal variability in the V band although no modulation is seen in the I band. The best fit sinusoid to the V band data has a period of 47.0±0.9 days and a shortest string analysis (Dworetsky 1983) shows a broad minimum at 46±3 days. The semi-amplitude of the oscillation is 0.011±0.0007 mag. The $B-V$ color of G121-42 is at the extreme of the stars Barnes (2007) used to derive gyro ages but still yields an age of 4.0±0.6 Gyr.

2MASS J1200+2048 is an active M7 with an Hα equivalent width of 2.9 Å (Gizis et al. 2000b; Reid & Cruz 2002). We combine this value with the χ parameter from Walkowicz et al. (2004) and measure log ($L_{H\alpha}/L_{Bol}$)=-4.8. The age/activity relation of West et al. (2009) suggests an age range of 5-7 Gyr for this object. Reid & Cruz (2002) found an absence of Lithium in the spectrum (<0.7 Å), which is in agreement with an older field age. That study also calculated (U, V, W)=(-35±3,26±2,-32±1) velocities for 2MASS J1200+2048 which place it outside of the Eggen box favoring an age > 2 Gyr.

Given these diagnostics we adopt an age for G 121-42 and 2MASS J1200+2048 of 4-5 Gyr. This is slightly younger then the age predicted for 2MASS J1200+ 2048 from the Hα activity; however because the activity level of M dwarfs can be variable, this younger range is perfectly reasonable.

3.4.4 UCD Mass Estimates

The evolutionary models from Burrows et al. (1997) were used to estimate masses for the nine UCD secondaries. Comparisons to the models were made using bolometric luminosities (L_{bol}), which were computed by combining distances (using parallax measurements or spectro-photometic distances) with apparent magnitudes and bolometric corrections with the exception of SDSS J1758+4633, whose luminosity was calculated in Section 4.2.6. For L and T dwarfs we converted K_s apparent magnitudes from the 2MASS photometric system into the MKO system using the relations from Stephens & Leggett (2004), and for M dwarfs we converted into the CIT photometric system using the color transformations from Carpenter (2001). The bolometric corrections were calculated using either the relation from Golimowski et al. (2004b) for L and T dwarfs or from the measurements in Reid & Hawley (2005) for M dwarfs. Figure 3.11 shows the estimated age vs. L_{bol} for the UCD secondaries against the evolutionary tracks from Burrows et al. (1997). In general, masses for the substellar objects are very uncertain if the system age was poorly constrained due to the rapid change in brown dwarf luminosities with time. We conclude that 2MASS J0003-2822, SDSS J0041+1341, SDSS J0207+1355, 2MASS J1200+2048, 2MASS J1320+0409, 2MASS J1320+0957,

and SDSS J1416+5006 have masses above the hydrogen burning limit and are very low temperature stars at the bottom of the traditional stellar main sequence. SDSS J1758+4633 falls below the hydrogen burning limit and is a brown dwarf. 2MASS J0025+4759 has a questionable age therefore an undetermined mass. Table 3.10 lists our estimated ages, masses, and pertinent spectral characteristics for all of the UCD companions.

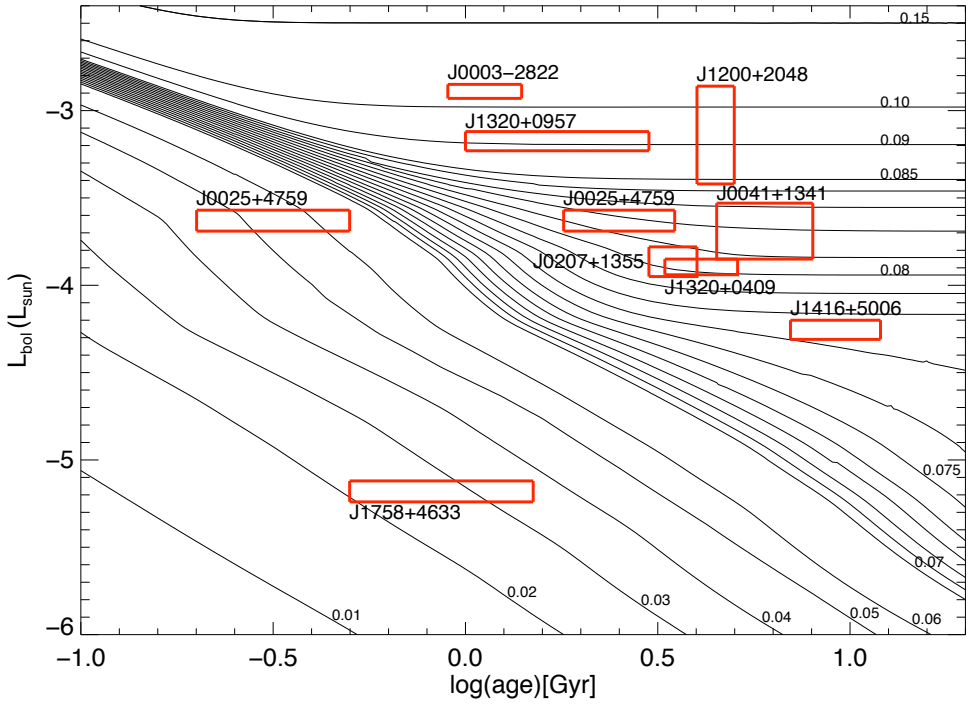

Figure 3.11: A plot of the Burrows et al. (1997) evolutionary models with parameters (age and luminosity) for the nine candidate UCDs in wide pairs indicated with labeled boxes. Masses from 0.01 through 0.15 $M_{\odot}$ are shown. Only SDSS J1758+4633 is clearly of substellar mass. 2MASS J0025+4759 is listed twice due to the discrepancy in age diagnostics of the primary and the secondary in this system. The box at left reflects the younger age calculated from the diagnostics of the secondary. The box at right reflects the older age calculated from the diagnostics of the primary.

3.5 Discussion

3.5.1 Dynamic Stability and Maximum Separation Scales

The separations of the nine companion systems discussed in this study are rather large for field UCDs and require a check as to whether or not they should have survived dynamical interactions within the Galaxy. We investigated this question using the formalism of Weinberg et al. (1987) where the impact of perturbations from giant molecular clouds (GMCs) and close stellar encounters was examined for wide companion systems. As in Burgasser et al. (2003c), and Close et al. (2003, 2007), the analytic solution of the Fokker Planck coefficients from Weinberg et al. (1987) describing the advective diffusion of a binary due to stellar encounters was used to investigate the sample. We work in the single kick limit[6] and investigate the occurrence of disruptive encounters using a rate which is proportional to mass and separation[7] as $f_{cat} \propto aM^{-1}$. All systems but that containing G 200-28 are subject to a frequency of disruptive encounters $<$ (20 Gyr) $^{-1}$. G 200-28 has a frequency of $\sim$ (9 Gyr)$^{-1}$ which is approaching the inverse lifetime of the Galaxy and within our age range estimate for this system. The characteristic diffusive timescale ($t_* \propto a^{-1}M$) yields values $>$ 15 Gyr for all of the systems. Therefore, close stellar encounters are not likely to affect these companions over the ages listed in Table 3.11. The impact parameter for interactions with giant molecular clouds is proportional to mass and separation as $b_{FP}^{GMC} \propto M^{-1/4}a^{3/4}$. This value is larger than the maximum impact parameter $b_{max} \propto a^{3/2}M^{-1/2}$ for each of the nine companions, so such interactions are also not likely to have disrupted these systems.

Recent results have shown that binding energies of the most weakly bound very low–mass (M_{tot} $<$0.2$M_\odot$) binaries in the field are $\sim$3 times larger than those of higher mass systems, suggesting a separation distribution of the field population that is sensitive to the conditions of formation. Burgasser et al. (2003c), and Close et al. (2003, 2007), find a minimum binding energy for very low–mass systems (nearly all of which have q $>$ 0.8 and M_{tot} $<$0.2$M_\odot$) of $\sim$2 x 10^{42} ergs. However this is clearly not the case for slightly more massive UCD systems. Figure 3.12 shows the binding energy (E_b) versus total mass for a compilation of companion systems. Stellar companions were gathered from the catalogs of Duquennoy & Mayor (1991), Fischer & Marcy (1992), and Tokovinin (1997); and young UCD companion systems from Kraus et al. (2005, 2006), Konopacky et al. (2007), Luhman et al. (2009), and Allers et al.

[6]Assuming $GM/\epsilon a V_{rel}^2 << (M/M_p)^2$

[7]In all calculations we use V_{rel}=20 km s^{-1}, ϵ=0.1, n_*=0.1 pc^{-3}, n_{GMC}=4 x 10^{-8} pc^{-3},R_{GMC}=20 pc, M_{GMC}=5 x 10^5 $M_\odot$, N_{clump}=25 and M_p=0.7 $M_\odot$ as in Weinberg et al. (1987) and Close et al. (2007)

Table 3.11. Estimated Ages of the Systems

Name (primary) (1)	Name (secondary) (2)	Age (primary) (Gyr) (3)	Age (secondary) (Gyr) (4)	Age (system) (Gyr) (5)
G 266-33	2MASS J0003-2822	0.9-1.4	0.1-1.0	0.9-1.4
G 171-58	2MASS J0025+4759	1.8-3.5	0.1-0.5	—-
NLTT 2274	2MASS J0041+1341	4.5-10	2-8	4.5-8
G 73-26	2MASS J0207+1355	3-4	2-8	3-4
G 121-42	2MASS J1200+2048	4-5	5-7	4-5
G 62-33	2MASS J1320+0409	3.3-5.1	2-8	3.3-5.1
G 63-23	2MASS J1320+0957	1.0-3	1-8	1.0-3
G 200-28	2MASS J1416+5006	7-12	—	7-12
G 204-39	2MASS J1758+4633	0.5-3	0.5-1.5	0.5-1.5

(2009). Details on the field UCD systems were gathered from the Very Low Mass Binary Archive[8]. Table 3.1 lists the systems with widely-separated (> 100 AU) UCD companions; i.e. those with the lowest binding energies. The addition of recent systems both young and old with varying q values and small total mass complicates the idea of a minimum binding energy set at formation. Four of the systems discussed in this study have $0.2M_{\odot} < M_{tot} < 0.6M_{\odot}$ but their binding energies are nearly ten times lower than the binding energies of the widest $M_{tot} < 0.2M_{\odot}$ field systems. Indeed, there are several field pairs now known with $M_{tot} > 0.1M_{\odot}$ and $E_b << 2 \times 10^{42}$ ergs, as well as young, lower mass, weakly bound systems (e.g. Close et al. 2007; Zuckerman & Song 2009). The system containing NLTT 2274 is especially interesting as it has $M_{tot} \sim 0.3M_{\odot}$, $E_b < 10^{42}$ ergs and an intermediate q value of ~ 0.4. These new systems indicate a gap in our sampling of intermediate mass companion systems, where a transition between weakly bound low–mass stellar companions and tight brown dwarf pairs occurs.

Zuckerman & Song (2009) have applied Jeans mass considerations to the problem of weakly bound very low- mass multiple systems. Using the minimum fragmentation mass of a typical molecular cloud (7 M_{Jup}; Low & Lynden-Bell 1976) and assuming an arbitrary separation cutoff of 300AU, they derive a binding energy cut-off as shown in Figure 3.12. However, a number of systems found in the field and young clusters violate this boundary indicating that 300 AU may not be a meaningful separation limit.

[8]http://vlmbinaries.org; see Burgasser et al. (2007b) and references therein.

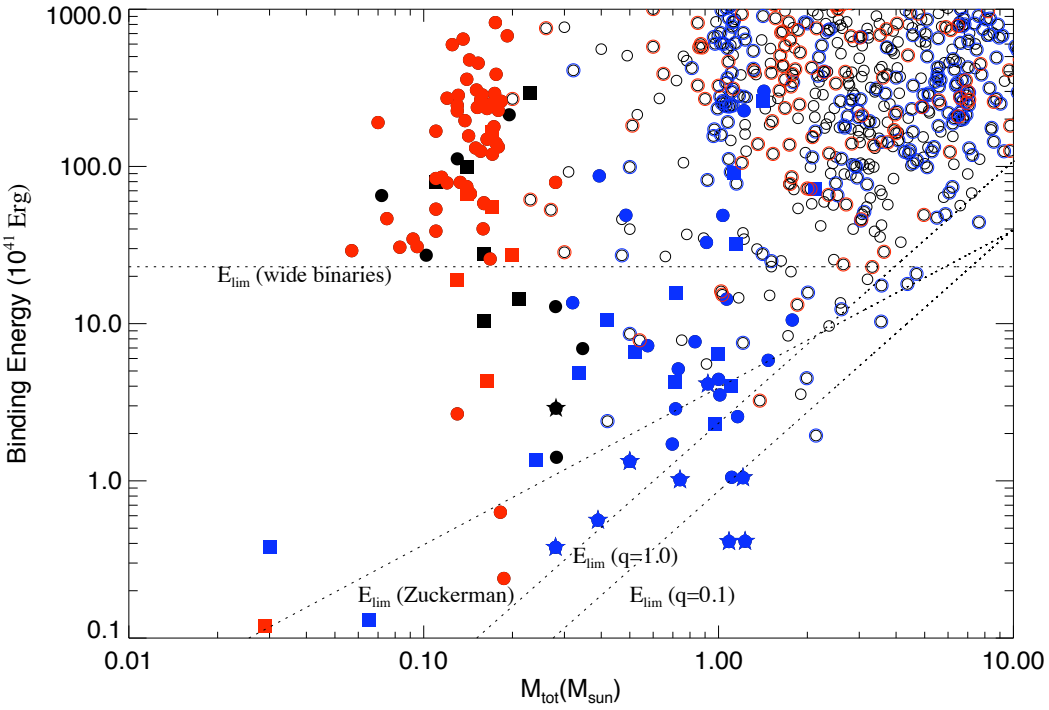

Figure 3.12: System binding energy vs. total mass. Mass ratios are color coded on this plot with red symbols indicating q > 0.7, blue symbols indicating q<0.3 and black symbols indicating 0.3<q<0.7. Filled circles indicate systems containing a UCD, filled squares indicate systems containing a UCD that is younger than 500 Myr. Open circles come from stellar companion catalogs. The nine systems discussed in this paper are marked as five point stars. The minimum wide binding energy for brown dwarf field binaries (Burgasser et al. 2003c; Close et al. 2007) is plotted as well as the minimum binding energy line from Zuckerman & Song (2009). The two lines at the far right are our Jeans length criteria for q=1.0 and q=0.1 systems, respectively.

Instead, we explored the Jeans mass criterion for wide companion systems using a Jeans length criterion to set the separation scale. Two cases were examined: (1) q=1.0 with the maximum separation equal to twice the Jeans length; (2) q=0.1 with the maximum separation equal to the sum of the Jeans length for a system of mass M_2 and a system of 10 x M_2. We are assuming that the minimal initial separation of a pair that formed together should roughly equal the Jeans length. Subsequent dynamics such as gravitational infall and scattering or sub-fragmentation at the time of formation will generally bring sources closer together and perturbations from Galactic

encounters will generally pull systems further apart. However the Jeans length is a good starting point for the widest separation of companions that formed from the same molecular cloud. The resultant binding energy cut-offs are shown in Figure 3.12. The difference between them is small and all but two of the systems discussed in this paper have binding energies that fall within the maximum scale set by the first fragmentation stage. Indeed the distribution of all systems shown in Figure 3.12 are well-constrained by these lines over $0.2M_{\odot}<M_{tot}<10M_{\odot}$, suggesting that this variable separation scale is a more realistic limit than an arbitrary fixed separation limit. This envelope does not attempt to explain why field systems with $M_{tot} < 0.2M_{\odot}$ are almost all at significantly tighter separations than what is predicted by the Jeans criterion. It may be that dynamical effects are more important in the initial formation of such low–mass objects than for more massive stellar systems (Reipurth & Clarke 2001; Bate et al. 2002), although we still cannot rule out insufficient sampling of the parameter space.

3.5.2 Higher Order Multiplicity Among Wide Systems

One explanation for the unusually low binding energies for some of the UCD systems plotted in Figure 3.12 is that one or both components may themselves be unresolved multiples. It has been suggested by Burgasser et al. (2005) that there is a higher binary frequency among brown dwarfs when they are found widely-separated from a common motion stellar primary versus those found isolated in the field. The larger binary fraction could be indicative of a formation mechanism which requires a higher order multiple system to keep all components gravitationally bound, or requires an exchange of angular momentum between wide and close components.

We have re-visited this conjecture with the objects listed in Table 3.1. There are 44 systems containing a UCD which is over 100 AU from the primary star, of which 20 have had their UCD secondaries targeted with adaptive optics or the Hubble Space Telescope to search for additional components down to 0.1″-0.5″ separations. This higher resolution probes the projected separation space within 20 AU, which characterizes the majority (∼90%) of UCD binaries (Allen 2007). From this subset we calculate a resolved binary frequency for UCDs of ϵ_b=50±11%. This is significantly larger than the resolved binary frequency for field UCDs, which typically range over 10-20% (e.g. Reid et al. 2001, 2006; Burgasser et al. 2003c, 2006b; Bouy et al. 2003; Siegler et al. 2003, 2007; Close et al. 2003). Our UCD multiplicity fraction is a $\sim 2\sigma$ deviation from the field, consistent with the results of Burgasser et al. (2005). We note that our companion sample is not a volume-complete one and complex selection effects (other than those associated with formation mechanisms) may be

present. In the worst case scenario of a magnitude limited sample that favors unresolved multiples, the binary fraction of isolated field sources increases to 10-30%. But this is still well below the ∼50% binary fraction found for the wide multiples. This large fraction of triples is surprising.

For comparison, the 8pc sample (Reid & Hawley 2005) contains 118 M dwarfs, with 55 single stars, 26 binaries, 6 triples, and 1 quadruple system. Hence the ratio of triples to binaries is roughly 1:4 and quadruples to binaries is 1:26. Our wide UCD companion sample includes 20 binaries, 12 triples, and 5 quadruples so we find these ratios to be 3:5 and 1:4 respectively. The addition of a third or fourth component to these wide binaries may be required to maintain the stability of the system. This high rate of multiplicity is also relevant to the binding energies plotted in Figure 3.12, as the addition of an unseen UCD or stellar companion could increase binding energies by as much as 50%.

3.5.3 Discrepancy Among the Ages

Establishing common proper motion, distance and radial velocity are important checks on the likelihood of a co-eval pair. However, for the UCD population, precise distances are difficult to establish and radial velocities are rare. Consequently, establishing a common age via activity, kinematic and/or metallicity diagnostics becomes a particularly important tool for confirming companionship. But, as seen in this work, discrepancies still arise among the available age diagnostics. While the differences in ages discussed in section 4 of this paper do not seem large enough to force us to disregard possible companions, they do serve as intriguing cases for examining current age-activity relations for both stellar and substellar objects. For instance, G 171-58 has chromospheric activity levels which likely place it as older then ∼1 Gyr while its companion, 2MASS J0025+4759, has strong Li absorption and is most likely younger then ∼0.5 Gyr. G 63-23 has both chromospheric and rotation ages which suggest it is younger than ∼3 Gyr while its companion, an Hα inactive M8, resembles an older field star. NLTT 2274 is a mid-type M dwarf which shows no Hα activity making it among the older field stars while its companion is an Hα active L0. These pairs may end up as excellent tests for the low mass-star and substellar activity relations. Regardless, we encourage future investigations of UCD companions to carefully examine coevality of a proposed system before assuming companionship.

3.6 Conclusions

We have provided a detailed analysis of nine wide companion systems containing UCDs. Seven of the systems have parallax measurements, six of which are precise Hipparcos measurements. Combining catalog information with new spectroscopic observations of the primary and secondary components, a best age range for each system was determined. Assuming co-evality with the secondaries and combining best age ranges with bolometric luminosity ranges, masses were estimated from the Burrows et al. (1997) evolutionary models. Seven of the UCDs were determined to be very low–mass stars, one was determined to be substellar, and one has a questionable age therefore undetermined mass. Two of the nine systems, G171-58 with 2MASS J0025+4759 and G 63-23 with 2MASS J1320+0957, have significant differences in the component system ages indicating possible shortcomings in our understanding of the age diagnostics of stars and ultracool dwarfs.

Using a compiled list of known wide companion systems containing a UCD, we find that the frequency of tight resolved binaries is at least twice as high for wide companion UCDs as for isolated field equivalents. The ratio of triples to binaries is 3:5 and quadruples to binaries is 1:4 for wide companion systems with resolved UCD secondaries versus 1:4 and 1:26 for the 8-parsec sample. The higher frequency of higher order multiples suggests that a third or fourth component may be required to maintain gravitational stability or to facilitate the exchange of angular momentum in these loosely bound systems.

The Jeans criterion was investigated against a large sample of companion systems and we conclude that using the Jeans length to set the separation scale is sufficient for constraining the lowest binding energy UCD companion systems down to M_{tot} $\sim$0.2$M_{\odot}$. However, the tight separation of the closely bound, near equal-mass UCD systems is not explained by the allowed envelope set by the Jeans length. The distinguishing characteristics of objects now known at varying mass ratios, total masses, separations, and ages suggests that more specific predictions from relevant theories will help distinguish the dominant formation mechanism for the UCD population.

3.7 Post-Publication

Since the publication of this work a number of relevant papers have followed. Recent simulations by Stamatellos & Whitworth (2010, 2009) have been successful in accounting for widely separated VLM binaries using gravitational fragmentation of massive extended disks. In their smoothed particle hydrodynamic (SPH) simulations, a system with M_{DISK}=0.7$M_{\odot}$, R_{DISK}=400AU,

M_{star}=0.7 $M_{\odot}$ is evolved for up to 20 kyr followed by an N-body dynamical evolution for up to 200 Kyr. After 12 simulations, 96 stars are formed with brown dwarf or low–mass secondaries and among those companions, 9 are tight VLM multiples. Based on statistics within their resultant systems, the authors conclude that gravitational fragmentation can account for a higher population of hierarchical systems when the UCD is widely separated from a more massive star. Furthermore, the simulations produce a significant population of low mass ($M_{secondary} < 100$ M_J) companions at distances out to 10,000 AU.

Dhital et al. (2010) presented a catalog of 1342 very-wide (projected separation >500 AU), low-mass (at least one mid-K to mid-M dwarf component) common proper motion pairs identified from astrometry, photometry, and proper motions in the Sloan Digital Sky Survey (catalog identified as SLoWPoKES) . Similar to our results, most of the SLoWPoKES pairs violate the previously defined empirical limits for maximum angular separation or binding energies. Dhital et al. (2010) used their sample to re-define empirical limitations and their new log-normal relation encompass all the systems reported in this chapter. They also report that the wide binary frequency (WBF) for the mid-K to mid-M spectral types decreases as a function of Galactic height, suggesting a time evolution of the WBF. In addition, the semi-major axes of the SLoWPoKES systems exhibit a distinctly bimodal distribution, with a break at separations (and corresponding binding energies) around 0.1 pc (beyond the boundary of our widest system). Compared with theoretical predictions for the disruption of binary systems with time, the authors conclude that the SLoWPoKES sample comprises two populations of both old yet tightly bound systems, and "young" weakly bound systems that will not survive more than a few Gyr.

Law et al. (2010) analyzed a sample of 36 wide (separations ranging from 600 - 6500 AU) M dwarf (M1- M5) binaries in the field in search of hierarchical multiples. They found ten new triple systems and one new quadruple system and reported a bias-corrected total high-order-multiple fraction of $45^{+18\%}_{-16\%}$. All the detected companions had masses similar to their primary components although they did detect two very low mass secondaries, including a candidate brown dwarf. They found a high-order-multiple fraction of $21^{+17\%}_{-7\%}$ for systems with separations up to 2000 AU compared to $77^{+9\%}_{-22\%}$ for systems with separations > 4000 AU. These results coincide with our own and suggest that the very widest M dwarf companion systems require higher masses to form or to survive.

Chapter 4

Parallaxes

Arguably, the most difficult and time-consuming astrometric measurement to make for a stellar or substellar object is a distance measurement. In this chapter I detail an extensive 2-4 y ear astrometric campaign to obtain parallaxes for a subset of the BDKP catalog. It would have been observationally impossible to obtain parallaxes for the entire sample described in chapter one, therefore we chose a subset of objects that had the highest potential of providing insight into the intrinsic physical and atmospheric properties of the overall population.

The following chapter is a manuscript in preparation for submission to the Astrophysical Journal.

4.1 Introduction

For any new class of astronomical objects identified, distances are crucial for investigating basic physical properties. Brown dwarfs, low mass mass objects that lack stable hydrogen burning in their core, are a recent addition to the plethora of objects studied in astronomy. They were first predicted by Kumar (1962) and Hayashi & Nakano (1963) but not observationally confirmed until the late 20th century (Nakajima et al. 1995; Rebolo et al. 1992). There are now over 500 spectrally confirmed brown dwarfs and two spectral classes designated for their classification: "L" for objects with temperatures ranging between 1300 and 2000K and "T" for objects cooler than 1300K (see Kirkpatrick 2005 and references there-in). Their masses range from $0.072 M_{\odot}$ at the high end to $0.012\ M_{\odot}$ at the low end thereby straddling the boundary between the lowest mass stars and the highest mass exoplanets (Saumon et al 1996; Chabrier & Baraffe 1997) . Distances are crucial for diagnosing the brown dwarf population as standard stellar evolution does not apply to them.

Rather than joining the main sequence, brown dwarfs do not have enough mass for stable hydrogen burning therefore they continually cool after some initial deuterium burning (Burrows et al. 1997). Distances are necessary for establishing the basic temperature and luminosity scale as well as identifying unresolved binary candidates. Moreover, brown dwarfs are among the closest systems to the Sun therefore determining distances is required for an overall census of the local solar neighborhood.

With the early parallax programs of Dahn et al (2002), Tinney, Burgasser, & Kirkpatrick (2003) and Vrba et al (2004) the near-IR color magnitude diagrams for brown dwarfs were first examined. Golimowski et al (2004) published a relation for obtaining the bolometric correction for ultracool dwarfs which was used in combination with parallax measurements to create the first temperature classes for brown dwarfs (see also Vrba et al 2004). From these works, initial spectrophotometric relations were created in the near-IR which were used to estimate absolute magnitudes and hence distances for spectrally classified brown dwarfs. Recent photometric work using Spitzer IRAC channels extended these relations into the mid-IR where the latest T dwarfs emit the majority of their flux (Patten et al 2006; Leggett et al 2010). Furthermore, objects were followed up with Hubble Space Telescope (HST) or adaptive optics observations, confirmed as close binary pairs and subsequently found to be over-luminous on color-magnitude diagrams(e.g. Gizis et al. 2003; Bouy et al. 2008; Burgasser et al. 2003c). Recent investigations have obtained dynamical masses of close binaries with trigonemetric parallaxes using orbital monitoring (Lane et al. 2001; Dupuy et al. 2008, 2009; Konopacky et al. 2010b).

One of the main puzzling features of brown dwarf color-magnitude diagrams is the significant scatter detected among similar effective temperature objects. Increasingly complex atmospheric and evolutionary models have explained this scatter as the result of variations in gravity, metallicity, sedimentation efficiency and/or binarity (e.g. Tsuji et al. 1996; Tsuji & Nakajima 2003; Burrows et al. 2006; Helling et al. 2008; Saumon & Marley 2008). Differing models disagree as to which parameter has the largest effect . Several groups have used models to investigate the variations of observational color-magnitude diagrams but the number of objects with independently measured "second parameters" is still sparse (Knapp et al 2004; Patten et al 2006; Leggett et al 2010). It is difficult to test the spread of color magnitude diagrams due to differing metallicities and/or gravities without a bona-fide sample of each subset. There are a handful of L subdwarfs known, objects with subsolar metallicity, but only a small fraction have parallax measurements (Cushing et al. 2009; Burgasser et al. 2009; Burgasser et al. 2003a;Burgasser 2004a;Schilbach et al. 2009). A number of low-surface gravity brown dwarfs have been identified in

the field, but until this work, none have had parallaxes reported (Cruz et al. 2009; Allers et al. 2010; Allers et al. 2007; Kirkpatrick et al. 2006). Investigating the absolute magnitudes of broadly different gravity and/or metallicity subsets of the brown dwarf population will help to disentangle the intrinsic physics which drive their evolution and population diversity.

Another major anomaly of brown dwarf color magnitude diagrams is an intriguing brightening in J (and to some extent H and K) band as objects transition between the warmer L and cooler T dwarf spectral classes . Clouds are especially influential on the 1 μm region for brown dwarfs therefore this significant brightening (up to 1.5 magnitude; Vrba et al 2004) is attributed to a redistribution of flux while cloud decks clear or sedimentation efficiency improves (e.g. Burgasser et al. 2002b; Knapp et al. 2004). In Golimowski et al (2004) a near constant temperature of $\sim$1450 K was obtained for L7-T4 objects supporting models that attribute the J band brightening to atmospheric effects and hinting at unresolved binarity among the sample. In the past decade, several L/T transition objects have been confirmed as flux reversal binaries indicating that the brightening is an intrinsic feature of brown dwarfs (e.g. Liu et al. 2006; Looper et al. 2008a;Gizis et al. 2003; Burgasser et al. 2006b). However, a significantly larger binary fraction across the L/T transition artificially enhances the bump (Burgasser 2007). Small numbers of L/T transition objects with parallax measurements has hindered investigating the true extent of this atmospheric transition.

In late 2006 we initiated the Brown Dwarf Kinematics Project (BDKP) in order to address persistent questions of brown dwarf evolution and atmospheric properties. The primary focus of the BDKP is to measure the proper motion, parallax, and radial velocity of all brown dwarfs within 20pc. Our aim is to search for spatial and kinematic association with moving groups as well as kinematic correlations with physical properties. Also, using parallaxes, we hope to construct a "clean" (free of binaries and extreme gravity and/or metallicity objects) absolute magnitude diagram. In so doing we aim to disentangle effects of gravity, metallicity, binarity, and/or atmospheric properties on the brown dwarf population. In this work we report parallaxes for 84 ultracool dwarfs (UCDs). We have primarily focused on objects that straddle the boundary between L and T dwarfs as well as those classified as low-surface gravity dwarfs. Section 4.2 describes the target list as well as the data acquisition and reduction. Section 4.3 describes the parallax pipeline used to determine distances. Section 4.4 uses all parallax measurements reported in this work in combination with literature values and photometric information obtained from various catalogs to investigate color-magnitude diagrams and spectrophotometric relations for the brown dwarf population. In section 4.5

an updated brown dwarf near-IR color magnitude diagram is examined using evolutionary models. Section 4.6 discusses the absolute magnitude vs. spectral type relation for low-surface gravity dwarfs. Section 4.7 reviews the kinematics for an ensemble of all known brown dwarfs with parallax measurements and section 4.8.3 describes individual objects of interest. Conclusions are reported in section 4.9.

4.2 Observations

4.2.1 Target List

We compiled the parallax target list from the BDKP astrometric sample reported in Faherty et al. (2009). Instrumental limitations precluded measuring parallaxes to the faintest, most distant L and T dwarfs so we focused primarily on ultracool dwarfs within 20pc. However we were also interested in subsets of the ultracool dwarf population which included low-surface gravity dwarfs (potentially young sources) and subdwarfs (potentially old sources). For these scientifically interesting subsets we relaxed our astrometric constraint to include sources whose predicted spectrophotometric distance was up to 50pc. Our full target list consisted of 84 ultracool dwarfs, including 19 M dwarfs, 37 L dwarfs and 28 T dwarfs (see Tables 4.1 - 4.2). Among this sample there were 17 low-surface gravity dwarfs and 3 subdwarfs.

Table 4.1: Target List

Name	Spectral Type[1]	Nights	Frames[2]	Ref Stars	Δt (yr)	J	H	K	Instrument	Note[3]
(1)	(2)	(3)	(4)	(5)	(6)	(7)	(8)	(9)	(10)	(11)
2MASS J00325584-4405058	L0γ	15	53	75	2.32	14.78± 0.04	13.86± 0.03	13.27± 0.04	ANDICAM	LG
2MASS J00345157+0523050	T6.5	5	23	38	0.97	15.53± 0.05	15.44± 0.08	16.24± 0.50	ISPI	
2MASS J0103320+193536	L6	5	19	54	1.13	16.29± 0.08	14.90± 0.06	14.15± 0.06	ISPI	
2MASS J02212859-6831400	M8β	16	58	41	2.66	13.97± 0.03	13.27± 0.03	12.81± 0.04	ANDICAM	LG
2MASS J02235464-5815067	L0γ	12	51	54	1.70	15.07± 0.05	14.00± 0.04	13.42± 0.04	ANDICAM	LG
2MASS J03185403-3421292	L7	7	31	25	1.29	15.57± 0.05	14.35± 0.04	13.51± 0.04	ISPI	
SDSS J032553.17+042540.1	T5.5	5	28	48	1.13	16.16± 0.06	16.20± 0.06	16.37± 0.06	ISPI	
2MASS J03341218-4953322	M9	19	68	65	2.96	11.38± 0.02	10.82± 0.03	10.39± 0.02	ANDICAM	
2MASS J03552337+1133437	L5γ	4	17	50	1.29	14.05± 0.02	12.53± 0.03	11.53± 0.02	ISPI	LG
2MASS J04221413+1530525:	M6γ	14	51	16	2.84	12.76± 0.02	11.77± 0.02	11.28± 0.02	ANDICAM	LG
2MASS J04362788-4114465	M7.5β	5	22	46	1.38	13.10± 0.03	12.42± 0.02	12.06± 0.03	ISPI	LG
2MASS J04390101-2353083	L6.5	14	52	58	3.00	14.41± 0.03	13.41± 0.03	12.82± 0.02	ANDICAM	
2MASS J04433761+0002051	M9β	5	21	44	1.38	12.52± 0.03	11.80± 0.02	11.17± 0.02	ISPI	LG
2MASS J04455387-3048204	L2	25	87	71	3.05	13.39± 0.03	12.58± 0.02	11.98± 0.02	ANDICAM	
2MASS J05012406-0010452	L4γ	19	77	86	2.92	14.98± 0.04	13.71± 0.03	12.96± 0.04	ANDICAM	LG
2MASS J05103520-4208140	T5	9	42	56	2.08	16.22± 0.09	16.24± 0.16	16.00± 0.28	ISPI	
2MASS J05160945-0445499	T5.5	9	38	34	2.08	15.98± 0.08	15.72± 0.17	15.49± 0.20	ISPI	
2MASS J05184616-2756457	L0	7	33	40	1.32	15.26± 0.04	14.30± 0.05	13.61± 0.04	ISPI	LG
2MASS J05185995-2828372	L7.5	8	38	56	2.08	15.98± 0.10	14.83± 0.07	14.16± 0.07	ISPI	B
2MASS J05361998-1920396	L1β	7	26	78	1.32	15.77± 0.08	14.69± 0.07	13.85± 0.06	ISPI	
LHS 1777	M5	21	94	32	2.84	10.21± 0.02	9.69± 0.02	9.37± 0.02	ANDICAM	Cal
2MASS J06085283-2753583	M8.5γ	26	91	89	3.04	13.60± 0.03	12.90± 0.03	12.39± 0.03	ANDICAM	LG
2MASS J06164006-6407194	sdL5	5	24	95	1.32	16.40± 0.11	16.27± 0.23	16.38± 0.50	ISPI	SD
2MASS J06195260-2903592	M6β	24	95	88	3.05	15.14± 0.03	14.19± 0.04	13.45± 0.05	ANDICAM	LG
2MASS J06244595-4521548	L5	21	68	65	2.86	14.48± 0.03	13.34± 0.03	12.60± 0.03	ANDICAM	
DENIS-P J065248.5-574137	M8β	14	55	40	2.83	13.63± 0.03	12.97± 0.02	12.45± 0.02	ANDICAM	B,LG
2MASS J07123786-6155528	L1β	6	23	82	1.32	15.30± 0.06	14.39± 0.04	13.67± 0.05	ISPI	LG
2MASS J07234305+0316218	sdM8	15	59	69	2.65	14.54± 0.03	14.12± 0.04	13.88± 0.04	ANDICAM	SD
2MASS J07290002-3954043	T8	9	38	98	2.08	15.92± 0.08	15.98± 0.18	15.29± 0.50	ISPI	
SDSS J074201.41+205520.5	T5	7	20	83	2.08	15.87± 0.06	15.91± 0.06	15.96± 0.06	ISPI	
2MASS J0746425+200032	L2	13	55	94	2.69	11.76± 0.02	11.01± 0.02	10.47± 0.02	ANDICAM	B,Cal
SDSS J083048.80+012831.1	T4.5	7	33	46	2.08	16.25± 0.06	16.12± 0.06	16.29± 0.10	ISPI	
2MASS J08472872-1532372	L2	24	87	69	2.89	13.51± 0.03	12.63± 0.03	12.06± 0.02	ANDICAM	
2MASS J0850359+105716	L6	7	45	50	2.08	16.47± 0.11	15.22± 0.09	14.47± 0.07	ISPI	B

Continued on Next Page...

Table 4.1 – Continued

Name	Spectral Type[1]	Nights	Frames[2]	Ref Stars	Δt (yr)	J	H	K	Instrument	Note[3]
(1)	(2)	(3)	(4)	(5)	(6)	(7)	(8)	(9)	(10)	(11)
2MASS J09393548-2448279	T8	7	24	63	2.07	15.98± 0.11	15.80± 0.15	16.56± 0.50	ISPI	B,Cal
2MASS J09490860-1545485	T2	8	36	50	2.08	16.15± 0.12	15.26± 0.11	15.23± 0.17	ISPI	
WT 248	M3	17	68	100	2.20	10.56± 0.02	10.10± 0.02	9.87± 0.02	ANDICAM	Cal
SDSS J100711.74+193056.2	L8	4	23	48	1.97	16.90± 0.10	15.79± 0.10	15.16± 0.06	ISPI	
2MASS J1010148-040649	L7	9	33	55	2.08	15.51± 0.06	14.39± 0.04	13.62± 0.05	ISPI	
2MASS J10220489+0200477	M9	5	25	49	1.32	14.10± 0.03	13.40± 0.03	12.90± 0.03	ISPI	LG
SDSS J103026.78+021306.4	L9.5	6	29	52	1.88	17.27± 0.10	16.22± 0.10	15.66± 0.10	ISPI	
2MASS J1036530-344138	L6	8	34	57	2.08	15.62± 0.05	14.45± 0.04	13.80± 0.04	ISPI	
SDSS J104335.08+121314.1	L7	7	24	63	2.07	15.96± 0.06	14.81± 0.06	14.23± 0.06	ISPI	
SDSS J104409.43+042937.6	L7	5	23	67	1.88	15.98± 0.06	14.91± 0.06	14.35± 0.06	ISPI	
2MASS J10584787-1548172	L3	15	55	28	2.48	14.15± 0.04	13.23± 0.03	12.53± 0.03	ANDICAM	Cal
2MASS J11020983-3430355	M8.5γ	21	82	92	2.89	13.03± 0.02	12.36± 0.02	11.89± 0.02	ANDICAM	LG
SDSS J11101001+011613.1	T5.5	5	22	33	2.08	16.34± 0.12	15.92± 0.14	15.13± 0.50	ISPI	
2MASS J11145133-2618235	T7.5	9	43	42	2.08	15.86± 0.08	15.73± 0.12	16.11± 0.50	ISPI	
TWA 26γ	M9	16	65	56	2.37	12.69± 0.03	12.00± 0.02	11.50± 0.02	ANDICAM	LG
2MASS J11553952-3727350	L2	21	80	97	2.53	12.81± 0.02	12.04± 0.03	11.46± 0.02	ANDICAM	
SDSS J115553.86+055957.5	L7.5	7	33	46	2.08	15.78± 0.06	14.68± 0.06	14.11± 0.06	ISPI	
SDSS J120747.17+024424.8	L8	7	31	61	1.88	15.56± 0.06	14.75± 0.06	14.28± 0.06	ISPI	
2MASS J12095613-1004008	T3	5	22	58	1.88	15.91± 0.07	15.33± 0.09	15.06± 0.14	ISPI	
2MASS J12154432-3420591	T4.5	7	35	79	2.08	16.24± 0.13	15.81± 0.19	16.32± 0.50	ISPI	
2MASS J13595510-4034582	L1	13	48	99	1.80	13.65± 0.03	13.03± 0.03	12.57± 0.03	ANDICAM	
2MASS J14044941-3159329	T2.5	10	36	84	2.08	15.58± 0.06	14.95± 0.07	14.54± 0.09	ISPI	
2MASS J14442067-2019222	sdM9	15	63	87	2.87	12.55± 0.02	12.14± 0.02	11.93± 0.02	ANDICAM	SD,Cal
SDSS J14460060+002452.0	L6	7	26	63	1.88	15.89± 0.08	14.51± 0.04	13.94± 0.05	ISPI	Cal
SDSS J150411.63+102718.4	T7	9	45	32	2.08	16.81± 0.06	16.88± 0.06	16.89± 0.06	ISPI	
SDSS J151114.66+060742.9	T0	8	54	52	2.08	16.01± 0.06	15.11± 0.06	14.51± 0.06	ISPI	
SDSS J152103.24+013142.7	T2	6	43	60	2.08	16.27± 0.06	15.58± 0.06	15.43± 0.06	ISPI	
2MASS J1526140+204341	L7	6	26	73	1.88	15.59± 0.05	14.50± 0.04	13.92± 0.05	ISPI	
2MASS J1553022+153236	T7	4	22	39	2.08	15.66± 0.06	15.72± 0.06	15.81± 0.06	ISPI	B
2MASS J16150413+1340079	T6	8	43	34	2.08	16.35± 0.09	16.49± 0.25	15.86± 0.50	ISPI	
SDSS J163022.92+081822.0	T5.5	6	33	73	1.88	16.46± 0.06	16.31± 0.06	16.30± 0.06	ISPI	
2MASS J16452211-1319516	L1.5	12	44	89	1.07	12.45± 0.03	11.69± 0.03	11.15± 0.03	ANDICAM	
2MASS J17545447+1649196	T5	6	25	97	1.88	15.81± 0.07	15.65± 0.13	15.56± 0.16	ISPI	
2MASS J18283572-4849046	T5.5	8	25	93	1.88	15.18± 0.06	14.91± 0.07	15.18± 0.14	ISPI	
2MASS J19360187-5502322	L5	12	42	71	1.32	14.49± 0.04	13.63± 0.04	13.05± 0.03	ANDICAM	
2MASS J20004841-7523070	M9β	5	38	52	0.84	12.73± 0.03	11.97± 0.03	11.51± 0.03	ISPI	LG

Continued on Next Page...

Table 4.1 – Continued

Name	Spectral Type[1]	Nights	Frames[2]	Ref Stars	Δt (yr)	J	H	K	Instrument	Note[3]
(1)	(2)	(3)	(4)	(5)	(6)	(7)	(8)	(9)	(10)	(11)
2MASS J20431769-1551031	L9	5	28	75	1.88	17.03± 0.06	15.96± 0.06	15.41± 0.06	ISPI	
SDSS J204749.61-071818.3	T0	6	22	77	1.34	16.88± 0.06	15.83± 0.06	15.33± 0.06	ISPI	
SDSS J205235.31-160929.8	T1	7	26	80	1.88	16.23± 0.08	15.40± 0.06	14.97± 0.06	ISPI	
2MASS J20575409-0252302	L1.5	20	73	93	2.20	13.12± 0.02	12.27± 0.02	11.72± 0.03	ANDICAM	
2MASS J21321145+1341584	L6	5	23	75	1.20	15.80± 0.06	14.60± 0.05	13.84± 0.06	ISPI	B
2MASS J21513839-4853542	T4	7	28	72	1.52	15.73± 0.07	15.17± 0.10	15.43± 0.18	ISPI	
2MASS J22282889-4310262	T6	6	30	52	1.52	15.66± 0.07	15.36± 0.12	15.30± 0.21	ISPI	
2MASS J23224684-3133231	L0β	9	34	79	1.39	13.58± 0.03	12.79± 0.02	12.32± 0.02	ANDICAM	LG
2MASS J2356547-155310	T5.5	6	25	32	1.52	15.76± 0.06	15.66± 0.06	15.62± 0.06	ISPI	Cal
2MASS J23594034-7335055	T8	8	40	55	1.52	16.16± 0.10	15.91± 0.19	15.16± 0.50	ISPI	

[1]M and L dwarfs are classified using red optical data. If that is unavailable the near-IR spectral type is used. T dwarfs are classified in the near-IR

[2]Number of frames used in the parallax solution

[3]LG is a low surface gravity dwarf, Cal is a calibrator ultracool dwarf, SD is an ultracool subdwarf, and B is a binary

Table 4.2: Astrometry of Targets

Name	Ref	Spectral Type	π_{rel} (mas)	π_{abs} (mas)	μ_α mas yr^{-1}	μ_δ mas yr^{-1}	v$_{tan}$ km s^{-1}
(1)	(2)	(3)	(4)	(5)	(6)	(7)	(8)
2MASS J00325584-4405058	5	L0γ	63.2 ± 2.3	65.7 ± 2.3	112.4 ± 2.3	-83.2 ± 2.3	10.1 ± 0.9
2MASS J00345157+0523050	1	T6.5	102.5 ± 1.6	107.1 ± 5.1	681.4 ± 4.4	177.8 ± 6.4	31.2 ± 1.6
2MASS J0103320+193536	10	L6	23.5 ± 7	26.2 ± 7.3	413.7 ± 14.2	82.8 ± 11.7	76.5 ± 32.8
2MASS J02212859-6831400	18	M8β	21.8 ± 1	25.5 ± 1	52.9 ± 1.2	0.7 ± 1.1	9.8 ± 1.6
2MASS J02235464-5815067	5	L0γ	31.1 ± 2.7	33.1 ± 2.7	76.5 ± 4.6	-42.1 ± 5.2	12.5 ± 3.2
2MASS J03185403-3421292	11	L7	79.5 ± 5.2	83.4 ± 5.9	343.5 ± 10.2	57.3 ± 11.2	19.8 ± 2.2
SDSS J032553.17+042540.1	2	T5.5	34.1 ± 20.3	36.8 ± 20.6	-144.3 ± 30.1	-44.9 ± 23.3	19.5 ± 37.6
2MASS J03341218-4953322	3	M9	128.8 ± 1	131.7 ± 1.1	2358.7 ± 1.3	483.8 ± 1.1	86.8 ± 0.4
2MASS J03552337+1133437	5	L5γ	119.8 ± 11.4	123.1 ± 12	186.6 ± 10.7	-678.4 ± 8	27.1 ± 2.9
2MASS J04221413+1530525:	18	M6γ	16 ± 0.9	24.4 ± 1.2	-8.4 ± 0.9	3.5 ± 0.8	1.8 ± 0.9
2MASS J04362788-4114465	3	M7.5β	113 ± 8.2	114.6 ± 8.2	76.8 ± 8.7	-54.1 ± 5.1	3.9 ± 0.8
2MASS J04390101-2353083	3	L6.5	104.3 ± 2.2	108.1 ± 2.2	-122.5 ± 2.3	-156.2 ± 2	8.7 ± 0.4
2MASS J04433761+0002051	8	M9β	139.7 ± 9.8	143 ± 11.9	34.5 ± 9.6	-139.4 ± 6.6	4.8 ± 1
2MASS J04455387-3048204	3	L2	78.4 ± 1.6	80.1 ± 1.6	145.4 ± 1.8	-407.6 ± 1.7	25.6 ± 0.7
2MASS J05012406-0010452	5	L4γ	87.7 ± 2.6	89.8 ± 2.6	182.6 ± 2.5	-142.9 ± 2.4	12.2 ± 0.7
2MASS J05103520-4208140	16	T5	49.1 ± 2.7	51.4 ± 3.4	98.3 ± 3.4	597 ± 3.8	55.8 ± 4.3
2MASS J05160945-0445499	1	T5.5	64.8 ± 2.6	67.6 ± 3	-192.2 ± 3.2	-189 ± 3.2	18.9 ± 1.5
2MASS J05184616-2756457	4	L0	3.6 ± 12.2	5.9 ± 12.4	2.1 ± 13	-9.7 ± 13.5	7.9 ± 11.8
2MASS J05185995-2828372	11	L7.5	53.3 ± 2.9	55.4 ± 3.3	-106.8 ± 4	-273.6 ± 3.7	25.1 ± 2.6
2MASS J05361998-1920396	4	L1β	60.9 ± 6.4	62.6 ± 6.7	52.2 ± 9.9	-83.7 ± 10.2	7.5 ± 2.4
LHS 1777	21	M5	77.5 ± 1	79.7 ± 1	-155.5 ± 1.1	951 ± 1	57.4 ± 0.7
2MASS J06085283-2753583	3	M8.5γ	38.6 ± 1.3	41.3 ± 1.3	8.9 ± 1.3	15.2 ± 1.3	2 ± 0.4
2MASS J06164006-6407194	6	sdL5	20.1 ± 5.6	22.4 ± 5.9	1351.3 ± 7.4	-48.6 ± 9	285.9 ± 64
2MASS J06195260-2903592	3	M6β	18.9 ± 1.3	21.6 ± 1.3	3.9 ± 1.3	2.5 ± 1.2	1 ± 0.8
2MASS J06244595-4521548	18	L5	102.2 ± 1.3	104.5 ± 1.4	-38.4 ± 1.8	374.6 ± 1.4	17.1 ± 0.3
DENIS-P J065248.5-574137	18	M8β	39.6 ± 1.2	41.7 ± 1.2	2.1 ± 1.2	26.9 ± 1.1	3.1 ± 0.5
2MASS J07123786-6155528	5	L1β	57 ± 4	58.3 ± 4.1	-18.8 ± 6.3	101.9 ± 6.2	8.4 ± 1.7
2MASS J07234305+0316218	13	sdM8	34.2 ± 1.5	36.4 ± 1.5	-115.2 ± 1.6	-407.1 ± 1.4	55.2 ± 3.2
2MASS J07290002-3954043	16	T8	114.8 ± 2.4	118 ± 3.5	-538.9 ± 2.8	1697 ± 2.6	71.6 ± 1.5
SDSS J074201.41+205520.5	1	T5	68.2 ± 3.6	69.9 ± 4	-319.3 ± 3.5	-231.6 ± 3.7	26.8 ± 2.2
2MASS J0746425+200032	10	L2	78.7 ± 2.8	79.9 ± 2.8	-324.8 ± 3.2	-68.7 ± 3.4	19.7 ± 1.1
SDSS J083048.80+012831.1	1	T4.5	34.6 ± 6	37.1 ± 6.3	-10 ± 5.5	32 ± 10.4	4.3 ± 3.7
2MASS J08472872-1532372	3	L2	75.5 ± 1.2	78.4 ± 1.2	139.3 ± 1.3	-199.4 ± 1.3	14.7 ± 0.4
2MASS J0850359+105716	9	L6	32.5 ± 7.5	34.9 ± 7.8	-144.2 ± 5.3	-37.7 ± 5.3	20.3 ± 11.3

Continued on Next Page...

Table 4.2 – Continued

Name	Ref	Spectral Type	π_{rel} (mas)	π_{abs} (mas)	μ_α mas yr^{-1}	μ_δ mas yr^{-1}	v$_{tan}$ km s^{-1}
(1)	(2)	(3)	(4)	(5)	(6)	(7)	(8)
2MASS J09393548-2448279	1	T8	184.8 ± 4.6	187.9 ± 7.2	548.9 ± 3.4	-1068 ± 2.4	30.3 ± 1
2MASS J09490860-1545485	1	T2	47.4 ± 7.3	49.8 ± 7.5	-101.9 ± 6.4	-0.1 ± 5.5	9.7 ± 4.3
WT 248	22	M3	29.6 ± 1.3	32.8 ± 1.4	-1223.3 ± 1.7	-108.4 ± 1.7	177.5 ± 6.1
SDSS J100711.74+193056.2	2	L8	57.7 ± 15.5	60 ± 15.6	-249.6 ± 8.2	-6.3 ± 5.1	19.8 ± 10.1
2MASS J1010148-040649	3	L7	76 ± 4.9	78.1 ± 5.3	-303.6 ± 5.9	-2.7 ± 5.1	18.4 ± 2.1
2MASS J10220489+0200477	18	M9	32.6 ± 10.5	33.7 ± 10.5	-129.2 ± 10.9	-400.2 ± 8.1	59.3 ± 29.1
SDSS J103026.78+021306.4	12	L9.5	42 ± 16.1	43.8 ± 16.2	57.2 ± 15.7	54.2 ± 15.8	8.5 ± 12
2MASS J1036530-344138	7	L6	73.4 ± 2.8	74.8 ± 2.9	17.7 ± 2.3	-560.1 ± 2	35.6 ± 1.7
SDSS J104335.08+121314.1	2	L7	73.4 ± 6.8	75.7 ± 7.4	98.2 ± 3.9	-199.1 ± 3.3	13.9 ± 2.7
SDSS J104409.43+042937.6	12	L7	52.8 ± 23.3	54.6 ± 23.4	-18.5 ± 20.9	95.3 ± 17.9	8.4 ± 13
2MASS J10584787-1548172	9	L3	59.6 ± 2.5	62.1 ± 2.5	-259.1 ± 2	43.5 ± 2	20.1 ± 1.5
2MASS J11020983-3430355	3	M8.5γ	29.9 ± 1.3	33.7 ± 1.4	-58.4 ± 1.3	-1.1 ± 1.3	8.2 ± 1.3
SDSS J11101001+011613.1	1	T5.5	33 ± 6.1	35.1 ± 6.4	-187.9 ± 3.4	-262.9 ± 4.2	43.7 ± 13.3
2MASS J11145133-2618235	1	T7.5	185.8 ± 3.3	188.6 ± 4.7	-3000.6 ± 3	-367.4 ± 3.4	76.1 ± 1
TWA 26	23	M9γ	35.6 ± 0.8	43 ± 1.1	-79.2 ± 0.8	-11.6 ± 0.7	8.8 ± 0.7
2MASS J11553952-3727350	7	L2	108.3 ± 1.8	112 ± 1.9	44.1 ± 1.7	-785 ± 2	33.3 ± 0.6
SDSS J115553.86+055957.5	12	L7.5	45.1 ± 6.2	51.2 ± 6.3	-403.1 ± 4.1	-13.3 ± 4.3	37.4 ± 6.7
SDSS J120747.17+024424.8	8	L8	67.6 ± 6	68.6 ± 6	-516.9 ± 7.7	143.1 ± 4.7	37.1 ± 4.1
2MASS J12095613-1004008	11	T3	59.5 ± 7.3	62.7 ± 7.3	267.5 ± 7.6	-312.8 ± 6.7	31.1 ± 5.3
2MASS J12154432-3420591	16	T4.5	41.4 ± 4.8	43.4 ± 4.8	-243.5 ± 5.8	-360.1 ± 4.1	47.5 ± 7.4
2MASS J13595510-4034582	18	L1	70.8 ± 2.5	72 ± 2.5	38.7 ± 3.1	-499 ± 2.9	33 ± 1.5
2MASS J14044941-3159329	15	T2.5	31.2 ± 1.5	34.2 ± 1.6	347.4 ± 2	-23.9 ± 2	48.3 ± 3.5
2MASS J14442067-2019222	19	sdM9	59.7 ± 1.2	61.6 ± 1.2	-2905.1 ± 1	-1953.9 ± 1	269.6 ± 2.6
SDSS J14460060+002452.0	8	L6	42.9 ± 6	44.8 ± 6	150.3 ± 7.8	-79.2 ± 7.5	18 ± 5.5
SDSS J150411.63+102718.4	2	T7	85.7 ± 4.2	88.4 ± 4.2	403.2 ± 4.4	-295 ± 4.2	26.8 ± 1.7
SDSS J151114.66+060742.9	2	T0	28.5 ± 2.5	31.8 ± 2.5	-245.9 ± 3.3	-237.3 ± 2.9	51 ± 6.4
SDSS J152103.24+013142.7	1	T2	40.2 ± 2.8	42.4 ± 2.8	-159.7 ± 3.8	75.5 ± 2.1	19.8 ± 2.9
2MASS J1526140+204341	10	L7	44.4 ± 11.3	46.2 ± 11.3	-194.3 ± 13.6	-333.8 ± 9.2	39.7 ± 15.3
2MASS J1553022+153236	1	T7	106.5 ± 4.4	109.1 ± 4.4	-322.7 ± 4.2	162.6 ± 6.2	15.7 ± 1
2MASS J16150413+1340079	16	T6	88.9 ± 3.3	90.8 ± 3.4	274.2 ± 4.1	-357.5 ± 4	23.5 ± 1.2
SDSS J163022.92+081822.0	2	T5.5	58.4 ± 8.2	60.1 ± 8.2	-84 ± 11.4	-99.7 ± 10.1	10.3 ± 3.6
2MASS J16452211-1319516	7	L1.5	99.9 ± 2.7	102.6 ± 2.7	-367.5 ± 4.8	-784.5 ± 4.7	40.1 ± 1.1
2MASS J17545447+1649196	20	T5	163.3 ± 2.7	165 ± 2.7	67.6 ± 3	-167.6 ± 3.6	5.2 ± 0.2
2MASS J18283572-4849046	1	T5.5	85.8 ± 1.8	87.3 ± 1.8	235 ± 3.1	96.3 ± 2.4	13.8 ± 0.5
2MASS J19360187-5502322	18	L5	52.9 ± 3	55.5 ± 3	235.5 ± 5.4	-303.9 ± 6.3	32.9 ± 2.6
2MASS J20004841-7523070	18	M9β	48.7 ± 3.7	50.9 ± 3.7	64.4 ± 10.4	-155 ± 12.2	15.7 ± 2.6

Continued on Next Page...

Table 4.2 – Continued

Name	Ref	Spectral Type	π_{rel} (mas)	π_{abs} (mas)	μ_α mas yr^{-1}	μ_δ mas yr^{-1}	v$_{tan}$ km s^{-1}
(1)	(2)	(3)	(4)	(5)	(6)	(7)	(8)
2MASS J20431769-1551031	2	L9	77.1 ± 11	79.1 ± 11	38.7 ± 12.2	-111.9 ± 9.4	7.1 ± 2.7
SDSS J204749.61-071818.3	1	T0	46.6 ± 5.9	48.5 ± 5.9	60.8 ± 9.5	-205.4 ± 10.8	21 ± 5.2
SDSS J205235.31-160929.8	2	T1	70.8 ± 6.6	73.1 ± 6.6	460.1 ± 9.9	207.9 ± 10.2	32.8 ± 3.9
2MASS J20575409-0252302	3	L1.5	71.1 ± 1.3	74.2 ± 1.4	-6.2 ± 1.4	-87.2 ± 1.3	5.6 ± 0.3
2MASS J21321145+1341584	4	L6	38.2 ± 14.6	40.3 ± 14.6	2.6 ± 13.7	-149.2 ± 19.7	17.6 ± 17.3
2MASS J21513839-4853542	1	T4	51.9 ± 1.2	54 ± 1.2	415.8 ± 2.6	-202.1 ± 2.5	40.6 ± 1.3
2MASS J22282889-4310262	1	T6	90.3 ± 9.3	92.9 ± 9.3	95.4 ± 15.6	-325 ± 13.2	17.3 ± 2.8
2MASS J23224684-3133231	18	L0β	70.7 ± 2.7	72.5 ± 2.8	-185.4 ± 3.6	-554.1 ± 3.6	38.2 ± 1.7
2MASS J2356547-155310	1	T5.5	71.8 ± 2.7	74.1 ± 2.8	-418 ± 5	-618.2 ± 6.2	47.8 ± 1.9
2MASS J23594034-7335055	17	T8	94.9 ± 2.6	96.3 ± 2.6	299.2 ± 4.6	76.2 ± 4.9	15.2 ± 0.7

[1]Discovery Reference Key: 1=Burgasser et al. (2006) 2=Chiu et al. (2006) 3=Cruz et al (2003) 4=Cruz et al. (2007) 5=Cruz, Kirkpatrick, & Burgasser (2009) 6=Cushing et al. (2009) 7=Gizis (2002) 8=Hawley et al. (2002) 9=Kirkpatrick et al. (1999) 10=Kirkpatrick et al. (2000) 11=Kirkpatrick et al. (2008) 12=Knapp et al. (2004) 13=Lepine et al (2005) 14=Lepine, Rich, & Shara (2003) 15=Looper et al. (2008) 16=Looper, Kirkpatrick, and Burgasser (2007) 18=Reid et al. (2008) 19=Scholz et al (2004) 20=This paper 21=Harrington et al (1993) 22=Wroblewski et al (1991) 23=Gizis et al (2002)

4.2.2 Data Collection and Reduction

ANDICAM

We obtained parallax frames with the ANDICAM (A Novel Double-Imaging CAMera- DePoy 2003) imager between November 2006 and March 2010 ($\sim$ 500 hours of observations). ANDICAM is a dual channel near-IR and CCD imager located on the 1.3m telescope at Cerro Tololo InterAmerican Observatory (CTIO). The optical detector is a 1024 x 1024 CCD and the near-IR channel uses a Rockwell 1024 x 1024 HgCdTe Hawaii array. The near-IR field of view is $\sim$2.4 arcminutes with a plate scale of $\sim$0.274 $''$/pixel. The optical CCD field of view is slightly larger, $\sim$6.2 arcminutes, with a plate scale of $\sim$0.369 $''$/pixel. The optical and near-IR channels operate independently with a dichroic filter directing light to the two independent cameras. Therefore, we were able to take a set of near-IR images while integrating in the optical.

All ANDICAM data were acquired through queue observing with telescope time allocated through the SMARTS (Small and Moderate Aperture Research Telescope System) consortium. To ensure the same reference stars for each parallax frame, we required the target star to always be placed in the same X,Y position on the detector. We also required all observations to be made within $\pm$30 minutes of meridian crossing to minimize the corrections for differential color refraction (DCR–see section 4.3.1 below). Typical seeing was 1$''$ and useable conditions for our parallax program were up to 2 $''$.

In the optical we observed in the I_c band with integration times that ranged from 265s for our brightest targets to 610s for our faintest. In the near-IR we observed in the J band with integration times that ranged from 20s with 5 coadds for our brightest targets to 130s with 8 coadds for our faintest. We acquired 5-7 near-IR images in a 10 $''$ dither pattern.

The optical ANDICAM data was processed with overscan subtraction and flat-fielding, prior to distribution. Initially we intended to use the near-IR data for parallaxes and the CCD data as a check on the astrometric quality. However, we quickly realized that the optical images were far superior to the near-IR, which were plagued with imaging artifacts, an occasional elongated PSF, and a smaller field of view (therefore fewer reference stars). As a result we report parallaxes in this paper based only on the optical imaging.

Infrared Side Port Imager (ISPI)

We collected parallax data for our faintest targets with the Infrared Side Point Imager (ISPI) on the CTIO 4m Blanco telescope van der Bliek et al. 2004). Observations were conducted over a period of just over 2 years (from early March 2008 through late April 2010) and 15 observing runs. As opposed

to ANDICAM, ISPI data were collected classically. All observations were carried out in the J band under seeing conditions up to $2''$ full width half maximum (FWHM) with typical conditions between 0.8-1.1$''$. Most of the parallax observations were made when the target was within $\pm$30 minutes of the meridian to minimize the corrections for DCR (see section 4.3.1 below). However, due to observational constraints (weather, instrument issues, etc) some targets were observed within $\pm$1 hr of meridian crossing.

ISPI has an $\sim$ 8 arcminute field of view and nominal plate scale of 0.303 $''$ /pixel. In order to minimize the effects of distortion and to ensure the same reference stars in each frame, we placed the target star on the same X,Y pixel position for each parallax frame. On the first observing run for a target, the frame was initially offset from the center of the chip to avoid the four-quadrant seam along the detector. This initial frame was used in all subsequent observing runs as a reference for determining where to place the parallax star.

Integration times were set by the magnitude of the target and the conditions at the telescope. They ranged from 30 to 60s with 5-10 coadds and 5-10 images in a 10 $''$ dither pattern. Depending on the weather and seeing conditions, the typical integration time was between 15-40 minutes.

Dark frames and lights on/off dome flats were obtained at the start of each evening. Reduction procedures were based on the prescriptions put together by the ISPI team[1] utilizing a combination of IRAF routines. J band flats were created by median combining the lights on and lights off images then subtracting the two. Bad pixel masks were created from a dome flat image. Individual parallax frames were flat-fielded and corrected for bad pixels with the resultant calibration images. All images were flipped to orient North up and East to the left using the IRAF routine *osiris* in the *cirred* package. Finally, the IRAF routine *xdimsum* was used to perform sky subtractions and mask resultant holes from bright stars.[2]

4.3 Parallax Pipeline

4.3.1 Source Extraction

Once all data were reduced, we used the Carnegie Astrometric Planet Search software (from here-on ATPa) to extract all point sources and solve

[1] *http* : *//www.ctio.noao.edu/instruments/ir_instruments/ispi/*

[2] We note that during observations the primary mirror would randomly slip causing he PSF to appear elongated. When this occured we would halt and restart an integration. The problem was sporadic but did not effect any of the final images.

for parallaxes (Boss et al. 2009). Images were not co-added, rather sources were extracted on every image at every dither position. We initiated the ATPa centroiding algorithm by (1) defining the FWHM of each set of images (2) defining the plate scale for the instrument and (3) designating the highest quality image in the set as a template. The ATPa algorithm first detected all point sources in the template image then used that list as a reference for detection in all subsequent images taken on a given night. The centroiding algorithm fit a one-dimensional PSF profile in both X and Y directions. A number of apertures (typically 3) spaced by 0.20 pixels were used to determine the centroid and the average was adopted as the final position.

Once sources were extracted we used custom IDL routine to refine the reference star list. We ensured that the target star was acquired in each frame and that spurious sources, such as cosmic rays or CCD artifacts, were not selected as reference sources. Each parallax frame had a text file associated with it (from now on referred to as plate files) containing, X, Y, and photometric information of at least 20-25 common reference stars. We compared the relative positions for all stars in an image and the scatter was used to estimate positional uncertainties for individual stars. The typical positional uncertainty for parallax targets in ISPI and ANDICAM was $\sim$0.01 pixels.

DCR corrections are typically required because the parallax star and reference stars have very different colors. As a result, their positions shift relative to one another due to different amounts of atmospheric refraction. The effect is wavelength, weather, and zenith distance dependent. Stone (1996, 2002) present a theoretical method for determining DCR effects. In that work, they demonstrated that maintaining small zenith distances, DCR effects in I and longer wavelengths (such as J) are minimal (typically < 1 mas). Similar results were found using the empirical methodology proposed by Monet et al. (1992). The low-mass star optical parallax program of Jao et al. (2005) and the brown dwarf optical parallax program of Dahn et al. (2002) also found negligible I band DCR corrections (typically < 1 mas) as did the near-IR T dwarf parallax program of Tinney et al. (2003). Therefore, DCR corrections are not applied to the positions in our pipeline. To ensure that even this small effect was minimized, we observed targets (with few exceptions) within $\pm$ 30 minutes of meridian crossing.

4.3.2 Parallax Solution

The reference stars in an image were used to transform the plate coordinates to sky coordinates and model the motion of each star. For this we used the Astrometric Iterative Solution available in the ATPa package. The solution was initiated with the right ascension (RA) and declination (DEC)

coordinates of the brightest star in the field. The highest quality image obtained for a given parallax source was used as the template frame to which everything was matched.

After one iteration a linear transformation was applied to each plate catalog to constrain the field rotation, plate scale and match all reference sources to the template. Higher order transformations were tested but yielded negligible differences from linear solutions in both ANDICAM and ISPI images. The apparent trajectory of each star was fit to a standard astrometric model included in the ATPa software. The algorithms follow the astrometric solution prescriptions laid out in the Hipparcos (Perryman et al. 1997) and Tycho Catalogue (Hog et al. 2000) descriptions[3]. A subset of well-behaved stars (RMS $<$ 5 mas and at least 5 observations) was chosen and the second iteration begun using those as reference point sources. All steps were automated and we set the number of total iterations to 3-5 and required at least 10 stars (typically 20) to converge upon the astrometric solution. The convergence was monitored by propagating the RMS positional uncertainty of all stars and determining the average RMS for the well-behaved reference sources.

The initial astrometric solution was used to identify the well-behaved stars and to ensure that the following objects were not used as solution sources: (1) the target parallax star, (2) high proper motion stars in the field, (3) saturated stars, and (4) elongated or extended sources (e.g. galaxies). The parallax plates were then processed a second time with an "exclusion" list of objects that were not to be used as reference stars.

The final catalog that was output by ATPa contained the following five astrometric parameters and their uncertainties: (1) X position, (2) Y position, (3) proper motion in RA (μ_α), (4) proper motion in DEC (μ_δ), and (5) parallax (π). It also contained information about the number of observations employed, the RMS of the residuals per epoch, and the reduced χ^2 of the astrometric solution for each star (Boss et al. 2009) :

$$\chi^2_\nu = \frac{1}{2N_{epochs} - N_{pars}} \sum_i^{N_{epochs}} \left[\frac{(x^i_{obs} - x_{model})^2}{\sigma_i^2} + \frac{(y^i_{obs} - y_{model})^2}{\sigma_i^2} \right] \qquad (4.1)$$

where N_{epochs} is the number of epochs, N_{pars} is the number of model parameters to be fit, x^i_{obs} and y^i_{obs} are the measured positions of the star in a local coordinate system, x_{model} and y_{model} are the positions predicted by the best fit model, and the summation is over all epochs. Each observation is weighted using its own standard deviation σ_i.

As described in Boss et al (2009), to ensure that the uncertainties in the

[3] $http://www.rssd.esa.int/SA/HIPPARCOS/docs/vol1_all.pdf$

parameters from the astrometric least squares solution were more realistic than the ones obtained using only the intra-night scatter, a small uncertainty was added in quadrature to the estimated uncertainty derived from the calibration step until an effective χ^2_ν=1 was obtained. The final uncertainty for the parallax star was obtained by adding the uncertainty of the least squares solution to the positional uncertainty for the parallax source.

4.3.3 Correction from relative to absolute parallax

The final parallaxes from the astrometric solution are relative to the motion of the background stars chosen as references. A correction is required based upon the true parallaxes of the reference stars to convert to an absolute measurement.

Typically there are three ways to convert from relative to absolute parallaxes: (1) using statistical methods which rely on a well-determined model of the Galaxy and is most relevant for faint distant reference stars, (2) spectroscopic parallaxes which rely on spectral data obtained for every reference star, or (3) photometric parallaxes for all reference stars. We determined the parallax corrections using the third method because the reference stars are primarily the brightest in the field and spectral data are not generally available for all stars in the field.

In order to measure photometric parallaxes for the reference stars we assume that all sources are main-sequence dwarfs. Following the prescription described in Vrba et al. (2004), we obtained 2MASS photometry for all reference stars then converted J,H,K_s values to California Institute of Technology (CIT) colors using the transformations detailed in Carpenter (2001). The CIT J-H and H-K colors were used to estimate spectral types of the background stars based on the relations detailed in Bessell & Brett (1988) for main sequence dwarfs. Absolute V magnitudes were taken from color spectral type relations described in Kitchin (2004) and then converted to M_J and M_K via the Bessell & Brett (1988) calibrations[4]. Distances to reference stars were determined by averaging $(m\text{-}M)_J$ and $(m\text{-}M)_K$ values which were typically in good agreement.

Each reference star was given equal weight in the astrometric solution. As a result we averaged the parallaxes in mas to calculate the distance correction and used a standard deviation of the mean for the correction uncertainty. We added the distance correction to our relative parallax and added the correction uncertainty in quadrature with our parallax uncertainty to obtain the final

[4]To our knowledge there is no relation for directly converting from JHK values to M_{JHK} and spectral type.

absolute parallax. The average correction to absolute parallax for the full list of targets is 2.3±0.3 mas ranging from [0.9,4.0] mas. See Table 4.2 for the final parallaxes with absolute corrections.

4.3.4 Comparison of Calibrators

There were 9 calibrator stars in our full astrometric sample; 4 imaged with ISPI and 5 imaged with ANDICAM, that we obtained as a check on the reliability of our methods. Table 4.3 lists the astrometry for the calibrators measured in this work and compares those values with previous results reported in the literature (see Figure 4.1). For our calibrators we chose primarily nearby brown dwarfs with J band magnitudes comparable to our sources. Of the 9 calibrators, 6 match within 1 σ and all match within 2σ. The mean difference and scatter between literature and BDKP values is 0.11± 3.6 mas. No systematic trends are detected in the parallax measurements. This indicates that our parallax pipeline with conversion to absolute parallaxes produces reliable results.

As a check on non-calibrator stars we show how well the proper motion values match literature values for all sources in our sample (see Table 4.1 for references). The two lower panels in Figure 4.1 show plots of μ_α and μ_δ from the literature versus our calculated values with uncertainties. We find that 30% of the sample match both components within 1σ, 63% match within 2σ, 82% match within 3σ and all match within 4σ. The mean difference between μ_α and μ_δ values was 2.2±32.0 mas and -1.6±29.6 mas respectively and no systematic trends were detected between values. This is significantly different from a Gaussian error distribution. The deviation from a Gaussian distribution could indicate an underestimation of uncertainty in either literature values or within our astrometric solution.

4.4 Absolute Magnitude Relations

As of June 2010 there were 81 L and T dwarfs with published parallax measurements. We have added 65 to this list, doubling the number of measurements in some spectral bins (see Table 4.4). With a substantial increase in the number of measurements, we can re-evaluate the color-magnitude and spectral type-magnitude trends originally defined by Dahn et al (2002), Tinney, Burgasser, & Kirkpatrick (2003), and Vrba et al (2004), particularly across the poorly sampled L/T transition region.

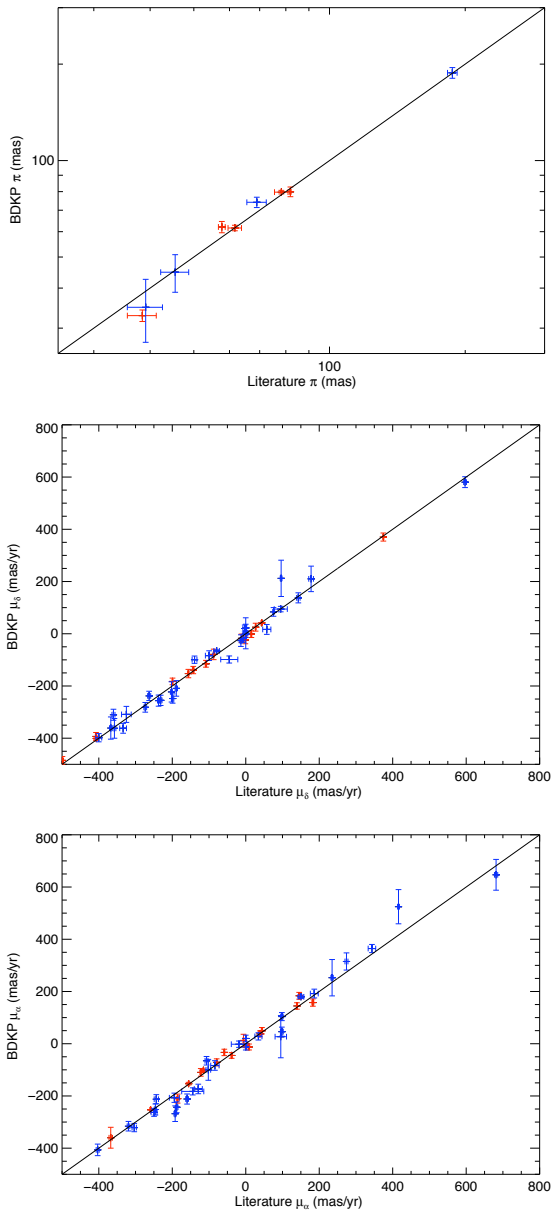

Figure 4.1: Top plot: The parallax measurement comparison of the 9 calibrator dwarfs. Middle and lower plots: Comparison of literature proper motion components to those measured in this work. In each plot blue crosses represents dwarfs that were measured with ISPI and red crosses were measured with ANDICAM.

Table 4.3. Astrometric Calibrators

Name	π_{abs} (mas) (BDKP)	μ_α $''$yr^{-1} (BDKP)	μ_δ $''$yr^{-1} (BDKP)	π_{abs} (mas) (Lit)	μ_α $''$yr^{-1} (Lit)	μ_δ $''$yr^{-1} (Lit)	Inst.[a]	ref
(1)	(2)	(3)	(4)	(5)	(6)	(7)	(8)	(9)
LHS 1777	79.71 ± 1.02	-155.49 ± 1.10	951.02± 1.00	78.20± 2.70	-153.00± 5.00	957.00± 5.00	A	1
				79.72± 1.89				2
				80.11± 2.34				3
WT 248	32.82± 1.36	-1223.26± 1.74	-108.36± 1.74	38.44± 2.83	-1191.00± 13.00	-115.00± 13.00	A	1
2MASS J0746+2000	79.93± 2.78	-324.75± 3.22	-68.66± 3.37	81.90± 0.30	-374.04± 0.31	-57.91± 0.65	A	4
2MASS J0850+1057	34.85± 7.75	-144.17± 5.29	-37.70± 5.30	39.10± 3.50	-144.50± 2.00	-7.57± 2.27	I	4
2MASS J0939-2448	187.88± 7.20	548.88± 3.39	-1067.96± 2.41	187.30± 4.60	573.40± 2.30	-1044.70± 2.50	I	6
2MASS J1058-1548	62.05± 2.52	-259.14± 2.03	43.54± 2.01	57.70± 1.00	-252.93± 0.50	41.42± 0.45	A	4
2MASS J1444-2019	61.61± 1.22	-2905.12± 0.97	-1953.86± 1.01	61.67± 2.12	-2906.15± 2.41	-1963.12± 2.71	A	7
SDSS J1446+0024	44.84± 6.02	150.27± 7.84	-79.24± 7.47	45.46± 3.25	179.60± 6.68	-65.58± 4.07	I	5
2MASS J2356-1553	74.11± 2.75	-417.99± 5.01	-618.16± 6.24	68.97± 3.42	-443.44± 2.07	-600.15± 2.48	I	5

[a]A=ANDICAM and I=ISPI

References. — 1=Yale Trigonometric Parallaxes, van Altena 1995, 2=CTIOPI Jao et al 2005, 3=Costa et al. 2005, 4=Dahn et al 2002, 5=Vrba et al. (2004), 6=Burgasser et al. (2008b), 7=Schilbach et al. (2009)

Table 4.4. Absolute Magnitudes

Spectral Type (1)	BDKP (2)	Literature (3)	Total[a] (4)	Binaries (5)	M_J (6)	M_H (7)	M_K (8)
M6	0	8	8	0	10.23 ± 0.43	9.67 ± 0.42	9.33 ± 0.41
M7	0	4	4	0	10.93 ± 0.20	10.28 ± 0.13	9.90 ± 0.09
M8	0	6	6	0	10.99 ± 0.75	10.30 ± 0.71	9.87 ± 0.67
M9	1	2	3	0	11.74 ± 0.54	11.06 ± 0.62	10.58 ± 0.62
L0	0	6	6	2	11.69 ± 0.25	11.05 ± 0.19	10.51 ± 0.21
L1	3	4	7	0	12.39 ± 0.64	11.41 ± 0.43	10.80 ± 0.46
L2	4	2	6	2	12.89 ± 0.09	12.13 ± 0.13	11.49 ± 0.22
L3	1	5	6	2	12.93 ± 0.21	12.10 ± 0.17	11.36 ± 0.11
L4	0	4	4	1	12.90 ± 0.55	12.01 ± 0.36	11.03 ± 0.40
L5	2	5	7	2	13.37 ± 0.53	12.50 ± 0.45	11.81 ± 0.40
L6	4	3	7	2	14.48 ± 0.46	13.48 ± 0.45	12.27 ± 0.50
L7	5	7	12	5	14.86 ± 0.39	13.82 ± 0.37	13.03 ± 0.39
L8	1	9	10	1	14.64 ± 0.33	13.70 ± 0.30	13.00 ± 0.33
T0	1	0	1	0	0.00 ± 0.00	0.00 ± 0.00	0.00 ± 0.00
T1	1	2	3	1	15.36 ± 0.54	14.77 ± 0.62	14.32 ± 0.56
T2	3	2	5	1	14.54 ± 0.18	13.77 ± 0.17	13.69 ± 0.13
T3	1	2	3	1	14.54 ± 0.42	14.23 ± 0.35	14.16 ± 0.24
T4	3	1	4	0	14.37 ± 0.44	13.90 ± 0.18	14.23 ± 0.34
T5	6	3	9	1	14.88 ± 0.22	15.05 ± 0.23	15.08 ± 0.29
T6	3	8	11	1	15.36 ± 0.38	15.70 ± 0.41	15.77 ± 0.54
T7	3	5	8	1	15.96 ± 0.60	16.42 ± 0.58	16.63 ± 0.81
T8	3	3	6	1	16.53 ± 0.79	16.91 ± 1.02	17.04 ± 1.48

[a] All low-gravity and subdwarfs are excluded from totals. Four objects, 2MASS J2043-1551, 2MASS J1764+1649, 2MASS J1511+0607, and SDSS 1110+0116, have been disregarded because they are suspiciously over or under-luminous sources

4.4.1 Absolute Magnitude/Spectral Type Relations

Color-magnitude diagrams and spectrophotometric relations are used to investigate physical parameters that influence brown dwarf evolution and to establish distances for spectroscopically confirmed objects. All brown dwarfs have highly structured energy distributions, and magnitudes in JHK are extremely sensitive to the exact filter bandpass used. Therefore, we converted all magnitudes onto the Mauna Kea Observatory filter set (MKO; Tokunaga et al. 2002), whose narrow bandpasses are less affected by atmospheric absorption than the CIT and 2MASS filter sets (particularly at J). If required, the transformations from Stephens & Leggett (2004) were used to convert from 2MASS to MKO magnitudes.

Most of the L dwarfs in our sample were classified spectrally from red optical data following the scheme of Kirkpatrick et al. (1999), while the T dwarfs were largely classified in the near-IR (Burgasser et al. 2006). An optical spectral type was used for any object classified as an L dwarf and a near-IR spectral type was used for any object classified as a T dwarf. For any L dwarf lacking optical data we used its near-IR spectral type.

We combined our parallax measurements from this work with all previous measurements, excluding known binaries, and objects classified as either low-surface gravity dwarfs or subdwarfs, and re-examined absolute magnitude trends and dispersions. Figure 4.2 shows the M_{JHK} sequences. Only objects with M_{JHK} uncertainties < 0.3 mag are shown. Table 4.4 shows the median absolute MKO J, H, and K magnitude values and their scatter for L0-T8 dwarfs (binned by 1 spectral type). Two objects, 2MASS J2043-1551 and 2MASS J 1754+1649, are significantly under-luminous. Two other objects, 2MASS J1511+0607 and SDSS 1110+0116, are over-luminous with the former is suspected to be a close binary (Burgasser et al 2010). These objects are discussed in detail in section 4.8.3 below.

We have used our new parallaxes to revisit the usefulness of spectrophotometric relations as predictors of absolute magnitude for field dwarfs that lack parallax measurements. Table 4.5 lists the coefficients of a sixth order polynomial fit to MKO JHK absolute magnitudes (excluding binaries, low-surface gravity dwarfs, and subdwarfs). Among the three near-IR bands, we find K band is the most reliable near-IR relation to use for absolute magnitudes. The RMS scatter is equivalent for all bands in Table 4.4, but the significant and still poorly understood transition bump is least prominent in K (see this section). We have used resolved photometry for 8 of the L/T transition binaries for a more detailed look at the spectrophotometric relation. Two known binary sources, 2MASS J0518-2828 and 2MASS J1404-3159, had parallax measurements reported in this work as did one suspected binary 2MASS J1511+0607

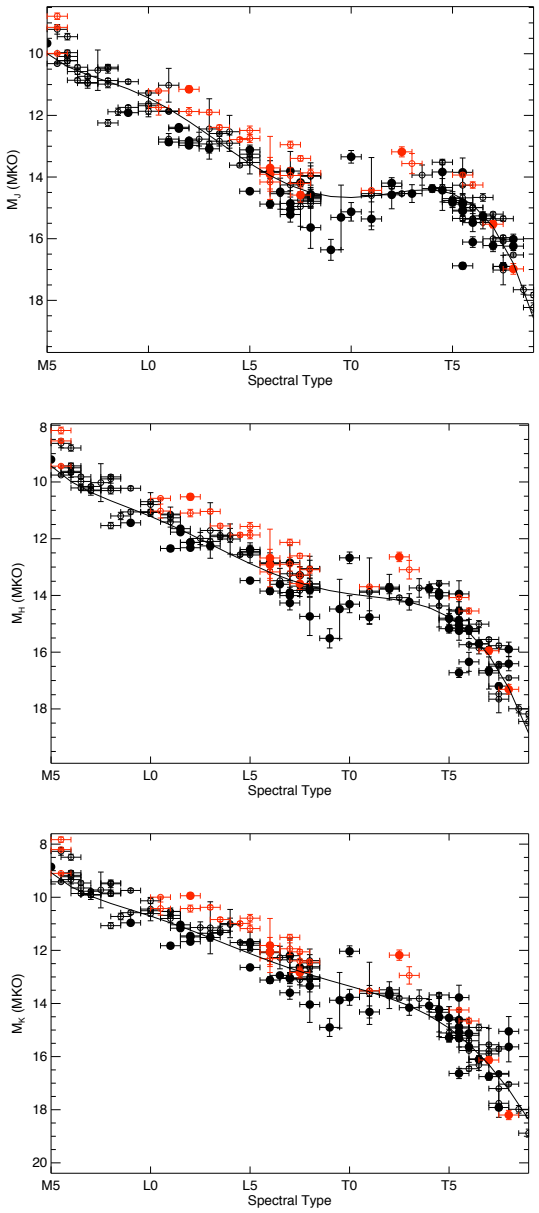

Figure 4.2: Spectral type versus absolute magnitude in the MKO J, H, and K filters for late-type M through T dwarfs. Unfilled circles are ultracool dwarfs with parallax measurements gathered from the literature. Filled circles are ultracool dwarfs with parallaxes measured in this work. Red symbols represent known binaries. Overplotted on each is the best fit polynomial (see Table 4.5).

Table 4.5. Coefficients of Polynomial Fits for L0 -T8 Dwarfs

MKO Filter (1)	c_0 (2)	c_1 (3)	c_2 (4)	c_3 (5)	c_4 (6)	c_5 (7)	c_6	rms
M_J	-1.578	5.480	-9.937E-1	9.048E-2	-4.087E-3	8.622E-5	-6.516E-7	0.32
M_H	-1.594	4.841	-8.105E-1	7.094E-2	-3.177E-3	6.814E-5	-5.364E-7	0.32
M_K	-1.672	4.721	-7.934E-1	7.034E-2	-3.271E-3	7.556E-5	-6.749E-7	0.32
M_J[a]	-2.059	5.417	-9.484E-1	8.662E-2	-4.042E-3	9.074E-5	-7.649E-7	0.32
M_K[a]	-1.673	4.722	-7.936E-1	7.035E-2	-3.272E-3	7.557E-5	-6.750E-7	0.32
$M_{3.6}$	3.260	1.155	-6.163E-2	1.269E-3	—	—	—	0.17
$M_{4.5}$	3.784	9.910E-1	-4.640E-2	8.315E-4	—	—	—	0.11
$M_{5.8}$	2.185	1.402	-7.881E-2	1.569E-3	—	—	—	0.17
$M_{8.0}$	1.475	1.489	-8.233E-2	1.587E-3	—	—	—	0.17

[a]Including 8 L/T transition binaries with resolved photometry: SD0423-0414, 2M0518-2828, SD1021-0304, 2M1404-3159, 2M1711+2232, SD1511+0607, epsIndi, SD1534+1615

Note. — Polynomial fits to optical L dwarfs and NIR T dwarfs (L dwarfs with no optical spectral type have NIR spectral types) excluding subdwarfs, low gravity dwarfs, and binaries. Function is defined as $M_{J,H,K}=\sum_{i=0}^{n} c_i(\mathrm{SpT})^i$ and is valid for spectral types L0-T8 where 10=L0, 20=T0, etc.

(Burgasser et al 2010). The polynomial fit for this sample is listed in Table 4.5 and demonstrated in Figure 4.3.

The initial JHK-SpT relations for brown dwarfs set by Vrba et al. (2004) used a linear fit for L0 to L8 dwarfs and a second order polynomial fit for T0.5 to T8 dwarfs. Subsequently a number of objects were found to be unresolved binaries. Liu et al (2006) re-visited the relations and derived two polynomial fits, one excluding all resolved binary systems and potential candidates and one excluding only the former. Most recently, Looper et al (2008) re-visited the absolute magnitude relations and found a sixth-degree polynomial fit for L0 to T8 dwarfs. The scatter in M_J,M_H,M_K in that work was 0.29,0.29, and 0.33 respectively, similar albeit slightly smaller than what we found for a larger sample.

We also examined the absolute magnitude/spectral type relations in the mid-IR Spitzer (IRAC) bands using source photometry from Leggett et al (2010) and Patten et al (2006). Only a small percentage of the full astrometric sample has reported mid-IR photometry but we have included the coefficients to a third order polynomial fit in Table 4.5. Figure 4.4 shows the $IRAC$ color sequence vs. spectral type. Spectrophotometric scatter is smallest in the $M_{4.5}$ as noted by Warren et al 2007, Stephens et al 2009, and Leggett et al 2010. With decreasing temperature, the coldest brown dwarfs emit significant portions of their light in mid-IR wavelengths. Leggett et al (2010) noted that

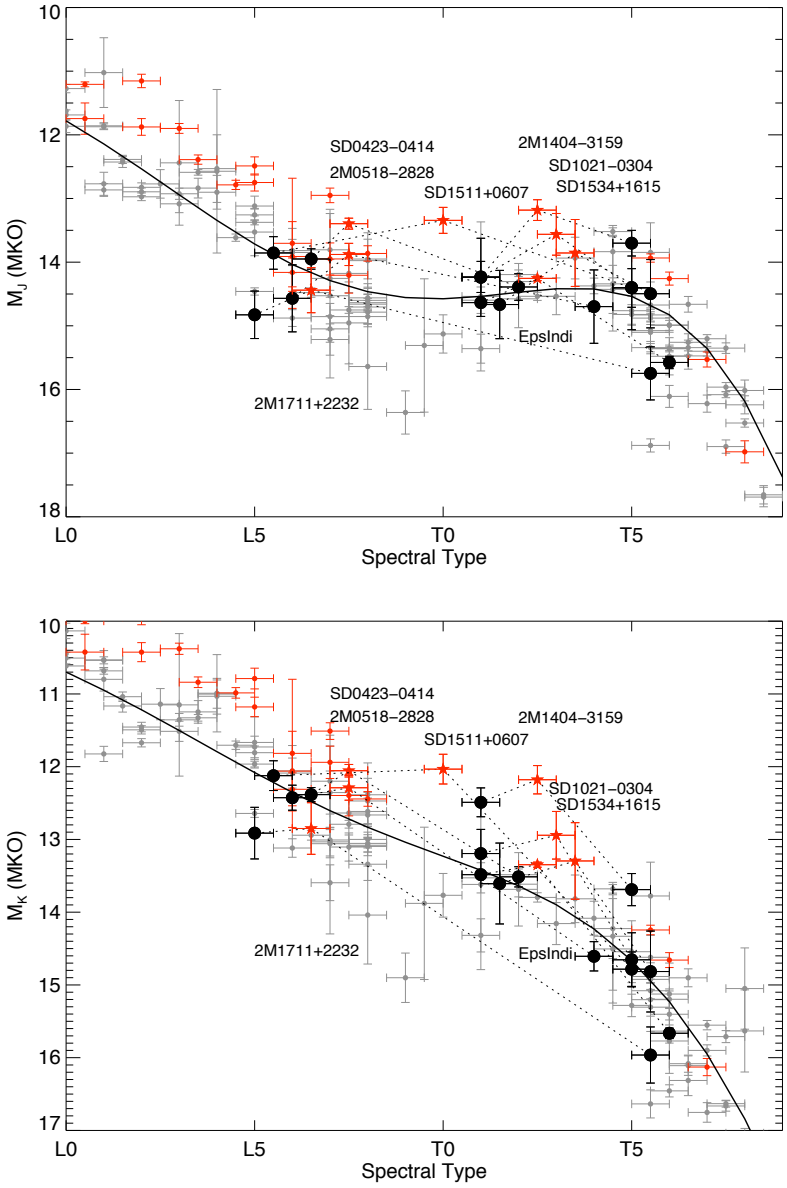

Figure 4.3: Spectral type versus absolute magnitude in the MKO J, and K filters for L and T dwarfs with resolved binary components. Light grey filled circles represent field dwarfs (excluding subdwarfs and low surface gravity objects). Red symbols are known binaries with five point stars representing L/T transition binaries with resolved photometry. Black filled circles are the subsequent resolved absolute magnitudes of the binary components. Overplotted on each panel is the best fit polynomial (see Table 4.5).

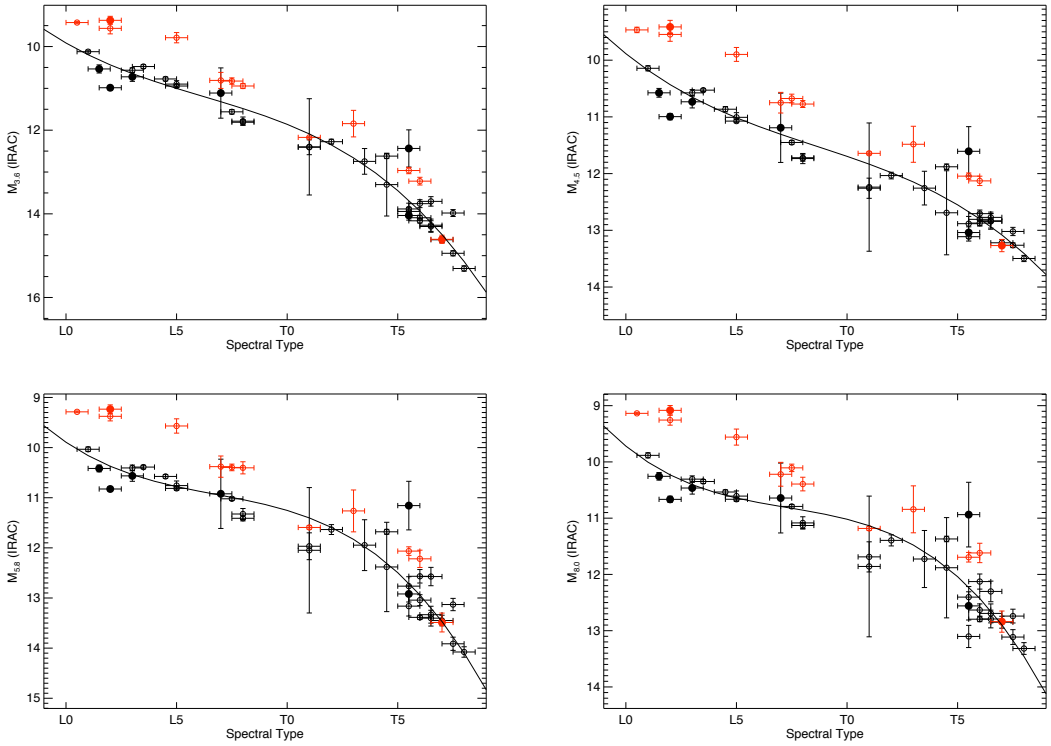

Figure 4.4: Spectral type versus absolute magnitude in the *IRAC* 3.6, 4.5, 5.8, and 8.0 filters for L and T dwarfs. Unfilled circles are ultracool dwarfs with parallax measurements gathered from the literature. Filled circles are ultracool dwarfs with parallaxes measured in this work. Red symbols represent known binaries. Overplotted on each is the best fit polynomial (see Table 4.5).

the drop in luminosity was much milder in the mid-IR than in the near-IR. We confirm this trend.

The brightening of early T dwarfs is most apparent in J where there is a 1 mag difference between mean M_J at T1 (mean M_J=15.36±0.54) to the M_J maximum at T4 (mean M_J=14.37±0.44). At H there is a similar although less significant (0.8 mag) brightening. At K the brightening has largely turned into a plateau between T1 and T4; although there is a 0.6 magnitude brightening between T1 and T2 dwarfs. L8 dwarfs have a surprisingly tight spread in each filter (0.33, 0.30, 0.33 in J, H, and K respectively) even though they are the gateway to the J band brightening.

In general, the loci for L dwarfs is tighter at J (median σ_J of 0.39 compared to 0.47), H (median σ_H of 0.32 compared to 0.47), and K (median σ_K of 0.34 compared to 0.57) than for the T dwarf sequence. Unresolved binarity or

significant variations in the age, metallicity, and/or atmospheric properties of the T dwarfs compared to the L dwarfs could account for the difference in spreads. Vrba et al (2004) found a broader distribution in v_{tan} values for the T dwarfs in their astrometric sample compared to the L dwarfs hinting that the T dwarfs were kinematically older than the L dwarfs. Leggett et al (2010) and Patten et al (2006) found evidence for significant gravity effects on the latest-type T dwarf samples.

As temperatures cool among the T dwarfs, there is a significant increase in the M_{JHK} scatter for the latest spectral types. The T8 dwarfs have the largest spread in all bands (σ_J=0.79; σ_H=1.02; σ_K=1.48). There are 5 objects included in the mean and spread calculation for this bin and those are broken down into 3 T8.0 dwarfs and 2 T8.5 dwarfs. If we narrow down the calculation to half bins and compare the T8.0 to the T8.5 we find that the scatter diminishes to σ_J=0.26; σ_H=0.50; σ_K=1.02 for T8.0 objects and σ_J=0.03; σ_H=0.20; σ_K=0.35 for T8.5 dwarfs. This indicates that temperature differences between late T-dwarf subtypes are more pronounced than for early T's or L dwarfs. As noted in the literature, significant temperature changes may not cause large enough spectral variations to warrant a later spectral type (Warren et al. 2007; Burningham et al. 2009).

4.4.2 Color-Magnitude Trends for L and T dwarfs

We have collected photometric information for all known L and T dwarfs with parallaxes, totaling 146 (see Tables 4.1 - 4.2). We examined various combinations of optical, near-IR and mid-IR colors to find the color-magnitude diagrams that provided the strongest insight into differentiating brown dwarf spectral types and/or physical properties of the population. Figures 4.5 - 4.7 show some of those diagrams. The colors demarcate L0-L4 dwarfs (red filled circles), L5-L8 dwarfs (blue filled circles), T0-T4 dwarfs (purple filled circles), and T5-T8/T9 dwarfs (black filled circles).

We found three prominent trends among the various color plots. The first are color vs. absolute magnitude diagrams that can be categorized as tightly correlated in a (generally) monotonic relationship. Figure 4.5 shows two representative examples. Patten et al (2006) found a relatively smooth progression of M through T dwarfs in the M_{K_s} versus K_s-[4.5] diagram. We verify that this relation separates the early and mid L dwarfs ($0.5 < K$-[4.5] < 1.4) from the early and mid T dwarfs ($1.2 < K$-[4.5] < 3.8). However, it does not show a monotonic progression with the later T dwarf spectral types. The degeneracy is most clearly depicted for the T6.0 and T6.5 dwarfs which show a nearly 2.0 mag spread in K-[4.5] color. We also show the M_H versus H-[4.5] diagram (bottom panel of Figure 4.5) as this color is a good tracer of effective temper-

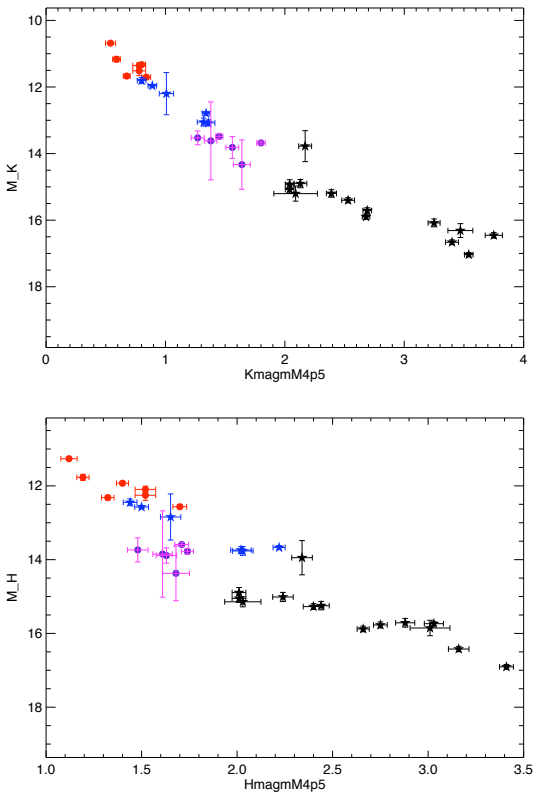

Figure 4.5: Color-Magnitude diagrams for L and T dwarfs with measured parallaxes. The M_K vs. K-[4.5] and M_H vs H - [4.5] demonstrate the tight transition between L and T dwarfs. L0-L4 dwarfs are red filled circles, L5-L8 dwarfs are blue filled circles, purple filled circles are T0-T4 dwarfs, and black filled circles are the latest type T dwarfs (T5-T8).

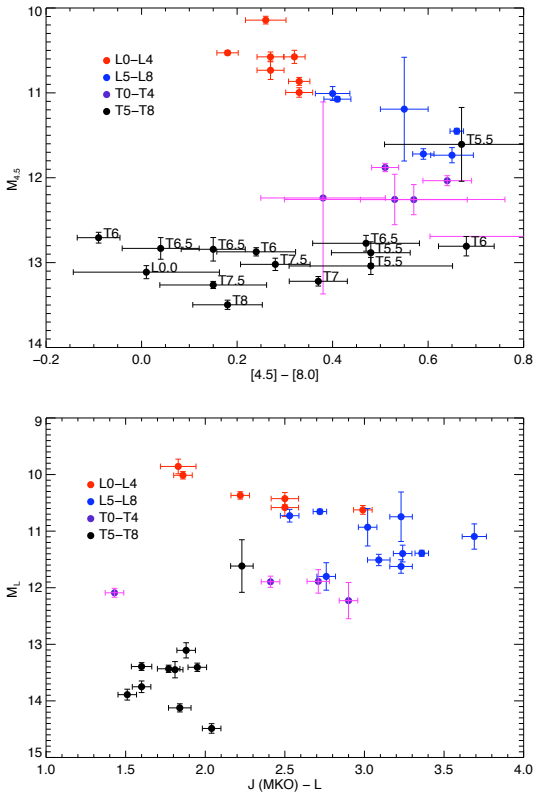

Figure 4.6: Color-Magnitude diagrams for L and T dwarfs with measured parallaxes. The $M_{[4.5]}$ vs. [4.5]-[8.0] and M_L vs J - L demonstrate the color reversal seen between the L dwarf and T dwarf sequences. L0-L4 dwarfs are red filled circles, L5-L8 dwarfs are blue filled circles, purple filled circles are T0-T4 dwarfs, and black filled circles are the latest type T dwarfs (T5-T8).

ature for the coldest brown dwarfs (Warren et al 2009; Stephens et al 2009; Leggett et al 2010). The early to mid L dwarfs are nearly monotonic on this figure as are the latest T dwarfs; however L7.5 through mid T dwarfs show near constant M_H as the H - [4.5] color gets increasingly blue before reddening through the mid to late T dwarfs. Interestingly, these two color-magnitude diagrams are strikingly different from the J - [4.5] plot shown in Figure 4.7 indicating that they are less sensitive to gravity, metallicity, or atmospheric changes.

The second prominent trend is a color reversal as objects transition from L into T dwarfs. The most studied version of this trend is the J - K color reversal discussed in Section 4.5 below. Figure 4.6 shows two other representative examples. The top panel of Figure 4.6 shows the $M_{4.5}$ versus [4.5] - [8.0] color and the bottom shows the M_L versus J - L color. Condensate cloud opacity is likely the dominate contributor to the increasingly red colors of L dwarfs. In Figure 4.6, the effect is much more pronounced in the near-IR (2.5 mag spread) as opposed to the mid-IR (0.5 mag spread) demonstrating that atmospheric changes accompany this trend. As temperatures drop into the T dwarf regime, clouds clear causing a brightening in J as well as [4.5] while CH_4 and H_2O absorption remove significant flux in both L and [8.0] causing the color reversal (Cushing et al 2006; 2008). This is enhanced in the [4.5]-[8.0] color as there is a strong CO feature in the [4.5] band which remains relatively constant with decreasing temperature. In the top panel of Figure 4.6, it is interesting to note the near-uniform $M_{4.5}$ magnitude for the late T dwarfs as the [4.5] - [8.0] color becomes increasingly blue.

The third prominent trend of color-magnitude diagrams is two parallel linear sequences for the L and T dwarfs, with L-T transition objects curving back on themselves. The two sequences are similar in color but the L dwarfs are generally 2-3 magnitudes brighter than the T dwarfs. Figure 4.7 shows two representative examples of this case. The top plot shows the M_J versus J-[4.5] diagram with the L dwarf sequence brighter but separated from the T dwarf sequence. The bottom plot shows the $M_{3.6}$ versus H-[3.6] diagram demonstrating larger scatter among the late-type T dwarf colors but a larger magnitude break between L and T dwarfs. As in the above color reversal trend, the L dwarfs redden through the later spectral types due to condensate opacity removing significant flux in the near-IR. At the L/T transition, clouds disperse and objects brighten in J and H band just as CH_4 absorption begins to remove significant flux in the [3.6] and some portion of the [4.5] bands. Contrary to what happens in the color reversal described above, a significant fraction of the flux shifts to mid-IR wavelengths for the T dwarfs (see Leggett et al 2010) causing them to once again redden with decreasing temperature.

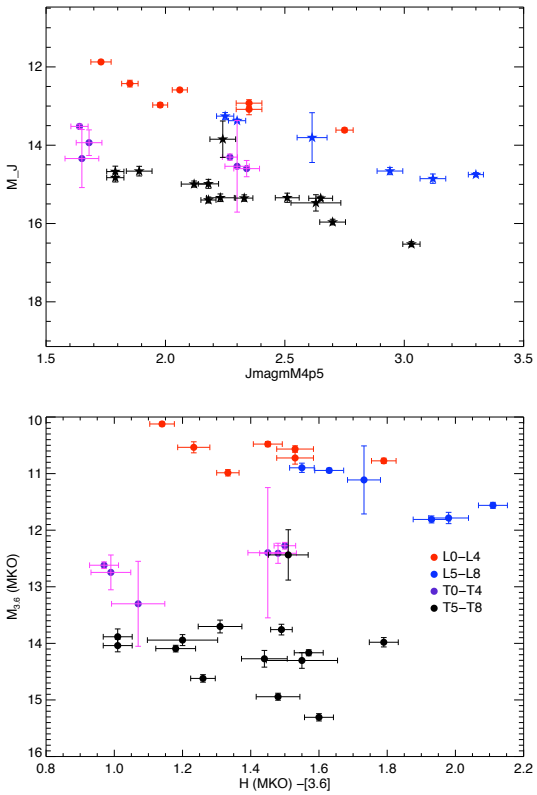

Figure 4.7: Color-Magnitude diagrams for L and T dwarfs with measured parallaxes. The M_J vs. J-[4.5] and $M_{[3.6]}$ vs H - [3.6] demonstrate the L dwarf and T dwarf sequences with similar slopes, separated by 1-2 magnitudes. L0-L4 dwarfs are red filled circles, L5-L8 dwarfs are blue filled circles, purple filled circles are T0-T4 dwarfs, and black filled circles are the latest type T dwarfs (T5-T8).

4.5 Comparison to Evolutionary Models

To put the observed trends on color-magnitude diagrams in context, we compared the data to two sets of evolutionary models. Saumon & Marley (2008) present a set of evolutionary models that include a cloud sedimentation parameter which can be varied to explain (with different levels of accuracy) the near-IR color magnitude diagram for L and T dwarfs. Burrows et al (2006) present a model for refractory clouds as well as a completely cloudless model with varying gravity and metallicity parameters. In Figures 4.8 and 4.9 we examine the M_K vs. J-K diagram for L and T dwarfs using the full sample with trigonometric parallaxes and the respective evolutionary models. In Figure

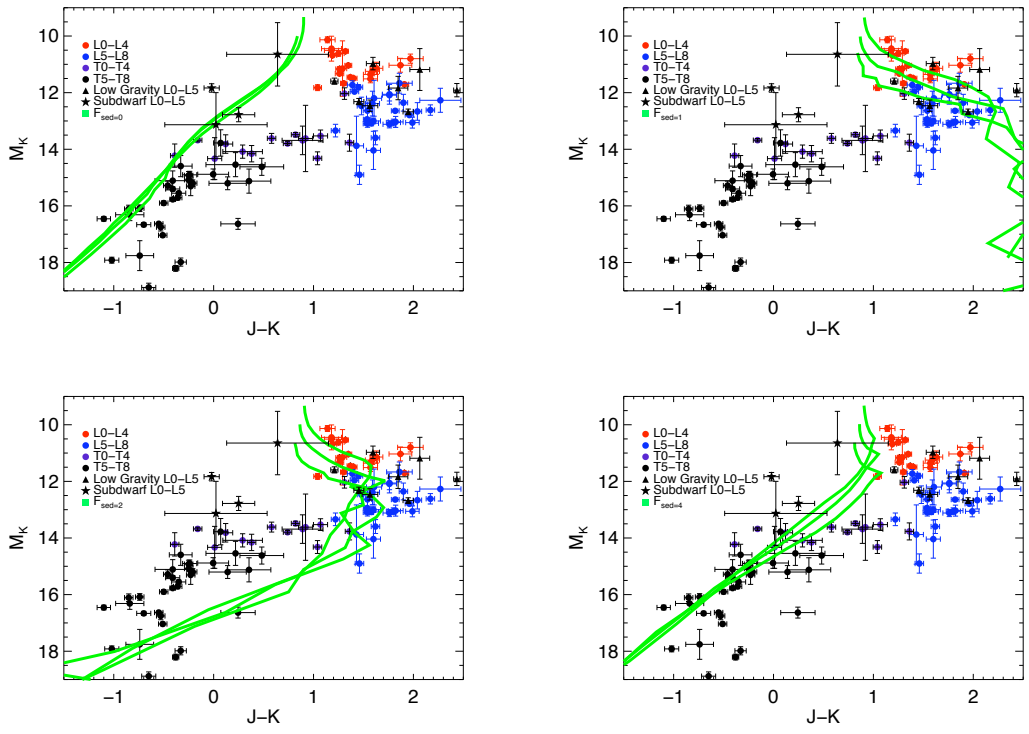

Figure 4.8: The M_K vs J-K diagram for L and T dwarfs with the evolutionary models of over-plotted. Varying the cloud thickness parameter f_{sed} fits the L and T dwarf sequences with varying degrees of accuracy.

4.8 the sedimentation parameter (f_{sed}) from Saumon & Marley (2008) is shown with increasing value to represent decreasing cloud thickness. In Figure 4.9 the metallicity and gravity are varied using the clear model (upper left panel) and refractory cloud model (three remaining panels) of Burrows et al (2006). All early and late-type L and T dwarfs, low-surface gravity objects, and subdwarfs with trigonometric parallaxes ($\sigma_{M_K} < 0.3$ mag) are over-plotted.

4.5.1 L Dwarfs

Varying gravity and metallicity within the cloud model of Burrows et al (2006) encompasses the majority of early L dwarfs (top right and bottom two panels of Figure 4.9); however, late-type L dwarfs are still poorly represented. Compared to the highest gravity, super solar metallicity track, there are a number of late-type L dwarfs that are fainter and redward of predictions. In Figure 4.8, the L dwarf sequence is best modeled with the f_{sed}=1,2 parameters

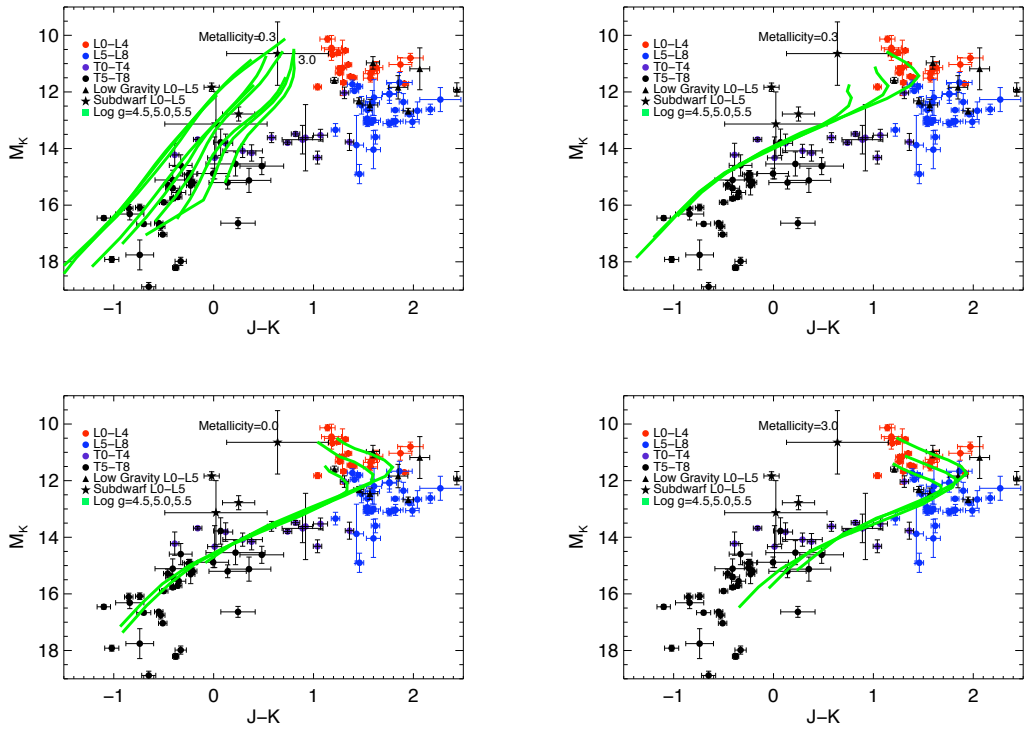

Figure 4.9: The M_K vs J-K diagram for L and T dwarfs with the evolutionary models of Burrows et al. (2006) over-plotted. Varying the metallicity and gravity fits the L and T dwarf sequences with varying degrees of accuracy.

(top and middle plot of Figure 4.8). There are a handful of red or potentially "ultra-cloudy" objects that are not fit by the models. Significant outliers include 2MASS J1442+6603, which is a close (∼30 AU) companion to the M1.5 dwarf G239-25 (Forveille 2004), and 2MASS J0619-5802 which is a companion (∼260 AU) to the young K2 star AB Pic (Chauvin et al 2005). 2MASS J1841+3117 is also significantly redward of the models. It is classified as an L4pec by Kirkpatrick et al (2000) because it shows feature strengths that match an L4 but its optical color (between 6300 and 10000A) is too blue.

T Dwarfs

The mid to late-type T dwarfs are best fit using the clear model from Burrows et al (2006) and the f_{sed}=4 track from Saumon & Marley (2008). In the case of the latter model (bottom right panel of Figure 4.8) the predicted range in both M_K and J-K shows very little spread whereas empirical measurements show significant scatter. There are a handful of T dwarfs including 2MASS J1114-2618, ULAS J0034-0052, and 2MASS J1754+1649 which are notably under-luminous and red compared to the f_{sed}=4 model predictions. The colors of these late-type T dwarfs are better fit by the f_{sed}=2 parameter (thicker clouds) which also encompasses the majority of mid to late-type L dwarfs. Comparing the spread to the Burrows et al (2006) clear model (top panel of Figure 4.9) predictions show similar red, under-luminous outliers. The solar and super solar metallicity tracks on the cloud model (bottom panels of Figure 4.9) fit a portion of the late-type T dwarfs but significant outliers remain. Inconsistencies with both models indicates that thick condensate clouds might continue to play a role in the photospheres of cooler dwarfs (see discussion in Burgasser et al. 2010b, Marley et al. 2010). Measurements of the age of each of these individual objects would prove useful as Burgasser et al. (2010b) suggests that thick clouds could explain spectral features of the low-surface gravity (young) T dwarf Ross 458C.

4.5.2 L/T Transition Dwarfs

The L-T transition objects can not all be fit by a single f_{sed} parameter using the Saumon & Marley (2008) models nor by any single combination of gravity and/or metallicity on the Burrows et al (2006) models[5]. To address this problem we created a hybrid cloud model using the Saumon & Marley tracks. Similar to the work of Burgasser et al. (2002b) we varied the sedimentation parameter between the f_{sed}=2 and f_{sed}=4 models across the region

[5]Burrows et al 2006 also note that variations in cloud particle size can not account for the transition objects.

between 13.0< M_K < 15.0. We started with the f_{sed}=2 color, then added the f_{sed}=4 color in 10% increments across the transition. The result is plotted in Figure 4.10. The L-T transition objects lie within an absolute magnitude range corresponding to model temperatures spanning ±150 K from a mean T_{eff} that depends on the log(g) chosen.

The steady and significant decrease in $J-K$ color with near constant M_K for the objects in the transition region indicates (as noted in Burgasser et al 2002 and Knapp et al 2004) that the clearing of clouds or change in cloud thickness could explain a large part of the J band brightening. Two objects, 2MASS J0559-1404 and SDSS J0830+0128, are blueward of the hybrid model predictions and brighter by nearly a magnitude at M_K than the late-type T dwarf sequence. 2MASS J0559-1404 has been examined with HST for a near-equal mass companion to explain its over-luminosity but nothing has been resolved (Burgasser et al. 2003c, Zapatero Osorio et al. 2007[6]). SDSS J0830+0128 has no spectral peculiarities noted within the literature.

4.5.3 L Subdwarfs

The four L subdwarfs with measured parallaxes demonstrate a range in color. The Burrows et al (2006) models account for variations of both metallicty and gravity parameters. Three of the subdwarfs, 2MASS J0616-6407, 2MASS J0532+8246, and 2MASS J1256-0224 are fit with the clear model in the upper right panel of Figure 4.9; however their large uncertainties preclude distinguishing between metallicities. The L4 subdwarf 2MASS J1626+3925 fits nicely along the subsolar metallicity track of the clear model. L subdwarf fits to the clear vs cloudy model indicates that cloud coverage may be correlated with age. Younger L dwarfs might be dustier than older subdwarfs (see section 4.6 below). However, we note that the low-metallicity is also driving the cloudless properties (see Burgasser et al (2003, 2007); Gizis & Harvin 2006).

4.6 Low Surface Gravity Dwarfs

A subset of the parallax sample are the low surface gravity dwarfs. Within this subsample there are 10 M dwarfs and 7 L dwarfs. Their optical spectra are characterized by unusual spectral features such as weak FeH absorption, weak Na I and K I doublets and very strong vanadium oxide bands which imply low surface gravities (Cruz et al. 2009; Allers et al. 2010; Allers et al.

[6]The Zapatero Osorio et al. (2007) null detection was using radial velocity variability

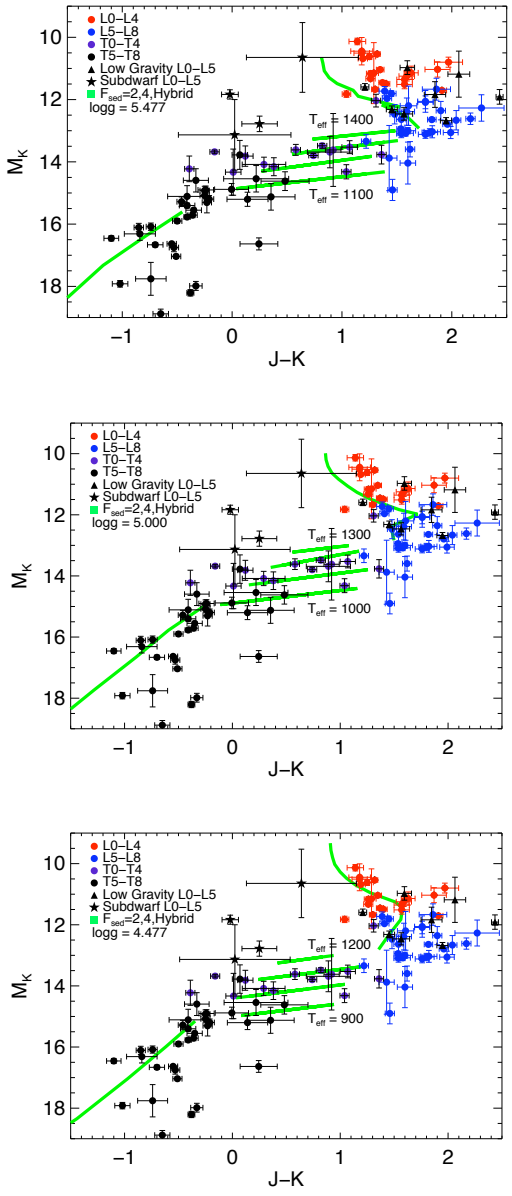

Figure 4.10: The M_K vs J-K diagram for the evolutionary models of Saumon & Marley 2008 over-plotted using the best-fit for the late-type L and T dwarfs (f_{sed}=2,4 respectively) and our hybrid model created by varying the cloud thickness between the two in 10% increments.

Table 4.6. Low Gravity Dwarfs

Name (1)	Spt (2)	M_J (3)	M_H (4)	M_K (5)	Δ_{M_J} [a] (6)	Δ_{M_H} [a] (7)	Δ_{M_K} [a] (8)
2MASS J06195260-2903592	M6.0β	11.70 ± 0.30	10.91 ± 0.30	10.08 ± 0.3	-2.0	-1.7	-1.0
2MASS J04221413+1530525	M6.0γ	9.60 ± 0.24	8.72 ± 0.24	8.17 ± 0.2	0.9	1.4	1.8
2MASS J04362788-4114465	M7.5β	13.34 ± 0.34	12.72 ± 0.34	12.33 ± 0.3	-4.5	-5.2	-5.7
DENIS-P J065248.5-574137	M8.0β	11.66 ± 0.15	11.09 ± 0.15	10.52 ± 0.2	-0.7	-0.9	-0.8
2MASS J02212859-6831400	M8.0β	10.93 ± 0.21	10.33 ± 0.21	9.81 ± 0.2	0.1	0.0	0.1
2MASS J06085283-2753583	M8.5γ	11.60 ± 0.16	11.00 ± 0.16	10.44 ± 0.2	-0.7	-0.8	-0.7
2MASS J11020983-3430355	M8.5γ	10.60 ± 0.20	10.02 ± 0.20	9.49 ± 0.2	0.4	0.3	0.4
2MASS J04433761+0002051	M9.0β	13.21 ± 0.39	12.62 ± 0.39	11.91 ± 0.4	-1.6	-1.5	-1.3
2MASS J 20004841-7523070	M9.0β	10.89 ± 0.40	10.22 ± 0.40	9.71 ± 0.4	0.9	0.8	0.9
TWA 26	M9.0γ	10.78 ± 0.13	10.19 ± 0.13	9.64 ± 0.1	1.4	1.2	1.3
2MASS J00325584-4405058	L0.0γ	13.77 ± 0.19	12.97 ± 0.18	12.32 ± 0.2	-4.7	-5.2	-4.5
2MASS J02235464-5815067	L0.0γ	12.57 ± 0.41	11.63 ± 0.39	10.97 ± 0.4	-1.3	-1.0	-0.8
2MASS J23224684-3133231	L0.0β	12.80 ± 0.19	12.11 ± 0.19	11.59 ± 0.2	-2.5	-2.8	-2.7
2MASS J05361998-1920396	L1.0β	13.68 ± 0.80	12.78 ± 0.79	11.84 ± 0.8	-0.9	-1.1	-0.8
2MASS J07123786-6155528	L1.0β	14.03 ± 0.37	13.27 ± 0.35	12.46 ± 0.4	-1.6	-2.4	-2.0
2MASS J05012406-0010452	L4.0γ	14.63 ± 0.16	13.52 ± 0.16	12.68 ± 0.2	-2.4	-2.9	-2.9
2MASS J03552337+1133437	L5.0γ	14.35 ± 0.46	13.05 ± 0.46	11.91 ± 0.5	-1.0	-0.6	-0.1

[a]Δ values are calculated from the mean absolute magnitudes in Table 4.4. Negative values indicate under-luminous objects.

2007; Kirkpatrick et al. 2006). They have extreme red near-IR colors and small tangential velocities relative to the rest of the brown dwarf population (Faherty et al 2009). Kirkpatrick et al. 2006 and Cruz et al. 2009 have suggested that a number of the low-surface gravity dwarfs are candidate members of nearby moving groups such as β Pictoris, Tucana-Horlogium, and AB Doradus, implying ages roughly spanning 10- 50 Myr.

Figure 4.11 shows the near-IR absolute magnitude vs. spectral type diagrams for mid-type M through late-type L dwarfs with binaries removed. Table 4.6 lists the absolute magnitude for each object in J,H, and K as well as the deviation from the median M_J, M_H, and M_K values for each spectral bin. Thirty percent of the objects (5 out of 17) are at least 2σ (and at most $\sim 5.7\sigma$) under-luminous for their spectral bin which translates to 10-50% closer than expected. The average difference in M_J, M_H, and M_K values are (-0.8,-0.7,-0.6) mag respectively. On Figure 4.11 we have plotted the β and γ designations assigned for each object to indicate intermediate and low-gravity respectively (see discussion in Kirkpatrick et al 2005, 2006; Cruz et al 2009). Within this sample, there does not appear to be a correlation between σ_{M_J,M_H,M_K} and the strength of low-surface gravity features.

The trend of low-surface gravity dwarfs appearing under-luminous for their

spectral type is counter-intuitive. According to the evolutionary tracks of Burrows et al (1997); 10 Myr objects with masses ranging from 10-75 M_{Jup} have radii which are 25-75% larger than 1- 3 Gyr equivalent temperature objects. This translates into a luminosity or magnitude difference (overluminosity) between 0.2-0.6 mag. For 50 Myr objects radii can be 13-50% larger and have magnitude differences between 0.1-0.4 mag. There are at least two factors that could contribute to the under-luminosity: (1) Spectral types assigned to low gravity objects do not necessarily correspond (in temperature or luminosity) to spectral types assigned for field dwarfs. The low-surface gravity effects produce weaker alkali lines which in field dwarf classification translates into earlier spectral types. Low surface gravity objects may be skewed toward earlier types thereby making them seem "under-luminous" on an H-R diagram. The same issue occurs among the metal-poor subdwarfs and the solution is to derive a new spectra type/T_{eff} mapping for these outliers (Burgasser et al 2007). (2) Young objects could be dustier than field-aged dwarfs. Observationally, both low-surface gravity dwarfs and dusty L dwarfs show near-IR colors that are redder than normal field objects. They also share similar spectral characteristics (Looper et al 2008, Allers et al 2010). Evolutionary models demonstrate that the lower gravity and dustier (lower f_{sed}) tracks have redder near-IR colors than intermediate, high gravity, or larger f_{sed} tracks (see Figure 4.12).

In Figure 4.12 we isolate the low-surface gravity L dwarfs on a color-magnitude diagram with the Saumon & Marley (2008) and Burrows et al (2006) evolutionary tracks overplotted. The L0.0γ and L1.0β dwarfs 2MASS J0223-5815 and 2MASS J0536-1920 fall within the f_{sed}=1 low gravity track of Saumon & Marley (2008) and the low gravity solar - super solar metallicity tracks from Burrows et al (2006). The L5.0γ dwarf 2MASS J0355+1133 is redward of all predictions from either model. The L0.0β dwarf 2MASS J2322-3133 falls closest to the high gravity track or nearly 1 mag fainter than predicted for the lowest gravity track on both models. The L4.0γ dwarf 2MASS J2322-3133 has the same problem on the Saumon & Marley (2008) models. Using the Burrows et al (2006) models, it is redward of all predictions. The L0.0γ and L1.0β dwarfs 2MASS J0032-4405 and 2MASS J0712-6155 are best traced by the f_{sed}=2 (thinner cloud) model however all three gravity tracks converge on their position. They are nearly 1.5 magnitudes fainter than the lowest gravity f_{sed}=1 (thicker cloud) model. The Burrows et al (2006) models show very little gravity variation in the color space occupied by these dwarfs on the HR diagram.

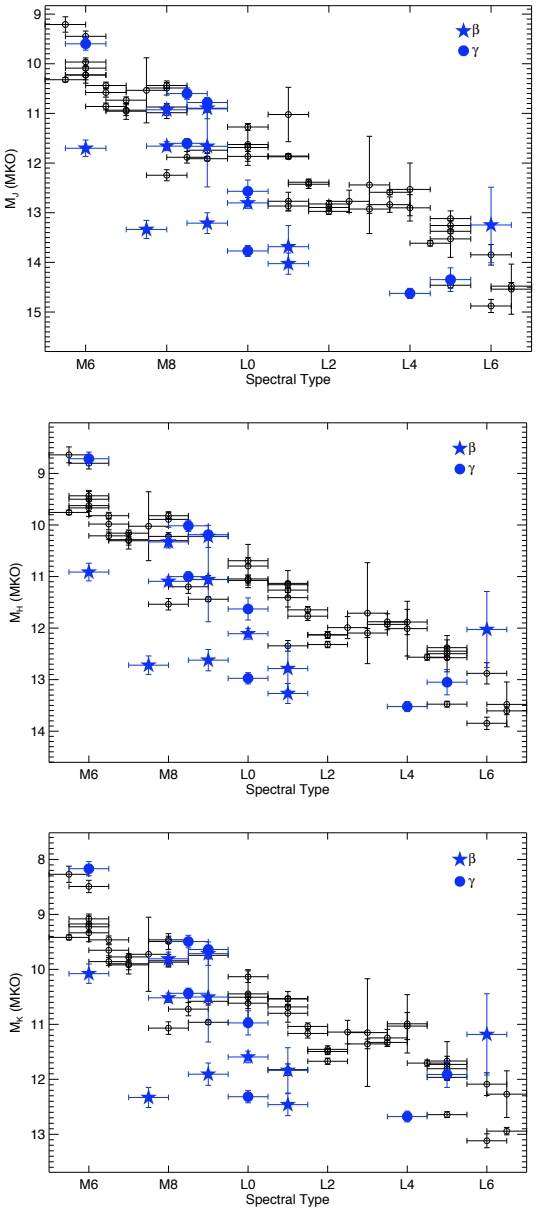

Figure 4.11: Spectral type versus absolute magnitude in the MKO J, H, and K filters for late-type M through mid-L dwarfs. Unfilled circles are ultracool dwarfs with parallax measurements gathered from the literature. Blue filled circles and five point stars are low-surface gravity dwarfs with parallaxes measured in this work.

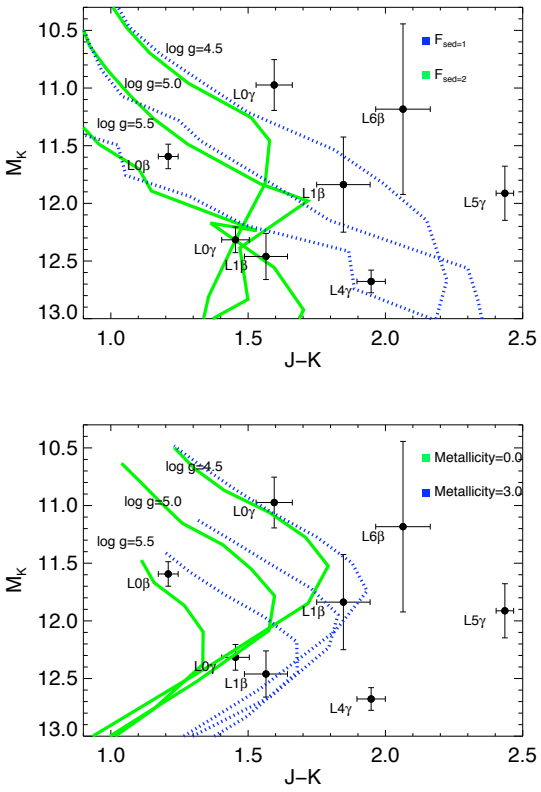

Figure 4.12: The M_K vs J-K diagram for L and T dwarfs with the evolutionary models of Saumon & Marley 2008 (top panel) and Burrows et al (2006-bottom panel) over-plotted with the seven low-surface gravity L dwarfs in our parallax sample. The the log g=[4.477,5.000,5.477], f_{sed}=1,2 parameters of the former are shown as are the log g=[4.5,5.0,5.5], Metallicity=[0.0,3.0] parameters of the later.

4.7 Kinematics

Combining the absolute parallax with the relative proper motion gives the tangential velocity (v_{tan}) of a source (see Table 4.2 for v_{tan} values of objects studied in this work). Our full astrometric sample is composed of objects in the general solar vicinity therefore v_{tan} values can be used as a rough indicator of age. In general, older objects will have had enough time to interact with objects in the Galactic disk and have their orbits perturbed while younger objects will maintain a nascent smaller value. The dispersion of a population is more informative than individual values for determining age characteristics. The full sample contains low-surface gravity objects and subdwarfs, as well as normal field L and T dwarfs. Omitting the first two subsets from the general population and using only objects with v_{tan} uncertainties < 10 km s^{-1}, we compared the distribution of v_{tan} values for L and T dwarfs. The median V_{tan} and σ_{tan} values for the 60 L dwarfs are 28 km s^{-1} and 19 km s^{-1} respectively. For the 50 T dwarfs we find slightly larger values of 36 km s^{-1} and 21 km s^{-1} respectively. These values are consistent with the kinematic results of previous works (Dahn et al 2002; Vrba et al 2004; Osorio et al 2008). Based on the significant difference in dispersion between the L and T dwarfs Vrba et al (2004) concluded from their much smaller sample of UCDs that the L dwarfs were a kinematically younger population than the T dwarfs. In part, their conclusion was drawn from the fact that there were no T dwarfs with v_{tan} values < 20 km s^{-1}. In the full sample examined here, we find 15 T dwarfs with v_{tan} values < 20 km s^{-1}. Regardless we find a similar significant difference between the L and T dwarfs indicating a kinematic age difference between the two populations.

We isolated the low-surface gravity dwarfs and the subdwarfs and compared their kinematics to the overall sample (note that we have included late-type M objects in each subset). The former have significantly smaller v_{tan} values and tighter dispersions than the overall population and the latter significantly larger values. The median v_{tan} and σ_{tan} values for the 17 low-surface gravity dwarfs are 11 km s^{-1} and 10 km s^{-1} respectively. For the 4 subdwarfs, the median v_{tan} and σ_{tan} values are 204 km s^{-1} and 114 km s^{-1} respectively. The considerable difference in values for each subset compared to the overall population further confirms expectations that they are younger (low surface gravity objects) and older (subdwarfs) than the overall ultracool dwarf population.

4.8 Individual Objects

4.8.1 New low v_{tan} objects

As noted in previous works, individual v_{tan} values are a poor indicator of individual ages. However extreme differences in kinematics from the overall population in combination with spectral or photometric peculiarity can be informative about an individual object. Within the full astrometric sample we looked for extreme kinematic outliers (both significantly fast and significantly slow movers).

We found no new significantly fast movers ($v_{tan} > 100$ km s^{-1}) but we did identify two considerably slow ($v_{tan} < 5$ km s^{-1}) objects. The T4.5 dwarf 2MASS J0830+0128 and the L6.5 dwarf 2MASS J1711+2232 move with v_{tan} values of 4±4 km s^{-1} and 4±3 km s^{-1} respectively. Neither object exhibits low surface gravity features. In fact, in apparent contradiction, 2MASS J0830+0128 appears slightly blue for its spectral type (J-K_s=-0.04±0.12 as opposed to the mean value of 0.26 for T4 dwarfs) and is identified as a potentially high surface gravity dwarf in Knapp et al (2004) from its H-K color. 2MASS J1711+2232 was originally classified by Kirkpatrick et al (2000) as an L6.5 dwarf using optical data. Given this spectral type, this dwarf is significantly redder than equivalently classified objects (J-K_s=2.36±0.20 as opposed to the mean value of 1.75 for L6 dwarfs). The red outlier quality would suggest a younger age (see Faherty et al 2009; Schmidt et al 2010); however, Burgasser et al (2010) examined the near-IR spectrum and derived a later yet poorly constrained near-infrared classification of L9±2. Furthermore, they use composite spectra and find this object to be a strong candidate for an unresolved binary (L5.0±0.4 primary T5.5±1.2 secondary Δ J=0.92±0.30; see Figure 4.3). Radial velocity measurements for both of these dwarfs would be informative for investigating the kinematic age using the full space motion.

4.8.2 2MASS J0616-6407

Cushing et al. (2009) reported the discovery of 2MASS J0616-6407 as the first outer halo L subdwarf, with a spectral type sdL5 and extreme kinematics (1.405±0.008 $''$ yr^{-1}; V_{rad} = 454±15 km s^{-1}). They estimated a distance of 57±9 pc using near-infrared absolute magnitude/spectral type relations constructed from a small sample of ultracool subdwarfs with parallax measurements. Our astrometry confirms the high proper motion of this source, and we measure a parallax of 22±6 mas (d = 45±13 pc), which is closer but statistically consistent with the spectrophotometric estimate of Cushing et al.

From these values we find UVW velocities[7] of (80±10,-525±34,45±59) km s^{-1} and V_{tan} = 286±32 km s^{-1}.

Using our parallax measurements, we re-examined the orbit of 2MASS J0616-6407, taking into account the uncertainties in its Galactic position and velocity vectors. We used the same axisymmetric Galactic potential model as described in Cushing et al. (2009), consistently primarily of Plummer spheres for the disk, dark matter halo and bulge, using parameters from Dauphole & Colin (1995). Orbits were computed over a 1 Gyr period centered on the current epoch in time steps of 0.1 Myr, using the halo-dominant mass model of Binney & Tremaine (2008). For each calculation, we randomly varied the input position and velocity vectors based on the uncertainties in position and velocity vectors, assuming the errors are gaussian. Figure 4.14 displays the results of these calculations, showing the distributions of maximum radius and maximum vertical displacement from the Galactic plane, as well as comparison between the nominal orbit and those with maximum and minimum kinetic energies at the current epoch. The latter two plots illustrate how poorly constrained the orbit of this source is based on current position and velocity measurements; there is nearly a factor of 3 difference in the maximum orbit radius between these extremes, with a mean value of 20±6 kpc. Due to the large uncertainty in W, these orbits also vary from completely planar to $\mid Z \mid_{max}$ = 13 kpc (the mean $\mid Z \mid_{max}$ = 2.4±2.4 kpc). Nevertheless, the halo kinematics of 2MASS J0616-6407 is unambiguous; its orbit is completely retrograde to the rotation of the Galactic disk. However, more precise distance and radial velocity measurements are needed to constrain the shape of this orbit .

4.8.3 Over and Under-Luminous Sources

As noted in section 4.4.1 four sources were disregarded in calculating the median M_{JHK} values for spectral type bins because they were particularly over or under-luminous compared to the rest of the field.

SDSS J1110+0116, originally identified in Geballe et al (2002) and classified as a T5.5 by Burgasser et al (2006), is $\sim$ 1 magnitude over-luminous in $M_{J,H,K}$ compared to the median value for its spectral bin. Knapp et al (2004) examined this source in detail and concluded that the depth of the KI lines implied a low-surface gravity. Comparing to the evolutionary models of Marley et al (2002) they predicted that this source had an age of 1-3Gyr and a mass ranging from 10-15$M_{Jupiter}$. Stephens et al. (2009) also examined this object in detail and

[7]We follow the convention that the U is positive toward the Galactic center (l=0, b=0) and velocities are reported with respect to the Local Standard of Rest (LSR) using the solar motion from Johnson & Soderblom (1987)

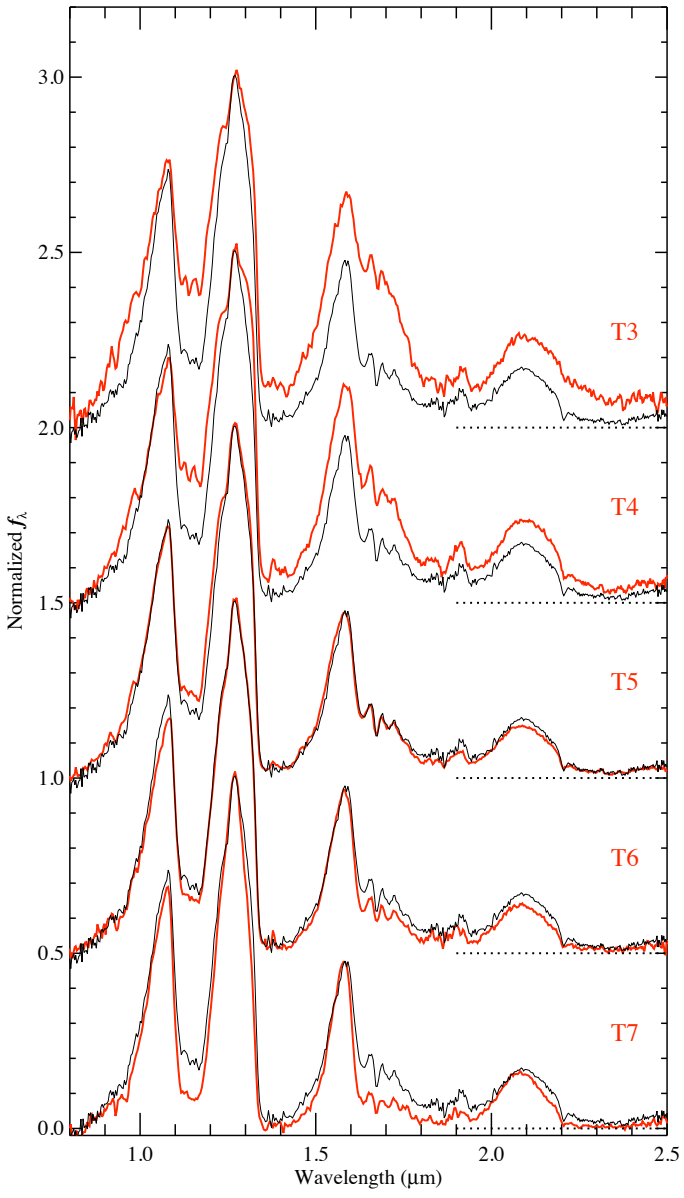

Figure 4.13: The near-IR spectrum of 2MASS J1754+1649 using SpeX. T3 - T7 standards are over-plotted in red. We find a best fit of T5.5.

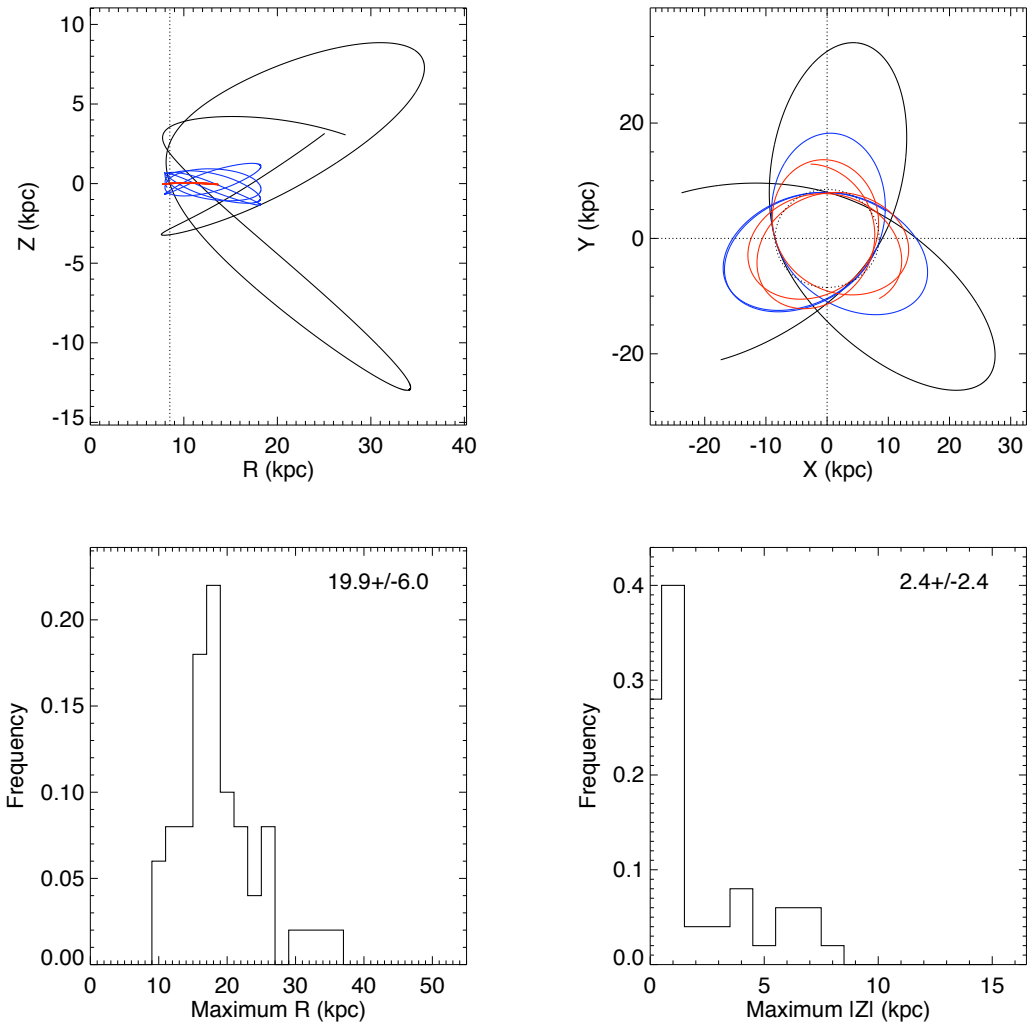

Figure 4.14: The upper panels show the distributions of maximum radius (upper left) and maximum vertical (upper right) displacement from the Galactic plane. The lower panels show a comparison between the nominal orbit (blue) and those with maximum (black–lower left panel) and minimum (red–lower right panel) kinetic energies at the current epoch. The latter two plots illustrate how poorly constrained the orbit of this source is based on current position and velocity measurements; there is nearly a factor of 3 difference in the maximum orbit radius between these extremes, with a mean value of 20±6 kpc.

concluded an even younger age of 0.1 - 1 Gyr and a mass of 7 - 25 $M_{Jupiter}$. As discussed in Section 4.6 above, the low-surface gravity L dwarfs appear under-luminous for their spectral type, contrary to model predictions that they should be noticeably over-luminous. The overluminosity of SDSS J1110+0116 could be attributed to an unresolved binary or to its youth.

2MASS J1511+0607, originally classified as a T0±2 in the near-IR, is more than 1 magnitude over-luminous in $M_{J,H,K}$ compared to the other unresolved T0 with a parallax measurement (2MASS J2047-0718). It is also $\sim$ 1 magnitude over-luminous in $M_{J,H,K}$ compared to the median value for T1 dwarfs. The near-IR spectrum of 2MASS J1511+0607 was characterized as peculiar compared to standard early T dwarfs as it had strong CH_4 absorption at 1.1 and 1.6 μm but very weak absorption at 2.2μm. Burgasser et al (2010) re-examined the spectrum using composite template fitting and found that an L5.5±0.8 primary and T5±0.4 secondary composite spectrum best-fit the source and suggested this as a strong candidate unresolved binary. We show the spectral components in Figure 4.3 and find that the overluminosity supports the binary hypothesis.

Three other sources in this parallax work were identified as weak binary candidates using the composite template method in Burgasser et al (2010). 2MASS J0949-1545 was identified as a likely T1.0±0.2 primary and T2.0±0.2 secondary with a ΔJ=-0.12±0.10. SDSS J2052-1609 was identified as a likely L7.5±0.6 primary and T2.0±0.2 secondary with a ΔJ=0.04±0.18. If true binaries, both would have smaller J flux reversals than other early T dwarf binaries. SDSS J1207+0244 was identified as a likely L6.5±0.7 primary and T2.5±0.5 secondary with a ΔJ=0.48±0.28.

Two sources appeared under-luminous compared to similar spectral type objects. 2MASS J2043-1551 is classified as an L9 in the near-IR by Chiu et al (2006). Only 3 L9 dwarfs have parallaxes although all have L8 optical spectral types. Given that 2MASS J2043-1551 does not have any optical spectral type for comparison, it is difficult to quantify if this source is truly under-luminous or if it anchors the tail of the L dwarf sequence. There are no reported indications of spectral peculiarities connected to 2MASS J2043-1551.

2MASS J1754+1649 stands out as being a particularly under-luminous and red T dwarf. It was originally discovered as part of a search of the 2MASS survey for bright, nearby T dwarfs (Burgasser et al. 2003; Tinney et al. 2004; Burgasser et al., in prep.). A low-resolution ($\lambda/\Delta\lambda \approx 120$) near-infrared spectrum of it was obtained with the IRTF SpeX spectrograph (Rayner et al. 2003) on 2006 June 1 (UT). Data were acquired and reduced (using SpeXtool; Vacca et al. 2003; Cushing et al. 2004) as described in Burgasser et al. (2004 - AJ, 127, 2856). Figure 4.13 compares this spectrum to a set of T dwarf

standards defined in Burgasser et al. (2006). The strengths of the various H_2O and CH_4 bands in the 1–2.5 μm region are most closely matched with the T5 spectral standard. From the spectral indices defined in Burgasser et al. (2006), we infer a numeric spectral type of T5.5. Comparison to a broader sample of spectral templates from the SpeX Prism Spectral Libraries[8] confirms this classification. 2MASS J1754+1649 is an almost identical match to the T5.5 dwarf 2MASS J1828-4849, for which we infer $M_J = 16.88 \pm 0.2$ from our parallax measurement, a full 2 magnitudes fainter at J. 2MASS J1754+1649 is also considerably redder than its counterparts. With J-K = -0.16±0.05, it is ∼0.2 mag redder than 2MASS J1828-4849 and ∼1 mag redder than T dwarfs with comparable M_K magnitudes. It is in fact quite isolated in the near-infrared color magnitude diagram (Figure 8), lying along the $f_{sed} = 2$ track from Saumon & Marley (2008). As such, the unusual presence of clouds may explain the unexpected faintness and redness of 2MASS J1754+1649, even though its near-infrared spectrum shows no obvious peculiarity.

4.9 Conclusions

We have measured 84 trigonometric parallaxes for late-type M, L and T dwarfs in the local solar neighborhood. The target list consisted of 19 M dwarfs, 37 L dwarfs, and 28 T dwarfs. Nine calibrator stars were included in the sample to verify the reliability of our pipeline. The focus of this project was on late-type M and L dwarfs including low surface gravity, L-T transition objects, late-type T dwarfs within 20 pc of the sun, and nearby subdwarfs. The 65 new L and T dwarf parallaxes significantly increases the number of brown dwarfs with accurate distance measurements.

We combined our sample with literature measurements for a brown dwarf astrometric catalog containing 146 objects. The loci for L dwarfs is tighter at M_{JHK} than the T dwarf sequence. Unresolved binarity or significant variation in the age, metallicity, and/or atmospheric properties of the T dwarfs compared to the L dwarfs could account for the difference in spreads. We used the full sample to re-define color-magnitude and spectrophotometric diagrams in JHK as well as $IRAC$ ([3.6], [4.5], [5.8], and [8.0]) bands. Scatter is smallest in the $IRAC$ [4.5] band although a smaller astrometric sample is available in the mid-IR.

The brightening of early T dwarfs is confirmed with a significantly larger scatter than previously measured. It is most apparent in J where there is a 1 mag difference between T1 and T4 dwarfs. There is also a 0.8 mag brightening

[8] `http://www.browndwarfs.org/spexprism`

in H and a plateau in K for the L/T transition objects. Significant scatter is detected among the latest type T dwarf spectral bins although when broken into half spectral bins the scatter is largely dispersed.

We investigated the color-magnitude diagrams for brown dwarfs and found that they can be categorized as (1) generally monotonic, (2) demonstrating a color reversal, or (3) as two sequences (the L and T) offset from one another by the transition objects that curve back on themselves. Falling into the first category, the M_K versus K - [4.5] diagram is the most efficient at distinguishing early and mid L and T dwarfs; however there is significant scatter among mid T dwarfs. The latter two effects are best explained by L dwarf reddening caused by condensate cloud opacity that affects the near-IR significantly more than the mid-IR. Colors reverse as clouds clear and CH_4 as well as H_2O absorption become prominent for cooler temperatures. In the third case, significant flux is shifted to longer wavelengths causing objects past the L/T transition to once again redden.

We compared the M_K vs. J-K data for the full astrometric catalog to the evolutionary models of Saumon & Marley (2008) and Burrows et al (2006). The f_{sed}=1,2 parameters best fit the L dwarf sequence and f_{sed}=4 (corresponding to a very thin cloud layer) best fit the late-type T dwarf sequence using the Saumon & Marley (2008) models. The cloud model with varying gravity and metallicity reproduce the L dwarfs and the clear model with similar variations fit the T dwarfs using the Burrows et al (2006) models. However comparisons to empirical data show significant red or potentially "ultra-cloudy" L dwarf outliers. Similarly there is significant scatter seen in the latest type T dwarfs that is unaccounted for in the clear and f_{sed}=4 models indicating that condensate clouds may play a role in the photospheres of these objects. The four L subdwarfs are well fit by the Burrows et al (2006) clear model in stark contrast to dusty field dwarfs. This supports evidence that cloudiness is correlated with metallicity and/or age.

No single f_{sed} parameter nor gravity or metallicity track in the evolutionary models can account for the L/T transition objects. We constructed a hybrid model between the f_{sed}=2 model which fits the latest type L's and f_{sed}=4 which fits the latest T dwarfs. Allowing the cloud layer to decrease in thickness by 10% (creating patchy clouds) for model temperatures corresponding to a range of $\pm$150 K (dependent upon log(g)) we reproduce NIR color-magnitude trends for the L-T transition objects.

The low-surface gravity objects with parallax measurements in this work are not explained by varying gravity in the evolutionary models. Among the 17 objects investigated, thirty percent appear at least 2σ (and as much as 5.7σ) under-luminous for their spectral bin or 10-50% closer than would be

predicted by standard spectrophotometric relations. Possible explanations for their underluminosity are that (1) low-surface gravity produces weaker alkali lines which in field dwarf classification translates into earlier spectral types, thereby making them seem under-luminous on an H-R diagram. (2) Young objects could be dustier than field-aged objects.

Investigations of the kinematics of the normal (no low-gravity or subdwarf) L and T dwarf v_{tan} dispersion shows differences between the two populations. While contrary to previous studies there do appear to be slow moving (v_{tan} < 20 km s^{-1}) T dwarfs, their larger dispersion compared to L dwarfs indicates that there is a kinematics age difference between the two consistent with populations synthesis models (e.g. Burgasser et al. 2004; Allen et al. 2005).

Chapter 5

Conclusion

5.1 Chapter Conclusions

Observational studies of brown dwarfs are only 15 years old. This was part of the appeal when I chose my research topic four years ago. Within this thesis I have made basic astrometric measurements and used them to study population characteristics. After an extensive observational campaign in both the Northern and Southern hemispheres to re-image known L and T dwarfs, I created a catalog of proper motions, tangential velocities (v_{tan}), and distances (either from spectrophotometric relations or parallax when available) for 90% of the known field brown dwarf population. Average kinematic and photometric values were updated for spectral bins using the large sample. I estimated rough ages from the dispersion in v_{tan} and the population was concluded to have a similar age to the predictions from population synthesis models. Photometric outliers were found to have significantly different kinematics than the "normal" population. I concluded that objects that were red or blue for their spectral type were statistically younger or older (respectively) than normal field aged dwarfs.

Using the large sample of proper motions I conducted a cross-catalog search for common proper motion companions in LSPM-North and Hipparcos. Detailed photometric and spectroscopic follow-ups were obtained for the nine high probability wide companion candidates. Age ranges were deduced for each system with varying degrees of precision. Some age discrepancies, based on the activity of the brown dwarf versus the main sequence star companion, suggest possible shortcomings in our understanding of the age diagnostics of stars and UCDs. I examined the binding energy for each of the new systems and compared it to the (albeit small) collection of known wide UCD multiples. The new multiples were among the lowest binding energy systems investigated

to date. The frequency of tight resolved binaries was found to be higher among widely separated systems (a result confirming previous studies). The ratio of triples to binaries and quadruples to binaries was higher for the collection of known wide UCD companions than compared to the field population. This hinted at the need for a third or fourth component in such loosely bound systems to maintain gravitational stability or to facilitate the exchange of angular momentum.

The largest previous contribution of parallax measurements for the brown dwarf population came over a 2 year period from 2002-2004 when three studies reported measurements for 58 L and T dwarfs. Until this thesis those measurements defined our understanding of the luminosity of brown dwarfs and sculpted the HR diagram that has been used by atmospheric and evolutionary models for just under a decade. With an increasingly large number of brown dwarfs reported including subsolar metallicity objects, low-surface gravity objects, low-temperature T dwarfs, red and blue photometric outliers, and flux reversal binaries it seemed appropriate to begin another large parallax study of the population. We conducted an observationally intensive campaign to measure parallaxes for 84 ultra cool dwarfs. Combining all objects with measured parallaxes resulted in a full sample of 146 UCDs. The J-band bump was quantified to be as much as 1 magnitude between T1 and T4 dwarfs but also significant at H (0.8 mag). Comparisons were made with evolutionary models and the observational color-magnitude diagram. Potentially "ultra-cloudy" L dwarfs were identified as were a collection of late-type T dwarfs which might have condensate clouds in their photospheres. No single cloud or metallicity parameter model could account for all of the L/T transition objects. A hybrid model allowing clouds to quickly dissipate in 10% increments reproduced the majority of the L/T transition portion of the NIR color-magnitude diagram. Low surface gravity objects were not fit by any model and the majority were redward and underluminous of predictions. Investigations of the kinematics of the normal (no low-gravity or subdwarf) L and T dwarf v_{tan} dispersion shows significant differences between the two populations. Contrary to previous studies there do appear to be slow moving ($v_{tan} < 20$ km s^{-1}) T dwarfs, but their larger dispersion compared to L dwarfs indicates that there is a kinematics age difference between the two.

5.2 Thesis Follow-Ups

The large body of observational astrometric work conducted in this thesis is primarily complete. Below I detail the tasks that remain with the data in hand and with follow-up that will be conducted over the next few years.

5.2.1 Completion of Brown Dwarf Parallaxes

A number of objects had parallax observations started over the course of this thesis but due to inclement weather or too few astrometric frames, I was not able to converge upon a parallax solution. The original target list that I started with contained 36 L/T transition (L6 through T5) objects and 48 low surface gravity objects visible in the South. Twenty of the low-surface gravity dwarfs were in fields too sparse to target with ANDICAM and they were too bright to become a high priority target with ISPI. Fifteen of the L/T transition objects had parallax frames started but at the time of this publication there are not enough epochs to converge upon a solution or to report an uncertainty $< 10\%$.

To refine parallax uncertainties, obtain enough frames for parallax convergence, and/or to target low surface gravity objects in sparse fields, I plan on applying for more NOAO ISPI time. ISPI was recently decommissioned from the 4.0m Blanco telescope to make room for the wide field NIR imager NEWFIRM. However, if one can justify why ISPI is the only instrument that can be used for a project then it can be requested.

Looking into the future there are a number of parallax programs I foresee or am already pursing. The parallax targets pursued in my thesis are in the South but I would like to get a Northern sample completed as well. I have already begun a project with collaborators Kelle Cruz and Sebastien Lepine targeting low surface gravity L dwarfs using the MDM telescope and optical imager at Kitt Peak. Parallax observations were begun at various times over the past 12 months and I will pursue them over the next few years.

ANDICAM has proven to be a stable optical astrometric instrument and the queue mode is optimal for long term multi-epoch imaging. I have been collaborating with graduate student Dagny Looper at the University of Hawaii whose thesis involved identifying new low-mass members of the TW Hydrae association. We would like to use ANDICAM in the future to measure parallaxes for the brighter targets in her thesis to confirm membership.

5.2.2 Pursuing New Binaries

In section 8 of chapter 4, I reported that SDSS J1110+0116 and 2MASS J1511+0607 appear overluminous by more than 1 magnitude in M_{JHK} when compared to similar spectral type dwarfs. 2MASS J1511+0607 is a candidate tight binary in Burgasser et al. (2010a) and follow-up observations with Adaptive Optics (AO) at Keck by collaborators has verified a second closely separated component in this system. Three other sources with parallaxes reported in this thesis, 2MASS J0949-1545, SDSS 2052-1609, and SDSS 1207+0244,

are suspected binaries based on composite template fitting (Burgasser et al. 2010a). Stumpf et al. (2010) recently published AO observations resolving SDSS 2052-1609 into two near-equal components. Further high resolution imaging using either AO or Hubble Space Telescope (HST) observations are necessary for investigating the binary nature of the remaining systems. If true binaries like 2MASS J1511+0607 and SDSS 2052-1609, all of these low-mass systems would have two L/T transition components. Combined with a well constrained distance would make these systems important tests for atmospheric and evolutionary models. A current campaign is underway by a number of collaborators using the Keck LGO system to follow-up on all of the binary candidates listed within this thesis.

5.2.3 Radial Velocities

Radial velocities are the third kinematic parameter which is missing from our population analysis. Combining the new proper motion and distance measurements reported in this work with radial velocities, we would be able to search for spatial and kinematic association with moving groups as well as examine kinematic correlations with physical properties. While we did a great deal of kinematic analysis without radial velocity measurements, they are required to derive U,V,W values, the true measure of an object's Galactic space motion. Precise U,V,W velocities are also required to confirm membership in moving groups. As reported in Cruz et al. (2009), a number of the low surface gravity dwarfs with parallaxes reported in this thesis are candidate members of AB Doradus, β Pictoris, Tucana Horlogium, and other young associations.

Current collaborative efforts are underway or observationally complete for this portion of the project. Radial velocity data has been obtained in the Northern hemisphere with Phoenix on Gemini, NIRSPEC on Keck, TripleSpec on ARC and in the Southern hemisphere with MagE and FIRE on Magellan.

5.3 Future of Brown Dwarf Discovery and Astrometry Surveys

The Two Micron All Sky Survey (2MASS), the DEep Near Infrared Survey of the Southern Sky (DENIS), the Sloan Digital Sky Survey (SDSS), the Canada France Hawaii Telescope Legacy Survey (CFHTLS), and the UKIRT Infrared Deep Sky Survey (UKIDSS) were instrumental over the past 15 years in identifying brown dwarfs. While candidates are still being collected from each of these catalogs, astronomers are looking ahead to the next major mis-

sions that will identify the lowest temperature brown dwarfs and/or measure large numbers of parallaxes.

- **Wide-field Infrared Survey Explorer (WISE):** December of 2009 saw the launch of WISE which will provide an all-sky survey from 3.4 to 22 μm. It will image the sky in the [3.4], [4.6], [12], and [22] μm bands; optimal for searches for the coldest brown dwarfs. 2MASS and SDSS were extremely successful at detecting large numbers of L and T dwarfs hotter than 750K. The UKIDDS survey produced a handful of colder candidates but WISE, operating at longer wavelengths where the coldest objects emit the majority of their light, is projected to find hundreds of low-temperature objects (see Figure 5.1). Depending on the space density, WISE should detect brown dwarfs with temperatures of $\sim$ 450K out to a distance of 23 pc; 300K objects out to 6 pc; and 150K objects out to 3 pc[1]. As analysis continues over the next few years, WISE should generate a new large and diverse catalog of substellar mass objects (see first results published in Mainzer et al. 2010).

  Moreover, since WISE is an all-sky survey, it will provide mid-IR magnitudes for the known collection of L and T dwarfs allowing population studies at longer wavelengths. It will also lead to the first all-sky near-IR to mid-IR proper motion catalog. By imaging the entire sky $\sim$ 9-12 years after 2MASS, WISE will provide a significant baseline for measuring proper motions down to $\sim$50 mas yr^{-1}. Using reduced near-IR or mid-IR proper motion diagrams we will be able to select brown dwarf candidates without the color biases that have been used throughout the past decade.

- **Panoramic Survey Telescope & Rapid Response System (Pan-STARRS):** Pan-STARRS is a wide field imaging facility being developed at the University of Hawaii that will observe the entire available sky several times each month. It will be composed of four individual optical systems (one of which obtained first light in 2006), each with a 1.8m mirror observing the same region of the sky simultaneously. The field of view of each detector will be three degrees with a 0.3 $''$/pixel platescale. Exposure times will vary between 30 and 60 seconds in the *grizy* bands and the expected limiting magnitude is 24.

  The main goal of Pan-STARRS is to catalog and monitor near-Earth or potentially hazardous asteroids. However there is also a great deal of brown dwarf science that will be possible. Over the course of a few

[1] see the WISE science objects as listed on http://wise.ssl.berkeley.edu/sciencebrowndwarfs.html

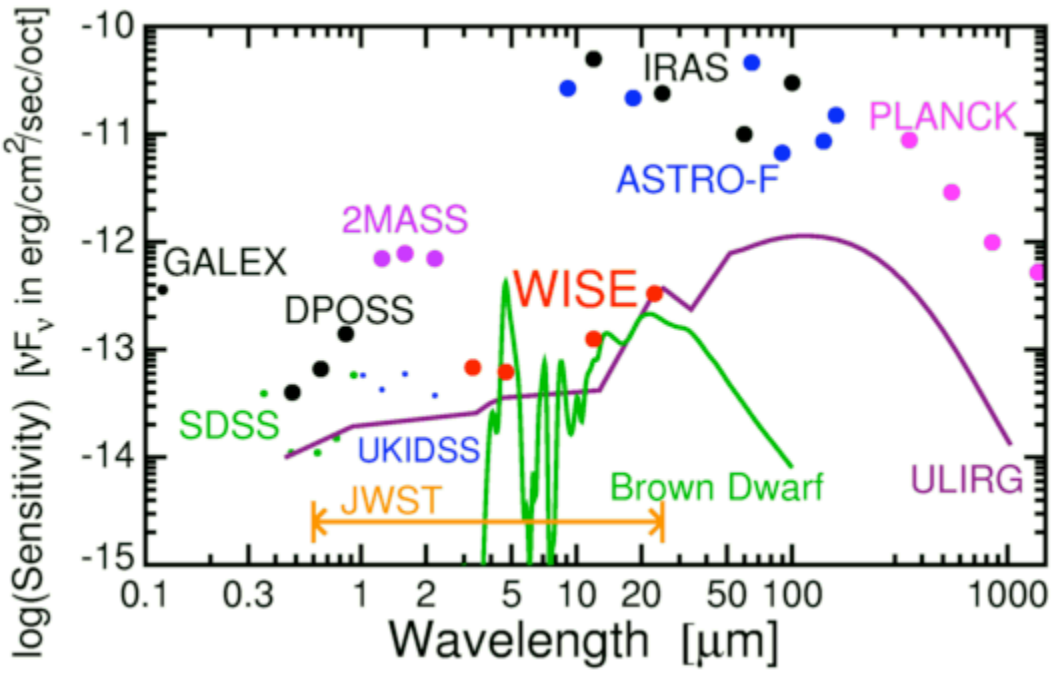

Figure 5.1: This figure[2] shows the 5 sigma point source sensitivities of WISE and previous or planned all-sky surveys. The planned wavelength range for the JWST is indicated. The dot size shows the planned sky coverage. GALEX is a small Explorer (SMEX) which was launched by NASA in 2003, SDSS is the ground-based Sloan Digital Sky Survey, DPOSS is the groundbased Digital Palomar Observatory Sky Survey, ASTRO-F is the Japanese satellite, renamed Akari after launch on 22 Feb 2006, and Planck is the European CMB mission to be launched in 2009 which also includes a good sub-mm survey capability.

years, the continuous monitoring of the sky by Pan-STARRS will allow parallax measurements for an estimated ∼4 x 10^5 stars within 100 pc (Dupuy & Liu 2009). Using astrometry combined with the iz and y filters, numerous brown dwarf discoveries are expected. Pan-STARRS should produce a volume-limited sample of T dwarfs out to 50 pc, and an even larger catalog of T dwarfs based on izy-band color selection (Liu et al. 2007). The results will be an order of magnitude gain over 2MASS and SDSS surveys and will include a substantial number of cold brown dwarfs (see Figure 5.2). The depth of Pan-STARRS will allow parallax measurements for all known brown dwarfs in the ∼ 75% of the sky covered by this survey as well as a measurement for any new objects discovered.

- **Large Synoptic Survey Telescope (LSST):** LSST is a wide field imaging facility planned on being built in central Chile that is likely to get first light in this decade[3]. It will be composed of an 8.4m telescope with a 1.6x3.0 meter camera that covers a 3.5 degree field of view with a 0.2 ″/pixel platescale. The filter bandpasses currently slated include $grizy$ and exposure times of 15 seconds should reach depths of r∼24.5-26.5. The design of LSST will allow it to scan the available Southern sky once every 1-2 nights.

  There are numerous science objectives for LSST. Among the main topics will be studying the nature of dark energy, monitoring and discovering new solar system bodies (e.g. Kuiper belt objects–KBO's, near-earth objects–NEO's), exploring the transient optical sky, and studying Galactic structure. LSST is an optimal survey for studying stellar populations. Accurate parallaxes will be reported for all stellar types within 10pc and most stellar types within 100pc. As with Pan-STARRS, brown dwarfs will be discovered using izy-band color selection. Parallaxes can be measured for all new sources discovered and known objects in the ∼75% of the sky LSST will monitor. Between these two surveys, the Northern and Southern hemisphere will be covered offering an unprecedented sample of new brown dwarf candidates and astrometric information for all of them.

5.4 Summary

This dissertation is a body of work aimed at measuring the most basic observational features of the brown dwarf population. At the very core, my

[3]The 2010 decadel survey ranked LSST the highest priority ground-based project

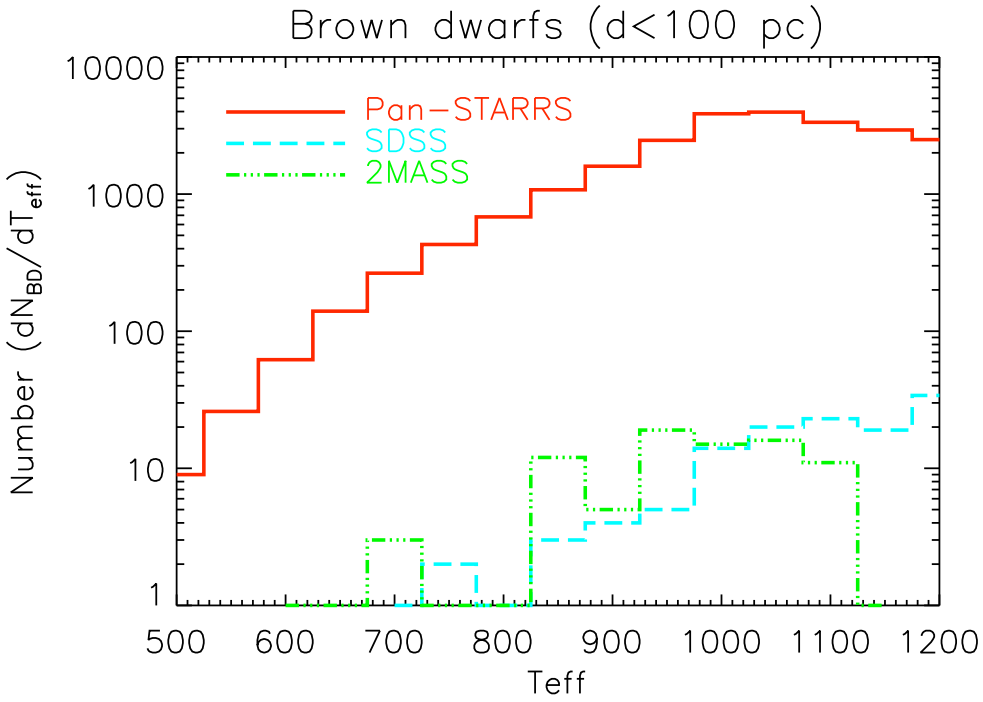

Figure 5.2: A comparison of the brown dwarf discovery capabilities of Pan-STARRS, 2MASS, and SDSS based on a Monte Carlo simulation of the solar neighborhood from Liu et al. (2007). The simulation assumes a constant star formation rate and an initial mass function of $dN/dM \sim M^{-1}$, normalized to the local density of 0.1 - 1.0 $M_{\odot}$ stars. The Pan-STARRS advantage is substantial. (Note that the gain of Pan-STARRS relative to previous surveys is independent of the assumed IMF slope.) Furthermore, while 2MASS and SDSS provide only color information, Pan-STARRS will also measure parallaxes for many of the brown dwarfs that it identies.

thesis was about conducting simple measurements and using them to probe complex characteristics of a class of objects. Astrometric measurements can be linked to some of the most important and historical breakthroughs in the field and the need for precise measurements persists. The number of objects studied in this thesis is a large addition to the astrometric sample that was available in the past decade and will inform evolutionary and astrometric models over the coming years. The future astrometric missions will build upon this sample but the expected numbers will far exceed anything possible from a single user observing thesis. I look forward to the future of brown dwarf science which will be greatly advanced by the new astrometric surveys discussed in this chapter.

Bibliography

Ackerman, A. S. & Marley, M. S. 2001, ApJ, 556, 872

Ahmic, M., Jayawardhana, R., Brandeker, A., Scholz, A., van Kerkwijk, M. H., Delgado-Donate, E., & Froebrich, D. 2007, ApJ, 671, 2074

Allard, F., Hauschildt, P. H., Alexander, D. R., Tamanai, A., & Schweitzer, A. 2001, ApJ, 556, 357

Allard, N. F., Allard, F., Hauschildt, P. H., Kielkopf, J. F., & Machin, L. 2003, A&A, 411, L473

Allen, P. R. 2007, ApJ, 668, 492

Allen, P. R., Koerner, D. W., Reid, I. N., & Trilling, D. E. 2005, ApJ, 625, 385

Allers, K. N., Jaffe, D. T., Luhman, K. L., Liu, M. C., Wilson, J. C., Skrutskie, M. F., Nelson, M., Peterson, D. E., Smith, J. D., & Cushing, M. C. 2007, ApJ, 657, 511

Allers, K. N., Liu, M. C., Dupuy, T. J., & Cushing, M. C. 2010, ApJ, 715, 561

Allers, K. N., Liu, M. C., Shkolnik, E., Cushing, M. C., Dupuy, T. J., Mathews, G. S., Reid, I. N., Cruz, K. L., & Vacca, W. D. 2009, ArXiv e-prints

Arp, H. C., Baum, W. A., & Sandage, A. R. 1952, AJ, 57, 4

Artigau, É., Doyon, R., Lafrenière, D., Nadeau, D., Robert, J., & Albert, L. 2006, ApJ, 651, L57

Artigau, É., Lafrenière, D., Albert, L., & Doyon, R. 2009, ApJ, 692, 149

Artigau, É., Lafrenière, D., Doyon, R., Albert, L., Nadeau, D., & Robert, J. 2007, ApJ, 659, L49

Bailer-Jones, C. A. L. 2004, A&A, 419, 703

Baliunas, S. L., Donahue, R. A., Soon, W. H., Horne, J. H., Frazer, J., Woodard-Eklund, L., Bradford, M., Rao, L. M., Wilson, O. C., Zhang, Q., Bennett, W., Briggs, J., Carroll, S. M., Duncan, D. K., Figueroa, D., Lanning, H. H., Misch, T., Mueller, J., Noyes, R. W., Poppe, D., Porter, A. C., Robinson, C. R., Russell, J., Shelton, J. C., Soyumer, T., Vaughan, A. H., & Whitney, J. H. 1995, ApJ, 438, 269

Barbanis, B. & Woltjer, L. 1967, ApJ, 150, 461

Barnes, S. A. 2007, ApJ, 669, 1167

Bartlett, J. L. 2007, PhD thesis, University of Virginia

Basri, G. & Brown, M. E. 2006, Annual Review of Earth and Planetary Sciences, 34, 193

Basri, G., Marcy, G. W., & Graham, J. R. 1996, ApJ, 458, 600

Bate, M. R. 2000, MNRAS, 314, 33

Bate, M. R., Bonnell, I. A., & Bromm, V. 2002, MNRAS, 336, 705

Becklin, E. E. & Zuckerman, B. 1988, Nature, 336, 656

Bensby, T., Oey, M. S., Feltzing, S., & Gustafsson, B. 2007, ApJ, 655, L89

Berriman, B., Kirkpatrick, D., Hanisch, R., Szalay, A., & Williams, R. 2003, in IAU Joint Discussion, Vol. 8, IAU Joint Discussion

Bessell, M. S. 1979, PASP, 91, 589

Bihain, G., Rebolo, R., Béjar, V. J. S., Caballero, J. A., Bailer-Jones, C. A. L., Mundt, R., Acosta-Pulido, J. A., & Manchado Torres, A. 2006, A&A, 458, 805

Biller, B. A., Kasper, M., Close, L. M., Brandner, W., & Kellner, S. 2006, ApJ, 641, L141

Billères, M., Delfosse, X., Beuzit, J.-L., Forveille, T., Marchal, L., & Martín, E. L. 2005, A&A, 440, L55

Binney, J. & Tremaine, S. 2008, Galactic Dynamics: Second Edition, ed. Binney, J. & Tremaine, S. (Princeton University Press)

Bochanski, J. J., Munn, J. A., Hawley, S. L., West, A. A., Covey, K. R., & Schneider, D. P. 2007a, AJ, 134, 2418

Bochanski, J. J., West, A. A., Hawley, S. L., & Covey, K. R. 2007b, AJ, 133, 531

Borysow, A., Jorgensen, U. G., & Zheng, C. 1997, A&A, 324, 185

Boss, A. P., Weinberger, A. J., Anglada-Escudé, G., Thompson, I. B., Burley, G., Birk, C., Pravdo, S. H., Shaklan, S. B., Gatewood, G. D., Majewski, S. R., & Patterson, R. J. 2009, PASP, 121, 1218

Bouvier, J., Kendall, T., Meeus, G., Testi, L., Moraux, E., Stauffer, J. R., James, D., Cuillandre, J., Irwin, J., McCaughrean, M. J., Baraffe, I., & Bertin, E. 2008, A&A, 481, 661

Bouy, H., Brandner, W., Martín, E. L., Delfosse, X., Allard, F., & Basri, G. 2003, AJ, 126, 1526

Bouy, H., Martín, E. L., Brandner, W., Forveille, T., Delfosse, X., Huélamo, N., Basri, G., Girard, J., Zapatero Osorio, M., Stumpf, M., Ghez, A., Valdivielso, L., Marchis, F., Burgasser, A. J., & Cruz, K. 2008, A&A, 481, 757

Bowler, B. P., Liu, M. C., & Cushing, M. C. 2009, ApJ, 706, 1114

Browning, M. K. 2008, ApJ, 676, 1262

Burgasser, A. J. 2004a, ApJ, 614, L73

—. 2004b, ApJS, 155, 191

—. 2007, ApJ, 659, 655

Burgasser, A. J., Burrows, A., & Kirkpatrick, J. D. 2006a, ApJ, 639, 1095

Burgasser, A. J., Cruz, K. L., Cushing, M., Gelino, C. R., Looper, D. L., Faherty, J. K., Kirkpatrick, J. D., & Reid, I. N. 2010a, ApJ, 710, 1142

Burgasser, A. J., Kirkpatrick, J. D., Brown, M. E., Reid, I. N., Burrows, A., Liebert, J., Matthews, K., Gizis, J. E., Dahn, C. C., Monet, D. G., Cutri, R. M., & Skrutskie, M. F. 2002a, ApJ, 564, 421

Burgasser, A. J., Kirkpatrick, J. D., Brown, M. E., Reid, I. N., Gizis, J. E., Dahn, C. C., Monet, D. G., Beichman, C. A., Liebert, J., Cutri, R. M., & Skrutskie, M. F. 1999, ApJ, 522, L65

Burgasser, A. J., Kirkpatrick, J. D., Burrows, A., Liebert, J., Reid, I. N., Gizis, J. E., McGovern, M. R., Prato, L., & McLean, I. S. 2003a, ApJ, 592, 1186

Burgasser, A. J., Kirkpatrick, J. D., Cruz, K. L., Reid, I. N., Leggett, S. K., Liebert, J., Burrows, A., & Brown, M. E. 2006b, ApJS, 166, 585

Burgasser, A. J., Kirkpatrick, J. D., Cutri, R. M., McCallon, H., Kopan, G., Gizis, J. E., Liebert, J., Reid, I. N., Brown, M. E., Monet, D. G., Dahn, C. C., Beichman, C. A., & Skrutskie, M. F. 2000a, ApJ, 531, L57

Burgasser, A. J., Kirkpatrick, J. D., & Lowrance, P. J. 2005, AJ, 129, 2849

Burgasser, A. J., Kirkpatrick, J. D., McElwain, M. W., Cutri, R. M., Burgasser, A. J., & Skrutskie, M. F. 2003b, AJ, 125, 850

Burgasser, A. J., Kirkpatrick, J. D., Reid, I. N., Brown, M. E., Miskey, C. L., & Gizis, J. E. 2003c, ApJ, 586, 512

Burgasser, A. J., Kirkpatrick, J. D., Reid, I. N., Liebert, J., Gizis, J. E., & Brown, M. E. 2000b, AJ, 120, 473

Burgasser, A. J., Looper, D. L., Kirkpatrick, J. D., Cruz, K. L., & Swift, B. J. 2008a, ApJ, 674, 451

Burgasser, A. J., Looper, D. L., Kirkpatrick, J. D., & Liu, M. C. 2007a, ApJ, 658, 557

Burgasser, A. J., Marley, M. S., Ackerman, A. S., Saumon, D., Lodders, K., Dahn, C. C., Harris, H. C., & Kirkpatrick, J. D. 2002b, ApJ, 571, L151

Burgasser, A. J. & McElwain, M. W. 2006, AJ, 131, 1007

Burgasser, A. J., McElwain, M. W., & Kirkpatrick, J. D. 2003d, AJ, 126, 2487

Burgasser, A. J., McElwain, M. W., Kirkpatrick, J. D., Cruz, K. L., Tinney, C. G., & Reid, I. N. 2004, AJ, 127, 2856

Burgasser, A. J., Reid, I. N., Siegler, N., Close, L., Allen, P., Lowrance, P., & Gizis, J. 2007b, in Protostars and Planets V, ed. B. Reipurth, D. Jewitt, & K. Keil, 427–441

Burgasser, A. J., Simcoe, R. A., Bochanski, J. J., Saumon, D., Mamajek, E. E., Cushing, M. C., Marley, M. S., McMurtry, C., Pipher, J. L., & Forrest, W. J. 2010b, ArXiv e-prints

Burgasser, A. J., Tinney, C. G., Cushing, M. C., Saumon, D., Marley, M. S., Bennett, C. S., & Kirkpatrick, J. D. 2008b, ApJ, 689, L53

Burgasser, A. J., Vrba, F. J., Lépine, S., Munn, J. A., Luginbuhl, C. B., Henden, A. A., Guetter, H. H., & Canzian, B. C. 2008c, ApJ, 672, 1159

Burgasser, A. J., Wilson, J. C., Kirkpatrick, J. D., Skrutskie, M. F., Colonno, M. R., Enos, A. T., Smith, J. D., Henderson, C. P., Gizis, J. E., Brown, M. E., & Houck, J. R. 2000c, AJ, 120, 1100

Burgasser, A. J., Witte, S., Helling, C., Sanderson, R. E., Bochanski, J. J., & Hauschildt, P. H. 2009, ArXiv e-prints

Burningham, B., Pinfield, D. J., Leggett, S. K., Tinney, C. G., Liu, M. C., Homeier, D., West, A. A., Day-Jones, A., Huelamo, N., Dupuy, T. J., Zhang, Z., Murray, D. N., Lodieu, N., Barrado y Navascues, D., Folkes, S., Galvez-Ortiz, M. C., Jones, H. R. A., Lucas, P. W., Morales Calderon, M., & Tamura, M. 2009, ArXiv e-prints

Burrows, A., Burgasser, A. J., Kirkpatrick, J. D., Liebert, J., Milsom, J. A., Sudarsky, D., & Hubeny, I. 2002, ApJ, 573, 394

Burrows, A., Dulick, M., Bauschlicher, Jr., C. W., Bernath, P. F., Ram, R. S., Sharp, C. M., & Milsom, J. A. 2005, ApJ, 624, 988

Burrows, A., Hubbard, W. B., & Lunine, J. I. 1989, ApJ, 345, 939

Burrows, A., Hubbard, W. B., Lunine, J. I., & Liebert, J. 2001, Reviews of Modern Physics, 73, 719

Burrows, A., Hubbard, W. B., Lunine, J. I., Marley, M., Guillot, T., Saumon, D., & Freedman, R. S. 1997, in Astronomical Society of the Pacific Conference Series, Vol. 119, Planets Beyond the Solar System and the Next Generation of Space Missions, ed. D. Soderblom, 9–+

Burrows, A. & Liebert, J. 1993, Reviews of Modern Physics, 65, 301

Burrows, A., Sudarsky, D., & Hubeny, I. 2006, ApJ, 640, 1063

Caballero, J. A. 2007, ApJ, 667, 520

Carpenter, J. M. 2001, AJ, 121, 2851

Casewell, S. L., Jameson, R. F., & Burleigh, M. R. 2008, MNRAS, 390, 1517

Chabrier, G. & Baraffe, I. 1997, A&A, 327, 1039

Chabrier, G., Baraffe, I., Allard, F., & Hauschildt, P. 2000, ApJ, 542, 464

Chanamé, J. & Gould, A. 2004, ApJ, 601, 289

Chauvin, G., Lagrange, A.-M., Dumas, C., Zuckerman, B., Mouillet, D., Song, I., Beuzit, J.-L., & Lowrance, P. 2004, A&A, 425, L29

Chauvin, G., Lagrange, A.-M., Lacombe, F., Dumas, C., Mouillet, D., Zuckerman, B., Gendron, E., Song, I., Beuzit, J.-L., Lowrance, P., & Fusco, T. 2005a, A&A, 430, 1027

Chauvin, G., Lagrange, A.-M., Zuckerman, B., Dumas, C., Mouillet, D., Song, I., Beuzit, J.-L., Lowrance, P., & Bessell, M. S. 2005b, A&A, 438, L29

Chereul, E., Crézé, M., & Bienaymé, O. 1999, A&AS, 135, 5

Chereul, E. & Grenon, M. 2001, in Astronomical Society of the Pacific Conference Series, Vol. 228, Dynamics of Star Clusters and the Milky Way, ed. S. Deiters, B. Fuchs, A. Just, R. Spurzem, & R. Wielen, 398–+

Chiba, M. & Beers, T. C. 2000, AJ, 119, 2843

Chiu, K., Fan, X., Leggett, S. K., Golimowski, D. A., Zheng, W., Geballe, T. R., Schneider, D. P., & Brinkmann, J. 2006, AJ, 131, 2722

Chiu, K., Liu, M. C., Jiang, L., Allers, K. N., Stark, D. P., Bunker, A., Fan, X., Glazebrook, K., & Dupuy, T. J. 2008, MNRAS, 385, L53

Close, L. M., Siegler, N., Freed, M., & Biller, B. 2003, ApJ, 587, 407

Close, L. M., Zuckerman, B., Song, I., Barman, T., Marois, C., Rice, E. L., Siegler, N., Macintosh, B., Becklin, E. E., Campbell, R., Lyke, J. E., Conrad, A., & Le Mignant, D. 2007, ApJ, 660, 1492

Costa, E., Méndez, R. A., Jao, W.-C., Henry, T. J., Subasavage, J. P., Brown, M. A., Ianna, P. A., & Bartlett, J. 2005, AJ, 130, 337

Costa, E., Méndez, R. A., Jao, W.-C., Henry, T. J., Subasavage, J. P., & Ianna, P. A. 2006, AJ, 132, 1234

Covey, K. R., Hawley, S. L., Bochanski, J. J., West, A. A., Reid, I. N., Golimowski, D. A., Davenport, J. R. A., Henry, T., Uomoto, A., & Holtzman, J. A. 2008, AJ, 136, 1778

Covey, K. R., Ivezić, Ž., Schlegel, D., Finkbeiner, D., Padmanabhan, N., Lupton, R. H., Agüeros, M. A., Bochanski, J. J., Hawley, S. L., West, A. A., Seth, A., Kimball, A., Gogarten, S. M., Claire, M., Haggard, D., Kaib, N., Schneider, D. P., & Sesar, B. 2007, AJ, 134, 2398

Cox, A. N. 2000, Allen's astrophysical quantities (Springer; 4th edition (April 20, 2001))

Cruz, K. L., Kirkpatrick, J. D., & Burgasser, A. J. 2009, AJ, 137, 3345

Cruz, K. L. & Reid, I. N. 2002, AJ, 123, 2828

Cruz, K. L., Reid, I. N., Kirkpatrick, J. D., Burgasser, A. J., Liebert, J., Solomon, A. R., Schmidt, S. J., Allen, P. R., Hawley, S. L., & Covey, K. R. 2007, AJ, 133, 439

Cruz, K. L., Reid, I. N., Liebert, J., Kirkpatrick, J. D., & Lowrance, P. J. 2003, AJ, 126, 2421

Cushing, M. C., Looper, D., Burgasser, A. J., Kirkpatrick, J. D., Faherty, J., Cruz, K. L., Sweet, A., & Sanderson, R. E. 2009, ApJ, 696, 986

Cushing, M. C., Marley, M. S., Saumon, D., Kelly, B. C., Vacca, W. D., Rayner, J. T., Freedman, R. S., Lodders, K., & Roellig, T. L. 2008, ApJ, 678, 1372

Cushing, M. C., Saumon, D., & Marley, M. S. 2010, AJ, 140, 1428

Cushing, M. C., Vacca, W. D., & Rayner, J. T. 2004, PASP, 116, 362

Dahn, C. C., Harris, H. C., Vrba, F. J., Guetter, H. H., Canzian, B., Henden, A. A., Levine, S. E., Luginbuhl, C. B., Monet, A. K. B., Monet, D. G., Pier, J. R., Stone, R. C., Walker, R. L., Burgasser, A. J., Gizis, J. E., Kirkpatrick, J. D., Liebert, J., & Reid, I. N. 2002, AJ, 124, 1170

Dantona, F. & Mazzitelli, I. 1985, ApJ, 296, 502

de Bruijne, J. H. J., Hoogerwerf, R., & de Zeeuw, P. T. 2001, A&A, 367, 111

Deacon, N. R. & Hambly, N. C. 2007, A&A, 468, 163

Deacon, N. R., Hambly, N. C., & Cooke, J. A. 2005, A&A, 435, 363

Deacon, N. R., Hambly, N. C., King, R. R., & McCaughrean, M. J. 2009, MNRAS, 394, 857

Dehnen, W. & Binney, J. J. 1998, MNRAS, 298, 387

Delfosse, X., Forveille, T., Martín, E. L., Guibert, J., Borsenberger, J., Crifo, F., Alard, C., Epchtein, N., Fouqué, P., Simon, G., & Tajahmady, F. 2001, A&A, 366, L13

Delfosse, X., Tinney, C. G., Forveille, T., Epchtein, N., Bertin, E., Borsenberger, J., Copet, E., de Batz, B., Fouque, P., Kimeswenger, S., Le Bertre, T., Lacombe, F., Rouan, D., & Tiphene, D. 1997, A&A, 327, L25

Delfosse, X., Tinney, C. G., Forveille, T., Epchtein, N., Borsenberger, J., Fouqué, P., Kimeswenger, S., & Tiphène, D. 1999, A&AS, 135, 41

Delgado-Donate, E. J., Clarke, C. J., Bate, M. R., & Hodgkin, S. T. 2004, MNRAS, 351, 617

Dhital, S., West, A. A., Stassun, K. G., & Bochanski, J. J. 2010, AJ, 139, 2566

Dotter, A., Sarajedini, A., Anderson, J., Aparicio, A., Bedin, L. R., Chaboyer, B., Majewski, S., Marín-Franch, A., Milone, A., Paust, N., Piotto, G., Reid, I. N., Rosenberg, A., & Siegel, M. 2010, ApJ, 708, 698

Dupuy, T. J. & Liu, M. C. 2009, ApJ, 704, 1519

Dupuy, T. J., Liu, M. C., & Bowler, B. P. 2009, ApJ, 706, 328

Dupuy, T. J., Liu, M. C., & Ireland, M. J. 2008, ArXiv e-prints

Duquennoy, A. & Mayor, M. 1991, A&A, 248, 485

Durney, B. R., De Young, D. S., & Roxburgh, I. W. 1993, Sol. Phys., 145, 207

Dworetsky, M. M. 1983, MNRAS, 203, 917

Eggen, O. J. 1989, PASP, 101, 54

—. 1990, PASP, 102, 166

—. 1993, AJ, 106, 1885

Eggen, O. J. & Iben, I. J. 1989, AJ, 97, 431

Ellis, S. C., Tinney, C. G., Burgasser, A. J., Kirkpatrick, J. D., & McElwain, M. W. 2005, AJ, 130, 2347

Epchtein, N., de Batz, B., Capoani, L., Chevallier, L., Copet, E., Fouqué, P., Lacombe, P., Le Bertre, T., Pau, S., Rouan, D., Ruphy, S., Simon, G., Tiphène, D., Burton, W. B., Bertin, E., Deul, E., Habing, H., Borsenberger, J., Dennefeld, M., Guglielmo, F., Loup, C., Mamon, G., Ng, Y., Omont, A., Provost, L., Renault, J.-C., Tanguy, F., Kimeswenger, S., Kienel, C., Garzon, F., Persi, P., Ferrari-Toniolo, M., Robin, A., Paturel, G., Vauglin, I., Forveille, T., Delfosse, X., Hron, J., Schultheis, M., Appenzeller, I., Wagner, S., Balazs, L., Holl, A., Lépine, J., Boscolo, P., Picazzio, E., Duc, P.-A., & Mennessier, M.-O. 1997, The Messenger, 87, 27

EROS Collaboration, Goldman, B., Delfosse, X., Forveille, T., Afonso, C., Alard, C., Albert, J. N., Andersen, J., Ansari, R., Aubourg, É., Bareyre, P., Bauer, F., Beaulieu, J. P., Borsenberger, J., Bouquet, A., Char, S., Charlot, X., Couchot, F., Coutures, C., Derue, F., Ferlet, R., Fouqué, P., Glicenstein, J. F., Gould, A., Graff, D., Gros, M., Haissinski, J., Hamilton, J. C., Hardin, D., de Kat, J., Kim, A., Lasserre, T., Lesquoy, É., Loup, C., Magneville, C., Mansoux, B., Marquette, J. B., Martín, E. L., Maurice, É., Milsztajn, A., Moniez, M., Palanque-Delabrouille, N., Perdereau, O., Prévot, L., Regnault, N., Rich, J., Spiro, M., Vidal-Madjar, A., Vigroux, L., & Zylberajch, S. 1999, A&A, 351, L5

Faherty, J. K., Burgasser, A. J., Cruz, K. L., Shara, M. M., Walter, F. M., & Gelino, C. R. 2009, AJ, 137, 1

Famaey, B., Jorissen, A., Luri, X., Mayor, M., Udry, S., Dejonghe, H., & Turon, C. 2005, A&A, 430, 165

Famaey, B., Pont, F., Luri, X., Udry, S., Mayor, M., & Jorissen, A. 2007, A&A, 461, 957

Famaey, B., Siebert, A., & Jorissen, A. 2008, A&A, 483, 453

Fan, X., Knapp, G. R., Strauss, M. A., Gunn, J. E., Lupton, R. H., Ivezić, Ž., Rockosi, C. M., Yanny, B., Kent, S., Schneider, D. P., Kirkpatrick, J. D., Annis, J., Bastian, S., Berman, E., Brinkmann, J., Csabai, I., Federwitz, G. R., Fukugita, M., Gurbani, V. K., Hennessy, G. S., Hindsley, R. B., Ichikawa, T., Lamb, D. Q., Lindenmeyer, C., Mantsch, P. M., McKay, T. A., Munn, J. A., Nash, T., Okamura, S., Pauls, A. G., Pier, J. R., Rechenmacher, R., Rivetta, C. H., Sergey, G., Stoughton, C., Szalay, A. S., Szokoly, G. P., Tucker, D. L., York, D. G., & The SDSS Collaboration. 2000, AJ, 119, 928

Fazio, G. G., Hora, J. L., Allen, L. E., Ashby, M. L. N., Barmby, P., Deutsch, L. K., Huang, J.-S., Kleiner, S., Marengo, M., Megeath, S. T., Melnick,

G. J., Pahre, M. A., Patten, B. M., Polizotti, J., Smith, H. A., Taylor, R. S., Wang, Z., Willner, S. P., Hoffmann, W. F., Pipher, J. L., Forrest, W. J., McMurty, C. W., McCreight, C. R., McKelvey, M. E., McMurray, R. E., Koch, D. G., Moseley, S. H., Arendt, R. G., Mentzell, J. E., Marx, C. T., Losch, P., Mayman, P., Eichhorn, W., Krebs, D., Jhabvala, M., Gezari, D. Y., Fixsen, D. J., Flores, J., Shakoorzadeh, K., Jungo, R., Hakun, C., Workman, L., Karpati, G., Kichak, R., Whitley, R., Mann, S., Tollestrup, E. V., Eisenhardt, P., Stern, D., Gorjian, V., Bhattacharya, B., Carey, S., Nelson, B. O., Glaccum, W. J., Lacy, M., Lowrance, P. J., Laine, S., Reach, W. T., Stauffer, J. A., Surace, J. A., Wilson, G., Wright, E. L., Hoffman, A., Domingo, G., & Cohen, M. 2004, ApJS, 154, 10

Fischer, D. A. & Marcy, G. W. 1992, ApJ, 396, 178

Fleming, T. A., Schmitt, J. H. M. M., & Giampapa, M. S. 1995, ApJ, 450, 401

Folkes, S. L., Pinfield, D. J., Kendall, T. R., & Jones, H. R. A. 2007, MNRAS, 378, 901

Forrest, W. J., Barnett, J. D., Ninkov, Z., Skrutskie, M., & Shure, M. 1989, PASP, 101, 877

Forveille, T., Beuzit, J.-L., Delorme, P., Ségransan, D., Delfosse, X., Chauvin, G., Fusco, T., Lagrange, A.-M., Mayor, M., Montagnier, G., Mouillet, D., Perrier, C., Udry, S., Charton, J., Gigan, P., Conan, J.-M., Kern, P., & Michet, G. 2005, A&A, 435, L5

Freeman, K. & Bland-Hawthorn, J. 2002, ARA&A, 40, 487

Geballe, T. R., Knapp, G. R., Leggett, S. K., Fan, X., Golimowski, D. A., Anderson, S., Brinkmann, J., Csabai, I., Gunn, J. E., Hawley, S. L., Hennessy, G., Henry, T. J., Hill, G. J., Hindsley, R. B., Ivezić, Ž., Lupton, R. H., McDaniel, A., Munn, J. A., Narayanan, V. K., Peng, E., Pier, J. R., Rockosi, C. M., Schneider, D. P., Smith, J. A., Strauss, M. A., Tsvetanov, Z. I., Uomoto, A., York, D. G., & Zheng, W. 2002, ApJ, 564, 466

Gelino, C. R., Marley, M. S., Holtzman, J. A., Ackerman, A. S., & Lodders, K. 2002, ApJ, 577, 433

Gilmore, G. & Reid, N. 1983, MNRAS, 202, 1025

Gilmore, G., Wyse, R. F. G., & Kuijken, K. 1989, ARA&A, 27, 555

Gizis, J. E. 2002, ApJ, 575, 484

Gizis, J. E. & Harvin, J. 2006, AJ, 132, 2372

Gizis, J. E., Jao, W.-C., Subasavage, J. P., & Henry, T. J. 2007, ApJ, 669, L45

Gizis, J. E., Kirkpatrick, J. D., Burgasser, A., Reid, I. N., Monet, D. G., Liebert, J., & Wilson, J. C. 2001a, ApJ, 551, L163

Gizis, J. E., Kirkpatrick, J. D., & Wilson, J. C. 2001b, AJ, 121, 2185

Gizis, J. E., Monet, D. G., Reid, I. N., Kirkpatrick, J. D., & Burgasser, A. J. 2000a, MNRAS, 311, 385

Gizis, J. E., Monet, D. G., Reid, I. N., Kirkpatrick, J. D., Liebert, J., & Williams, R. J. 2000b, AJ, 120, 1085

Gizis, J. E., Reid, I. N., & Hawley, S. L. 2002, AJ, 123, 3356

Gizis, J. E., Reid, I. N., Knapp, G. R., Liebert, J., Kirkpatrick, J. D., Koerner, D. W., & Burgasser, A. J. 2003, AJ, 125, 3302

Golimowski, D. A., Henry, T. J., Krist, J. E., Dieterich, S., Ford, H. C., Illingworth, G. D., Ardila, D. R., Clampin, M., Franz, O. G., Wasserman, L. H., Benedict, G. F., McArthur, B. E., & Nelan, E. G. 2004a, AJ, 128, 1733

Golimowski, D. A., Leggett, S. K., Marley, M. S., Fan, X., Geballe, T. R., Knapp, G. R., Vrba, F. J., Henden, A. A., Luginbuhl, C. B., Guetter, H. H., Munn, J. A., Canzian, B., Zheng, W., Tsvetanov, Z. I., Chiu, K., Glazebrook, K., Hoversten, E. A., Schneider, D. P., & Brinkmann, J. 2004b, AJ, 127, 3516

Gontcharov, G. A. 2006, Astronomical and Astrophysical Transactions, 25, 145

Goodwin, S. P., Kroupa, P., Goodman, A., & Burkert, A. 2007, Protostars and Planets V, 133

Grossman, A. S., Hays, D., & Graboske, Jr., H. C. 1974, A&A, 30, 95

Halbwachs, J. L., Mayor, M., Udry, S., & Arenou, F. 2003, A&A, 397, 159

Hall, P. B. 2002, ApJ, 580, L77

Hambly, N. C., Davenhall, A. C., Irwin, M. J., & MacGillivray, H. T. 2001, MNRAS, 326, 1315

Hambly, N. C., Henry, T. J., Subasavage, J. P., Brown, M. A., & Jao, W.-C. 2004, AJ, 128, 437

Hänninen, J. & Flynn, C. 2002, MNRAS, 337, 731

Hauschildt, P. H., Allard, F., Ferguson, J., Baron, E., & Alexander, D. R. 1999, ApJ, 525, 871

Hauschildt, P. H., Baron, E., & Allard, F. 1997, ApJ, 483, 390

Hawkins, M. R. S. & Bessell, M. S. 1988, MNRAS, 234, 177

Hawley, S. L., Covey, K. R., Knapp, G. R., Golimowski, D. A., Fan, X., Anderson, S. F., Gunn, J. E., Harris, H. C., Ivezić, Ž., Long, G. M., Lupton, R. H., McGehee, P. M., Narayanan, V., Peng, E., Schlegel, D., Schneider, D. P., Spahn, E. Y., Strauss, M. A., Szkody, P., Tsvetanov, Z., Walkowicz, L. M., Brinkmann, J., Harvanek, M., Hennessy, G. S., Kleinman, S. J., Krzesinski, J., Long, D., Neilsen, E. H., Newman, P. R., Nitta, A., Snedden, S. A., & York, D. G. 2002, AJ, 123, 3409

Hayashi, C. & Nakano, T. 1963, Progress of Theoretical Physics, 30, 460

Helling, C., Ackerman, A., Allard, F., Dehn, M., Hauschildt, P., Homeier, D., Lodders, K., Marley, M., Rietmeijer, F., Tsuji, T., & Woitke, P. 2008, MNRAS, 391, 1854

Henry, T. J., Jao, W.-C., Subasavage, J. P., Beaulieu, T. D., Ianna, P. A., Costa, E., & Méndez, R. A. 2006, AJ, 132, 2360

Henry, T. J., Soderblom, D. R., Donahue, R. A., & Baliunas, S. L. 1996, AJ, 111, 439

Henry, T. J., Subasavage, J. P., Brown, M. A., Beaulieu, T. D., Jao, W.-C., & Hambly, N. C. 2004, AJ, 128, 2460

Hog, E., Fabricius, C., Makarov, V. V., Urban, S., Corbin, T., Wycoff, G., Bastian, U., Schwekendiek, P., & Wicenec, A. 2000, VizieR Online Data Catalog, 1259, 0

Holmberg, J., Nordstroem, B., & Andersen, J. 2008, VizieR Online Data Catalog, 5128, 0

Ibukiyama, A. & Arimoto, N. 2002, VizieR Online Data Catalog, 339, 40927

Irwin, M., McMahon, R. G., & Reid, N. 1991, MNRAS, 252, 61P

Iwanowska, W. 1980, Ap&SS, 73, 435

Jameson, R. F., Casewell, S. L., Bannister, N. P., Lodieu, N., Keresztes, K., Dobbie, P. D., & Hodgkin, S. T. 2008a, MNRAS, 384, 1399

Jameson, R. F., Lodieu, N., Casewell, S. L., Bannister, N. P., & Dobbie, P. D. 2008b, MNRAS, 385, 1771

Jao, W., Henry, T. J., Subasavage, J. P., Brown, M. A., Ianna, P. A., Bartlett, J. L., Costa, E., & Méndez, R. A. 2005, AJ, 129, 1954

Johnson, D. R. H. & Soderblom, D. R. 1987, AJ, 93, 864

Johnson, H. L. & Mitchell, R. I. 1958, ApJ, 128, 31

Kendall, T. R., Delfosse, X., Martín, E. L., & Forveille, T. 2004, A&A, 416, L17

Kendall, T. R., Mauron, N., Azzopardi, M., & Gigoyan, K. 2003, A&A, 403, 929

Kendall, T. R., Tamura, M., Tinney, C. G., Martín, E. L., Ishii, M., Pinfield, D. J., Lucas, P. W., Jones, H. R. A., Leggett, S. K., Dye, S., Hewett, P. C., Allard, F., Baraffe, I., Barrado Y Navascués, D., Carraro, G., Casewell, S. L., Chabrier, G., Chappelle, R. J., Clarke, F., Day-Jones, A., Deacon, N., Dobbie, P. D., Folkes, S., Hambly, N. C., Hodgkin, S. T., Nakajima, T., Jameson, R. F., Lodieu, N., Magazzù, A., McCaughrean, M. J., Pavlenko, Y. V., Tadashi, N., & Zapatero Osorio, M. R. 2007, A&A, 466, 1059

Kharchenko, N. V., Piskunov, A. E., & Scholz, R. 2004, VizieR Online Data Catalog, 3239, 0

Kirkpatrick, J. D. 2005, ARA&A, 43, 195

Kirkpatrick, J. D., Barman, T. S., Burgasser, A. J., McGovern, M. R., McLean, I. S., Tinney, C. G., & Lowrance, P. J. 2006, ApJ, 639, 1120

Kirkpatrick, J. D., Beichman, C. A., & Skrutskie, M. F. 1997, ApJ, 476, 311

Kirkpatrick, J. D., Cruz, K. L., Barman, T. S., Burgasser, A. J., Looper, D. L., Tinney, C. G., Gelino, C. R., Lowrance, P. J., Liebert, J., Carpenter, J. M., Hillenbrand, L. A., & Stauffer, J. R. 2008, ApJ, 689, 1295

Kirkpatrick, J. D., Dahn, C. C., Monet, D. G., Reid, I. N., Gizis, J. E., Liebert, J., & Burgasser, A. J. 2001a, AJ, 121, 3235

Kirkpatrick, J. D., Henry, T. J., & Liebert, J. 1993, ApJ, 406, 701

Kirkpatrick, J. D., Henry, T. J., & McCarthy, Jr., D. W. 1991, ApJS, 77, 417

Kirkpatrick, J. D., Liebert, J., Cruz, K. L., Gizis, J. E., & Reid, I. N. 2001b, PASP, 113, 814

Kirkpatrick, J. D., Looper, D. L., Burgasser, A. J., Schurr, S. D., Cutri, R. M., Cushing, M. C., Cruz, K. L., Sweet, A. C., Knapp, G. R., Barman, T. S., Bochanski, J. J., Roellig, T. L., McLean, I. S., McGovern, M. R., & Rice, E. L. 2010, ApJS, 190, 100

Kirkpatrick, J. D., McGraw, J. T., Hess, T. R., Liebert, J., & McCarthy, Jr., D. W. 1994, ApJS, 94, 749

Kirkpatrick, J. D., Reid, I. N., Liebert, J., Cutri, R. M., Nelson, B., Beichman, C. A., Dahn, C. C., Monet, D. G., Gizis, J. E., & Skrutskie, M. F. 1999, ApJ, 519, 802

Kirkpatrick, J. D., Reid, I. N., Liebert, J., Gizis, J. E., Burgasser, A. J., Monet, D. G., Dahn, C. C., Nelson, B., & Williams, R. J. 2000, AJ, 120, 447

Kitchin, C. R. 2004, Astronomy Now (ISSN 0951-9726), Vol. 18, No. 4, p. 24 (2004), 18, 040000

Knapp, G. R., Leggett, S. K., Fan, X., Marley, M. S., Geballe, T. R., Golimowski, D. A., Finkbeiner, D., Gunn, J. E., Hennawi, J., Ivezić, Z., Lupton, R. H., Schlegel, D. J., Strauss, M. A., Tsvetanov, Z. I., Chiu, K., Hoversten, E. A., Glazebrook, K., Zheng, W., Hendrickson, M., Williams, C. C., Uomoto, A., Vrba, F. J., Henden, A. A., Luginbuhl, C. B., Guetter, H. H., Munn, J. A., Canzian, B., Schneider, D. P., & Brinkmann, J. 2004, AJ, 127, 3553

Konopacky, Q. M., Ghez, A. M., Barman, T. S., Rice, E. L., Bailey, J. I., White, R. J., McLean, I. S., & Duchêne, G. 2010a, ApJ, 711, 1087

Konopacky, Q. M., Ghez, A. M., Barman, T. S., Rice, E. L., Bailey, III, J. I., White, R. J., McLean, I. S., & Duchene, G. 2010b, ArXiv e-prints

Konopacky, Q. M., Ghez, A. M., Rice, E. L., & Duchêne, G. 2007, ApJ, 663, 394

Kraus, A. L., White, R. J., & Hillenbrand, L. A. 2005, ApJ, 633, 452

—. 2006, ApJ, 649, 306

Kumar, S. S. 1962, AJ, 67, 579

Lachaume, R., Dominik, C., Lanz, T., & Habing, H. J. 1999, A&A, 348, 897

Lafrenière, D., Jayawardhana, R., Brandeker, A., Ahmic, M., & van Kerkwijk, M. H. 2008, ApJ, 683, 844

Lane, B. F., Zapatero Osorio, M. R., Britton, M. C., Martín, E. L., & Kulkarni, S. R. 2001, ApJ, 560, 390

Lasker, B. M., Lattanzi, M. G., McLean, B. J., Bucciarelli, B., Drimmel, R., Garcia, J., Greene, G., Guglielmetti, F., Hanley, C., Hawkins, G., Laidler, V. G., Loomis, C., Meakes, M., Mignani, R., Morbidelli, R., Morrison, J., Pannunzio, R., Rosenberg, A., Sarasso, M., Smart, R. L., Spagna, A., Sturch, C. R., Volpicelli, A., White, R. L., Wolfe, D., & Zacchei, A. 2008, AJ, 136, 735

Latham, D. W., Schechter, P., Tonry, J., Bahcall, J. N., & Soneira, R. M. 1984, ApJ, 281, L41

Latham, D. W., Stefanik, R. P., Torres, G., Davis, R. J., Mazeh, T., Carney, B. W., Laird, J. B., & Morse, J. A. 2002, AJ, 124, 1144

Law, N. M., Dhital, S., Kraus, A., Stassun, K. G., & West, A. A. 2010, ApJ, 720, 1727

Law, N. M., Hodgkin, S. T., & Mackay, C. D. 2006, MNRAS, 368, 1917

Leggett, S. K. 1992, ApJS, 82, 351

Leggett, S. K., Allard, F., Dahn, C., Hauschildt, P. H., Kerr, T. H., & Rayner, J. 2000, ApJ, 535, 965

Leggett, S. K., Burningham, B., Saumon, D., Marley, M. S., Warren, S. J., Smart, R. L., Jones, H. R. A., Lucas, P. W., Pinfield, D. J., & Tamura, M. 2010, ApJ, 710, 1627

Leggett, S. K., Cushing, M. C., Saumon, D., Marley, M. S., Roellig, T. L., Warren, S. J., Burningham, B., Jones, H. R. A., Kirkpatrick, J. D., Lodieu, N., Lucas, P. W., Mainzer, A. K., Martín, E. L., McCaughrean, M. J., Pinfield, D. J., Sloan, G. C., Smart, R. L., Tamura, M., & Van Cleve, J. 2009, ApJ, 695, 1517

Leggett, S. K. & Hawkins, M. R. S. 1988, MNRAS, 234, 1065

Leggett, S. K., Saumon, D., Albert, L., Cushing, M. C., Liu, M. C., Luhman, K. L., Marley, M. S., Kirkpatrick, J. D., Roellig, T. L., & Allers, K. N. 2008, ApJ, 682, 1256

Lépine, S. 2005, AJ, 130, 1680

Lépine, S. & Bongiorno, B. 2007, AJ, 133, 889

Lépine, S., Rich, R. M., & Shara, M. M. 2003, ApJ, 591, L49

Lépine, S., Shara, M. M., & Rich, R. M. 2002, AJ, 124, 1190

Liebert, J. & Gizis, J. E. 2006, PASP, 118, 659

Liebert, J., Kirkpatrick, J. D., Cruz, K. L., Reid, I. N., Burgasser, A., Tinney, C. G., & Gizis, J. E. 2003, AJ, 125, 343

Lindblad, B. 1925, ApJ, 62, 191

Linsky, J. L. 1969, ApJ, 156, 989

Linsky, J. L., Hunten, D. M., Sowell, R., Glackin, D. L., & Kelch, W. L. 1979, ApJS, 41, 481

Liu, M. C., Fischer, D. A., Graham, J. R., Lloyd, J. P., Marcy, G. W., & Butler, R. P. 2002, ApJ, 571, 519

Liu, M. C., Leggett, S. K., Golimowski, D. A., Chiu, K., Fan, X., Geballe, T. R., Schneider, D. P., & Brinkmann, J. 2006, ApJ, 647, 1393

Liu, M. C., Magnier, E., Brandner, W., Brown, T., Covey, K., Cushing, M., Dupuy, T., Goldman, B., Gouliermis, D., Gredel, R., Hambly, N., Henning, T., Hodapp, K., Joergens, V., Lister, T., Mamajek, E., Mosoni, L., & Science Consortium, P. 2007, in Bulletin of the American Astronomical Society, Vol. 38, Bulletin of the American Astronomical Society, 806–+

Lodieu, N., Scholz, R.-D., & McCaughrean, M. J. 2002, A&A, 389, L20

Lodieu, N., Scholz, R.-D., McCaughrean, M. J., Ibata, R., Irwin, M., & Zinnecker, H. 2005, A&A, 440, 1061

Looper, D. L., Gelino, C. R., Burgasser, A. J., & Kirkpatrick, J. D. 2008a, ApJ, 685, 1183

Looper, D. L., Kirkpatrick, J. D., & Burgasser, A. J. 2007, AJ, 134, 1162

Looper, D. L., Kirkpatrick, J. D., Cutri, R. M., Barman, T., Burgasser, A. J., Cushing, M. C., Roellig, T., McGovern, M. R., McLean, I. S., Rice, E., Swift, B. J., & Schurr, S. D. 2008b, ApJ, 686, 528

Low, C. & Lynden-Bell, D. 1976, MNRAS, 176, 367

Lowrance, P. J., McCarthy, C., Becklin, E. E., Zuckerman, B., Schneider, G., Webb, R. A., Hines, D. C., Kirkpatrick, J. D., Koerner, D. W., Low, F., Meier, R., Rieke, M., Smith, B. A., Terrile, R. J., & Thompson, R. I. 1999, ApJ, 512, L69

Lowrance, P. J., Schneider, G., Kirkpatrick, J. D., Becklin, E. E., Weinberger, A. J., Zuckerman, B., Plait, P., Malmuth, E. M., Heap, S. R., Schultz, A., Smith, B. A., Terrile, R. J., & Hines, D. C. 2000, ApJ, 541, 390

Luhman, K. L., Mamajek, E. E., Allen, P. R., Muench, A. A., & Finkbeiner, D. P. 2009, ApJ, 691, 1265

Luhman, K. L., Patten, B. M., Marengo, M., Schuster, M. T., Hora, J. L., Ellis, R. G., Stauffer, J. R., Sonnett, S. M., Winston, E., Gutermuth, R. A., Megeath, S. T., Backman, D. E., Henry, T. J., Werner, M. W., & Fazio, G. G. 2007, ApJ, 654, 570

Luhman, K. L. & Rieke, G. H. 1999, ApJ, 525, 440

Luyten, W. J. 1973, in IAU Symposium, Vol. 54, Problems of Calibration of Absolute Magnitudes and Temperature of Stars, ed. B. Hauck & B. E. Westerlund, 11–+

Luyten, W. J. 1979, LHS catalogue. A catalogue of stars with proper motions exceeding 0”5 annually (Minneapolis: University of Minnesota, 1979, 2nd ed.)

—. 1988, Ap&SS, 142, 17

—. 1995, VizieR Online Data Catalog, 1098, 0

Mainzer, A., Cushing, M. C., Skrutskie, M., Gelino, C. R., Kirkpatrick, J. D., Jarrett, T., Masci, F., Marley, M., Saumon, D., Wright, E., Beaton, R., Dietrich, M., Eisenhardt, P., Garnavich, P., Kuhn, O., Leisawitz, D., Marsh, K., McLean, I., Padgett, D., & Rueff, K. 2010, ArXiv e-prints

Mamajek, E. E. & Hillenbrand, L. A. 2008, ApJ, 687, 1264

Marley, M. S., Saumon, D., & Goldblatt, C. 2010, ApJ, 723, L117

Marley, M. S., Seager, S., Saumon, D., Lodders, K., Ackerman, A. S., Freedman, R. S., & Fan, X. 2002, ApJ, 568, 335

Marshall, J. L., Burles, S., Thompson, I. B., Shectman, S. A., Bigelow, B. C., Burley, G., Birk, C., Estrada, J., Jones, P., Smith, M., Kowal, V., Castillo, J., Storts, R., & Ortiz, G. 2008, in Society of Photo-Optical Instrumentation Engineers (SPIE) Conference Series, Vol. 7014, Society of Photo-Optical Instrumentation Engineers (SPIE) Conference Series

Martin, E. L., Brandner, W., & Basri, G. 1999, Science, 283, 1718

Martín, E. L., Brandner, W., Bouy, H., Basri, G., Davis, J., Deshpande, R., & Montgomery, M. M. 2006, A&A, 456, 253

Martín, E. L., Delfosse, X., Basri, G., Goldman, B., Forveille, T., & Zapatero Osorio, M. R. 1999, AJ, 118, 2466

Martín, E. L., Magazzù, A., Delfosse, X., & Mathieu, R. D. 2005, A&A, 429, 939

Martin, E. L., Rebolo, R., & Magazzu, A. 1994, ApJ, 436, 262

McElwain, M. W. & Burgasser, A. J. 2006, AJ, 132, 2074

McGovern, M. R., Kirkpatrick, J. D., McLean, I. S., Burgasser, A. J., Prato, L., & Lowrance, P. J. 2004, ApJ, 600, 1020

McLean, I. S., McGovern, M. R., Burgasser, A. J., Kirkpatrick, J. D., Prato, L., & Kim, S. S. 2003, ApJ, 596, 561

Ménard, F., Delfosse, X., & Monin, J.-L. 2002, A&A, 396, L35

Metchev, S. A. & Hillenbrand, L. A. 2004, ApJ, 617, 1330

—. 2006, ApJ, 651, 1166

Mihalas, D. & Binney, J. 1981, Galactic astronomy: Structure and kinematics /2nd edition/, ed. Mihalas, D. & Binney, J.

Mitchell, R. I. & Johnson, H. L. 1957, ApJ, 125, 414

Mohanty, S. & Basri, G. 2003, ApJ, 583, 451

Mohanty, S., Basri, G., Shu, F., Allard, F., & Chabrier, G. 2002, ApJ, 571, 469

Mohanty, S., Jayawardhana, R., & Basri, G. 2004, ApJ, 609, 885

Monet, D. 1998, USNO-A2.0, ed. Monet, D.

Monet, D. G., Dahn, C. C., Vrba, F. J., Harris, H. C., Pier, J. R., Luginbuhl, C. B., & Ables, H. D. 1992, AJ, 103, 638

Monet, D. G., Levine, S. E., Canzian, B., Ables, H. D., Bird, A. R., Dahn, C. C., Guetter, H. H., Harris, H. C., Henden, A. A., Leggett, S. K., Levison, H. F., Luginbuhl, C. B., Martini, J., Monet, A. K. B., Munn, J. A., Pier, J. R., Rhodes, A. R., Riepe, B., Sell, S., Stone, R. C., Vrba, F. J., Walker, R. L., Westerhout, G., Brucato, R. J., Reid, I. N., Schoening, W., Hartley, M., Read, M. A., & Tritton, S. B. 2003, AJ, 125, 984

Montes, D., López-Santiago, J., Gálvez, M. C., Fernández-Figueroa, M. J., De Castro, E., & Cornide, M. 2001, MNRAS, 328, 45

Mugrauer, M., Seifahrt, A., & Neuhäuser, R. 2007, MNRAS, 378, 1328

Mugrauer, M., Seifahrt, A., Neuhäuser, R., & Mazeh, T. 2006, MNRAS, 373, L31

Murdoch, K. A., Hearnshaw, J. B., & Clark, M. 1993, ApJ, 413, 349

Nakajima, T., Oppenheimer, B. R., Kulkarni, S. R., Golimowski, D. A., Matthews, K., & Durrance, S. T. 1995, Nature, 378, 463

Neuhäuser, R. & Guenther, E. W. 2004, A&A, 420, 647

Neuhäuser, R., Guenther, E. W., Wuchterl, G., Mugrauer, M., Bedalov, A., & Hauschildt, P. H. 2005, A&A, 435, L13

Nordström, B., Mayor, M., Andersen, J., Holmberg, J., Pont, F., Jørgensen, B. R., Olsen, E. H., Udry, S., & Mowlavi, N. 2004, A&A, 418, 989

Nordstrom, B., Mayor, M., Andersen, J., Holmberg, J., Pont, F., Jorgensen, B. R., Olsen, E. H., Udry, S., & Mowlavi, N. 2008, VizieR Online Data Catalog, 5117, 0

Oort, J. H. 1927, Bull. Astron. Inst. Netherlands, 4, 79

Oppenheimer, B. R., Kulkarni, S. R., & Stauffer, J. R. 2000, Protostars and Planets IV, 1313

Ortega, V. G., de la Reza, R., Jilinski, E., & Bazzanella, B. 2002, ApJ, 575, L75

Parenago, P. P. 1950, AZh, 27, 41

Parker, E. N. 1955, ApJ, 122, 293

—. 1993, ApJ, 408, 707

Patten, B. M., Stauffer, J. R., Burrows, A., Marengo, M., Hora, J. L., Luhman, K. L., Sonnett, S. M., Henry, T. J., Raghavan, D., Megeath, S. T., Liebert, J., & Fazio, G. G. 2006, ApJ, 651, 502

Pavlenko, Y. V. & Magazzu, A. 1996, A&A, 311, 961

Perryman, M. A. C., Brown, A. G. A., Lebreton, Y., Gomez, A., Turon, C., Cayrel de Strobel, G., Mermilliod, J. C., Robichon, N., Kovalevsky, J., & Crifo, F. 1998, A&A, 331, 81

Perryman, M. A. C., Lindegren, L., Kovalevsky, J., Hoeg, E., Bastian, U., Bernacca, P. L., Crézé, M., Donati, F., Grenon, M., van Leeuwen, F., van der Marel, H., Mignard, F., Murray, C. A., Le Poole, R. S., Schrijver, H., Turon, C., Arenou, F., Froeschlé, M., & Petersen, C. S. 1997, A&A, 323, L49

Phan-Bao, N., Bessell, M. S., Martín, E. L., Simon, G., Borsenberger, J., Tata, R., Guibert, J., Crifo, F., Forveille, T., Delfosse, X., Lim, J., & de Batz, B. 2008, MNRAS, 383, 831

Phan-Bao, N., Bessell, M. S., Martín, E. L., Simon, G., Guibert, J., Forveille, T., Delfosse, X., Crifo, F., Epchtein, N., Wood, P., & Tajahmady, F. 2006, MNRAS, 366, L40

Phan-Bao, N., Crifo, F., Delfosse, X., Forveille, T., Guibert, J., Borsenberger, J., Epchtein, N., Fouqué, P., Simon, G., & Vetois, J. 2003, A&A, 401, 959

Phan-Bao, N., Guibert, J., Crifo, F., Delfosse, X., Forveille, T., Borsenberger, J., Epchtein, N., Fouqué, P., & Simon, G. 2001, A&A, 380, 590

Phan-Bao, N., Martín, E. L., Reylé, C., Forveille, T., & Lim, J. 2005, A&A, 439, L19

Pinfield, D. J., Jones, H. R. A., Lucas, P. W., Kendall, T. R., Folkes, S. L., Day-Jones, A. C., Chappelle, R. J., & Steele, I. A. 2006, MNRAS, 368, 1281

Pinsonneault, M. H., Kawaler, S. D., & Demarque, P. 1990, ApJS, 74, 501

Potter, D., Martín, E. L., Cushing, M. C., Baudoz, P., Brandner, W., Guyon, O., & Neuhäuser, R. 2002, ApJ, 567, L133

Pourbaix, D., Tokovinin, A. A., Batten, A. H., Fekel, F. C., Hartkopf, W. I., Levato, H., Morell, N. I., Torres, G., & Udry, S. 2005, VizieR Online Data Catalog, 5122, 0

Probst, R. G. & Liebert, J. 1983, ApJ, 274, 245

Radigan, J., Lafrenière, D., Jayawardhana, R., & Doyon, R. 2008, ApJ, 689, 471

—. 2009, ArXiv e-prints

Reach, W. T., Megeath, S. T., Cohen, M., Hora, J., Carey, S., Surace, J., Willner, S. P., Barmby, P., Wilson, G., Glaccum, W., Lowrance, P., Marengo, M., & Fazio, G. G. 2005, PASP, 117, 978

Rebolo, R., Martin, E. L., & Magazzu, A. 1992, ApJ, 389, L83

Rebolo, R., Zapatero Osorio, M. R., Madruga, S., Bejar, V. J. S., Arribas, S., & Licandro, J. 1998, Science, 282, 1309

Rebolo, R., Zapatero Osorio, M. R., & Martín, E. L. 1995, Nature, 377, 129

Reid, I. N. & Cruz, K. L. 2002, AJ, 123, 2806

Reid, I. N., Cruz, K. L., Burgasser, A. J., & Liu, M. C. 2008a, AJ, 135, 580

Reid, I. N., Cruz, K. L., Kirkpatrick, J. D., Allen, P. R., Mungall, F., Liebert, J., Lowrance, P., & Sweet, A. 2008b, AJ, 136, 1290

Reid, I. N., Gizis, J. E., Kirkpatrick, J. D., & Koerner, D. W. 2001, AJ, 121, 489

Reid, I. N. & Hawley, S. L. 2005, New light on dark stars : red dwarfs, low-mass stars, brown dwarfs (New Light on Dark Stars Red Dwarfs, Low-Mass Stars, Brown Stars, by I.N. Reid and S.L. Hawley. Springer-Praxis books in astrophysics and astronomy. Praxis Publishing Ltd, 2005. ISBN 3-540-25124-3)

Reid, I. N., Kirkpatrick, J. D., Gizis, J. E., Dahn, C. C., Monet, D. G., Williams, R. J., Liebert, J., & Burgasser, A. J. 2000, AJ, 119, 369

Reid, I. N., Kirkpatrick, J. D., Liebert, J., Burrows, A., Gizis, J. E., Burgasser, A., Dahn, C. C., Monet, D., Cutri, R., Beichman, C. A., & Skrutskie, M. 1999, ApJ, 521, 613

Reid, I. N., Lewitus, E., Allen, P. R., Cruz, K. L., & Burgasser, A. J. 2006, AJ, 132, 891

Reid, I. N. & Walkowicz, L. M. 2006, PASP, 118, 671

Reid, L. N. & Gilmore, G. 1981, MNRAS, 196, 15P

Reid, N., Tinney, C. G., & Mould, J. 1994, AJ, 108, 1456

Reiners, A. & Basri, G. 2008, ApJ, 684, 1390

—. 2009, ApJ, 705, 1416

Reipurth, B. & Clarke, C. 2001, AJ, 122, 432

Retterer, J. M. & King, I. R. 1982, ApJ, 254, 214

Reylé, C. & Robin, A. C. 2004, A&A, 421, 643

Ribas, I. 2003, A&A, 400, 297

Rocha-Pinto, H. J. & Maciel, W. J. 1998, A&A, 339, 791

Roman, N. G. 1950, ApJ, 112, 554

—. 1952, ApJ, 116, 122

Ross, F. E. 1926, AJ, 36, 124

Ruiz, M. T., Leggett, S. K., & Allard, F. 1997, ApJ, 491, L107+

Ruiz, M. T., Wischnjewsky, M., Rojo, P. M., & Gonzalez, L. E. 2001, ApJS, 133, 119

Salim, S., Lépine, S., Rich, R. M., & Shara, M. M. 2003, ApJ, 586, L149

Sandage, A. & Wallerstein, G. 1960, ApJ, 131, 598

Sandage, A. R. 1953, AJ, 58, 61

Saumon, D., Bergeron, P., Lunine, J. I., Hubbard, W. B., & Burrows, A. 1994, ApJ, 424, 333

Saumon, D. & Marley, M. S. 2008, ApJ, 689, 1327

Saumon, D., Marley, M. S., Leggett, S. K., Geballe, T. R., Stephens, D., Golimowski, D. A., Cushing, M. C., Fan, X., Rayner, J. T., Lodders, K., & Freedman, R. S. 2007, ApJ, 656, 1136

Schilbach, E., Röser, S., & Scholz, R. 2009, A&A, 493, L27

Schmidt, S. J., Cruz, K. L., Bongiorno, B. J., Liebert, J., & Reid, I. N. 2007, AJ, 133, 2258

Schmidt, S. J., West, A. A., Hawley, S. L., & Pineda, J. S. 2010, AJ, 139, 1808

Schmitt, J. H. M. M., Fleming, T. A., & Giampapa, M. S. 1995, ApJ, 450, 392

Schneider, D. P., Greenstein, J. L., Schmidt, M., & Gunn, J. E. 1991, AJ, 102, 1180

Schneider, D. P., Knapp, G. R., Hawley, S. L., Covey, K. R., Fan, X., Ramsey, L. W., Richards, G. T., Strauss, M. A., Gunn, J. E., Hill, G. J., MacQueen, P. J., Adams, M. T., Hill, G. M., Ivezić, Ž., Lupton, R. H., Pier, J. R., Saxe, D. H., Shetrone, M., Tufts, J. R., Wolf, M. J., Brinkmann, J., Csabai, I., Hennessy, G. S., & York, D. G. 2002, AJ, 123, 458

Scholz, R.-D., Irwin, M., Ibata, R., Jahreiß, H., & Malkov, O. Y. 2000, A&A, 353, 958

Scholz, R.-D., Lodieu, N., Ibata, R., Bienaymé, O., Irwin, M., McCaughrean, M. J., & Schwope, A. 2004, MNRAS, 347, 685

Scholz, R.-D., McCaughrean, M. J., Lodieu, N., & Kuhlbrodt, B. 2003, A&A, 398, L29

Scholz, R.-D., McCaughrean, M. J., Zinnecker, H., & Lodieu, N. 2005, A&A, 430, L49

Scholz, R.-D. & Meusinger, H. 2002, MNRAS, 336, L49

Searle, L. & Zinn, R. 1978, ApJ, 225, 357

Seifahrt, A., Guenther, E., & Neuhäuser, R. 2005a, A&A, 440, 967

Seifahrt, A., Mugrauer, M., Wiese, M., Neuhäuser, R., & Guenther, E. W. 2005b, Astronomische Nachrichten, 326, 974

Seifahrt, A., Reiners, A., Almaghrbi, K. A. M., & Basri, G. 2010, A&A, 512, A37+

Shu, F. H., Adams, F. C., & Lizano, S. 1987, ARA&A, 25, 23

Siegler, N., Close, L. M., Burgasser, A. J., Cruz, K. L., Marois, C., Macintosh, B., & Barman, T. 2007, AJ, 133, 2320

Siegler, N., Close, L. M., Mamajek, E. E., & Freed, M. 2003, ApJ, 598, 1265

Silvestri, N. M., Hawley, S. L., West, A. A., Szkody, P., Bochanski, J. J., Eisenstein, D. J., McGehee, P., Schmidt, G. D., Smith, J. A., Wolfe, M. A., Harris, H. C., Kleinman, S. J., Liebert, J., Nitta, A., Barentine, J. C., Brewington, H. J., Brinkmann, J., Harvanek, M., Krzesiński, J., Long, D., Neilsen, Jr., E. H., Schneider, D. P., & Snedden, S. A. 2006, AJ, 131, 1674

Sivarani, T., Lépine, S., Kembhavi, A. K., & Gupchup, J. 2009, ApJ, 694, L140

Skrutskie, M. F., Cutri, R. M., Stiening, R., Weinberg, M. D., Schneider, S., Carpenter, J. M., Beichman, C., Capps, R., Chester, T., Elias, J., Huchra, J., Liebert, J., Lonsdale, C., Monet, D. G., Price, S., Seitzer, P., Jarrett, T., Kirkpatrick, J. D., Gizis, J. E., Howard, E., Evans, T., Fowler, J., Fullmer, L., Hurt, R., Light, R., Kopan, E. L., Marsh, K. A., McCallon, H. L., Tam, R., Van Dyk, S., & Wheelock, S. 2006, AJ, 131, 1163

Skumanich, A. 1972, ApJ, 171, 565

Smart, R. L., Jones, H. R. A., Lattanzi, M. G., Leggett, S. K., Warren, S. J., Adamson, A. J., Burningham, B., Casali, M., Evans, D. W., Irwin, M. J., & Pinfield, D. 2010, A&A, 511, A30+

Soderblom, D. R. 1983, ApJS, 53, 1

Soderblom, D. R., Duncan, D. K., & Johnson, D. R. H. 1991, ApJ, 375, 722

Song, I., Zuckerman, B., & Bessell, M. S. 2003, ApJ, 599, 342

Soubiran, C., Bienaymé, O., & Siebert, A. 2003, A&A, 398, 141

Spitzer, Jr., L. & Schwarzschild, M. 1953, ApJ, 118, 106

Stahler, S. W. 1988, ApJ, 332, 804

Stamatellos, D. & Whitworth, A. 2009, ArXiv e-prints

—. 2010, ArXiv e-prints

Stephens, D. C. & Leggett, S. K. 2004, PASP, 116, 9

Stephens, D. C., Leggett, S. K., Cushing, M. C., Marley, M. S., Saumon, D., Geballe, T. R., Golimowski, D. A., Fan, X., & Noll, K. S. 2009, ApJ, 702, 154

Stern, D., Kirkpatrick, J. D., Allen, L. E., Bian, C., Blain, A., Brand, K., Brodwin, M., Brown, M. J. I., Cool, R., Desai, V., Dey, A., Eisenhardt, P., Gonzalez, A., Jannuzi, B. T., Menendez-Delmestre, K., Smith, H. A., Soifer, B. T., Tiede, G. P., & Wright, E. 2007, ApJ, 663, 677

Stone, R. C. 1996, PASP, 108, 1051

—. 2002, PASP, 114, 1070

Strauss, M. A., Fan, X., Gunn, J. E., Leggett, S. K., Geballe, T. R., Pier, J. R., Lupton, R. H., Knapp, G. R., Annis, J., Brinkmann, J., Crocker, J. H., Csabai, I., Fukugita, M., Golimowski, D. A., Harris, F. H., Hennessy, G. S., Hindsley, R. B., Ivezić , Ž., Kent, S., Lamb, D. Q., Munn, J. A., Newberg, H. J., Rechenmacher, R., Schneider, D. P., Smith, J. A., Stoughton, C., Tucker, D. L., Waddell, P., & York, D. G. 1999, ApJ, 522, L61

Stumpf, M. B., Geißler, K., Bouy, H., Brandner, W., Goldman, B., & Henning, T. 2010, ArXiv e-prints

Tarter, J. C. 1975, PhD thesis, California Univ., Berkeley.

Teegarden, B. J., Pravdo, S. H., Hicks, M., Lawrence, K., Shaklan, S. B., Covey, K., Fraser, O., Hawley, S. L., McGlynn, T., & Reid, I. N. 2003, ApJ, 589, L51

Teixeira, R., Ducourant, C., Sartori, M. J., Camargo, J. I. B., Périé, J. P., Lépine, J. R. D., & Benevides-Soares, P. 2000, A&A, 361, 1143

Thompson, M. J., Christensen-Dalsgaard, J., Miesch, M. S., & Toomre, J. 2003, ARA&A, 41, 599

Thorstensen, J. R. & Kirkpatrick, J. D. 2003, PASP, 115, 1207

Tinney, C. G. 1996, MNRAS, 281, 644

Tinney, C. G., Burgasser, A. J., & Kirkpatrick, J. D. 2003, AJ, 126, 975

Tinney, C. G., Burgasser, A. J., Kirkpatrick, J. D., & McElwain, M. W. 2005, AJ, 130, 2326

Tinney, C. G., Delfosse, X., Forveille, T., & Allard, F. 1998, A&A, 338, 1066

Tinney, C. G., Mould, J. R., & Reid, I. N. 1993, AJ, 105, 1045

Tokovinin, A. A. 1997, A&AS, 124, 75

Tokunaga, A. T., Simons, D. A., & Vacca, W. D. 2002, PASP, 114, 180

Tsuji, T. 2002, ApJ, 575, 264

—. 2005, ApJ, 621, 1033

Tsuji, T. & Nakajima, T. 2003, ApJ, 585, L151

Tsuji, T., Ohnaka, K., Aoki, W., & Nakajima, T. 1996, A&A, 308, L29

Tsvetanov, Z. I., Golimowski, D. A., Zheng, W., Geballe, T. R., Leggett, S. K., Ford, H. C., Davidsen, A. F., Uomoto, A., Fan, X., Knapp, G. R., Strauss, M. A., Brinkmann, J., Lamb, D. Q., Newberg, H. J., Rechenmacher, R., Schneider, D. P., York, D. G., Lupton, R. H., Pier, J. R., Annis, J., Csabai, I., Hindsley, R. B., Ivesić, Ž., Munn, J. A., Thakar, A. R., & Waddell, P. 2000, ApJ, 531, L61

Ushomirsky, G., Matzner, C. D., Brown, E. F., Bildsten, L., Hilliard, V. G., & Schroeder, P. C. 1998, ApJ, 497, 253

Vacca, W. D., Cushing, M. C., & Rayner, J. T. 2003, PASP, 115, 389

van Altena, W. F., Lee, J. T., & Hoffleit, E. D. 1995, The general catalogue of trigonometric [stellar] paralaxes (New Haven, CT: Yale University Observatory, —c1995, 4th ed., completely revised and enlarged)

van Biesbroeck, G. 1944, AJ, 51, 61

—. 1961, AJ, 66, 528

van de Kamp, P. 1967, ZAp, 67, 319

van der Bliek, N. S., Norman, D., Blum, R. D., Probst, R. G., Montane, A., Galvez, R., Warner, M., Tighe, R., Delgado, F., & Martinez, M. 2004, in Society of Photo-Optical Instrumentation Engineers (SPIE) Conference Series, Vol. 5492, Society of Photo-Optical Instrumentation Engineers (SPIE) Conference Series, ed. A. F. M. Moorwood & M. Iye, 1582–1589

Vandenberg, D. A. & Bridges, T. J. 1984, ApJ, 278, 679

Voges, W., Aschenbach, B., Boller, T., Brauninger, H., Briel, U., Burkert, W., Dennerl, K., Englhauser, J., Gruber, R., Haberl, F., Hartner, G., Hasinger, G., Pfeffermann, E., Pietsch, W., Predehl, P., Schmitt, J., Trumper, J., & Zimmermann, U. 2000, VizieR Online Data Catalog, 9029, 0

Vrba, F. J., Henden, A. A., Luginbuhl, C. B., Guetter, H. H., Munn, J. A., Canzian, B., Burgasser, A. J., Kirkpatrick, J. D., Fan, X., Geballe, T. R., Golimowski, D. A., Knapp, G. R., Leggett, S. K., Schneider, D. P., & Brinkmann, J. 2004, AJ, 127, 2948

Walkowicz, L. M. & Hawley, S. L. 2009, AJ, 137, 3297

Walkowicz, L. M., Hawley, S. L., & West, A. A. 2004, PASP, 116, 1105

Warren, S. J., Mortlock, D. J., Leggett, S. K., Pinfield, D. J., Homeier, D., Dye, S., Jameson, R. F., Lodieu, N., Lucas, P. W., Adamson, A. J., Allard, F., Barrado Y Navascués, D., Casali, M., Chiu, K., Hambly, N. C., Hewett, P. C., Hirst, P., Irwin, M. J., Lawrence, A., Liu, M. C., Martín, E. L., Smart, R. L., Valdivielso, L., & Venemans, B. P. 2007, MNRAS, 381, 1400

Weinberg, M. D., Shapiro, S. L., & Wasserman, I. 1987, ApJ, 312, 367

West, A. A., Bochanski, J. J., Hawley, S. L., Cruz, K. L., Covey, K. R., Silvestri, N. M., Reid, I. N., & Liebert, J. 2006, AJ, 132, 2507

West, A. A., Hawley, S. L., Bochanski, J. J., & & Covey, K. R. 2009, AJ, submitted

West, A. A., Hawley, S. L., Bochanski, J. J., Covey, K. R., Reid, I. N., Dhital, S., Hilton, E. J., & Masuda, M. 2008, AJ, 135, 785

West, A. A., Hawley, S. L., Walkowicz, L. M., Covey, K. R., Silvestri, N. M., Raymond, S. N., Harris, H. C., Munn, J. A., McGehee, P. M., Ivezić, Ž., & Brinkmann, J. 2004, AJ, 128, 426

West, A. A., Walkowicz, L. M., & Hawley, S. L. 2005, PASP, 117, 706

White, R. J., Ghez, A. M., Reid, I. N., & Schultz, G. 1999, ApJ, 520, 811

Whitworth, A. P. & Stamatellos, D. 2006, A&A, 458, 817

Wielen, R. 1977, A&A, 60, 263

Willstrop, R. V. 1965, MmRAS, 69, 83

Wilson, J. C. 2002, PhD thesis, AA(CORNELL UNIVERSITY)

Wilson, J. C., Kirkpatrick, J. D., Gizis, J. E., Skrutskie, M. F., Monet, D. G., & Houck, J. R. 2001, AJ, 122, 1989

Wilson, J. C., Miller, N. A., Gizis, J. E., Skrutskie, M. F., Houck, J. R., Kirkpatrick, J. D., Burgasser, A. J., & Monet, D. G. 2003, in IAU Symposium, Vol. 211, Brown Dwarfs, ed. E. Martín, 197–+

Wilson, O. C. 1963, ApJ, 138, 832

Wolf, M. 1919, Veroeffentlichungen der Badischen Sternwarte zu Heidelberg, 7, 195

Yoo, J., Chanamé, J., & Gould, A. 2004, ApJ, 601, 311

York, D. G., Adelman, J., Anderson, Jr., J. E., Anderson, S. F., Annis, J., Bahcall, N. A., Bakken, J. A., Barkhouser, R., Bastian, S., Berman, E., Boroski, W. N., Bracker, S., Briegel, C., Briggs, J. W., Brinkmann, J., Brunner, R., Burles, S., Carey, L., Carr, M. A., Castander, F. J., Chen, B., Colestock, P. L., Connolly, A. J., Crocker, J. H., Csabai, I., Czarapata, P. C., Davis, J. E., Doi, M., Dombeck, T., Eisenstein, D., Ellman, N., Elms, B. R., Evans, M. L., Fan, X., Federwitz, G. R., Fiscelli, L., Friedman, S., Frieman, J. A., Fukugita, M., Gillespie, B., Gunn, J. E., Gurbani, V. K., de Haas, E., Haldeman, M., Harris, F. H., Hayes, J., Heckman, T. M., Hennessy, G. S., Hindsley, R. B., Holm, S., Holmgren, D. J., Huang, C.-h., Hull, C., Husby, D., Ichikawa, S.-I., Ichikawa, T., Ivezić, Ž., Kent, S., Kim, R. S. J., Kinney, E., Klaene, M., Kleinman, A. N., Kleinman, S., Knapp, G. R., Korienek, J., Kron, R. G., Kunszt, P. Z., Lamb, D. Q., Lee, B., Leger, R. F., Limmongkol, S., Lindenmeyer, C., Long, D. C., Loomis, C., Loveday, J., Lucinio, R., Lupton, R. H., MacKinnon, B., Mannery, E. J., Mantsch, P. M., Margon, B., McGehee, P., McKay, T. A., Meiksin, A., Merelli, A., Monet, D. G., Munn, J. A., Narayanan, V. K., Nash, T., Neilsen, E., Neswold, R., Newberg, H. J., Nichol, R. C., Nicinski, T., Nonino, M., Okada, N., Okamura, S., Ostriker, J. P., Owen, R., Pauls, A. G., Peoples, J., Peterson, R. L., Petravick, D., Pier, J. R., Pope, A., Pordes, R., Prosapio, A., Rechenmacher, R., Quinn, T. R., Richards, G. T., Richmond, M. W., Rivetta, C. H., Rockosi, C. M., Ruthmansdorfer, K., Sandford, D., Schlegel, D. J., Schneider, D. P., Sekiguchi, M., Sergey, G., Shimasaku, K., Siegmund, W. A., Smee, S., Smith, J. A., Snedden, S., Stone, R., Stoughton, C., Strauss, M. A., Stubbs, C., SubbaRao, M., Szalay, A. S., Szapudi, I., Szokoly, G. P., Thakar, A. R., Tremonti, C., Tucker, D. L., Uomoto, A., Vanden Berk, D., Vogeley, M. S., Waddell, P., Wang, S.-i., Watanabe, M., Weinberg, D. H., Yanny, B., & Yasuda, N. 2000, AJ, 120, 1579

Zapatero Osorio, M. R., Béjar, V. J. S., Martín, E. L., Rebolo, R., Barrado y Navascués, D., Mundt, R., Eislöffel, J., & Caballero, J. A. 2002, ApJ, 578, 536

Zapatero Osorio, M. R., Lane, B. F., Pavlenko, Y., Martín, E. L., Britton, M., & Kulkarni, S. R. 2004, ApJ, 615, 958

Zapatero Osorio, M. R., Martín, E. L., Béjar, V. J. S., Bouy, H., Deshpande, R., & Wainscoat, R. J. 2007, ApJ, 666, 1205

Zuckerman, B. & Song, I. 2009, A&A, 493, 1149